AN EVALUATION OF THE SUITABILITY OF DIFFERENT ELECTRODE ARRAYS FOR GEOHYDROLOGICAL STUDIES IN KAROO ROCKS USING ELECTRICAL RESISTIVITY TOMOGRAPHY

Arnaud Hamidou Tamssar

Submitted in fulfilment of the requirements for the degree

Magister Scientiae in Geohydrology

in the

Faculty of Natural and Agricultural Sciences

(Institute for Groundwater Studies)

at the

University of the Free State

Supervisor: Dr François D. Fourie

Co-supervisor: Prof Gideon Steyl

January 2013

DECLARATION

I, Arnaud HAMIDOU TAMSSAR, hereby declare that, the present thesis, submitted to the Institute for Groundwater Studies, Faculty of Natural and Agricultural Sciences, University of the Free State, Bloemfontein, South Africa, in the fulfilment for the degree of Magister Scientiae, is my own work. It has not previously been submitted by me to any other institution of higher education. In addition, I declare that all sources cited have been acknowledged by means of a list of references.

I furthermore cede copyright of the thesis in favour of the University of the Free State.

_____

Arnaud HAMIDOU TAMSSAR

17 January 2013

ACKNOWLEDGMENTS

I hereby wish to express my sincere gratitude to all who have motivated and helped me in the completion of this thesis:

- **The Institute for Groundwater Studies**, to whom I express my gratefulness for financing my studies and providing the equipment used to conduct this research.
- My promoter, **Dr François D. Fourie**, to whom I express my deep respect and all my recognition for the confidence he testified in me, by personally accepting the direction of my thesis; Thanks for his time and invaluable input in ensuring the success of this project, for the use of the software dongle that allowed full access to the capabilities of RES2DMOD and RES2DINV.
- **Prof. Gideon Steyl**, for his financial assistance, encouragement and contribution during this research;
- **Prof. Gerrit van Tonder** and **Dr Danie P. D. Vermeulen,** for their academic guidance.
- **Mr Eelco Lukas**, for his kind assistance, particularly with the WISH program.
- **Mrs Dora du Plessis,** for her kind help in editing the present dissertation.
- **Mrs. Lorinda Rust** for all administrative arrangements.
- **Mr Charl Yssel**, for accepting the research being undertaken on his farm.
- **Ms Suleen H. Vermaas**, for her time and help granted throughout my field works.
- My lovely parents, **David Tamssar** and **Bernadette Assana**, who are my source of encouragement. May they find in this achievement the greatest reward of their support, joint to my deep gratitude.
- Last but most importantly the Almighty GOD, who takes care of me day after day and provides for my needs, HIM without who I could not have made anything.

LIST OF ACRONYMS AND SYMBOLS

AC : Alternating Current

C1, C2, A, B : Current Electrodes

DC : Direct Current

ERT : Electrical Resistivity Tomography

IP : Induced Polarization

Ma : Mega annum

P1, P2, M, N : Potential Electrodes

RMS : Root-Mean-Squared

SAS : Signal Averaging System

VES : Vertical Electrical Sounding

1-D : One Dimensional

2-D : Two Dimensional

3-D : Three Dimensional

% : Percentage

TABLE OF CONTENTS

1 INTRODUCTION 1

1.1 RESEARCH FRAMEWORK 1

1.2 AIM AND OBJECTIVES 2

1.3 THESIS STRUCTURE 3

2 GEOLOGICAL AND GEOHYDROLOGICAL FRAMEWORKS 5

2.1 GEOLOGY 5

2.2 GEOHYDROLOGY 8

3 INTRODUCTION TO RESISTIVITY METHODS 10

3.1 GENERAL BACKGROUND ON RESISTIVITY METHODS 10

3.1.1 Basic resistivity theory 12

3.1.2 Electrical properties of some Earth materials 16

3.1.3 2-D Electrical Resistivity Tomography 17

3.2 APPLICATIONS OF 2-D ERT METHOD 18

3.2.1 2-D ERT method for groundwater exploration 18

3.2.2 Time-lapse ERT measurements during a pumping test (Loke, 2012) 22

4 SOME CHARACTERISTICS OF ELECTRODE ARRAYS 25

4.1 THE SENSITIVITY FUNCTION 28

4.2 THE DEPTH OF INVESTIGATION 30

4.3 MEASUREMENT PROPERTIES OF THE WENNER ARRAY 34

4.4 MEASUREMENT PROPERTIES OF THE DIPOLE-DIPOLE ARRAY 36

4.5 MEASUREMENT PROPERTIES OF THE WENNER-SCHLUMBERGER ARRAY 39

4.6 MEASUREMENT PROPERTIES OF THE POLE-POLE ARRAY 42

5 CASE STUDIES ON ERT SURVEYS USING DIFFERENT ARRAYS 44

5.1 MAPPING KARST ZONES OF VULNERABILITY 44

5.2 MAPPING FRACTURED CRYSTALLINE-ROCK TERRAIN 48

5.3 DELINEATING AN UNDERGROUND CAVITY 50

6 MODELLING INVESTIGATIONS 56

6.1 THE INFLUENCE OF SELECTED MODEL PARAMETERS 56

6.1.1 Comparison of L1 and L2-norm inversion methods 56

6.1.2 Noise-contaminated data sets 58

6.2 MODELLING DYKES ALONE 59
6.2.1 Construction of the input resistivity models 60
6.2.2 Inverse model resistivity sections 62
6.3 MODELLING SILLS ALONE 69
6.3.1 Construction of the input resistivity models 69
6.3.2 Inverse model resistivity sections 70
6.4 MODELLING DYKES WITH SILLS 73
6.4.1 Construction of the input resistivity models 74
6.4.2 Inverse model resistivity sections 77
6.5 MODELLING WEATHERED ZONE 88
6.5.1 A conceptual model of a weathered zone 88
6.5.2 Inverse model resistivity sections 89
6.6 MODELLING BOUNDARIES 91
6.7 MODELLING FAULT ZONES 96

7 FIELD SURVEYS 100
7.1 SITE DESCRIPTIONS 100
7.2 METHOD OF INVESTIGATIONS 103
7.3 RESULTS OF THE FIELD INVESTIGATIONS 108
7.3.1 Field survey across a dolerite sill 109
7.3.2 Field survey across a dolerite dyke 116
7.3.3 Field survey across a dolerite sill intruded by a dyke 122
7.4 COMPARISONS OF FIELD RESULTS TO THEORETICAL CONSIDERATIONS 128
7.4.1 Results obtained from surveys across dolerite sills 129
7.4.2 Results obtained from surveys across dolerite dykes 129
7.4.3 Results obtained from surveys across dolerite sill intruded by dyke 130

8 CONCLUSIONS AND RECOMMENDATIONS 133

REFERENCES 139

APPENDICES 147
APPENDIX 1: Vertical and dipping dyke's apparent resistivity pseudo-sections 147
A. VERTICAL THIN DYKE 147
B. DIPPING THIN DYKE 148
C. VERTICAL THICK DYKE 149
D. DIPPING THICK DYKE 151

APPENDIX 2: Sill's apparent resistivity pseudo-sections 152
A. THIN SILL 152
B. THICK SILL 153
APPENDIX 3: Sill intruded by vertical and dipping dyke's pseudo-sections 154
A. VERTICAL THIN DYKE WITH THIN SILL 154
B. DIPPING THIN DYKE WITH THIN SILL 155
C. VERTICAL THICK DYKE WITH THIN SILL 155
D. DIPPING THICK DYKE WITH THIN SILL 156
E. VERTICAL THIN DYKE WITH THICK SILL 158
F. DIPPING THIN DYKE WITH THICK SILL 159
G. VERTICAL THICK DYKE WITH THICK SILL 160
H. DIPPING THICK DYKE WITH THICK SILL 161
APPENDIX 4: Weathered zone's apparent resistivity pseudo-sections 163
A. WEATHERED ZONE 163
APPENDIX 5: Contacts and boundary's apparent resistivity pseudo-sections 164
A. VERTICAL CONTACT 164
B. DIPPING CONTACT 165
C. HORIZONTAL CONTACT 166
APPENDIX 6: Fault's apparent resistivity pseudo-sections 167
A. VERTICAL FAULT 167
B. DIPPING FAULT 168
Abstract 169
Opsomming 171

LIST OF TABLES

Table 3-1: Resistivities of some common rocks, minerals and chemicals (Loke, 1999).....17
Table 4-1: The median depth of investigation (Ze) for the different arrays (Edwards, 1977) 33
Table 6-1: RMS errors of the vertical and dipping dyke models after seven iterations 67
Table 6-2: RMS errors of the sill models after seven iterations 72
Table 6-3: RMS errors of the sill intruded by vertical and dipping dyke models after seven iterations.....87
Table 6-4: RMS errors of the boundary models after seven iterations 94
Table 6-5: RMS errors of the fault models after seven iterations.....98
Table 7-1: All possible measurements taken for each electrode array 106
Table 7-2: Resistivity profile lines coordinates 107
Table 7-3: Possible measurements for a typical field surveys.....115
Table 7-4: Summary regarding the advantages/disadvantages of the arrays.....132

LIST OF FIGURES

Figure 2-1: Geological map of South Africa (www.sanparks.org).....5
Figure 2-2: Dyke and sill formations.....7
Figure 3-1: General setup for resistivity surveying.....10
Figure 3-2 : Pseudo-section data pattern (a) and apparent resistivity pseudo-section (b).....11
Figure 3-3: Flow of current from a point current source and the resulting potential distribution (Loke, 2012).....14
Figure 3-4: Potential distribution caused by a pair of current electrodes (Loke, 2012).....15
Figure 3-5: A conventional four electrode array.....15
Figure 3-6: Apparent resistivities measured during dry (top) and wet (bottom) seasons (Agramakova, 2005).....20
Figure 3-7: Results of the inversions for data set collected during dry and wet seasons (Agramakova, 2005).....20
Figure 3-8: Pseudo-section and inverse model sections for a pumping test (Loke, 2012).....22
Figure 3-9: Percentage relative change in the subsurface resistivity values (Loke, 2012).....23
Figure 3-10: Use of Archie's Law for the Hoveringham pumping test (Loke, 2012).....24
Figure 4-1: Common arrays used in resistivity surveys (Loke, 1999).....26
Figure 4-2: Sensitivity patterns for the (a) Wenner (b) Wenner-Schlumberger and (c) Dipole-Dipole arrays.....27
Figure 4-3: Sensitivity function calculation at a point $d\tau(x,y,z)$ within a half-space.....28
Figure 4-4: The geometry of the Wenner array.....34
Figure 4-5: 2-D sensitivity sections for the Wenner array (Loke, 2012).....35
Figure 4-6: The geometry of the Dipole-Dipole array.....36
Figure 4-7: The 2-D sensitivity sections for the Dipole-Dipole array (Loke, 2012).....38
Figure 4-8: The geometry of the Wenner-Schlumberger array.....39
Figure 4-9: A comparison of the (i) electrode arrangement and (ii) pseudo-section data pattern for the Wenner and Wenner-Schlumberger arrays (Loke, 2012).....40
Figure 4-10: 2-D sensitivity sections for the Wenner-Schlumberger array (Loke, 2012).....41
Figure 4-11: The geometry of the Pole-Pole array.....42
Figure 4-12: The 2-D sensitivity section of the Pole-Pole array (Loke, 2012).....43
Figure 5-1: Conceptual model of formation of a cover-collapse sinkhole (Zhou et al., 2002)45
Figure 5-2: Resistivity pseudo-sections for the sinkhole formation model (Zhou et al., 2002).....46
Figure 5-3: Modelled resistivity sections over a sinkhole collapse area (Zhou *et al*., 2002) ..47
Figure 5-4: Measured and calculated apparent resistivity data using the Wenner array.....51
Figure 5-5: Measured and calculated apparent resistivity data using the Dipole-Dipole array.....51
Figure 5-6: 3-D resistivity model obtained by a Wenner array as horizontal depth slices.....52
Figure 5-7: Iso-resistivity surface of the highest resistivity zones obtained by (a) Wenner array and (b) Dipole-Dipole array.....53
Figure 5-8: 3-D resistivity model obtained by a Dipole-Dipole array as horizontal depth slices.....55
Figure 6-1: Robust inverse model constraint (a) and least-square smoothness-constraint (b) 57
Figure 6-2: Modelled resistivity sections for noise-contaminated data sets.....59

Figure 6-3: Input resistivity model for a vertical thin dyke 60
Figure 6-4: Input resistivity model for a dipping thin dyke 61
Figure 6-5: Input resistivity model for a vertical thick dyke 61
Figure 6-6: Input resistivity model for a dipping thick dyke 62
Figure 6-7: Resistivity profiles showing the measured (top) and calculated (centre) apparent resistivity pseudo-sections and the inverse model resistivity section (bottom) 63
Figure 6-8: Modelled resistivity sections for a vertical thin dyke 64
Figure 6-9: Modelled resistivity sections for a dipping thin dyke 65
Figure 6-10: Modelled resistivity sections for a vertical thick dyke 66
Figure 6-11: Modelled resistivity sections for a dipping thick dyke 67
Figure 6-12: Input resistivity model for a thin sill 70
Figure 6-13: Input resistivity model for a thick sill 70
Figure 6-14: Modelled resistivity sections for a thin sill 71
Figure 6-15: Modelled resistivity sections for a thick sill 72
Figure 6-16: Input resistivity model for a thin sill intruded by a vertical thin dyke 74
Figure 6-17: Input resistivity model for a thin sill intruded by a dipping thin dyke 74
Figure 6-18: Input resistivity model for a thin sill intruded by a vertical thick dyke 75
Figure 6-19: Input resistivity model for a thin sill intruded by a dipping thick dyke 75
Figure 6-20: Input resistivity model for a thick sill intruded by a vertical thin dyke 76
Figure 6-21: Input resistivity model for a thick sill intruded by a dipping thin dyke 76
Figure 6-22: Input resistivity model for a thick sill intruded by a vertical thick dyke 77
Figure 6-23: Input resistivity model for a thick sill intruded by a dipping thick dyke 77
Figure 6-24: Modelled resistivity sections for a thin sill intruded by a vertical thin dyke 79
Figure 6-25: Modelled resistivity sections for a thin sill intruded by a dipping thin dyke 80
Figure 6-26: Modelled resistivity sections for a thin sill intruded by a vertical thick dyke 81
Figure 6-27: Modelled resistivity sections for a thin sill intruded by a dipping thick dyke 82
Figure 6-28: Modelled resistivity sections for a thick sill intruded by a vertical thin dyke 83
Figure 6-29: Modelled resistivity sections for a thick sill intruded by a dipping thin dyke 84
Figure 6-30: Modelled resistivity sections for a thick sill intruded by a vertical thick dyke 85
Figure 6-31: Modelled resistivity sections for a thick sill intruded by a dipping thick dyke 86
Figure 6-32: Input resistivity model for a weathered zone 89
Figure 6-33: Modelled resistivity sections for a weathered zone 90
Figure 6-34: Input resistivity model for a vertical boundary 91
Figure 6-35: Input resistivity model for a dipping boundary 91
Figure 6-36: Input resistivity model for a horizontal boundary 92
Figure 6-37: Modelled resistivity sections for a vertical contact zone 92
Figure 6-38: Modelled resistivity sections for a dipping contact zone 93
Figure 6-39: Modelled resistivity sections for a horizontal contact zone 94
Figure 6-40: Input resistivity model for a vertical fault 96
Figure 6-41: Input resistivity model for a dipping fault 97
Figure 6-42: Modelled resistivity sections for a vertical fault 97
Figure 6-43: Modelled resistivity sections for a dipping fault 98
Figure 7-1: Geographical location of the three study sites 100
Figure 7-2: Geographical location of the Krugersdrift site (Google Earth) 101
Figure 7-3: Geographical location of the Paradise site (Google Earth) 102

Figure 7-4: Geographical location of Meadows site (Google Earth).....102
Figure 7-5: Dolerite dyke direction at Meadows site (Google Earth) 103
Figure 7-6: Resistivity equipment.....104
Figure 7-7: Arrangement of the equipment for a 2-D survey (Modified from Loke, 2012)..105
Figure 7-8: Cable joint (a) and cable joint connected to a cable (b) (ABEM, 2010).....105
Figure 7-9: Data points distribution for all possible measurements taken with Wenner_L (a) and Wenner_S (b) 106
Figure 7-10: Modelled resistivity sections across a dolerite sill at the Paradise site.....110
Figure 7-11: Borehole log.....111
Figure 7-12: Inverse resistivity models for data recorded across a sill using the Dipole-Dipole array. Data sets have been truncated to include data points with standard deviations less than 50% (top), 20% (middle) and 10% (bottom) 114
Figure 7-13: Data points distribution for rapid surveys with (a) Wenner_L and (b) Wenner_S 115
Figure 7-14: Modelled sections using the typical survey protocols across a dolerite sill at the Paradise site 116
Figure 7-15: Thick dolerite dyke outcropping at the Krugersdrift site.....117
Figure 7-16: Magnetic profile across a dolerite dyke at the Krugersdrift site 117
Figure 7-17: Modelled resistivity sections across a dolerite dyke at the Krugersdrift site....118
Figure 7-18: Inverse resistivity models for data recorded across a dyke using the Dipole-Dipole array. Data sets have been truncated to include data points with standard deviations less than 50% (top), 20% (middle) and 10% (bottom) 121
Figure 7-19: Modelled sections using the typical survey protocols across a dolerite dyke at the Krugersdrift site 122
Figure 7-20: Trench showing the dyke thickness at the Meadows site 123
Figure 7-21: Modelled resistivity sections across a sill intruded by a dyke at the Meadows site 124
Figure 7-22: Inverse resistivity models for data recorded across a sill intruded by a dyke using the Dipole-Dipole array. Data sets have been truncated to include data points with standard deviations less than 50%, 20% 10%, 5% and 2% 126
Figure 7-23: Modelled sections using the typical survey protocols across a sill intruded by a dyke at the Meadows site.....127

1 INTRODUCTION

1.1 RESEARCH FRAMEWORK

The resistivity method has been used since the 1920s, when it was initially applied for quantitative interpretations; the one-dimensional (1-D) survey was carried out doing either profiling (lateral investigation) or vertical electrical sounding (VES) which had several limitations. Overcoming these limitations led to the introduction of the two-dimension (2-D) and three-dimension (3-D) resistivity methods in the 1990s; more accurate, serviceable, comfortable, convenient, field worthy and automatic. Nowadays, the 2-D Electrical Resistivity Tomography (ERT) method has become one of the most significant geophysical techniques for investigating near-surface underground structures. It is a well-established tool for environmental studies, geohydrology, archaeological and engineering site investigation, and is routinely applied in mapping freshwater aquifers and unconsolidated sediments, detecting contaminant plumes, characterising geologic structures and other applications.

Geohydrologists, geophysicists and engineers have also applied the 2-D ERT technique in the Karoo for many purposes, among which: groundwater exploration, detection of pollution, and location of ore deposits. The geology of the Karoo formations reveals the presence of many intrusive rocks, particularly dolerite dykes and sills. During plutonic intrusions, fractured zones are created at the contact between the intrusive magmas and the surrounding host rock. These fracture zones are generally sought during groundwater exploration and during groundwater pollution studies, because of their hydraulic conductivity properties. When conducting ERT surveys, a frequently occurring problem is the need to determine **which of the many existing electrode arrays will respond the best to the target material**, since each electrode configuration has its advantages and disadvantages in terms of:

- the sensitivity of the array to vertical and horizontal changes in the subsurface resistivity,
- the depth of investigation,
- the horizontal data coverage, and
- the signal strength (Loke, 1999).

Different electrode geometries are known to be more or less sensitive to certain changes in the Earth's resistivities: some are more sensitive to lateral changes; others are more sensitive to vertical changes. The question is: **How important is the choice of an array when conducting surveys across geological features such as dykes and sills?** This has an important consequence for groundwater exploration and groundwater pollution studies, since the aim of such studies is to detect the contact zones between the intrusive rocks and their hosts in order to target the fractured zones.

1.2 AIM AND OBJECTIVES

The present thesis aims to evaluate the suitability of different electrode arrays used during ERT surveys. Since different electrode geometries may be used during geohydrological investigations in Karoo formations, the general objectives of the study are:

- Determining which array is the most suitable in mapping the boundaries of vertical structures such as dykes,
- Ascertaining which array is the best in mapping the boundaries of horizontal structures such as sills,
- Establishing which array is the most suitable in mapping weathered zones, faults and other features.

The specific objectives of the project are to:

- carry out a thorough literature review regarding the sensitivities, depths of investigation, signal strengths and horizontal data coverage of various electrode arrays;
- perform a literature study to evaluate past research into the sensitivities of electrode arrays and their potential applications;
- execute forward and inverse modelling investigations in order to study the expected responses of different arrays for ERT measurements over different geological structures;
- perform field measurements at a number of selected sites where the field conditions (geology) are known (the surveys will be done across known dykes and sills);

- make a comparison of the results of the different arrays to see which arrays are the most successful in defining the vertical/horizontal contacts;
- give a critical evaluation of the field results as compared to the theoretical considerations; and
- draw some conclusions regarding the application of the electrode arrays to groundwater exploration and pollution studies in Karoo rocks.

1.3 THESIS STRUCTURE

The thesis is structured in eight chapters, including the introduction (Chapter 1):

Chapter 2 reviews the geology and the geohydrology of the Karoo rocks, with a particular focus on the dolerite dyke and sill intrusions, as well as some Karoo aquifer properties.

Chapter 3 gives an introduction to resistivity methods. It describes the basic resistivity theory, the electrical properties of some Earth materials, the 2-D ERT method and some of its applications.

Chapter 4 presents some characteristics of the Wenner, the Schlumberger, the Dipole-Dipole and the Pole-Pole arrays. It explains how the sensitivity function and the depth of investigation of each array are calculated.

Chapter 5 comments on case studies performed by authors on the sensitivity of various electrode arrays. The case studies concern the mapping of Karst zones and fractured crystalline rock terrain, as well as the delineation of an underground cavity, using the common electrode arrays.

Chapter 6 describes the modelled responses from the Forward and Inverse Modelling investigations. Several numerical models simulating geological features are evaluated through the Wenner, the Schlumberger, the Dipole-Dipole and the Pole-Pole arrays.

Chapter 7 provides information on the field method of investigations after describing the three study areas selected for the current research. It also compares the results of the different arrays to determine qualitatively which arrays are the most successful in defining the vertical/horizontal contacts, and finally makes a critical evaluation of the field results as compared to the theoretical considerations.

Chapter 8 draws conclusions on the application of the electrode arrays for geohydrological studies in Karoo rocks and provides recommendations for future research on groundwater investigations using the ERT method.

2 GEOLOGICAL AND GEOHYDROLOGICAL FRAMEWORKS

2.1 GEOLOGY

The present research is conducted on different sites located within the Karoo Supergroup (Figure 2-1), more specifically, in the Adelaide Subgroup of the Beaufort Group. The Karoo Supergroup mainly consists of sandstone, mudstone, shale and siltstone sedimentary rocks (Woodford *et al.*, 2002).

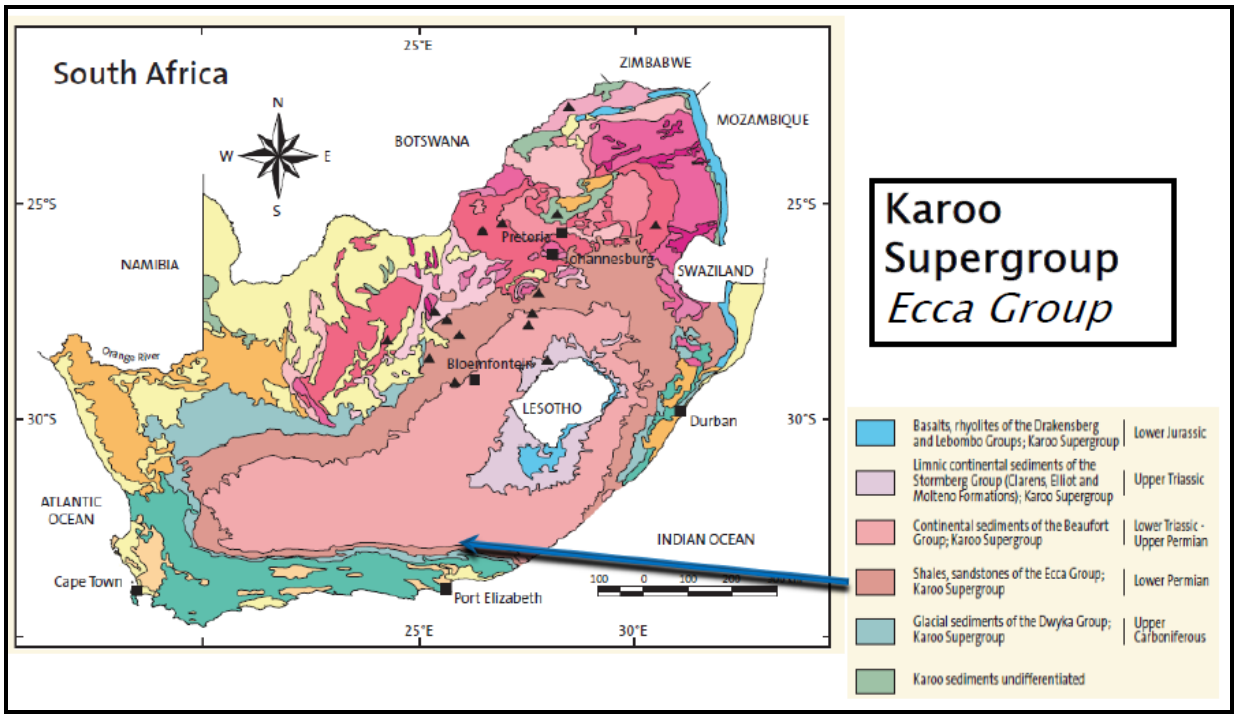

Figure 2-1: Geological map of South Africa (www.sanparks.org)

The Karoo Supergroup, which ranges in age from Carboniferous to Jurassic, is well known for its thick glacial deposits (approximately 12 km in the south-eastern part of the basin) and extensive flood basalts with their associated dolerite dykes and sills (Woodford *et al.*, 2002). Johnson *et al.* (2006) stated that deposition in the Main Karoo Basin began with the Dwyka Group, mostly formed by tillites or glacial sediments, at mid-Carboniferous times. Deposition of shales and sandstones which constitutes the Ecca Group followed afterwards, at Early Permian times. The Beaufort Group mainly composed of continental sediments was deposit later. This group is divided into the Adelaide and the Tarkastad Subgroups. Deposition of the Adelaide Subgroup occurred in Late Permian times (approximately 260 Ma ago), while deposition of the Tarkastad Subgroup occurred at Early Triassic times (approximately 240 Ma ago). Bloemfontein is situated in the Adelaide Subgroup. Deposition of the

Stormberg Group, predominantly consisting of limnic continental sediments, followed thereafter. This group can also be divided into the Molteno, Elliot and Clarens Formations. The Molteno Formation was deposited from Middle Triassic till Late Triassic ages (approximately 220 Ma ago). Depositions of the Elliot Formation occurred in the Late Triassic to Early Jurassic ages (approximately 195 Ma ago) and are overlain by the Middle Jurassic Clarens Formation (approximately 180 Ma). Sedimentation in the Main Karoo basin was terminated during the Middle Jurassic with the outpouring of at least 1400 m of basaltic lavas: the Drakensberg Group. The Drakensberg Group, essentially formed by basalts and rhyolites, constitutes the uppermost unit of the Karoo Supergroup.

The Jurassic dolerite dykes and sills (Figure 2-2) were intruded into the sediments of the Karoo Supergroup during a period of extensive magmatic activity, that took place over almost the entire Southern African subcontinent during one of the phases in the Gondwanaland break-up (Chevallier *et al.,* 2001). They represent the roots and the feeders of the extrusive Drakensberg basalt that are dated around 180 Ma (Duncan and Marsh, 2006; Duncan *et al.,* 1997; Fitch and Miller, 1984; Richardson, 1984). The Karoo dolerite, which includes a wide range of petrological facies, consists of an interconnected network of dykes and sills and it is nearly impossible to single out any particular intrusive or tectonic event (Woodford *et al.,* 2002).

Dykes: Dolerite dykes are vertical to sub-vertical intrusions that may act as semi- to impermeable barriers to the movement of groundwater (Woodford *et al*., 2002). Dolerite dykes have always been and still are the preferred drilling target for groundwater in the Karoo (Darcy Groundwater Scientists and Consultants, 2004). Studies conducted by Woodford *et al*. (2002) revealed that the average thickness of Karoo dolerite dykes ranges between 2 and 10 m and their average strike length ranges between 5 and 30 km. Detailed information such as structural aspects, mapping and geneses of Karoo dolerites can be obtained from Chevallier and Woodford (1999); Du Toit (1905); Du Toit (1920); Maske (1966); Rogers and Du Toit (1903).

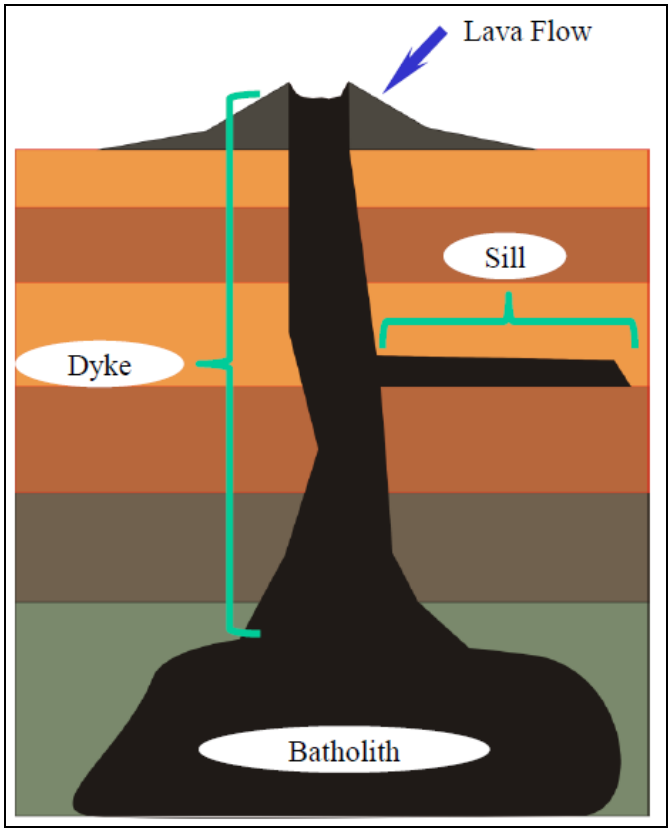

Figure 2-2: Dyke and sill formations

Sills: Sills in the Karoo formations are sheet-like forms of dolerite intrusions that tend to follow the bedding planes of the formations concordantly. These structures, whose thicknesses vary from less than a metre to hundreds of metres, represent the dominant form in which dolerite is emplaced in the Karoo Supergroup (Walker and Poldervaart, 1949). Sills may have very complex forms (Botha *et al.*, 1998).

Dolerite dykes (younger) that cut sills are often good targets for groundwater, especially in a valley-bottom situation where the sill material is highly weathered (Woodford *et al.*, 2002). The dyke-sill contact zone is generally not as wide or permeable as that of the dyke-sediment contact. This may be due to the more intense development of thermal-joints along dolerite sediment contacts as a result of differential cooling caused by the greater contrast in thermal conductance between the two rock types. Fractures are often well developed in the vicinity of the dyke/sill contacts. This fracturing probably resulted during the simultaneous cooling of the dyke and the sill (Woodford *et al.*, 2002).

Jointing is commonly developed along the contact of the dyke (thermal) and within the adjacent baked, disturbed sediment. Boreholes drilled into this zone are generally higher yielding than those drilled away from the dyke in the undisturbed host rock. Syn- or Post-

intrusion tectonic and/or hydrothermal reactivation of the structure often results in the development of more discrete fractures or fissures that transgress the dyke and extend into the country rock. Boreholes intersecting such fractures often have exceptionally high yields.

2.2 GEOHYDROLOGY

The Karoo aquifers occur within the rocks of the Karoo Supergroup, which consists of different groups of sediments, each with its own physical properties (Darcy Groundwater Scientists and Consultants, 2004). Aquifers with low permeability are the main features of the Karoo Supergroup. Boreholes drilled in Karoo formations, generally have low yields, less than 1 L/s (Woodford *et al*., 2002). Indeed, the common view is that Karoo aquifers do not contain large quantities of groundwater, hence the name Karoo, which is the Hottentot word for dry.

Exploration drilling has shown that water-bearing open fractures develop at specific locations within the dolerite and surrounding host rock, in the sediment above an up-stepping sill or at the base of an inner-sill (Woodford *et al*., 2002). In the first case, fracturing is much localised, whilst in the second and third cases shear and 'open' fractures can extend some distance away from the dolerite contact into the country rock. These zones represent challenging exploration targets that require drilling of deeper (200-350 m) boreholes (Woodford *et al*., 2002).

The Ecca Group consists mainly of shales of varying thicknesses. Since the shales are generally very dense, they are often overlooked as significant sources of groundwater (Woodford *et al*., 2002).

The Adelaide Subgroup of the Beaufort Group was extensively intruded by dolerite sills and by dolerite dykes. Within the rocks of the Adelaide Subgroup, groundwater generally occurs in joints and fractures on the contact zones, within weathered dolerite zones, weathered and jointed sedimentary rocks and on bedding planes (Botha *et al.*, 1998). Therefore, the Beaufort Group is often associated with aquifers with a high groundwater potential.

Dykes thicker than 10 m may serve as groundwater barriers, but those of a relatively smaller width are often permeable, as they developed cooling joints and fractures. Van Wyk (1963) reported that more than 80% of the successful boreholes (yield greater than 0.13 L/s) drilled in Karoo sediments in northern Kwazulu-Natal are directly or indirectly related to dolerite

intrusions. Sami *et al.* (2002) noted that the yield of boreholes adjacent to dolerite dykes intruding the fractured sandstone or mudstone of Karoo aquifers is significantly higher than elsewhere in the basin.

The following characteristics are some other features of the Karoo formations (Woodford *et al*., 2002):

- Boreholes with high yield (1.4 L/s) are generally encountered in the Molteno Formation;
- Low borehole yields can be expected far from dolerite intrusions in the Dwyka and Ecca Groups;
- The upper part of the Karoo Supergroup has good yields (1.4 to 25 L/s) because of the presence of several fractures in sandstone (horizontal bedding plane fractures);
- Groundwater is mostly located at dolerite seams in the Ecca Group. However, most of the boreholes below the Ecca shale are successful, particularly in the Northern Natal;
- Highest yields are obtained in boreholes which strike the water bearing seams under the water table where dolerite intrusion has occurred.

3 INTRODUCTION TO RESISTIVITY METHODS

The previous chapter presented a summary of the geology and the geohydrology of the Karoo Supergroup, with an emphasis on dolerite dyke and sill intrusions, as well as some properties of Karoo aquifers. The present chapter firstly gives a general background on resistivity method and secondly describes some applications of the 2-D ERT method in various fields of investigation.

3.1 GENERAL BACKGROUND ON RESISTIVITY METHODS

The resistivity method is a geophysical technique that can provide cost-effective answers to geological, geohydrological and engineering questions. It is a non-intrusive and intensively used geophysical technique for subsurface resistivity structure investigations. The method is based on the fact that different geological units (structures or formations) in the Earth's subsurface are more or less resistive to electrical current flow. A direct current (DC) or slowly varying alternating current (AC) is injected into the Earth by means of pairs of grounded current electrodes (Figure 3-1), A and B in this case. The voltage drops are then measured at selected positions of the surface, between different pairs of grounded potential electrodes M and N in this case. These voltage drops are dependent on the resistivities of the materials through which the electrical currents are flowing.

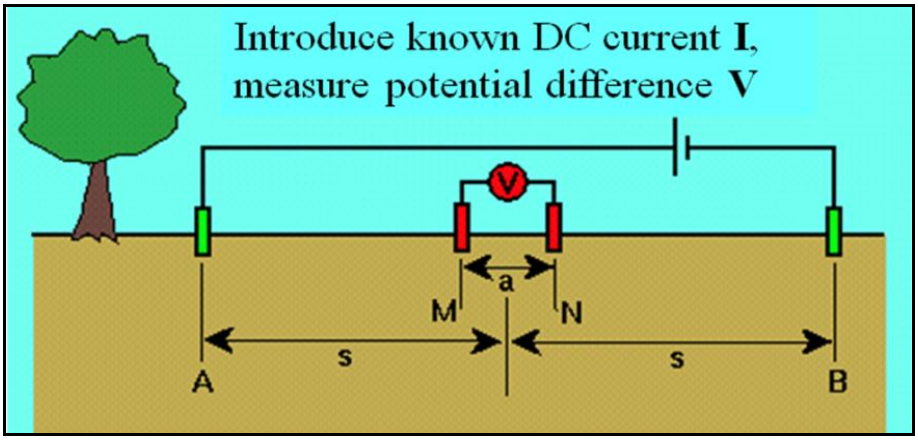

Figure 3-1: General setup for resistivity surveying

By assuming that the earth is homogeneous and isotropic, measurements of the injected electrical current and measured voltage drops, as well as the distances between the different electrodes, may be used to calculate an apparent resistivity for the Earth at a specific position and a pseudo-section of that half-space can be displayed. The pseudo-section plot is obtained

by contouring the apparent resistivity values calculated. The plot displays at its vertical scale the pseudodepth and its horizontal scale the horizontal distance along the survey line (Figure 3-2). The pseudo-section gives an approximate (but distorted) picture of the subsurface resistivity distribution and is useful as a means to present the measured apparent resistivity values in a pictorial form (Loke, 2012). The apparent resistivities recorded during a survey may be inverted to obtain a model of the resistivity distribution within the subsurface. The modelled resistivity distribution may now be interpreted in terms of the local geological conditions by incorporating known information on the geology of the site.

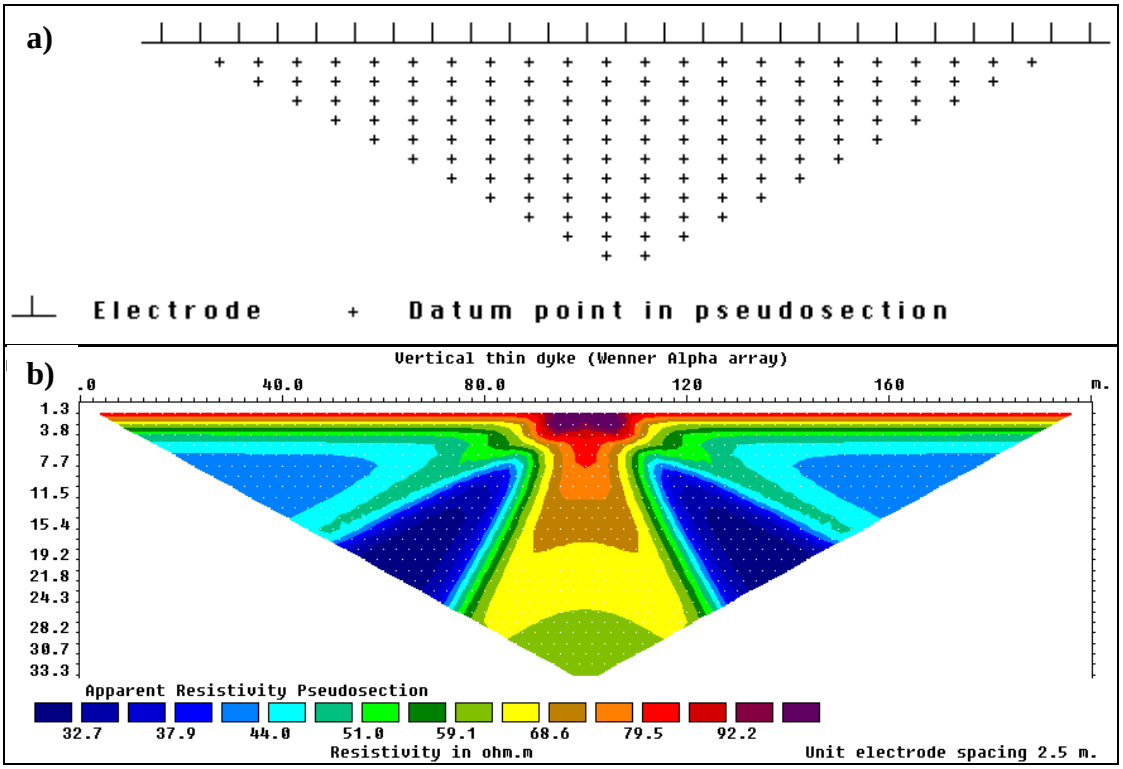

Figure 3-2 : Pseudo-section data pattern (a) and apparent resistivity pseudo-section (b)

Resistivity values of the earth materials are therefore calculated from measurements of the injected currents and measured voltages. These resistivity values are the weighted average values of the resistivities of the earth materials through which currents flow. The resistivity of soil and rocks in the subsurface depends on the degree of fluid saturation in the subsurface, the lithology, the porosity, and the ionic strength of subsurface fluids (Parasnis, 1997). By increasing or decreasing the distance between the electrodes, different volumes of the subsurface are investigated and additional information about resistivities at different depths is obtained.

The traditional resistivity method was carried out by a one dimensional (1-D) survey, conducted with either profiling or vertical electrical sounding (VES). The profiling technique was performed by moving a constant spacing electrode array along a line and plotting the variations against profiled distances, while the VES technique involved the increase of the electrode separations around a mid-point, usually with a logarithmic electrode separation distribution, in order to find the layering of strata. The interpretation of data acquired from such survey was undertaken with the assumption that the subsurface consists of horizontal layers. This method has given useful results for geological situations such as water-table where the 1-D model is approximately true (Loke, 2012).

Nowadays, the two-dimensional (2-D) and three-dimensional (3-D) resistivity imaging have replaced the 1-D method. The 2-D resistivity techniques, also called electrical resistivity tomography (ERT), allow rapid recording of resistivity data at different positions and depths along the survey line. The ERT systems usually employ multi-core cables that connect to numerous electrodes at constant spacings. A switcher unit automatically selects which electrode pairs on the cables act as current electrodes and potential electrodes. For each electrode selection an apparent resistivity value is calculated.

3.1.1 Basic resistivity theory

Loke (2012) gives a description of the basic theory of the resistivity technique. The purpose of electrical resistivity surveys is to determine the subsurface resistivity distribution by making measurements on the ground surface. From these measurements, the input resistivity of the subsurface can be estimated.

The fundamental physical law used in resistivity surveys is Ohm's Law which governs the flow of current in the ground. The Equation for Ohm's Law in vector form for current flow in a continuous medium is given by:

$$\mathbf{J} = \sigma \mathbf{E} \tag{3-1}$$

where σ is the conductivity of the medium, **J** is the current density and **E** is the electric field intensity. The resistivity (ρ) of the medium is the inverse of the conductivity ($\rho=1/\sigma$) and is more frequently used during resistivity surveys. The link between the electric potential and the field intensity is given by:

$$\mathbf{E} = -\nabla\phi \tag{3-2}$$

Combining Equations (3-1) and (3-2) gives:

$$\mathbf{J} = -\sigma\nabla\phi \tag{3-3}$$

In almost all surveys, the current sources are in the form of point sources. In this case, over an elemental volume ΔV surrounding the current source I, located at (x_s, y_s, z_s), the relationship between the current density and the current is given by (Dey and Morrison, 1979):

$$\nabla \cdot \mathbf{J} = \left(\frac{I}{\Delta V}\right)\delta(x - x_s)\delta(y - y_s)\delta(z - z_s) \tag{3-4}$$

where δ is the Dirac delta function. Equation (3-3) can then be rewritten as

$$-\nabla \cdot [\sigma(x,y,z)\nabla\phi(x,y,z)] = \left(\frac{I}{\Delta V}\right)\delta(x - x_s)\delta(y - y_s)\delta(z - z_s) \tag{3-5}$$

This is the basic equation that gives the potential distribution in the ground due to a point current source. This is the forward modelling problem, which is to determine the potential that would be observed over a given subsurface structure. Fully analytical methods have been used for simple cases, such as a sphere in a homogenous medium or a vertical fault between two areas each with a constant resistivity. For an arbitrary resistivity distribution, numerical techniques are more commonly used. For the 1-D case, where the subsurface is restricted to a number of horizontal layers, the linear filter method is commonly used (Koefoed, 1979). For 2-D and 3-D cases, the finite-difference and finite-element methods are the most versatile.

Data from a resistivity survey is usually presented in the form of values of apparent resistivity ρ_a, which is defined as **the resistivity of an electrically homogeneous and isotropic half-space that would yield the measured relationship between the applied current and potential difference for a particular arrangement and spacing of electrodes**.

Consider a homogeneous subsurface and a single point current source on a ground surface (Figure 3-3). The electric current (I) measured in amperes, flows radially away from the source, and the potential varies inversely with distance from the current source. The equipotential surfaces have a hemispherical shape, and the current flow is perpendicular to the equipotential surfaces. The electrical potential (ϕ), in this case is given by:

$$\phi = \frac{\rho I}{2\pi r} \tag{3-6}$$

where r is the distance of a point in the medium (also measured along the ground surface) from the electrode.

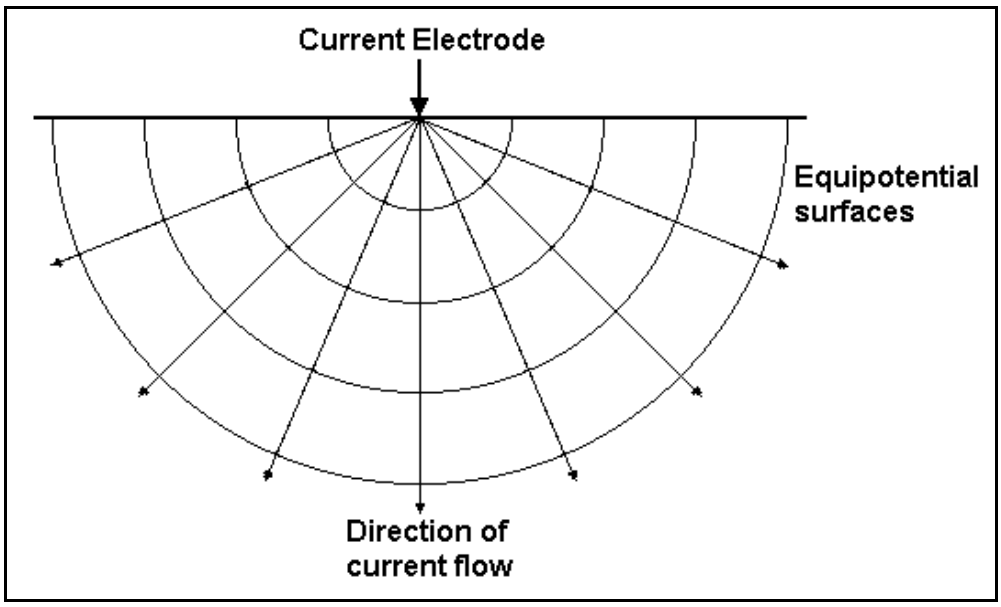

Figure 3-3: Flow of current from a point current source and the resulting potential distribution (Loke, 2012)

In practice, all resistivity surveys use at least two current electrodes – a positive current and a negative current source. For two current electrodes (Figure 3-4), the potential at a point is given by:

$$\phi = \rho\frac{I}{2\pi r_{c1}} - \rho\frac{I}{2\pi r_{c2}} = \rho\frac{I}{2\pi}\left[\frac{1}{r_{c1}} - \frac{1}{r_{c2}}\right] \tag{3-7}$$

where r_{c1} *and* r_{c2} are distances from the measurement point to electrodes c_1 and c_2.

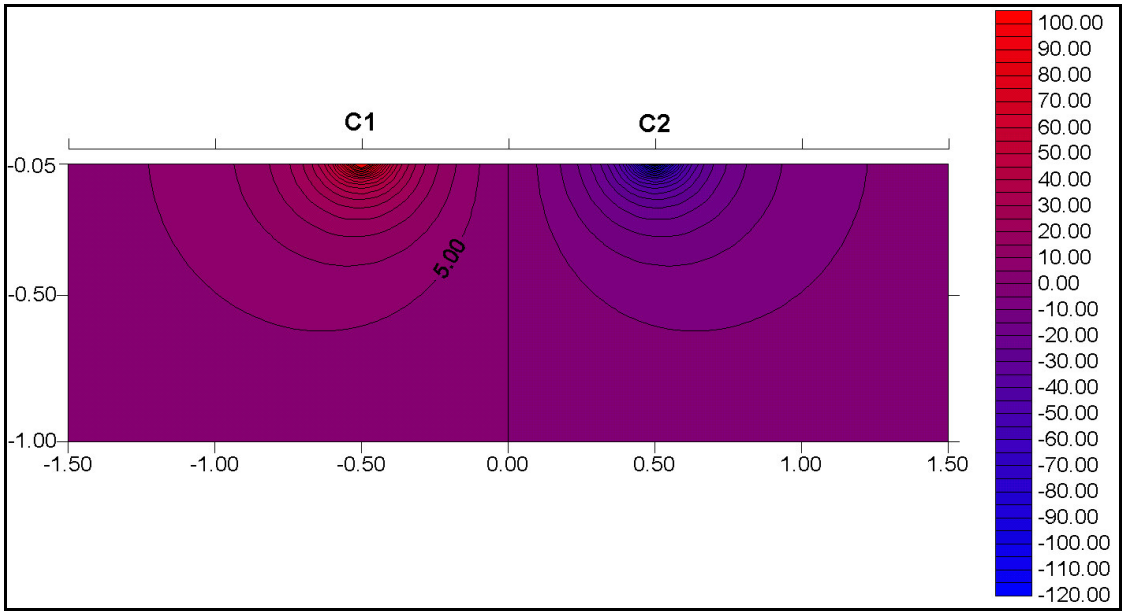

Figure 3-4: Potential distribution caused by a pair of current electrodes (Loke, 2012)

In practically all surveys, the potential difference between two points (normally on the ground surface) is measured. The resistivity measurements are normally made by injecting current into the ground through two current electrodes, C1 and C2, (Figure 3-5), and measuring the resulting voltage difference at two potential electrodes, P1 and P2.

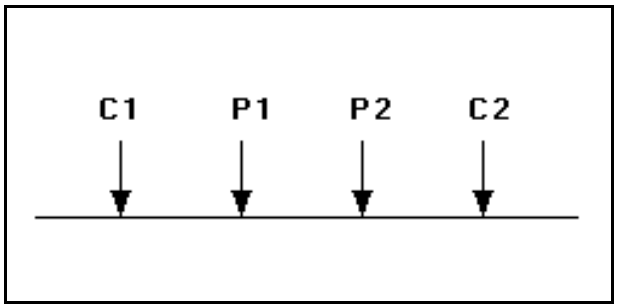

Figure 3-5: A conventional four electrode array

The potential difference is then given by:

$$V = \phi_{P1} - \phi_{P2} = \rho_a \frac{I}{2\pi}\left[\frac{1}{r_{c1P1}} - \frac{1}{r_{c2P1}} - \frac{1}{r_{c1P2}} + \frac{1}{r_{c2P2}}\right] \quad (3\text{-}8)$$

where ϕ_{P1} and ϕ_{P2} are the electrical potentials at P1 and P2 and r_{C1P1} is the distance between electrodes C1 and P1.

This Equation (3-8) gives the potential that would be measured over a homogeneous half-space with a four electrode arrays.

In the field, resistivity surveys are usually conducted over inhomogeneous mediums where the subsurface resistivity has a 3-D distribution. The resistivity measurements are still made by injecting a current into the ground through the two current electrodes C_1 and C_2 and measuring the voltage difference at two electrodes P_1 and P_2. From the current (I) and potential (V) values, an apparent resistivity (ρ_a) value is calculated by the Equation:

$$\rho_a = k\frac{V}{I}$$

$$\text{Where } k = \frac{2\pi}{\left[\frac{1}{r_{C_1P_1}} - \frac{1}{r_{C_2P_1}} - \frac{1}{r_{C_1P_2}} + \frac{1}{r_{C_2P_2}}\right]}$$

(3-9)

where k is a geometric factor that depends on the arrangement of the four electrodes.

Resistivity metres usually give a resistance value, $R=V/I$, so in practice the apparent resistivity value is calculated by:

$$\rho_a = kR$$

(3-10)

The calculated resistivity value is not the input resistivity of the subsurface, but an "apparent" value that is the resistivity of a homogeneous ground that will give the same resistance value for the same electrode arrangement. Determining the subsurface resistivity from the apparent resistivity values is an "inversion" problem (Loke, 2012).

3.1.2 Electrical properties of some Earth materials

Electrical properties of some rocks, soil and chemicals (Daniels and Alberty, 1966; Keller and Frischknecht, 1966; Telford *et al*., 1990) are shown in Table 3-1, where it can be seen that igneous and metamorphic rocks generally have high resistivity values. The resistivity of these rocks is greatly dependent on the degree of fracturing and the percentage of the fractures filled with groundwater. Thus a given rock type can have a large range of resistivity values spanning several orders of magnitude, depending on the degree of fracturing, weathering and water content. This characteristic is useful in the detection of fracture zones and other weathering features during engineering and groundwater surveys (Loke, 2012).

Table 3-1: Resistivities of some common rocks, minerals and chemicals (Loke, 1999)

Material	Resistivity (Ω.m)	Conductivity (Siemen/m)
Igneous and metamorphic rocks		
Granite	$5x10^{3}$ - 10^{6}	10^{-6} – $2x10^{-4}$
Basalt	10^{3} - 10^{6}	10^{-6} - 10^{-3}
Slate	$6x10^{2}$ – $4x10^{7}$	$2.5x10^{-8}$ - $1.7x10^{-3}$
Marble	10^{2} -$2.5x10^{8}$	$4x10^{-9}$ - 10^{-2}
Quartzite	10^{2} – $2x10^{8}$	$5x10^{-9}$ - 10^{-2}
Sedimentary Rocks		
Sandstone	8 – $4x10^{3}$	$2.5x10^{-4}$ - 0.125
Shale	20 – $2x10^{3}$	$5x10^{-4}$ - 0.05
Limestone	50 – $4x10^{2}$	$2.5x10^{-3}$ - 0.02
Soils and Waters		
Clay	1 - 100	0.01 - 1
Alluvium	10 - 800	$1.25x10^{-3}$ - 0.1
Groundwater (fresh)	10 - 100	0.01 - 0.1
Sea water	0 - 15	6.7
Chemicals		
Iron	$9.074x10^{-8}$	$1.102x10^{7}$
0.01 M Potassium chloride	0.708	1.413
0.01 M Sodium chloride	0.843	1.185
0.01 M acetic acid	6.13	0.163

3.1.3 2-D Electrical Resistivity Tomography

The resistivity method has been used since the 1920s due to the work of the Schlumberger brothers (Loke, 1999). Before the 1990s, surveys were normally carried out in a 1-D mode doing either profiling or VES. Conducting surveys in a 1-D mode had some limitations:

- During VES, the lateral changes in layer resistivities were not taken into account, which implied errors in interpreted layer resistivities and thicknesses.

- During profiling vertical changes in resistivity can go undetected.

Because of these limitations, a two-dimensional (2-D) survey was introduced in the 1990s. It yields a more accurate model of the subsurface, where the resistivity changes in both vertical and horizontal directions are estimated along a survey line. The ERT method is a technique in which many individual resistivities measured are combined to produce a 2-D resistivity cross-section or a 3-D resistivity model of the subsurface.

3.2 APPLICATIONS OF 2-D ERT METHOD

Electrical resistivity tomography has become one of the most significant geophysical techniques for investigating underground near-surface structures. It is a well-established tool for environmental, archaeological and engineering site investigation, and is routinely applied to:

- The mapping of freshwater aquifers and unconsolidated sediments (Acworth, 1987; Barker, 1996; Dahlin and Owen, 1998; Johansson and Dahlin, 1996),
- The detection of pollution (Daily *et al.,* 1998; Goes and Meekes, 2004),
- The characterization of geologic structures (Meads *et al.,* 2003),
- The characterization of engineered structures (Daily and Ramirez, 2000),
- Hydrogeological studies (Binley *et al.,* 2002; Sandberg *et al.,* 2002),
- Investigate building foundation site (Soupios *et al.,* 2007),
- Clarify the location of gold deposits (Park *et al.,* 2009),
- Archaeological investigations (El-Quady *et al.,* 2005; Ekinic and Kaya, 2007; Sultan *et al.,* 2006).

In order to resolve 2-D and 3-D ERT problem, several algorithms have been developed and are based on finite element, finite difference and integral methods (Dahlin and Bernstone, 1997; Dahlin and Loke, 1997; Loke and Barker, 1996; Spitzer, 1998; Tsourlos and Ogilvy, 1999; Zhao and Yedlin, 1996).

3.2.1 2-D ERT method for groundwater exploration

The electrical properties of many rocks are strongly influenced by their geohydrological characteristics, such as the nature and the amount of pore fluid, as well as the porosity of the fluid bearing material (Agramakova, 2005). As a result of this relation between the electrical properties and the geohydrological properties, the ERT method is well suited for groundwater exploration (Cassiani *et al.,* 2006; Daily *et al.,* 1992; Miller *et al.,* 2008). The ERT method can help to detect and delineate a productive aquifer and may also be used to evaluate the change in water content of the aquifer over a time interval when used in a time-lapse mode (Agramakova, 2005).

Case study: Time-Lapse ERT for groundwater investigation (Agramakova, 2005).

The study area is the island of Saint Lucia in the Caribbean Sea where the water demand was higher than the current supply due to the growth of the population as well as the seasonal variation in the amount of precipitation.

Geological studies of the area indicate the presence of tuffs lenses, and also lenses composed of the products of andesite weathering such as gravel and sandstones (which can be a good aquifer).

The resistivity survey was conducted during two periods: the dry and the wet season, in order to evaluate the potential and the feasibility of groundwater exploration. The first set of resistivity data was collected at the end of March, during the dry season. The preliminary interpretation of the data set indicated the existence of a possible aquifer just beneath the Thomazo River. For more accurate estimation, investigations of the same site during the rainy season was required and done in the middle of December.

The survey was performed along a profile of 100 m length. The resistivity line crosses the Thomazo River between 45 and 50 m from the origin of the line. The data were collected using the Dipole-Dipole array. In order to obtain good resolution at shallow depth, the unit electrode spacing was chosen to be equal to 5 m. To achieve larger depth of investigation, the unit electrode spacing was increased to 10 m.

Figure 3-6 shows the pseudo-sections of the apparent resistivities measured during the dry and wet seasons. The results of the inversion of each data set revealed a lens body of varying resistivity below the river from a depth of about 10 m, presumably overlain by a clay layer (Figure 3-7). As expected, the average resistivity of the lens decreased in the wet season. This result agrees with the consideration for the wet season when a larger amount of water is present in the lens. Based on the inversion results, the resistivity of the rock composing the potential aquifer is 150 Ω.m during the dry season and is 115 Ω.m during the wet season.

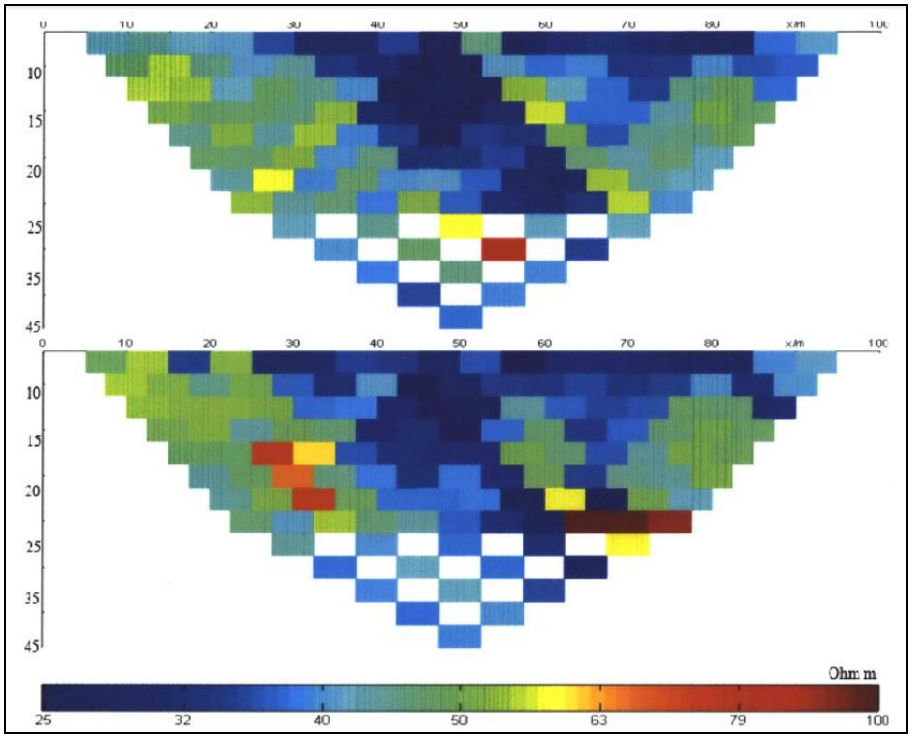

Figure 3-6: Apparent resistivities measured during dry (top) and wet (bottom) seasons (Agramakova, 2005)

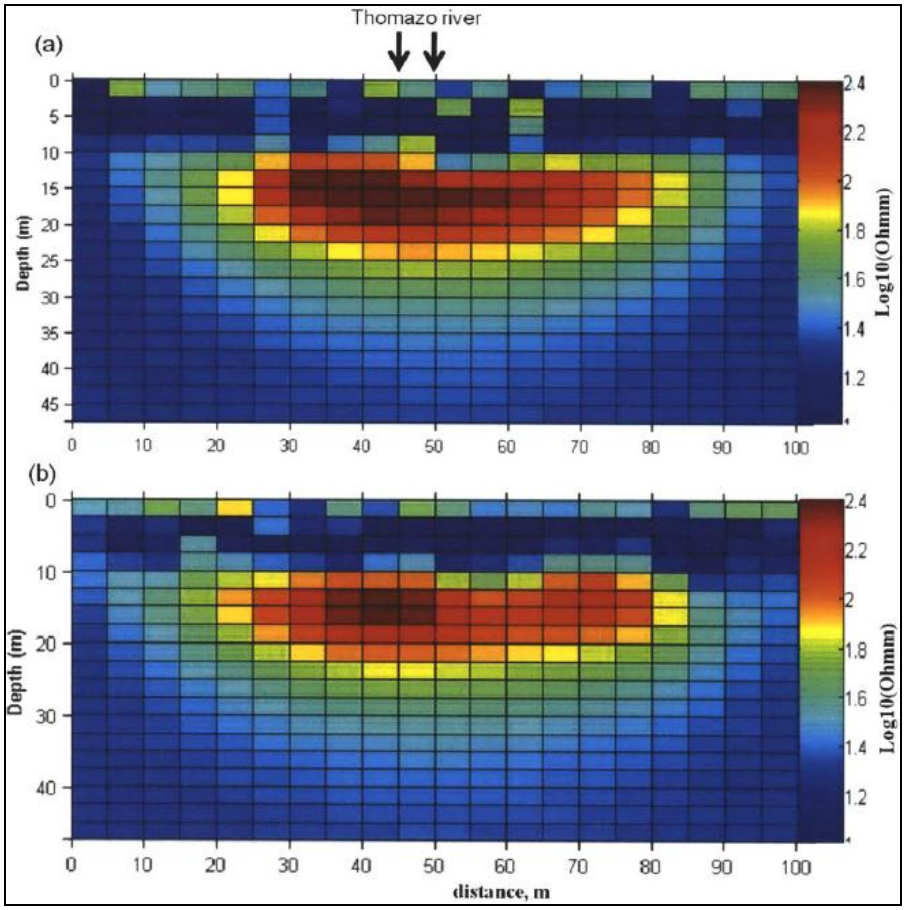

Figure 3-7: Results of the inversions for data set collected during dry and wet seasons (Agramakova, 2005)

The distribution of resistivity values corresponding to the subsurface layer of depth between 10 and 25 m reflects the overall decrease of resistivity of the aquifer during the wet season. It might imply that during the dry season, the aquifer contained less water than during the wet season.

The result of the inversion of the IP data indicates that the lens is not contaminated with clay; therefore the Archie's formula (Archie, 1942) can be applied to calculate the effective porosity of the aquifer.

$$\rho_e = \frac{a\rho w}{\varphi^m s_w^n} \tag{3-11}$$

where ρ_e is the resistivity of the rock and ρ_w the resistivity of water contained in the porous structure. The constant a varies between 0.5 and 2.5, depending on the m value and φ the effective porosity. The parameter s_w is the fraction of pores containing water and n the saturation exponent (ranging from 1.5 - 2.5, typically about 2.0 (Hallenburg, 1984)). The constant m is the cementation factor, which indicates the size of the pores, and has values ranging between 1.3 and 2.5.

The evaluation of the porosity with Archie's law, setting water resistivity equal to 40 Ω.m and bulk rock resistivity to 105 Ω.m, and assuming total saturation during the wet season and a cementation factor of 2, yields a porosity value of 59%. The high value of the porosity of the rock suggests that the aquifer is most likely composed of pumice whose porosity can be as high as 85%. Based on the results of the ERT survey, the thickness of the lens is 10 m, its width 35 m and its length 35 m. Therefore, the approximate volume of the potential aquifer is 12 250 m^3 which is equivalent to 12.25 x 10^6 L. Generally only about 40% of the groundwater can be extracted from an aquifer. The production of the aquifer (P) at the Thomazo River site during season may be estimated using Equation (3-12):

$$P = V\varphi E \tag{3-12}$$

where V is the volume of the aquifer (in litre) and E the groundwater extraction capacity as a percentage. The calculated production of the aquifer is 2.9 x 10^6 L. The time-lapse ERT interpretation showed that the change in groundwater content between dry and wet seasons is about 15%. During the dry season, the amount of groundwater would be 15% less compared to that during the wet season. It leads to the value of effective porosity of the aquifer equal to

50% in the dry season. Consequently, according to Equation (3-12), the estimated production of the aquifer during the dry season is 2.45 x 10^6 L.

It is important to mention that the above calculations do not take into account the groundwater recharge potential factor.

3.2.2 Time-lapse ERT measurements during a pumping test (Loke, 2012)

Resistivity imaging measurements were made during a pumping test in the Hoveringham area of East Central England where the aquifer is composed of sand and gravel layer overlying mudstone. Figure 3-8 (a) shows the initial apparent resistivity pseudo-section at the beginning of the test while the inverse model sections are shown in (b) at the beginning and (c) after 220 minutes of pumping.

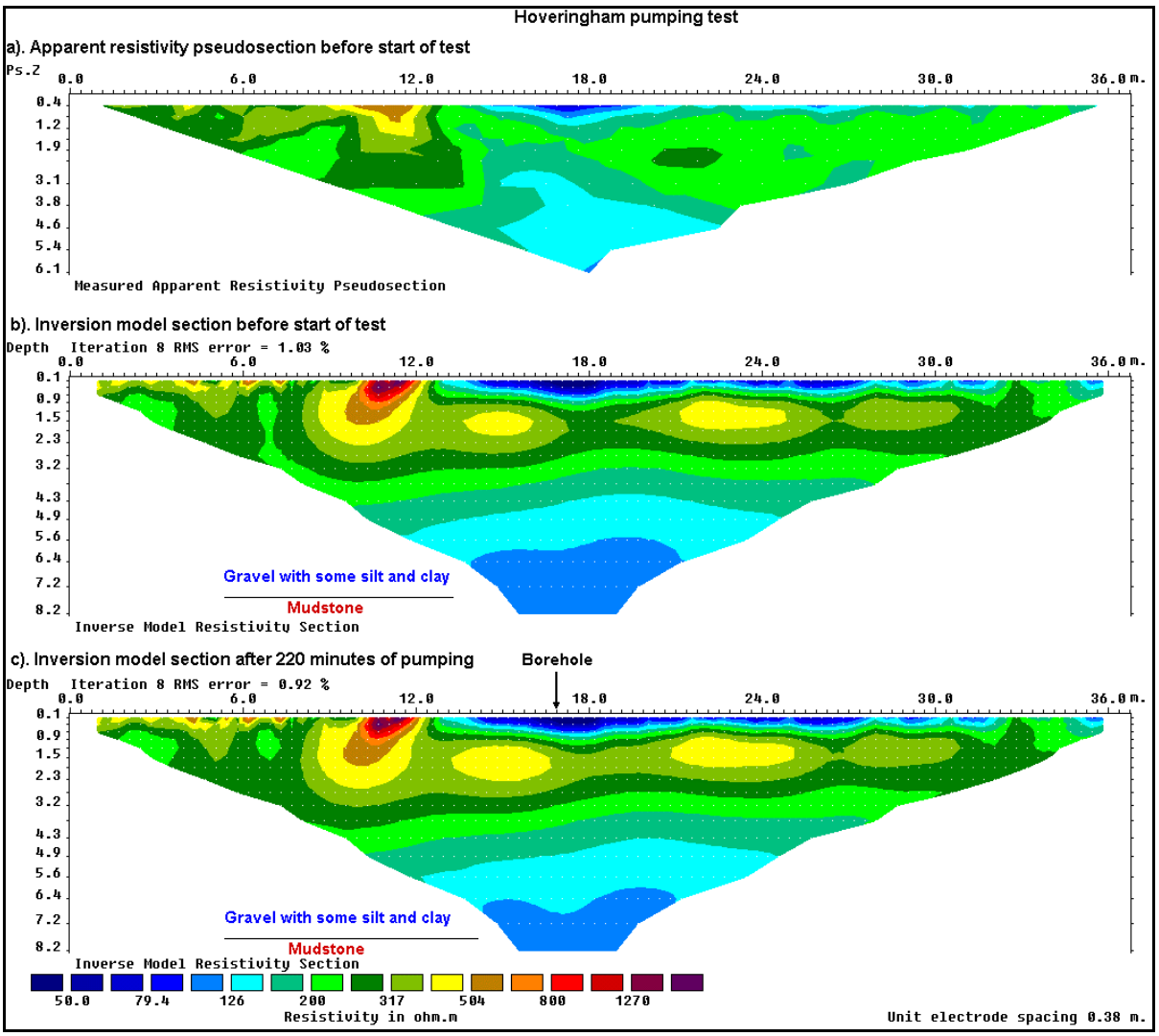

Figure 3-8: Pseudo-section and inverse model sections for a pumping test (Loke, 2012)

Figure 3-9 shows the relative change in the resistivity at 40, 120 and 220 minutes after the start of the pumping test. To highlight the changes in the subsurface resistivity, the changes in the model resistivity are shown and one can easily notice the increase in the model resistivity below the borehole with time. The figure clearly shows the increase in the zone with higher resistivity values with time due to the extraction of the water. By using Archie's Law, and assuming the water resistivity does not change with time, we can estimate the change in the water saturation values. The decrease in the water saturation level within the aquifer, or desaturation values, is shown in Figure 3-10. As Archie's Law assumes that the conduction is due to the water content alone, the desaturation values are likely to be lower than the true values if there is significant clay content. Archie's Law probably gives a lower limit for the actual change in the aquifer saturation.

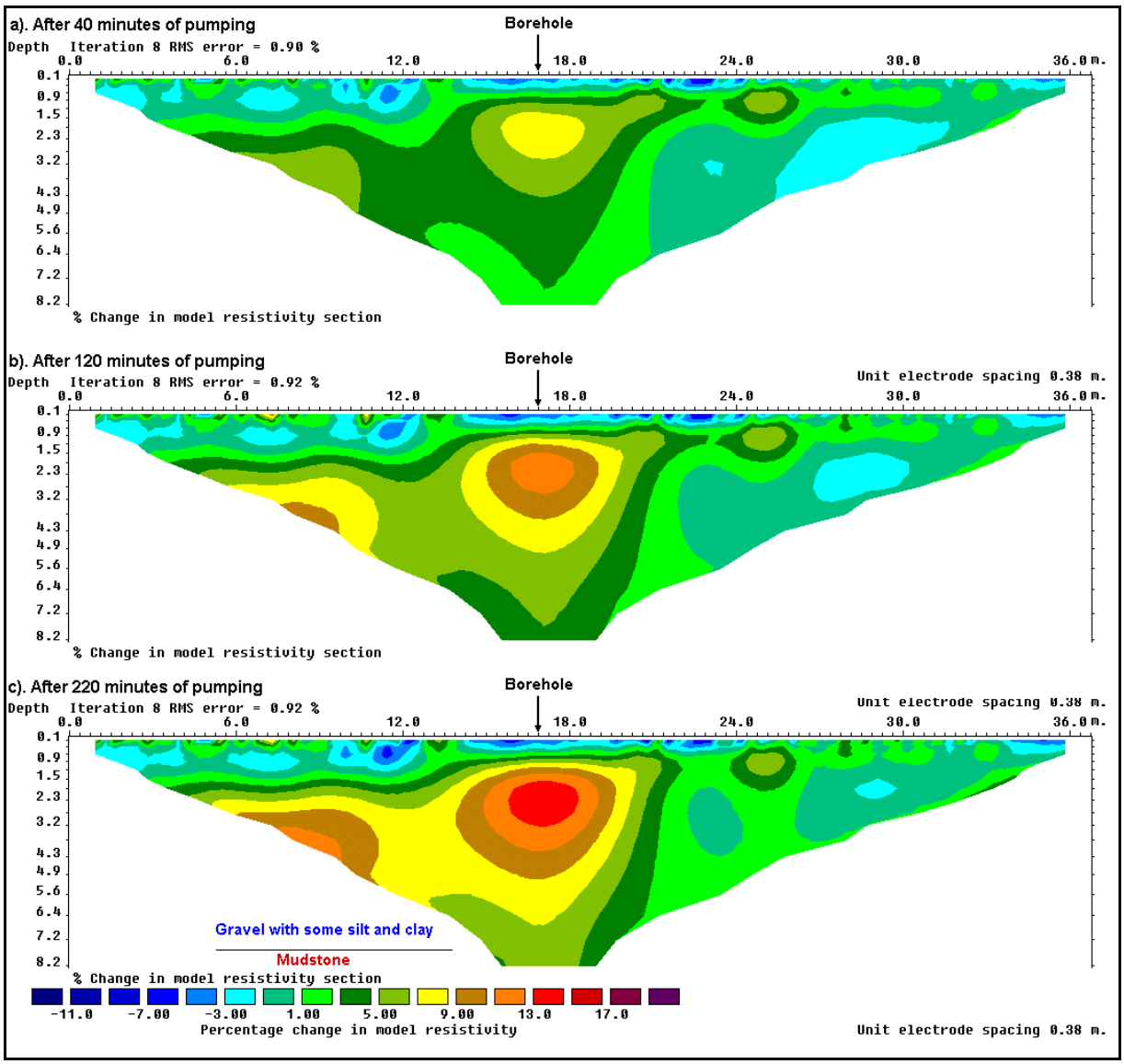

Figure 3-9: Percentage relative change in the subsurface resistivity values (Loke, 2012)

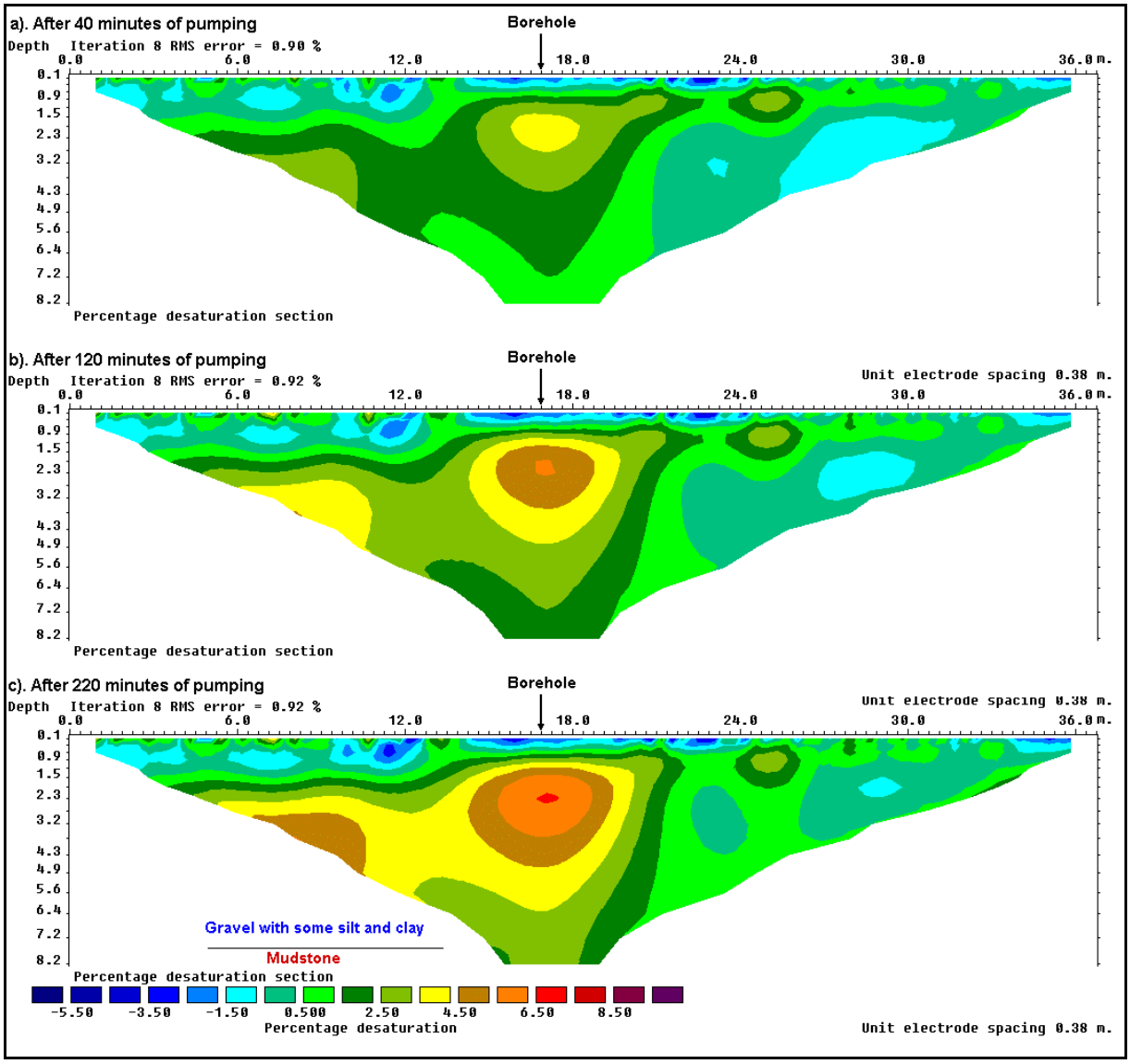

Figure 3-10: Use of Archie's Law for the Hoveringham pumping test (Loke, 2012)

4 SOME CHARACTERISTICS OF ELECTRODE ARRAYS

It was seen in Chapter 3 that resistivity measurements are made by injecting electrical current into the ground through two current electrodes, and measuring the resulting electrical potential difference at two potential electrodes. The arrangement of these electrodes for resistivity surveys is not always the same: sometimes the two potential electrodes are placed between the two current electrodes, other times they are placed outside or apart from the two current electrodes. Also, the distance (electrode spacing) between the four electrodes or each pair of electrodes is not always the same.

It is therefore the arrangement of these current electrodes and potential electrodes which implies different types of electrode arrays and consequently different sensitivities, different depths of investigation, different resolutions, different horizontal data coverage and different signals strengths.

The encyclopaedia dictionary (www.encyclopedia.com) defines an electrode configuration (electrode array) as a geometrical pattern of electrodes used in electrical sounding, constant-separation traversing, and induced polarization (IP) surveys. In other words, an electrode array is a configuration of electrodes used for measuring either an electrical current or a voltage.

Some arrays are more sensitive to vertical structures in the subsurface, and they might be appropriate or not to be used in areas with high background noise level, while other arrays are rather more sensitive to horizontal structures. Several electrode arrays are known in the application of the resistivity method. These arrays include the Wenner (alpha, beta, gamma, half), Wenner-Schlumberger, Schlumberger, Dipole-Dipole (equatorial, inline), Pole-Pole, Pole-Dipole (offset, forward, reverse), Pole-Bipole, Gamma, Gradient, and Midpoint-Potential-Referred arrays. In practice the arrays that are most commonly used for 2-D ERT surveys are the Wenner, the Dipole-Dipole, the Wenner-Schlumberger, the Schlumberger, the Pole-Pole and the Pole-Dipole arrays. Figure 4-1 displays the arrangement of some these arrays with their geometric factors.

Because the shape of the contours in the pseudo-section produced by different electrode arrays over the same structure can be very different, it is advantageous, before carrying out any survey, to know the type of structure to be mapped, the sensitivity of the resistivity meter, as well as the background noise level, in order to have a good understanding on the choice of the "best" electrode array for that particular field survey.

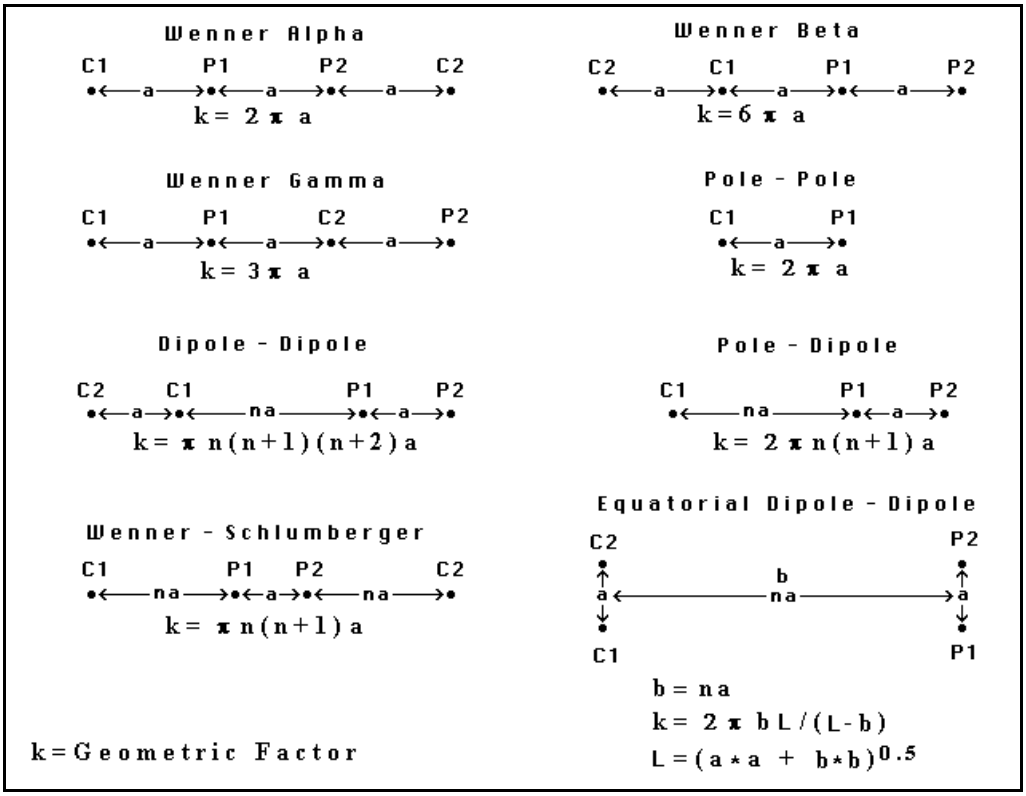

Figure 4-1: Common arrays used in resistivity surveys (Loke, 1999)

Each electrode array has its advantages and disadvantages, in terms of: the sensitivity of the array to vertical and horizontal changes in the subsurface resistivity, the depth of investigation, the horizontal data coverage and the signal strength (Loke, 1999).

The depth of investigation and the sensitivity of the array to vertical and horizontal changes are two characteristics that can be determined from the sensitivity function of the array for a homogeneous earth model. In Figure 4-2 for instance, a plot of the sensitivity function for the Wenner, Schlumberger and Dipole-Dipole arrays, applied to a homogeneous half-space, is shown. The sensitivity function shows the degree to which the change in the resistivity of a section of the subsurface will influence the electrical potential measured by the array (Loke, 1999). The higher the value of the sensitivity function, the greater is the influence of the section on the measurement.

It is seen (Figure 4-2) that the highest sensitivity values are near the electrodes for all three arrays. At larger distances from the electrodes, the shapes of the contours differ for the three arrays. The differences in the contour shapes of the sensitivity function plots explain the different responses of the arrays to different types of structures in terms of vertical and horizontal changes in the resistivities and the depth of investigation.

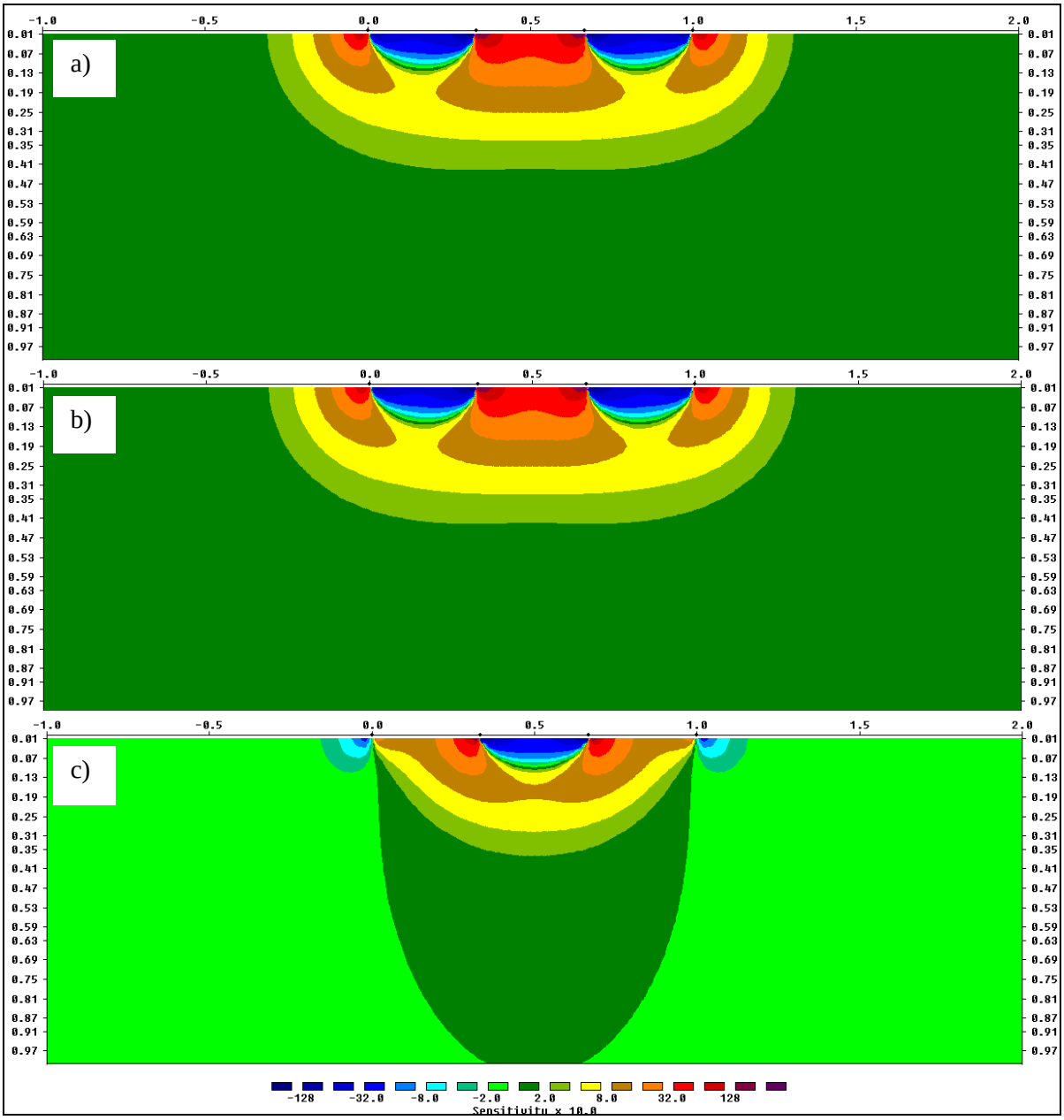

Figure 4-2: Sensitivity patterns for the (a) Wenner (b) Wenner-Schlumberger and (c) Dipole-Dipole arrays

4.1 THE SENSITIVITY FUNCTION

Mathematically, the sensitivity function for a homogenous half-space is given by the Frechet derivative (McGillivray and Oldenburg, 1990). Consider the collinear array configuration shown in Figure 4-3 with two current electrodes located at $A(x_A, y_A, z_A)$ and $B(x_B, y_B, z_B)$, and two potential electrodes located at $M(x_M, y_M, z_M)$ and $N(x_N, y_N, z_N)$. A current of 1 Ampere is injected into the ground through the current electrodes A and B. The resulting electrical potentials at electrodes M and N are Φ_M and Φ_N with a corresponding voltage $V = \Phi_M - \Phi_N$.

Suppose the resistivity of a volume of subsurface material, located at $d\tau(x,y,z)$ is changed by a small amount, $\delta\rho$. The corresponding changes in the potential, $\delta\Phi$, at the position of the volume element may be calculated by incorporating information on the distances to the different electrodes. In Figure 4-3 it is seen that the distances between the subsurface volume element and the surface electrodes may be calculated from:

$$r_A = [(x - x_A)^2 + (y - y_A)^2 + (z - z_A)^2]^{1/2}; \qquad r_M = [(x - x_M)^2 + (y - y_M)^2 + (z - z_M)^2]^{1/2}$$

$$r_N = [(x - x_N)^2 + (y - y_N)^2 + (z - z_N)^2]^{1/2}; \qquad r_B = [(x - x_B)^2 + (y - y_B)^2 + (z - z_B)^2]^{\frac{1}{2}}$$

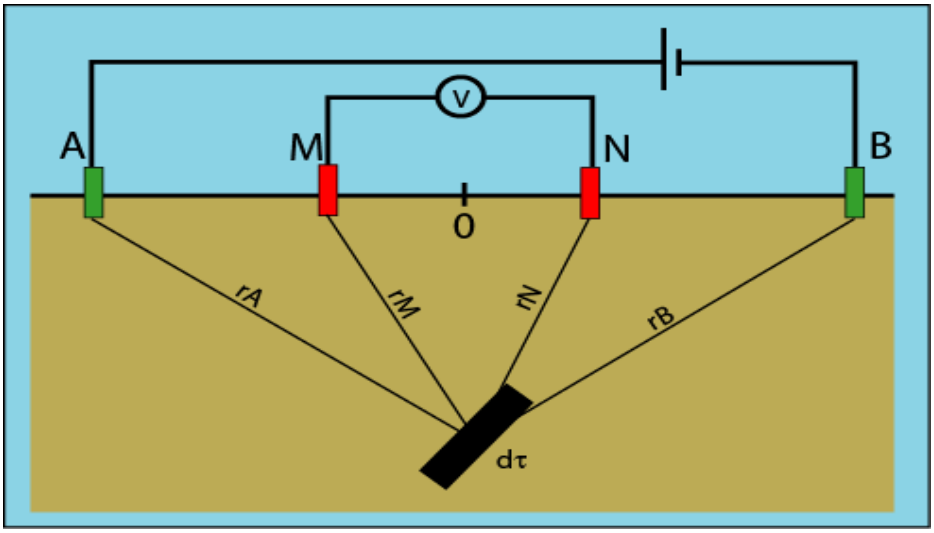

Figure 4-3: Sensitivity function calculation at a point dτ(x,y,z) within a half-space

From Equation (3-6), the electrical potential at the volume element due to the injection of electrical current (*I*) at electrodes A and B may be calculated as:

$$\Phi_A = \frac{\rho I}{2\pi r_A};\ \Phi_B = \frac{\rho I}{2\pi r_B}$$

It can be shown that the change in the electrical potential, $\delta\Phi$, due to a change, $\delta\rho$, in the resistivity of the volume element is given by:

$$\delta\Phi = \frac{\delta\rho}{\rho^2}\int_V [\nabla\Phi_A.\nabla\Phi_M + \nabla\Phi_A.\nabla\Phi_N + \nabla\Phi_B.\nabla\Phi_M + \nabla\Phi_B.\nabla\Phi_N]dxdydz \quad (4\text{-}1)$$

or

$$\frac{\delta\Phi}{\delta\rho} = \frac{1}{\rho^2}\int_V [\nabla\Phi_A.\nabla\Phi_M + \nabla\Phi_A.\nabla\Phi_N + \nabla\Phi_B.\nabla\Phi_M + \nabla\Phi_B.\nabla\Phi_N]dxdydz \quad (4\text{-}2)$$

with

$$\nabla\Phi_A.\nabla\Phi_N = \frac{\rho^2}{4\pi^2}\left[\frac{(x-x_A)(x-x_N)+(y-y_A)(y-y_N)+(z-z_A)(z-z_N)}{(r_A r_N)^3}\right] \quad (4\text{-}3)$$

$$\nabla\Phi_A.\nabla\Phi_M = \frac{\rho^2}{4\pi^2}\left[\frac{(x-x_A)(x-x_M)+(y-y_A)(y-y_M)+(z-z_A)(z-z_M)}{(r_A r_M)^3}\right] \quad (4\text{-}4)$$

$$\nabla\Phi_B.\nabla\Phi_N = \frac{\rho^2}{4\pi^2}\left[\frac{(x-x_B)(x-x_N)+(y-y_B)(y-y_N)+(z-z_B)(z-z_N)}{(r_B r_N)^3}\right] \quad (4\text{-}5)$$

$$\nabla\Phi_B.\nabla\Phi_M = \frac{\rho^2}{4\pi^2}\left[\frac{(x-x_B)(x-x_M)+(y-y_B)(y-y_M)+(z-z_B)(z-z_M)}{(r_B r_M)^3}\right] \quad (4\text{-}6)$$

The terms Φ_M and Φ_N from Equation (4-1) to Equation (4-6) are defined as

$$\Phi_M = \frac{\rho I}{2\pi r_M};\ \Phi_N = \frac{\rho I}{2\pi r_N}$$

Equation (4-2) reduces to:

$$\frac{\delta\Phi}{\sigma\rho} = \int_V \frac{1}{4\pi^2}\left[\frac{(x-x_A)(x-x_N)+(y-y_A)(y-y_N)+(z-z_A)(z-z_N)}{(r_A r_N)^3} + \frac{(x-x_A)(x-x_M)+(y-y_A)(y-y_M)+(z-z_A)(z-z_M)}{(r_A r_M)^3} + \frac{(x-x_B)(x-x_N)+(y-y_B)(y-y_N)+(z-z_B)(z-z_N)}{(r_B r_N)^3} + \frac{(x-x_B)(x-x_M)+(y-y_B)(y-y_M)+(z-z_B)(z-z_M)}{(r_B r_M)^3}\right] dxdydz \quad (4\text{-}7)$$

The 3-D Frechet derivative is then given by the integrand of Equation (4-7), namely:

$$F_{3D}(x,y,z) = \frac{1}{4\pi^2}\left[\frac{(x-x_A)(x-x_N)+(y-y_A)(y-y_N)+(z-z_A)(z-z_N)}{(r_A r_N)^3} + \frac{(x-x_B)(x-x_N)+(y-y_B)(y-y_N)+(z-z_B)(z-z_N)}{(r_B r_N)^3} + \frac{(x-x_A)(x-x_M)+(y-y_A)(y-y_M)+(z-z_A)(z-z_M)}{(r_A r_M)^3} + \frac{(x-x_B)(x-x_M)+(y-y_B)(y-y_M)+(z-z_B)(z-z_M)}{(r_B r_M)^3}\right] \quad (4\text{-}8)$$

Equation (4-8) gives the 3-D Frechet derivative or the general sensitivity function for all four-electrode arrays consisting of two current electrodes and two potential electrodes. Three- and two-electrode arrays are special cases for which the 3-D Frechet derivative may be calculated by setting certain terms in Equation (4-8) to zero.

4.2 THE DEPTH OF INVESTIGATION

It is well known in resistivity sounding surveys that the depth of investigation increases when the separation between the electrodes is increased (Loke, 2012). The depth of investigation in a homogeneous half-space can be obtained mathematically by deriving the sensitivity function formula or the Frechet derivative of the array. For example, the Frechet derivative for the Pole-Pole array, calculated by Loke (2012), can be written:

$$F_{3D}(x,y,z) = \frac{1}{4\pi^2}\cdot\frac{x(x-a)+y^2+z^2}{\left[x^2+y^2+z^2\right]^{1.5}\left[(x-a)^2+y^2+z^2\right]^{1.5}} \quad (4\text{-}9)$$

If the subsurface is assumed to consist of horizontal layers, each with different resistivities, the change in the potential measured by the array on the surface can be determined. For a horizontal layer, the *x* and *y* limits of the layer extends from -∞ to +∞. Thus the sensitivity function for a thin horizontal layer is obtained by integrating the 3-D sensitivity function in the *x* and *y* directions:

$$F_{1D}(z) = \frac{1}{4\pi^2} \int_{-\infty}^{+\infty} \int_{-\infty}^{+\infty} \frac{x(x-a) + y^2 + z^2}{[x^2 + y^2 + z^2]^{1.5}\,[(x-a)^2 + y^2 + z^2]^{1.5}} dxdy$$

(4-10)

Equation (4-10) has a simple analytical solution (Roy and Apparao, 1971), which is given by:

$$F_{1D}(z) = \frac{2}{\pi} \cdot \frac{z}{\left(a^2 + 4z^2\right)^{1.5}}$$

(4-11)

Equation (4-11) is the depth of investigation formula. It has been used by several authors to determine the properties of various arrays in resistivity sounding surveys (Barker, 1991; Edwards, 1977; Merrick, 1997). The depth of investigation does not depend on the measured apparent resistivity or the resistivity of the homogeneous earth model (Loke, 1999). Also, if there are large resistivity contrasts near the surface, the actual depth of investigation could be somewhat different.

The median depth of investigation for the different arrays can be observed in Table 4-1. The median depth of investigation of an electrode array, gives an idea of the depth to which subsurface structures might be mapped with that particular array. The median depth values are determined by integrating the sensitivity function with depth. In other words, the upper section of the Earth above the median depth of investigation has the same influence on the measured potential as the lower section. This shows how deep subsurface structures can be seen with an array. These depths are only valid for a homogeneous Earth model; however, they are sufficient for planning field surveys (Loke, 1999). In Table 4-1, for the Dipole-Dipole array, the Wenner-Schlumberger and the Pole-Dipole arrays, the median depth of investigation increases when the "n" factor is increased.

Numbers in brackets indicate signal-to-noise ratio of each array. This will be discussed later in the current chapter.

One of the goals of the present research being to define the contact zones between the vertical/horizontal structures (such as dykes and sills) and their hosts, the choice of the appropriate electrode arrays which will respond the best to the target material, is consequently based on their sensitivity to vertical/lateral subsurface resistivity changes. Only the most commonly used electrodes arrays are the subject of this study, namely the Wenner array, the Schlumberger array, the Dipole-Dipole array and the Pole-Pole array.

Table 4-1: The median depth of investigation (Ze) for the different arrays (Edwards, 1977)

Array type	Ze/a	Ze/L	Geometric Factor	Inverse Geometric Factor (Ratio)
Wenner Alpha	0.52	0.17	6.2832	0.15915 (1.0000)
Wenner Beta	0.42	0.14	18.85	0.05305 (0.3333)
Wenner Gamma	0.59	0.2	9.4248	0.10610 (0.6667)
Dipole-dipole n = 1	0.42	0.14	18.85	0.05305 (0.3333)
n = 2	0.7	0.17	75.398	0.01326 (0.0833)
n = 3	0.96	0.19	188.5	0.00531 (0.0333)
n = 4	1.22	0.2	376.99	0.00265 (0.0166)
n = 5	1.48	0.21	659.73	0.00152 (0.0096)
n = 6	1.73	0.22	1055.6	0.00095 (0.0060)
n = 7	1.98	0.22	1583.4	0.00063 (0.0040)
n = 8	2.24	0.22	2261.9	0.00044 (0.0028)
Equatorial dipole-dipole				
n = 1	0.45	0.32	21.452	0.04662 (0.2929)
n = 2	0.81	0.36	119.03	0.00840 (0.0528)
n = 3	1.18	0.37	367.31	0.00272 (0.0171)
n = 4	1.56	0.38	841.75	0.00119 (0.0075)
Wenner - Schlumberger				
n = 1	0.52	0.17	6.2832	0.15915 (1.0000)
n = 2	0.93	0.19	18.85	0.05305 (0.3333)
n = 3	1.32	0.19	37.699	0.02653 (0.1667)
n = 4	1.71	0.19	62.832	0.01592 (0.1000)
n = 5	2.09	0.19	94.248	0.01061 (0.0667)
n = 6	2.48	0.19	131.95	0.00758 (0.0476)
n = 7	2.86	0.19	175.93	0.00568 (0.0357)
n = 8	3.25	0.19	226.19	0.00442 (0.0278)
n = 9	3.63	0.19	282.74	0.00354 (0.0222)
n = 10	4.02	0.19	345.58	0.00289 (0.0182)
Pole-dipole n = 1	0.52		12.566	0.07958 (0.5000)
n = 2	0.93		37.699	0.02653 (0.1667)
n = 3	1.32		75.398	0.01326 (0.0833)
n = 4	1.71		125.66	0.00796 (0.0500)
n = 5	2.09		188.5	0.00531 (0.0334)
n = 6	2.48		263.89	0.00379 (0.0238)
n = 7	2.86		351.86	0.00284 (0.0178)
n = 8	3.25		452.39	0.00221 (0.0139)
Pole-Pole	0.87		6.28319	0.15915 (1.0000)

4.3 MEASUREMENT PROPERTIES OF THE WENNER ARRAY

The Wenner array, the most commonly used in resistivity is an array which was popularised by the pioneering works of the research group of The University of Birmingham (Griffiths and Turnbull, 1985; Griffiths *et al.*, 1990). Many of the early 2-D surveys were carried out with this array (Loke, 1999).

The array consists of four electrodes: two current electrodes A and B, and two potential electrodes M and N (Figure 4-4). These electrodes are equally spaced along a survey line and the distance between adjacent electrodes is called the array spacing, "a".

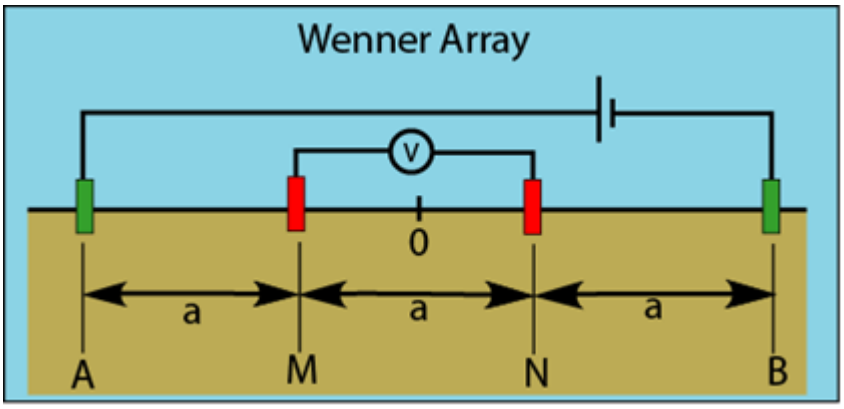

Figure 4-4: The geometry of the Wenner array

Considerer the configuration in Figure 4-4, with two current electrodes and two potential electrodes, located at:

$$A\left(\frac{-3a}{2},0,0\right); \qquad M\left(\frac{-a}{2},0,0\right); \qquad N\left(\frac{a}{2},0,0\right); \qquad B\left(\frac{3a}{2},0,0\right);$$

This means all four electrodes are on the ground surface and they are "a" distance units apart. A current of 1 ampere is injected into the ground through A and B, which results in a potential measured at M and N.

The sensitivity function for the Wenner array is given by:

$$F_{3D}(x,y,z) = \frac{1}{4\pi^2}\left[\frac{\left(x+\frac{3a}{2}\right)\left(x-\frac{a}{2}\right)+y^2+z^2}{(r_A r_N)^3} + \frac{\left(x+\frac{3a}{2}\right)\left(x+\frac{a}{2}\right)+y^2+z^2}{(r_A r_M)^3} + \frac{\left(x-\frac{3a}{2}\right)\left(x-\frac{a}{2}\right)+y^2+z^2}{(r_B r_N)^3} + \frac{\left(x-\frac{3a}{2}\right)\left(x+\frac{a}{2}\right)+y^2+z^2}{(r_B r_M)^3}\right] \quad (4\text{-}12)$$

The Wenner array has three different arrangements: Wenner-α, Wenner-β and Wenner-γ. However, the Wenner-α is considered to be the standard Wenner array (Carpenter and Habberjam, 1956). The electrode arrangements of the Wenner-α, Wenner-β and Wenner-γ configurations are shown in Figure 4-1. The Wenner Beta array is in fact a special case of the Dipole-Dipole array where the spacings between the electrodes are the same.

Figure 4-5 displays the 2-D sensitivity sections for the Wenner array. It can be seen that the sensitivity plot for the Wenner array has almost horizontal contours beneath the centre of the array. Because of this property of the sensitivity function, the Wenner array is relatively sensitive to vertical changes in the subsurface resistivity below the centre of the array. However, it is less sensitive to horizontal changes in the subsurface resistivity. In the other words, it provides good vertical resolution for horizontal structures. In general, the Wenner array is good in resolving vertical changes (horizontal structures), but relatively poor in detecting horizontal changes, in other words, narrow vertical structures (Loke, 1999).

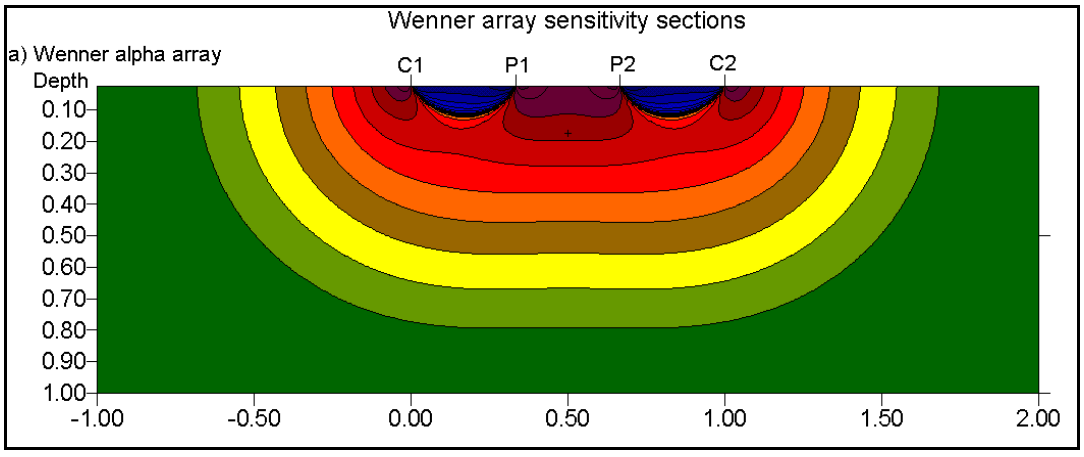

Figure 4-5: 2-D sensitivity sections for the Wenner array (Loke, 2012)

The median depth of investigation for the Wenner array is approximately 0.5 times the "a" spacing used (Table 4-1). It has a moderate depth of investigation, compared to other arrays.

Its signal strength is inversely proportional to its geometric factor "k = 2πa". This factor is smaller than the geometric factor for other arrays. However the Wenner array has the strongest signal strength, which is an important factor for surveys carried in areas with high background noise. The relatively poor horizontal coverage is one drawback of this array for 2-D surveys even when the electrode spacing is increased. This might be a problem when a system with a relatively small number of electrodes is used (Loke, 2012).

4.4 MEASUREMENT PROPERTIES OF THE DIPOLE-DIPOLE ARRAY

The Dipole-Dipole array is widely used in 2-D ERT surveys. The arrangement of the electrodes for this array is shown in Figure 4-1. The spacing between the current electrodes pair, AB, is given as "a" which is the same as the distance between the potential electrodes pair MN, "na" is the distance between the A and M electrodes.

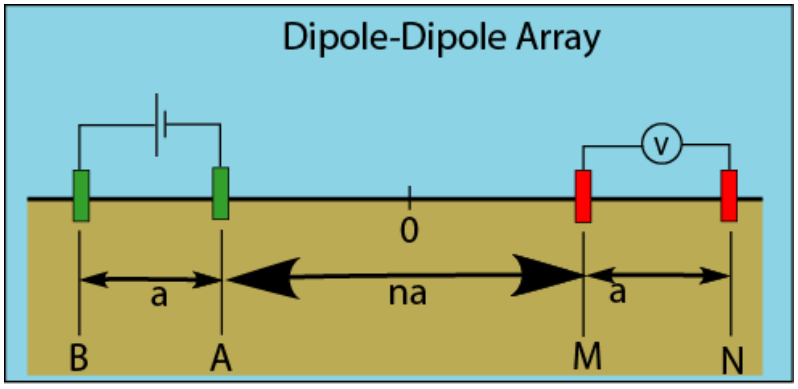

Figure 4-6: The geometry of the Dipole-Dipole array

With the origin of the coordinate system chosen at the centre of the configuration as shown in Figure 4-6 the positions of the four electrodes are:

$$A\left(\frac{-2a-na}{2},0,0\right);\qquad M\left(\frac{-na}{2},0,0\right);\qquad N\left(\frac{na}{2},0,0\right);\qquad B\left(\frac{2a+na}{2},0,0\right);$$

The sensitivity function for the Dipole-Dipole array is given by the Equation (4-13):

$$F_{3D}(x,y,z)=\frac{1}{4\pi^2}\left[\frac{\left(x+\frac{2a+na}{2}\right)\left(x-\frac{na}{2}\right)+y^2+z^2}{(r_A r_N)^3}+\frac{\left(x+\frac{2a+na}{2}\right)\left(x+\frac{na}{2}\right)+y^2+z^2}{(r_A r_M)^3}\right.$$
$$\left.+\frac{\left(x-\frac{2a+na}{2}\right)\left(x-\frac{na}{2}\right)+y^2+z^2}{(r_B r_N)^3}+\frac{\left(x-\frac{2a+na}{2}\right)\left(x+\frac{na}{2}\right)+y^2+z^2}{(r_B r_M)^3}\right] \quad (4\text{-}13)$$

Plots of the sensitivity function for the Dipole-Dipole array for "n" values ranging from 1 to 6 are displayed on Figure 4-7. It is noticed that the largest sensitivity values are located between C2-C1 and between P1-P2. This signifies that this array is most sensitive to resistivity changes below the electrodes in each dipole pair (Loke, 2012). The high sensitivity values become increasingly more concentrated beneath C1-C2 and P1-P2 electrodes, as the "n" factor is increased, while the sensitivity values beneath the centre of the array (between C1-P1) decreases. It is seen that the sensitivity values in pseudo-section becomes smaller for "n" values greater than 2. Near the electrodes the sensitivity contour pattern becomes almost vertical for "n" values greater than 2. The Dipole-Dipole array is therefore very sensitive to horizontal changes in resistivity, but relatively insensitive to vertical changes in the resistivity. That means this array is good in mapping vertical structures, such as dykes and cavities, but relatively poor in mapping horizontal structures such as sills or sedimentary layers (Loke, 2012). In the other words, the Dipole-Dipole array produces poorer vertical resolution but has better lateral resolution.

Generally the Dipole-Dipole array has a relatively high anomaly effects, yet more risk of noise contamination than other arrays (Table 4-1). It consequently produces low signal-ratio in surveys. It has symmetric electrode configurations for normal and reciprocal measurements. This facilitates the data quality control so as to obtain a reliable and good resolution image of the survey. However, its imaging resolution is comparable to Pole-Dipole array and better than others, particularly for the location of vertical and dipping structures whereas the depth resolution is not the best (Dahlin and Zhou, 2004). The Dipole-Dipole array is much more sensitive to the spacing errors (Zhou and Dahlin, 2003) and 3-D geological bodies than other arrays (Dahlin and Loke, 1997).

The median depth of investigation of the Dipole-Dipole array depends on both the "a" spacing and the "n" factor (Table 4-1). For example at n=1 the depth of investigation is 0.416 x a. For 2-D surveys, this array has better horizontal data coverage than the Wenner array. This array has been successfully used in many areas to detect structures such as cavities where the good horizontal resolution of this array is a major advantage.

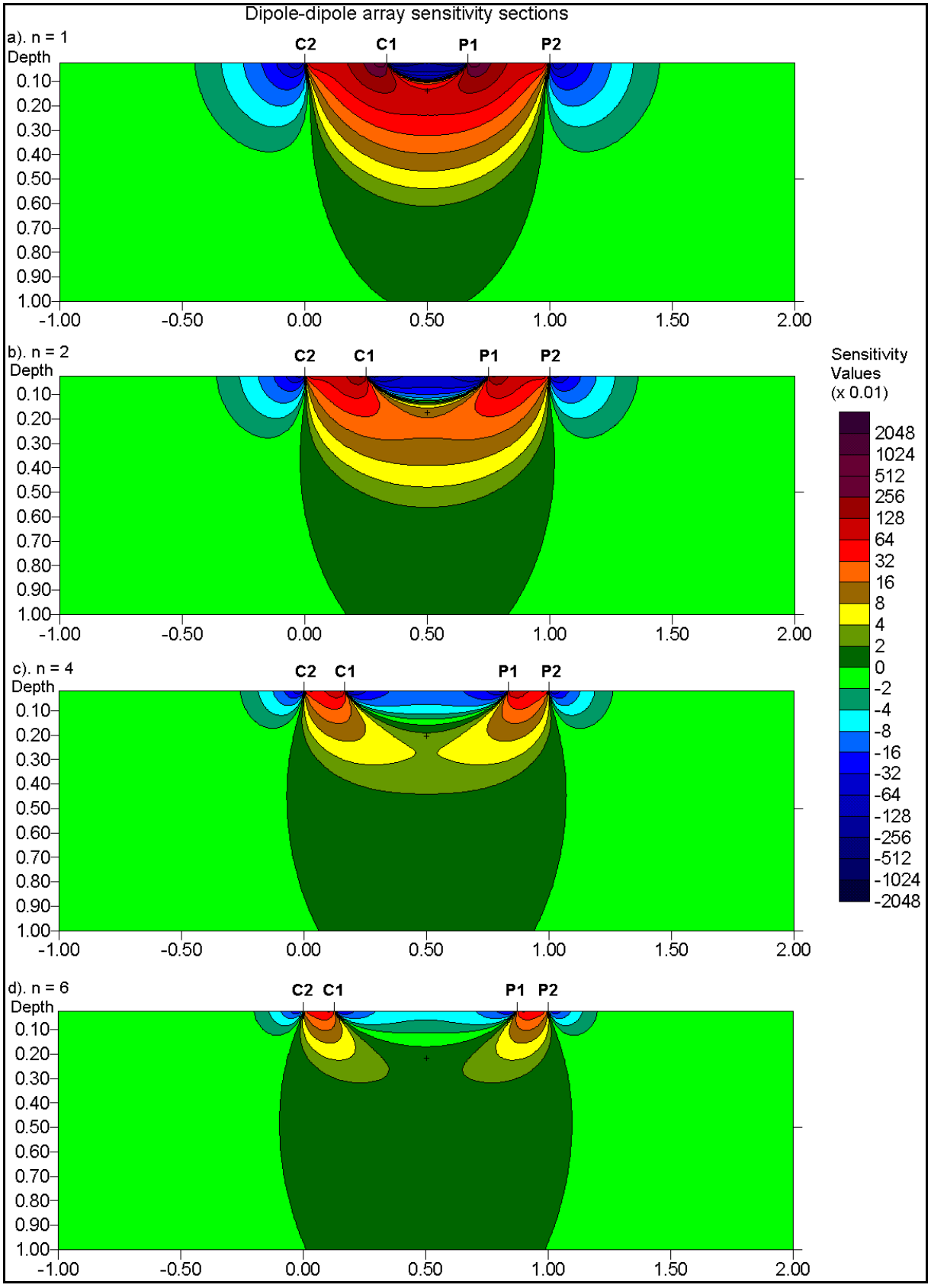

Figure 4-7: The 2-D sensitivity sections for the Dipole-Dipole array (Loke, 2012)

4.5 MEASUREMENT PROPERTIES OF THE WENNER-SCHLUMBERGER ARRAY

This array, one of the important used in 2-D ERT surveys, is a combination of the Wenner and Schlumberger configurations (Pazdirek and Blaha, 1996). The arrangements of electrodes are shown in Figure 4-1. It is seen that the Wenner array is a special case for this array where the "n" factor is equal to 1.

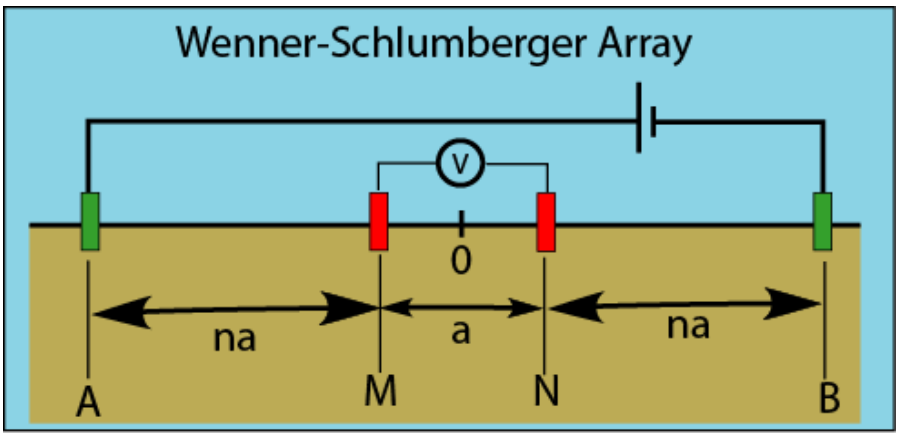

Figure 4-8: The geometry of the Wenner-Schlumberger array

With the origin of the coordinate system chosen at the centre of the configuration as shown in Figure 4-8, the positions of the four electrodes are:

$$A\left(\frac{-2na-a}{2},0,0\right); \qquad M\left(\frac{-a}{2},0,0\right); \qquad N\left(\frac{a}{2},0,0\right); \qquad B\left(\frac{2na+a}{2},0,0\right);$$

The sensitivity function of the Wenner-Schlumberger array is given by the Equation (4-14):

$$F_{3D}(x,y,z) = \frac{1}{4\pi^2}\left[\frac{\left(x+\frac{2na+a}{2}\right)\left(x-\frac{a}{2}\right)+y^2+z^2}{(r_A r_N)^3}+\frac{\left(x+\frac{2na+a}{2}\right)\left(x+\frac{a}{2}\right)+y^2+z^2}{(r_A r_M)^3}\right.$$
$$\left.+\frac{\left(x-\frac{2na+a}{2}\right)\left(x-\frac{a}{2}\right)+y^2+z^2}{(r_B r_N)^3}+\frac{\left(x-\frac{2na+a}{2}\right)\left(x+\frac{a}{2}\right)+y^2+z^2}{(r_B r_M)^3}\right] \tag{4-14}$$

The classical Schlumberger array is one of the most commonly array used for resistivity sounding surveys. A modified form of this array so that it can be used on a system with the electrodes arranged with a constant spacing is shown in Figure 4-9ib. The "n" factor for this array is the ratio of the distance between C1-P1 (or P2-C2) electrodes to the spacing between the P1-P2 potential pair.

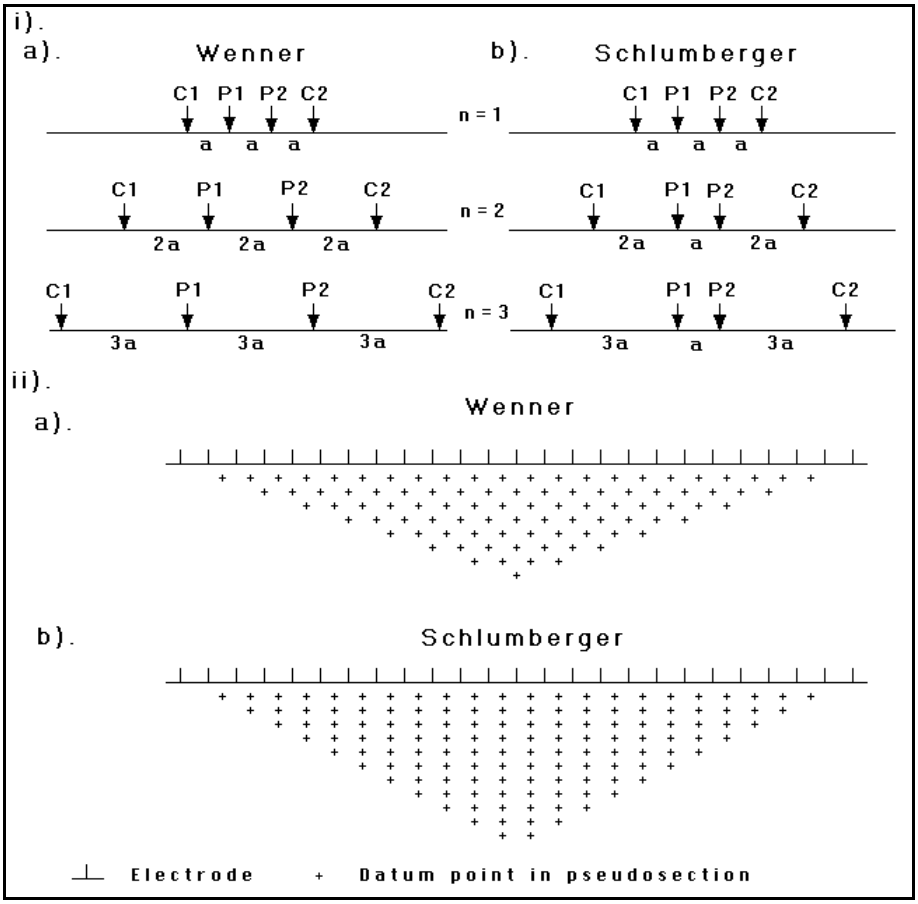

Figure 4-9: A comparison of the (i) electrode arrangement and (ii) pseudo-section data pattern for the Wenner and Wenner-Schlumberger arrays (Loke, 2012)

The sensitivity pattern for this array is displayed on Figure 4-10 where the "n" factor is increased from 1 (Wenner array) to 6 (the classical Schlumberger array). The area of highest positive sensitivity below the centre of the array becomes more concentrated beneath the central P1-P2 electrodes as the "n" factor is increased. Near the location of the plotting point at the median depth of investigation, the sensitivity contours have a slight vertical curvature below the centre of the array. At n=6, the high positive sensitivity lobe beneath P1-P2 electrodes becomes more separated from the high positive sensitivity values near C1 and C2 electrodes. As a result, this array is moderately sensitive to both horizontal (for low "n" values) and vertical structures (for high "n" values). For this reason, this array might be a good compromise between the Wenner and the Dipole-Dipole arrays in areas where both types of geological structures are expected (Loke, 2012).

The median depth of investigation for this array is about 10% larger than that for the Wenner array for the same distance between the outer (C1 and C2) electrodes for "n" values greater than 3. Its signal strength is approximately inversely proportional to the square of the "n"

value and is weaker than that for the Wenner array, but it is higher than the Dipole-Dipole array and twice that of the Pole-Dipole (Loke, 2012). This array has better horizontal coverage compared to Wenner array.

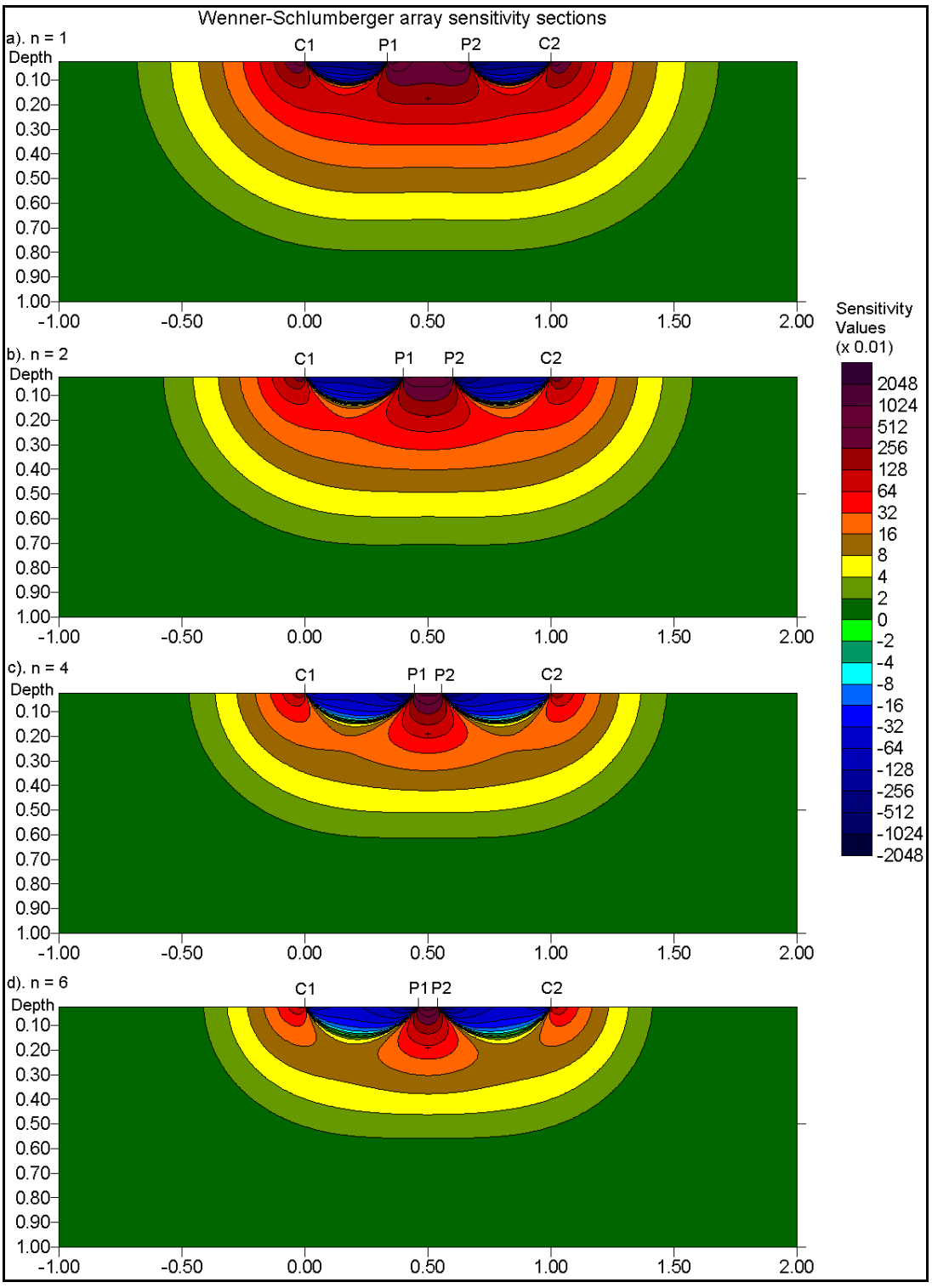

Figure 4-10: 2-D sensitivity sections for the Wenner-Schlumberger array (Loke, 2012)

4.6 MEASUREMENT PROPERTIES OF THE POLE-POLE ARRAY

The Pole-Pole array (not commonly used in ERT surveys), consists of only one current and one potential electrode (Figure 4-11). This does not exist in practice.

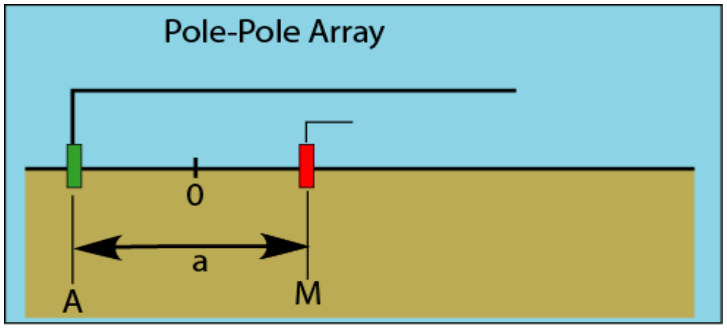

Figure 4-11: The geometry of the Pole-Pole array

With the origin of the coordinate system chosen to be at the centre of the array as shown in Figure 4-11, the positions of the four electrodes are:

$$A\left(\frac{-a}{2},0,0\right); \qquad M\left(\frac{a}{2},0,0\right); \qquad \mathrm{d}\tau(x,y,z)$$

The sensitivity function of this array is given in Equation (4-15):

$$F_{3D}(x,y,z) = \frac{1}{4\pi^2}\left[\frac{\left(x+\frac{a}{2}\right)\left(x-\frac{a}{2}\right)+y^2+z^2}{(r_A r_M)^3}\right] \tag{4-15}$$

The Pole-Pole array is the most simple electrode configuration that makes it easy to automate the data acquisition and to check data quality with reciprocity in a field, but it employs two remote electrodes that limit its applications to accessible sites. The anomaly effect and signal-to-noise ratio of the imaging survey may be relative high or low, depending on geological model, but the theoretical noise-contamination generally stays at moderate levels comparing with other arrays. However, the imaging resolution sits a low rank among the other electrode configurations (Dahlin and Zhou, 2004).

One drawback of this array is that it can pick up a large amount of telluric noise which can severely degrade the quality of the measurements. Thus this array is mainly used in surveys where relatively small electrode spacings (less than 10 m) are used. It has the widest horizontal data coverage and the deepest depth of investigation; however, the poorest resolution (Loke, 2012), which is reflected by the comparatively large spacing between the contours in the sensitivity function plot (Figure 4-12).

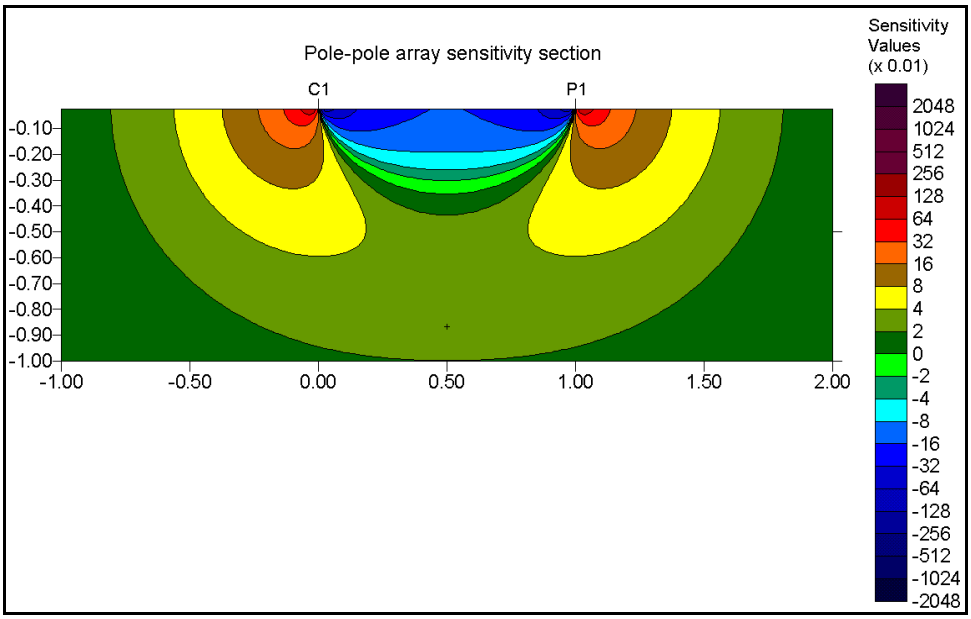

Figure 4-12: The 2-D sensitivity section of the Pole-Pole array (Loke, 2012)

5 CASE STUDIES ON ERT SURVEYS USING DIFFERENT ARRAYS

It was seen in the previous chapter that different electrode arrays have different sensitivities, different depths of investigation, different resolutions, different horizontal data coverage and different signal-to-noise ratio. For that reason, some are used in mapping Karst hazard areas, as well as fractured crystalline-rock terrain; meanwhile others are used in delineating underground cavities. Three case studies, performed by some authors, on the sensitivities of these electrode arrays are the main subject discussed in the present chapter.

5.1 MAPPING KARST ZONES OF VULNERABILITY

The ERT method, valuable tool in subsurface investigations (Zhou *et al.*, 1999), is becoming an efficient way to detect subsurface heterogeneities including voids and refilled cavities (Mochales *et al.*, 2008).

Zhou *et al.* (2002) investigated the success of different electrode arrays used during ERT for mapping karst hazards. Three commonly arrays were used during this investigation: the Wenner, the Schlumberger, and the Dipole-Dipole arrays. The aim of the study was to determine which of these arrays respond best in mapping karst hazard areas. The survey was carried out where a sinkhole had occurred.

- **A conceptual model of sinkhole formation**

A sinkhole results from either the transport of surface material downwards along enlarged channels or collapse of the rock roof over a large bedrock cavity. Of the sinkholes which occur in overburden, the cover-collapse sinkholes are the most unpredictable and are most likely to cause catastrophic damage to engineering works.

The goal of a geophysical investigation is to delineate the potential collapse area when the formation is still in process, where a void has developed but the soil has not collapsed yet. Figure 5-1 shows a conceptual model of a cover-collapse sinkhole formation for construction of apparent resistivity pseudo-sections. The model consists of two layers with 12 m of unconsolidated clayey soil underlain by thick-bedded limestone. A rectangular solution sinkhole is present on the bedrock surface and is filled with the clayey soil. A rectangular soil

cavity 2 m wide and 4 m high is sloping upwards within the soil. The resistivities of the soil, limestone and the air-filled cavity were chosen to be 100 Ω.m, 1 000 Ω.m, and 10 000 Ω.m, respectively.

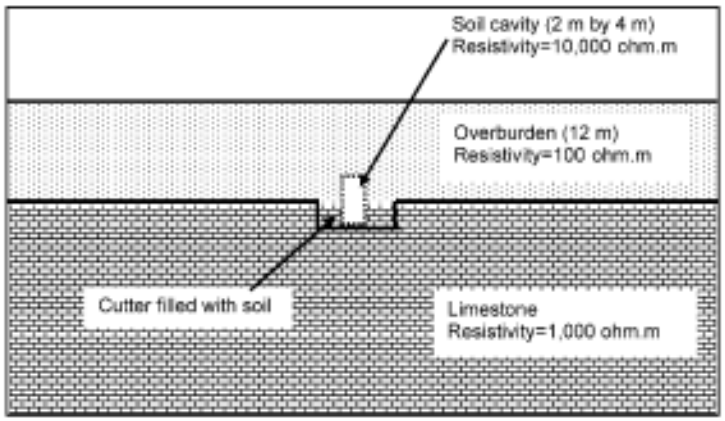

Figure 5-1: Conceptual model of formation of a cover-collapse sinkhole (Zhou et al., 2002)

❖ **The apparent resistivity pseudo-sections from different electrode arrays**

The software program RES2DMOD (Loke, 2002) was used to calculate the apparent resistivity of the model shown in Figure 5-1 by using the finite-difference method for the Wenner, Schlumberger, and Dipole-Dipole arrays. The resulting pseudo-sections are shown in Figure 5-2. It is noticeable that different arrays produce significantly different profiles. The Wenner array is the least sensitive to the potential collapse area. The large soil cavity does not even create a noticeable anomaly. The profile from the Schlumberger array shows two cutter-like signatures separated by a resistivity high. This resistivity high is most likely caused by the soil cavity, whereas the two low-resistivity anomalies are likely artifacts caused by the modelling processes.

The profile from the Dipole-Dipole array shows an isolated high-resistivity area near the surface directly above the feature. Below this high-resistivity area lies a low-resistivity area with high resistivity on both sides. It appears that the position of the soil cavity is in the low-resistivity area, which is likely an artifact of the modelling process. This simple modelling exercise indicates that:

- Detection of a potential sinkhole collapse area depends on an appropriate selection of an electrode array,
- Interpretation of the pseudo-sections requires knowledge of the applied array.

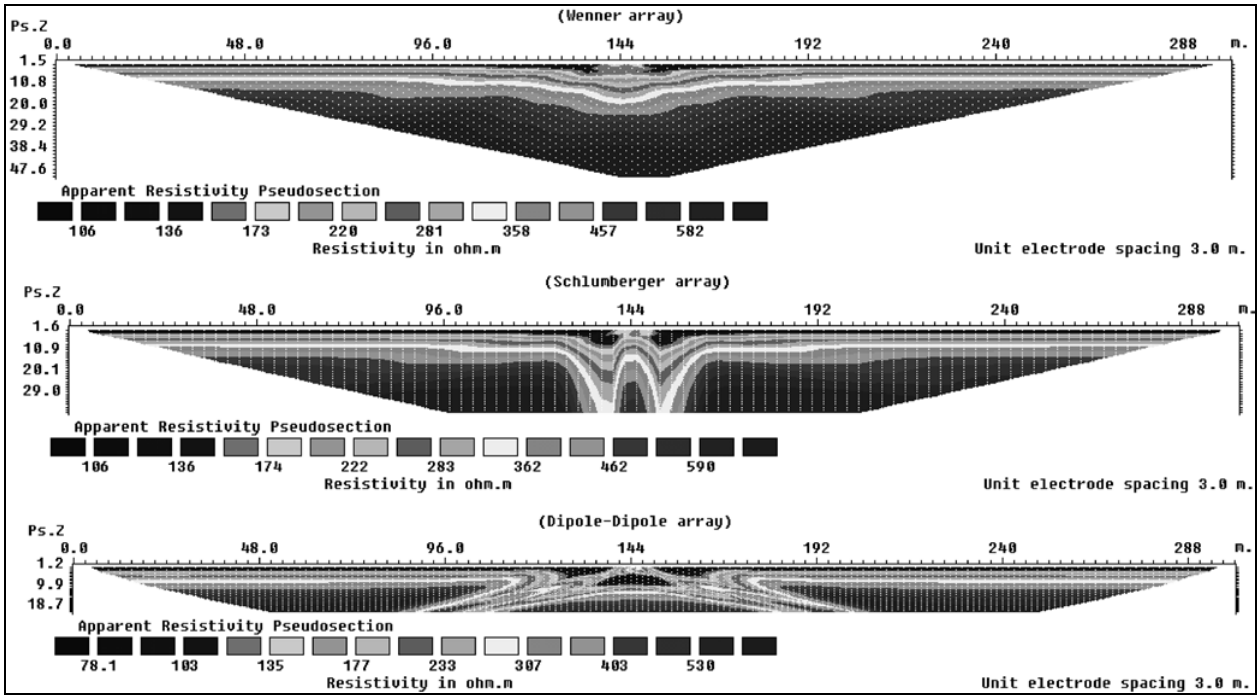

Figure 5-2: Resistivity pseudo-sections for the sinkhole formation model (Zhou et al., 2002)

❖ Resistivity profiles over a collapse area

The effectiveness of the various electrode arrays in delineating sinkhole areas was investigated along a section of I-70 in Frederick County, Maryland, where a significant number of sinkholes have occurred. The investigation was conducted over a newly collapsed sinkhole in the middle of the highway. The sinkhole is approximately 0.6 m in diameter and 1 m deep.

It appeared that the sinkhole was not filled with soil, which is similar to an air-filled cavity. The resistivity data were collected using the Sting/Swift system (Advanced Geosciences Inc., 1997) with 56 electrodes, 3 m apart. The resulting data were processed using the software program RES2DINV developed by Loke and Baker (1995).

Figure 5-3 shows the profiles for the Wenner, Schlumberger, Dipole-Dipole, and a mixed array. The mixed array combined all the data from the three standard arrays. The application of the mixed array was to determine whether a better representation of the subsurface could be obtained by taking advantage of the different properties of the three common arrays. A similar technique was employed by Kaufmann and Quinif (2001), who combined the data from the Dipole-Dipole and Schlumberger arrays to detect sinkhole-prone areas in Belgium.

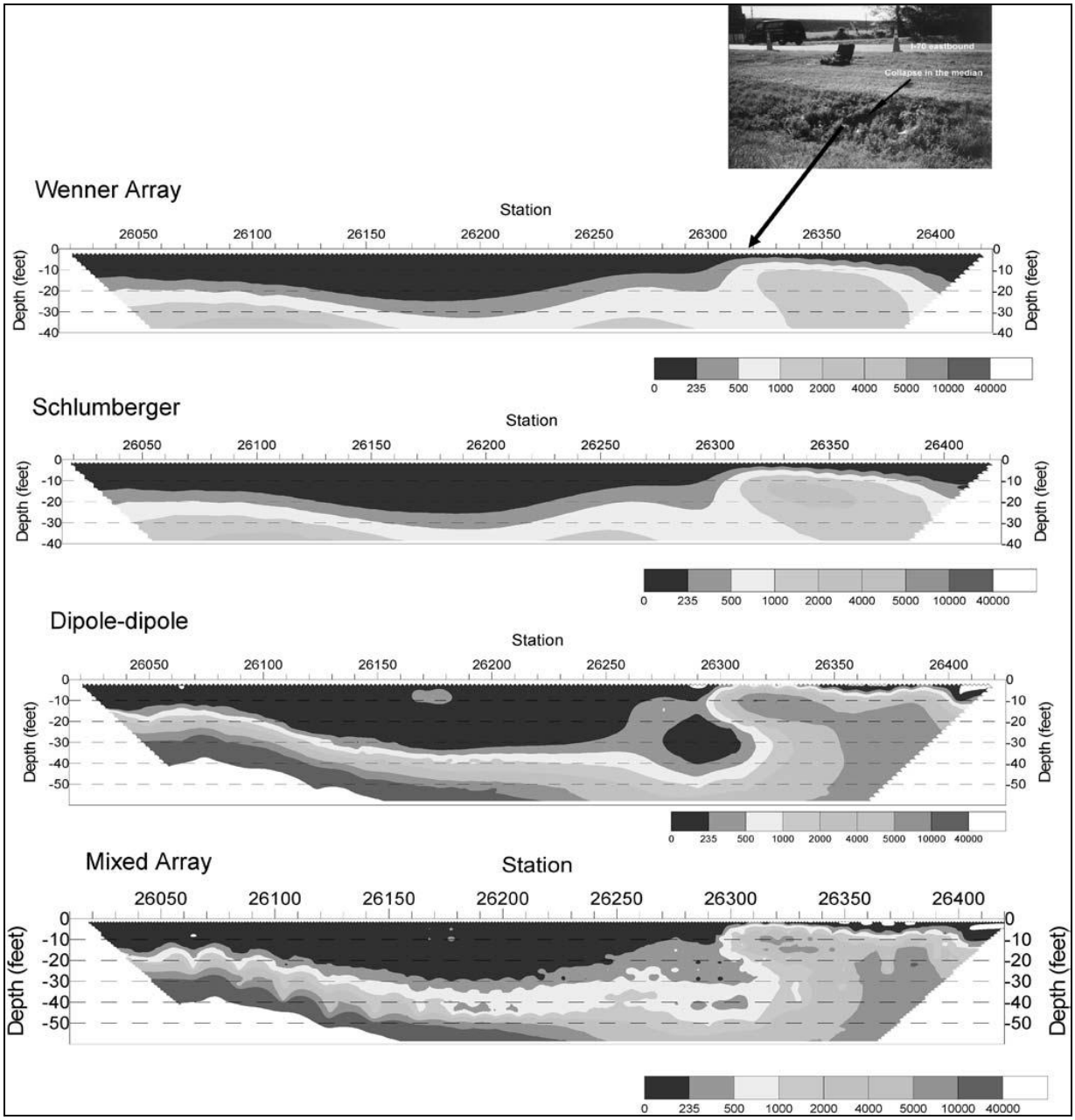

Figure 5-3: Modelled resistivity sections over a sinkhole collapse area (Zhou *et al*., 2002)

The picture at the upper right angle shows the collapse area, which is at station 26317 on the pseudo-sections. The profiles from the four investigated arrays are in reasonable agreement with each other until station 26250, to the left of which the geology does not seem to vary. However, the profiles are different over the collapsed area. The Wenner array seems to be the least sensitive, the Dipole-Dipole array the most sensitive, and the Schlumberger array is moderately sensitive. The geo-electric profile was enhanced to a certain degree in the mixed array. The collapsed area is more readily recognized. It is also apparent that the profile from the mixed array resembles that from the Dipole-Dipole array more than those from the Wenner and Schlumberger arrays.

Although the result from the mixed array provided a more representative signature of the collapse area, its application requires a significant increase in data-collection effort. For practical purposes, the standard arrays are commonly employed. Among the three standard arrays, the Dipole-Dipole array provides the highest precision of locating the sinkhole feature and has the greatest sensitivity to vertical resistivity boundaries. One drawback of the Dipole-Dipole array is that it does not provide a very high signal for measurement, and therefore it can produce somewhat noisy data. Other array geometries may provide a better signal-to-noise ratio but they do not have the resolving power of the Dipole-Dipole array.

Several other field investigations similarly to the previous have demonstrated that Dipole-Dipole ERT is able to delineate sinkhole collapse areas and is sensitive to vertical boundaries when it is properly employed.

5.2 MAPPING FRACTURED CRYSTALLINE-ROCK TERRAIN

Seaton and Burbey (2002) evaluated 2-D resistivity methods in fractured crystalline-rock terrain, in the Blue Ridge Province, Southwest Virginia, using the Wenner, Wenner-Schlumberger, the Dipole-Dipole and the Pole-Pole arrays. The goal of the research was to determine which electrode array will produce the highest data quality from the hydrogeological investigation within the crystalline bedrock aquifers. For that research, synthetic data (output of numeric modelling of synthetic geologic structures using forward modelling program) and field data of the apparent resistivity were used.

The numerical modelling was done using two synthetic resistivity models containing horizontal and vertical structures with varying resistivities as input to the forward modelling program. The inverse modelling of the synthetic data sets showed that the Dipole-Dipole array configuration reproduced the synthetic horizontal and vertical structures more accurately than the other array configurations.

Resistivity field data were collected in a farm where the subsurface consists of a shallow layer of unconsolidated soil and weathered rock varying in thickness from 0 to 20 m underlain by crystalline bedrock that is composed of metamorphosed igneous and sedimentary rocks including granite gneiss, biotite gneiss, mica schist, phyllite, and massive vein quartz. The bedrock is variably fractured and faulted making for a highly heterogeneous hydrogeological system.

The Wenner surveys were performed using all possible values of "a" for the given array. The Wenner-Schlumberger and Dipole-Dipole surveys were performed with increasing values for "n" and "a" which provide a higher resolution earth model and maximizes the depth of investigation.

The inverse models generated using the Dipole-Dipole data extended to depths of 30-35 m, showed significant variations in resistivity both vertically and horizontally, and had a thick transitional resistivity zone between the regolith and bedrock intervals. The Wenner-Schlumberger and Wenner profiles revealed more discreet and homogeneous high and low resistivity zones, thinner transitional resistivity zones, and extended to depths of only 25-30 m.

Borehole cuttings and geophysical well logs were used to correlate the different resistivity zones in the resistivity profiles to specific rock types. The modelled resistivity data from the Dipole-Dipole method approached the logged resistivity data in absolute value and mimicked the low resistivity zone in the well log. The models generated from the Wenner-Schlumberger and Wenner data underestimated the resistivities collected in the borehole and lacked the depth of investigation to detect the low resistivity interval in the borehole.

Conclusions of the research showed that:

- The arrays that have the potential electrodes placed inside the current path (Wenner and Wenner-Schlumberger) have a shallower depth of investigation, generally less resolution and sensitivity to geologic detail than arrays with the potential probes outside of the current path (Dipole-Dipole). The Pole-Pole array has significantly greater depth of investigation than the other arrays but lower resolution and sensitivity than the other configurations.

- The Dipole-Dipole array reproduced the shallow and the intermediate depth resistivity structures accurately.

- The Dipole-Dipole is very sensitive even to small structures with anomalously high and low resistivities in the subsurface.

- The Dipole-Dipole method has 20-25% greater depth penetration than the Wenner and Wenner–Schlumberger configuration.

- The higher resolution, greater depth of investigation, and high sensitivity to geologic detail offered by the Dipole-Dipole array outweighed the fact that it used more measurements than the Wenner or Wenner-Schlumberger configuration.

- The Dipole-Dipole configuration has low signal strength.

5.3 DELINEATING AN UNDERGROUND CAVITY

Ahmad *et al.* (2010) investigated the performances of the Wenner and the Dipole-Dipole arrays in mapping an underground three-dimensional cavity using the 3-D resistivity imaging. The objective of the study was to compare the Wenner and the Dipole-Dipole arrays in delineating an underground cavity at a site near the University of Malaya in Malaysia.

❖ **Data acquisition**

Measurements were collected along seven parallel lines, each covering 38 m with spacing of 2 m between the lines. Because the standard deviation is a valid indicator of the quality of the measurements (Tohon *et al.*, 2004), it was checked for each stack during the measurements and it was less than 2% and 4% for the Wenner and Dipole-Dipole arrays, respectively. All measured data sets were merged in order to perform the 3-D inversion using RES3DINV software (Loke, 2007). Two separate final sets of 938 and 364 apparent resistivity measurements were collected using a Terrameter SAS 4000 instrument (Dahlin, 1996).

❖ **Inversion of the data set**

The measured and calculated apparent resistivity data obtained along the seven parallel lines by the Wenner and Dipole-Dipole arrays are displayed as pseudo-sections in Figure 5-4 and Figure 5-5, respectively. Although the pseudo-sections can give some information about the locations of the cavity and the horizontal pipe, their size, depth and extent cannot be correctly estimated. Furthermore, the pseudo-section can be misleading if used as the basis for an interpretation of the true subsurface structure (Dahlin *et al.*, 2002). A 3-D inversion of the apparent resistivity data was then performed, in order to obtain a more reliable image of the cavity structure using the robust inversion technique.

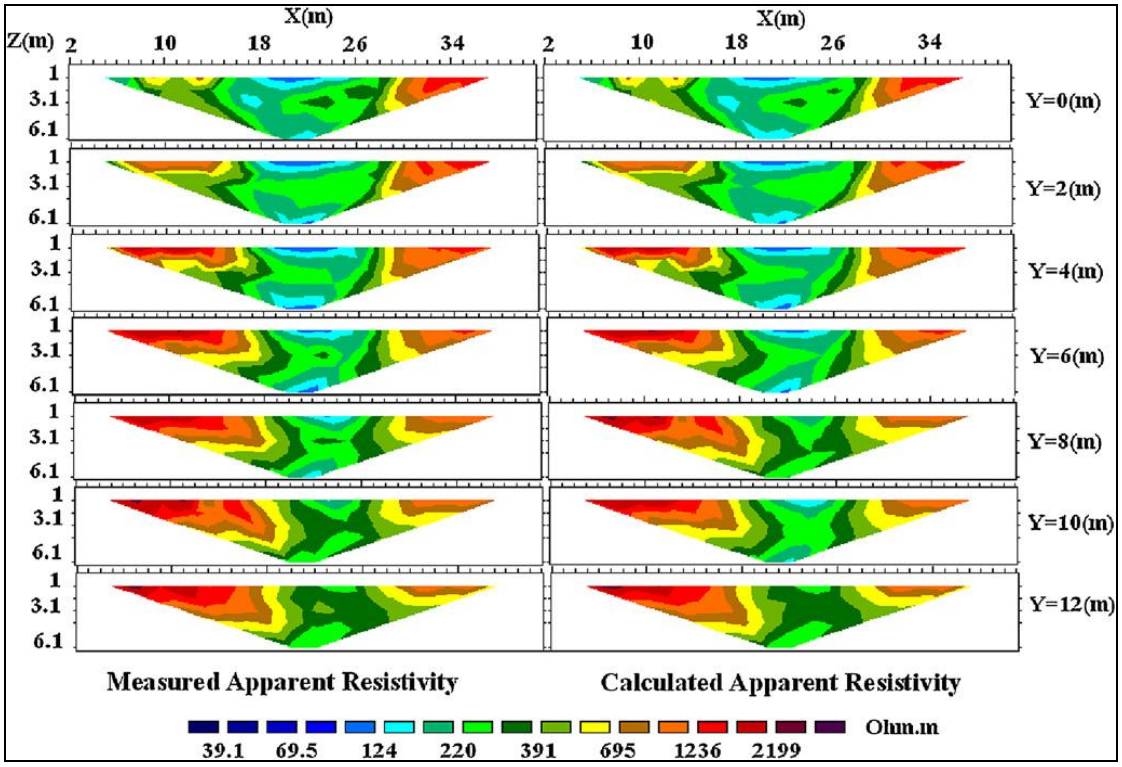

Figure 5-4: Measured and calculated apparent resistivity data using the Wenner array

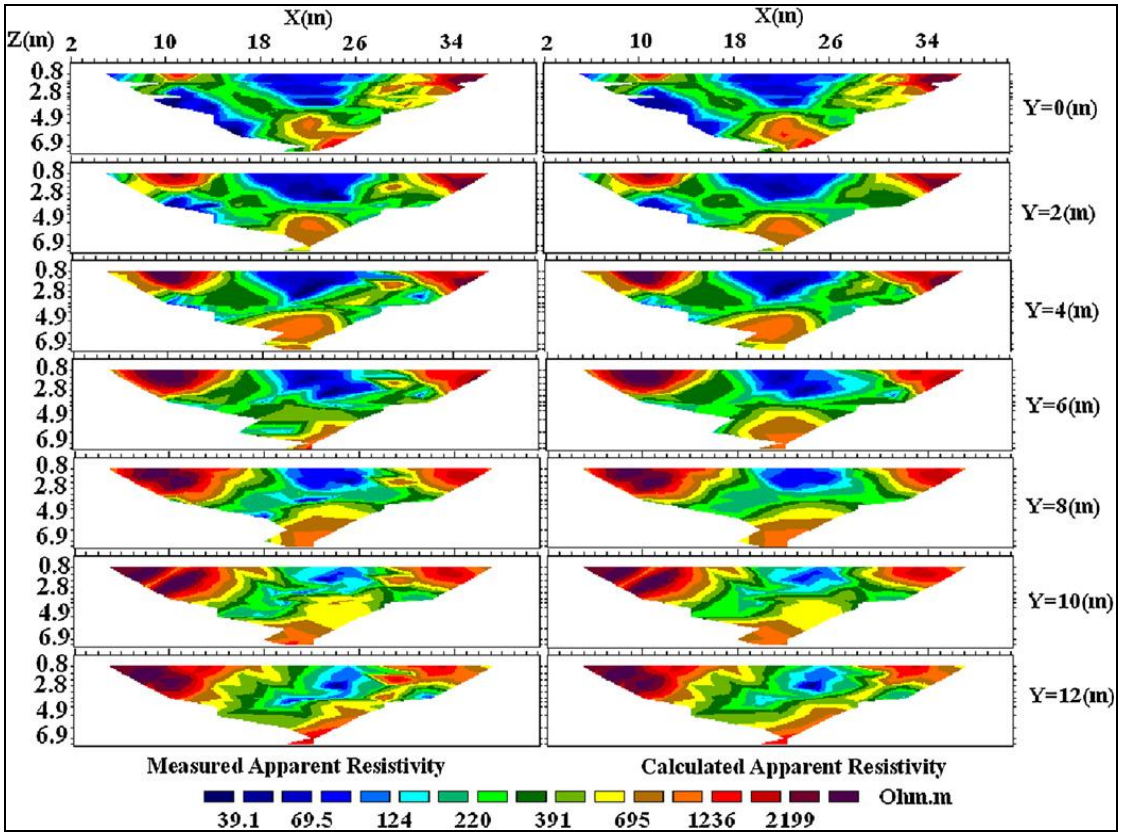

Figure 5-5: Measured and calculated apparent resistivity data using the Dipole-Dipole array

In order to determine the subsurface resistivity from the measured apparent resistivity, the widths of the interior blocks in the top two layers of the inverse model were set at half the unit electrode spacing, while the widths of the blocks in the deeper layers were kept equal to the electrode spacing (Dahlin *et al.*, 2002). The thickness of the first layer and the factor used to increase the layer thickness were set at 1.5 m and 1.15 m, respectively. Values of 0.15 and 0.01 were used for the initial and minimum damping factors, respectively, in the data inversion. These factors determine the relative importance given to reduce the data misfitting and the smoothness of the model (Ellis and Oldenburg, 1994). The finite difference method (Dey and Morrison, 1979) was used to calculate the apparent resistivity values as well as the elements of the Jacobian matrix (McGillivray and Oldenburg, 1990) for the inversion method.

- **Results**

Wenner array: The inversion process using the robust technique converged after six iterations with an RMS misfit of 4.52% for the apparent resistivity values. The 3-D resistivity model is shown as horizontal depth slices in Figure 5.6. The widths of the upper (11 m) and the lower (5 m) parts of the cavity (layers ‘a’ and ‘g’, respectively) are observed.

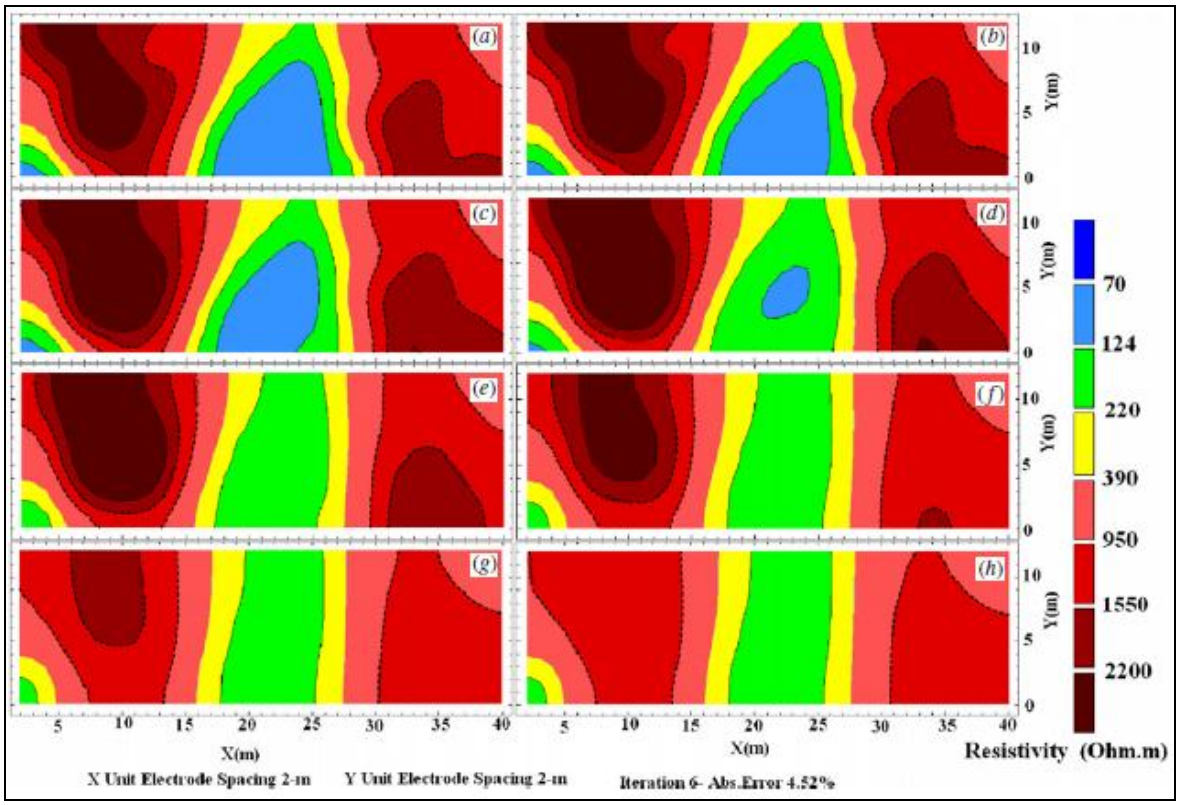

Figure 5-6: 3-D resistivity model obtained by a Wenner array as horizontal depth slices

The depth (m) for all the layers are as follows: (a) 0–0.5, (b) 0.5–1.1, (c) 1.1–1.7, (d) 1.7–2.5, (e) 2.5–3.4, (f) 3.4–4.4, (g) 4.4–5.5, and (h) 5.5–6.9.

According to Figure 5-6, the depth of the cavity is almost 5.5 m. The resistive zone, on the south side of the slices, also occurs at a depth of approximately 4.4 m. High resistivities are not observed near the middle of the site. In order to display the 3-D extent of the cavity and horizontal pipe, an iso-resistivity surface was also produced corresponding to resistivities higher than 1 550 Ω.m. The iso-surface connects data points of equal resistivity values (Figure 5-7a). As illustrated in the figure, the horizontal pipe and cavity were clearly detected.

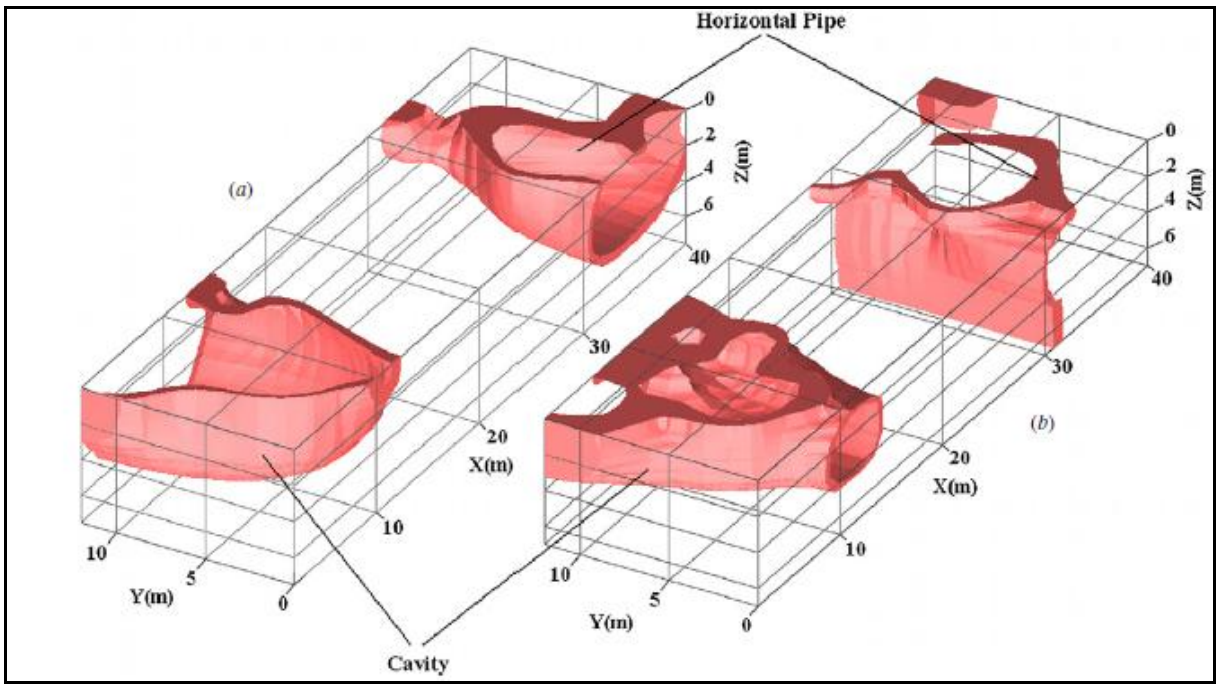

Figure 5-7: Iso-resistivity surface of the highest resistivity zones obtained by (a) Wenner array and (b) Dipole-Dipole array

Dipole-Dipole array: As a comparative study, the 3-D resistivity imaging data obtained by the Dipole-Dipole array were also inverted using the robust inversion method. After nine iterations, the inversion process converged with an RMS misfit of 14.09%, which is greater than the RMS misfit for the inversion obtained by the Wenner array (4.52%). This difference can be explained by the greater signal strength of the Wenner array than the Dipole-Dipole array, especially when a high resistivity contrast exists.

From the inverted data, horizontal depth slices (Figure 5-8) were extracted in order to display the lateral extent of the high resistivity zones. The depth (m) for the layers are as follows: (a) 0–0.5, (b) 0.5–1.0, (c) 1.0–1.6, (d) 1.6–2.3, (e) 2.3–3.0, (f) 3.0–3.9, (g) 3.9–5.0, (h) 5.0–6.9. While almost all features are well resolved in these depth slices, the inversion of the resistivity data obtained by the Dipole-Dipole array produces a greater depth for the resistive material surrounding the horizontal pipe (more than 6.9 m) and a smaller depth of 3.9 m for the cavity compared to the inversion result obtained by the Wenner array. It is clear that the Wenner array has better depth resolution than the Dipole-Dipole array.

On the other hand, vertical columns of high resistivity (A and B) are observed in the first slice (layer ‘a’ of Figure 5-8). These two columns are not observed in the inversion obtained from the Wenner array. This can be explained by the better horizontal resolution of the Dipole-Dipole array compared to the Wenner configuration.

In these slices, the cavity with a width of 14 m in its upper part (layer ‘a’, Figure 5-8) and about 5 m in its lower part (layer ‘f’) is observed. Although the horizontal changes in resistivity are in accordance with the findings obtained from known information about the investigation area, insufficient agreement in the vertical resistivity distribution was found, especially on the south side of the site.

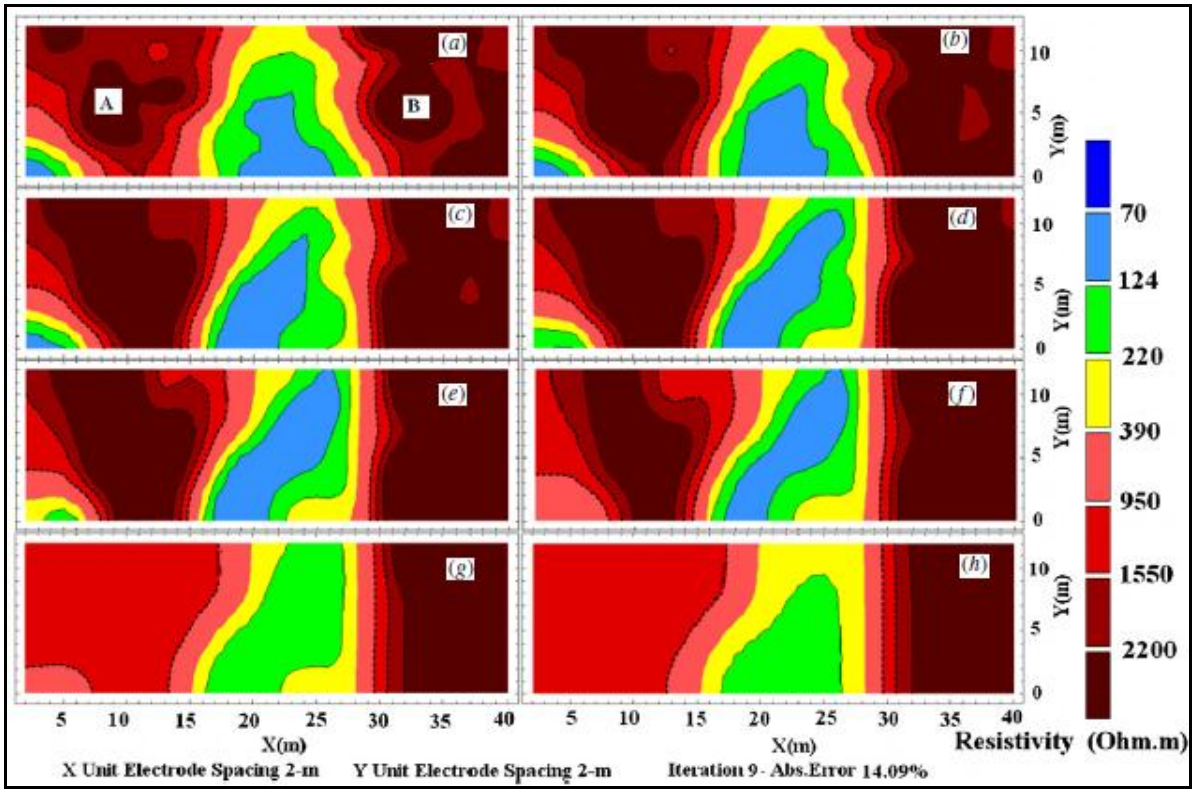

Figure 5-8: 3-D resistivity model obtained by a Dipole-Dipole array as horizontal depth slices

An iso-resistivity surface was also produced to display the 3-D extent of the cavity and horizontal pipe, which corresponds to resistivities higher than 1550 Ω.m (Figure 5-7b). It is seen that the cavity was clearly detected, but the vertical dimension of the pipe was not reliable.

In conclusion, although the Dipole-Dipole array produced a better lateral extent for the subsurface features, the results illustrate the superiority of the Wenner array over the Dipole-Dipole configuration for the determination of the vertical distribution of subsurface resistivity. Note that this research was done by the 3-D ERT methods.

6 MODELLING INVESTIGATIONS

Over the last two decades the 2-D ERT method has been widely used for many purposes in the Karoo. The present chapter aims to study the responses of different electrode to various geological features commonly encountered in Karoo formations (dykes, sills, faults, weathered zones) by means of 2-D forward and inverse modelling. The numerical modelling is done in order to assist in the selection of suitable array(s) prior to conducting ERT surveys on Karoo formations.

Forward modelling was done using the 2-D forward modelling software RES2DMOD, created by Loke (2002). The arrays supported by the software are the Wenner (Alpha, Beta and Gamma configurations), Pole-Pole, Gradient, equatorial Dipole-Dipole, inline Dipole-Dipole, Wenner-Schlumberger, Pole-Dipole, Offset, Forward and Reverse Pole-Dipole. For this research, only the four following electrode arrays were examined during the modelling investigation, because they are the commonly used in geohydrological studies:

- The Wenner Alpha array (referred as Wenner array only),
- The inline Dipole-Dipole array (referred as Dipole-Dipole array only),
- The Wenner-Schlumberger array (referred as Schlumberger array only), and
- The Pole-Pole array.

Inverse modelling was done using the software RES2DINV. Before simulating different geological models, some parameters, such as the L1 and L2-norm, as well as the inversions of noise-contaminated data sets, were examined.

6.1 THE INFLUENCE OF SELECTED MODEL PARAMETERS

6.1.1 Comparison of L1 and L2-norm inversion methods

The aim of geophysical inversion is to find a model of the subsurface whose response is the most alike to the measured field response. Consider a vertical dyke with a resistivity of 400 Ω.m, surrounded by rocks with low resistivity (40 Ω.m), overlain by an overburden with a resistivity of 100 Ω.m. For this conceptual model, the software RES2DINV offers two inversion options, namely: the robust inversion (Figure 6-1a), also called L1-norm inversion and the smoothness-constrained least-squares inversion (Figure 6-1b), also called L2-norm inversion.

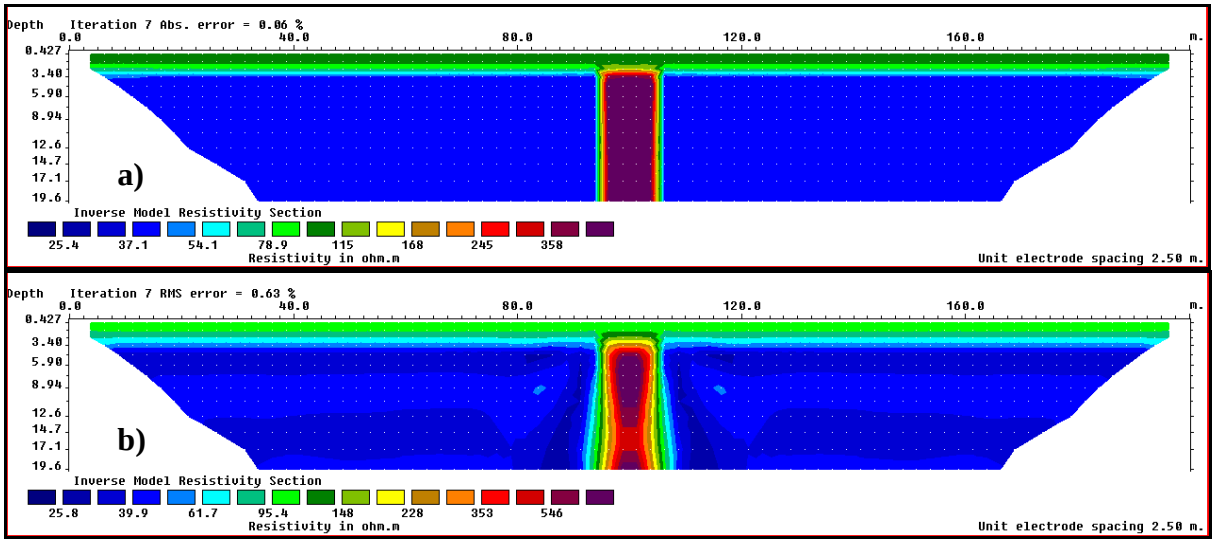

Figure 6-1: Robust inverse model constraint (a) and least-square smoothness-constraint (b)

It can be seen from Figure 6-1 a) and b) that the robust inversion (L1-norm) produces a model with sharp boundaries between the dyke, the host rock and the overburden while the smoothness-constrained least-squares inversion (L2-norm) produces a model with gradual transitions across zones of different resistivities.

The L1-norm attempts to find a model that minimises the absolute values of the data misfit. In other words, it attempts to minimise the square of the difference between the observed and the calculated apparent resistivity values of a model. Loke and Dahlin (2002) showed that the L1-norm is less sensitive to very noisy data points but might give a higher apparent resistivity RMS error. The L2-norm seeks a smooth model that minimises the squares of data misfit. It tends to give greater importance to data points with a larger misfit and this makes it more sensitive to the outliers in the data.

It is therefore recommended that the L2-norm be used if the subsurface resistivity changes in a smooth manner, conversely, the L1-norm should be used when there are sharp boundaries. The standard least-square smoothness-constraint inversion is a good optimisation choice when gradual changes are expected in the geology, or when dealing with contamination plumes in the mapping of groundwater pollution. The robust inversion optimisation method allows models with sharper variations in resistivity and is therefore a better optimisation choice when geological discontinuities are expected, for example in the Karoo formations (dykes, sills, faults).

The L1-norm optimisation method or robust inversion is most suited to the geology of the Karoo and was chosen in this study because the goal was to reproduce sharp geologic boundaries.

6.1.2 Noise-contaminated data sets

Consider a dolerite sill intrusion with a resistivity of 500 Ω.m, overlying a low resistivity formation (40 Ω.m), both overlain by overburden with a resistivity of 100 Ω.m. For this conceptual model, forward modelling using the Wenner, the Schlumberger, the Dipole-Dipole and the Pole-Pole arrays was performed. Random noise with an amplitude of 10% of the voltage was added to the calculated voltages of the first three arrays, while random noise of 10% was added to the apparent resistivity values of the Pole-Pole array. Inverse modelling was thereafter performed and the modelled resistivity sections for each array are displayed in Figure 6-2.

In Figure 6-2 it is seen that the Wenner array has less noise contamination and better signal-to-noise ratio than the other arrays. The Pole-Pole array has the weakest signal strength and is followed by the Dipole-Dipole array. The Schlumberger array is more at risk of contamination than the Wenner array, but has stronger signal strength compared to the Dipole-Dipole and Pole-Pole arrays. Similar experiments simulating several other geological models were performed during the modelling investigations in this research. Results showed that the Wenner array has the strongest signal strength, followed by the Schlumberger array, then the Dipole-Dipole array and finally the Pole-Pole array.

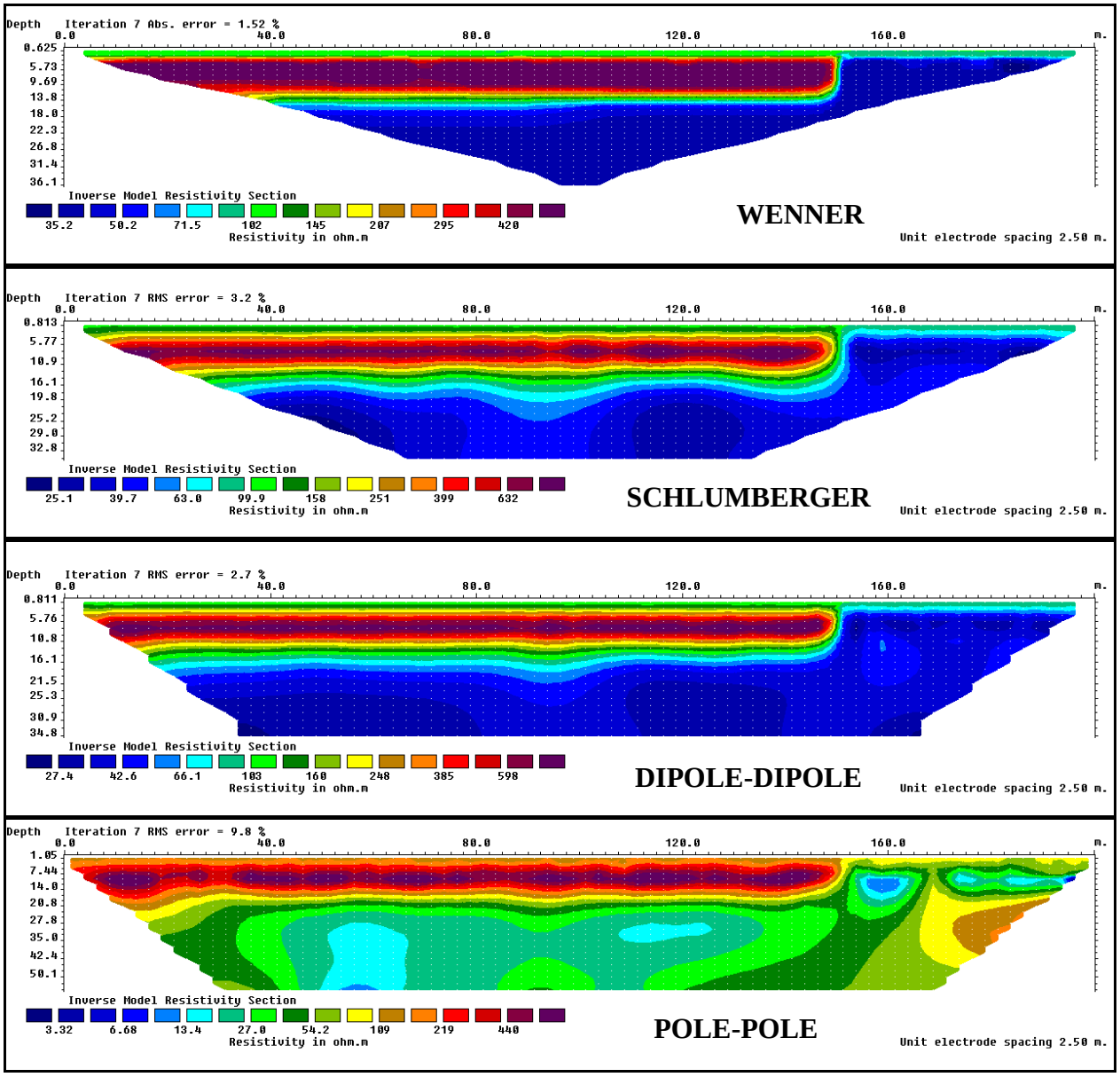

Figure 6-2: Modelled resistivity sections for noise-contaminated data sets

6.2 MODELLING DYKES ALONE

One of the main characteristics of the Karoo Supergroup is the presence of many dolerite dykes intrusions. In this section, four synthetic geological models, simulating a thin vertical dyke, a thin dipping dyke, a thick vertical dyke and a thick dipping dyke (similar to subsurface conditions in the Karoo formations) were used to examine the sensitivities of four electrode arrays. The apparent resistivity pseudo-sections for each model as obtained with different arrays are displayed in APPENDIX 1.

6.2.1 Construction of the input resistivity models

The input resistivity models for a vertical thin dyke (Figure 6-3), a dipping thin dyke (Figure 6-4), a vertical thick dyke (Figure 6-5) and a dipping thick dyke (Figure 6-6) intrusion were constructed in a text file with the extension **.**MOD so that it could be read by the software RES2DMOD. The thin dykes were assumed to be 10-m wide, while the thick dykes were assumed to be 20-m wide, as encountered in the Karoo. Dips of approximately 70^{o} were assigned to the dipping dykes. The input files contained the resistivity model values. A number of 81 electrodes were used for each model. For this research, the Terrameter SAS 1000 (ABEM Lund Imaging System) is used to conduct all the resistivity field surveys; this system, discussed in detail in Chapter 7, incorporates four cables and 81 electrodes: this justifies the reason of using 81 electrodes for the current modelling investigations. The number of apparent resistivity levels or pseudo-section data levels used was 26. The electrode spacings used was 2.5 m. Three resistivity values were used in the model: 500 Ω.m for the dolerite dyke (assuming it is not weathered), 100 Ω.m for the overburden material, and 40 Ω.m for the host rock. These resistivity values correspond to the typical formations encountered in the Karoo.

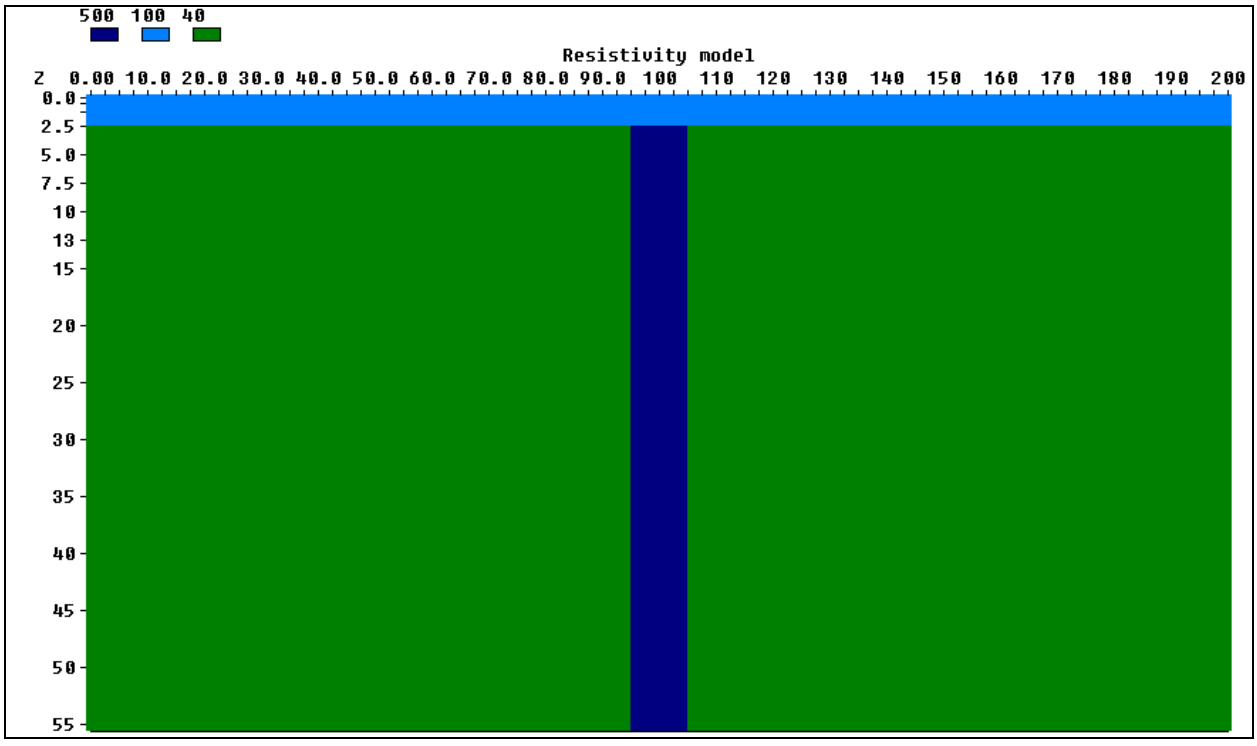

Figure 6-3: Input resistivity model for a vertical thin dyke

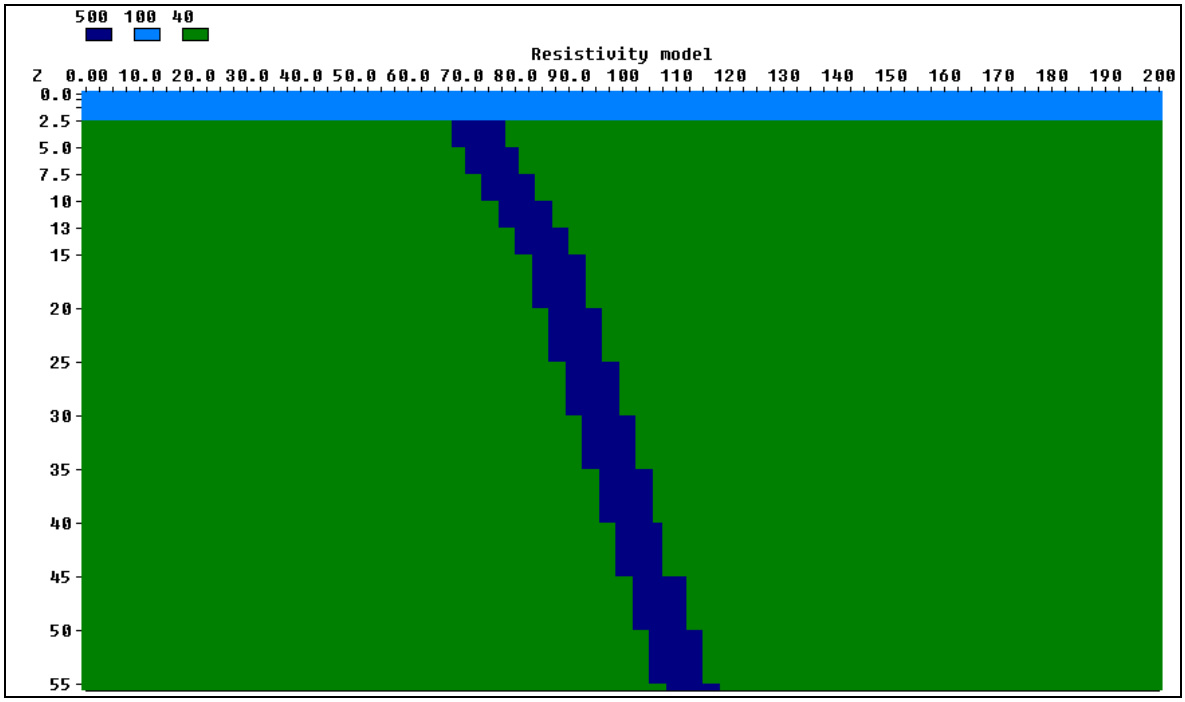

Figure 6-4: Input resistivity model for a dipping thin dyke

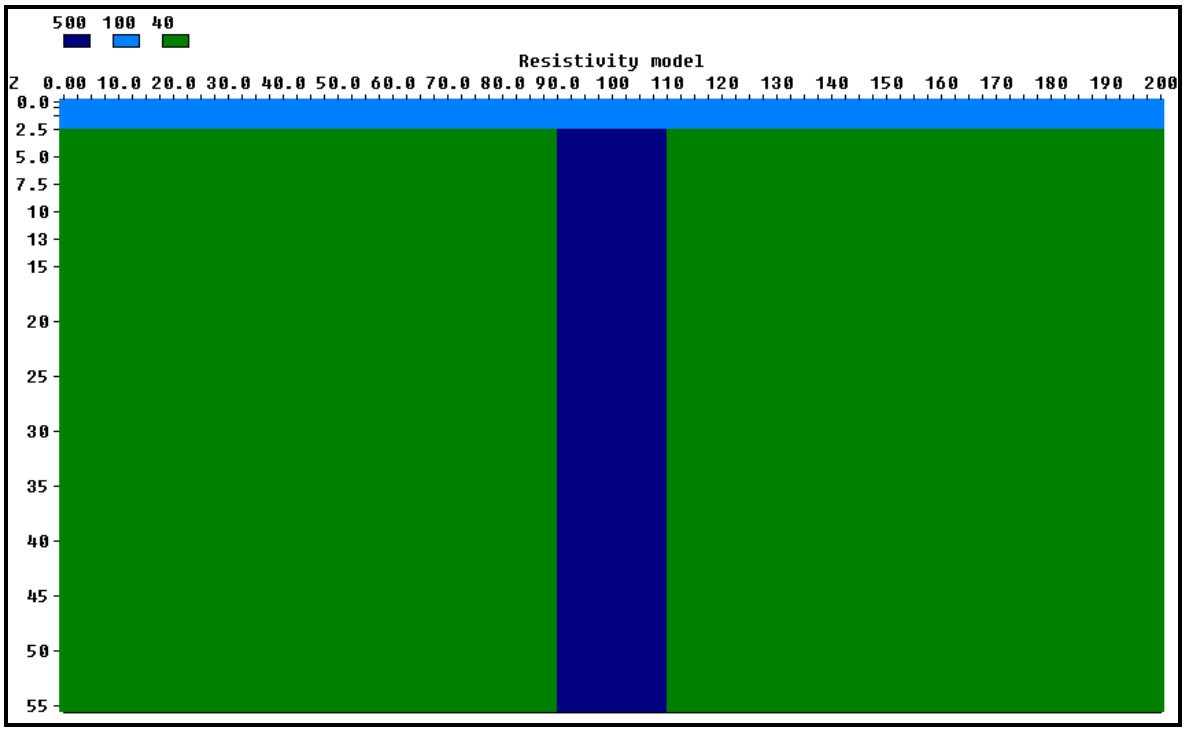

Figure 6-5: Input resistivity model for a vertical thick dyke

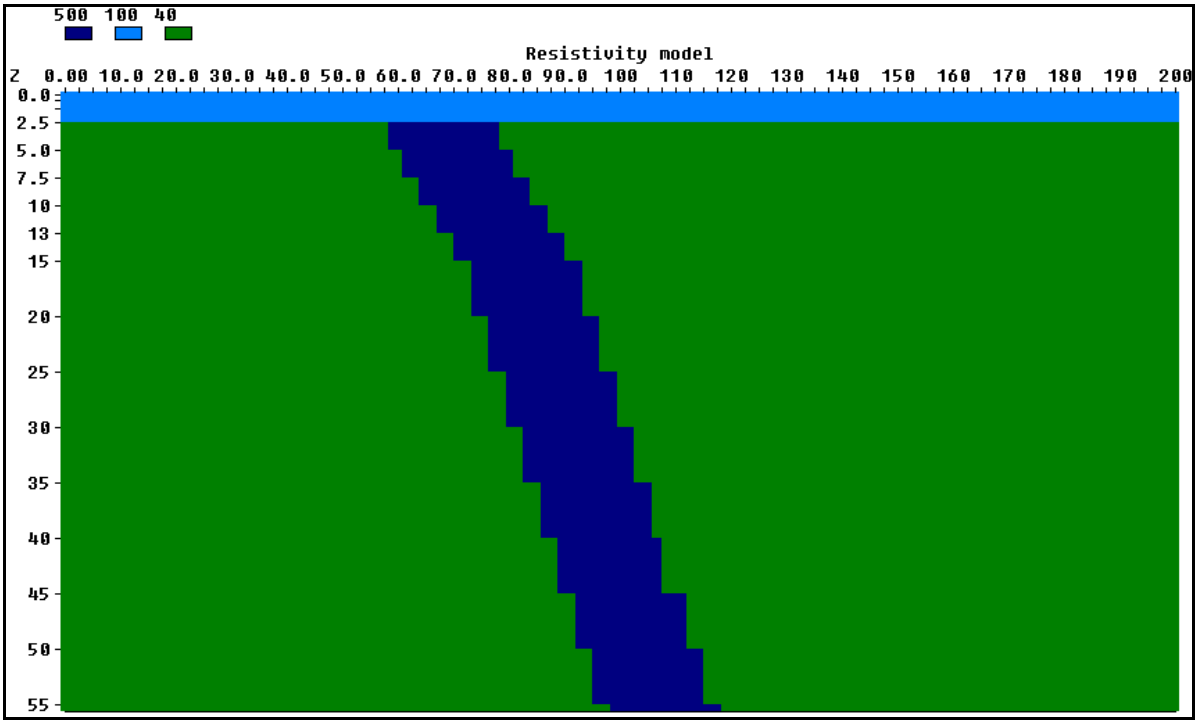

Figure 6-6: Input resistivity model for a dipping thick dyke

RES2DMOD was used to calculate the apparent resistivity values corresponding to the defined 2-D subsurface models, using the finite-difference technique. The Wenner, Schlumberger, Dipole-Dipole and Pole-Pole arrays were used to calculate the pseudo-sections of these arrays. These pseudo-sections are presented in APPENDIX 1. Results were later saved (first with no random noise and thereafter with 10% of random noise) with an extension of .DAT in order to be read by the software RES2DINV. The inverse modelling consists of converting apparent resistivity values into a resistivity model section that can be used for geological interpretation.

6.2.2 Inverse model resistivity sections

The software RES2DINV was used to carry out least-square inverse modelling of the four models obtained from the forwards modelling. RES2DINV displays a measured apparent resistivity pseudo-section, a calculated apparent resistivity pseudo-section and an inverse model resistivity section (Figure 6-7). The RMS error is given by the difference between the measured and the calculated apparent resistivity values. It generally decreases as the number of iterations increases. To allow comparison of the models for different arrays, seven iterations were used during all inversions of the synthetic models.

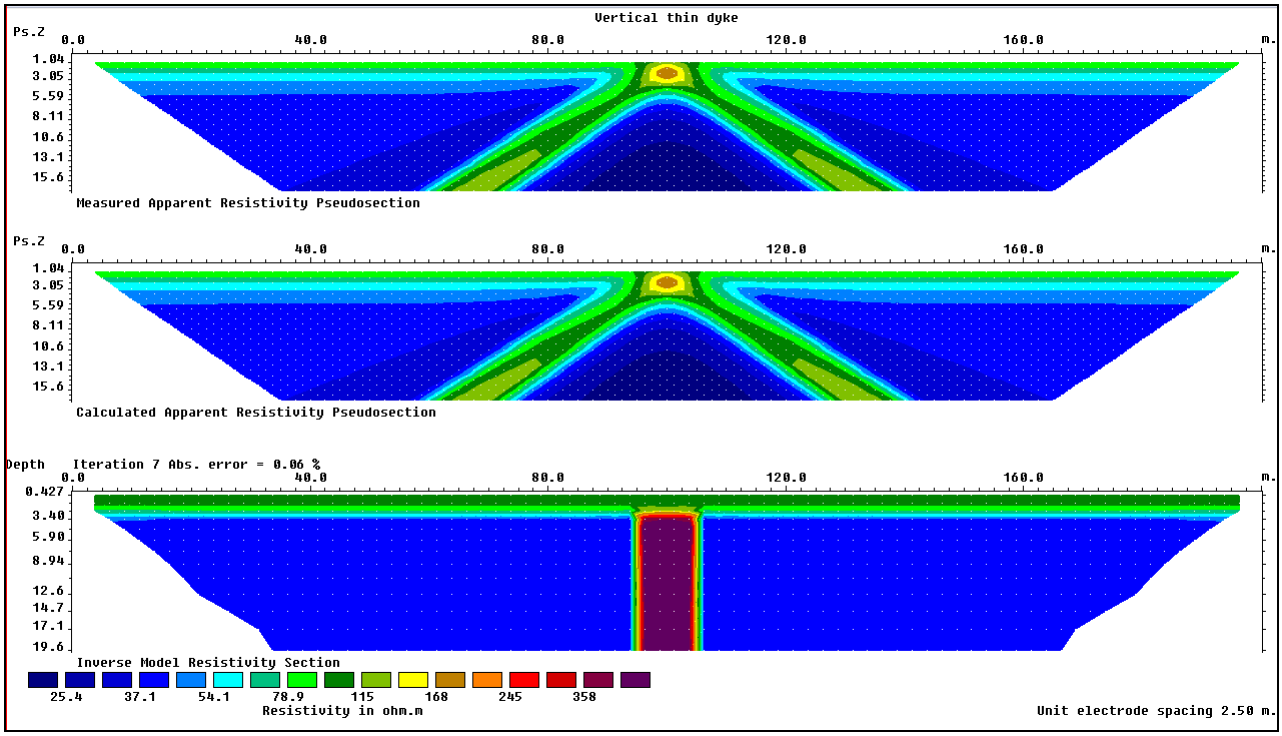

Figure 6-7: Resistivity profiles showing the measured (top) and calculated (centre) apparent resistivity pseudo-sections and the inverse model resistivity section (bottom)

Among the three resistivity sections shown in Figure 6-7, the inverse model resistivity section is the most important since it provides a model of the resistivity distribution that may give rise to the calculated pseudo-section. Therefore, only the inverse model resistivity sections will henceforth be presented in this dissertation. Even though only the inverse model will be shown, the agreement between the observed and modelled pseudo-sections will be reflected in the RMS errors displayed above the inverse models. For inversion the L1-norm (robust constraint) was selected. The modelled resistivity sections for the different electrode arrays used as generated by the software are presented in Figure 6-8 to Figure 6-11.

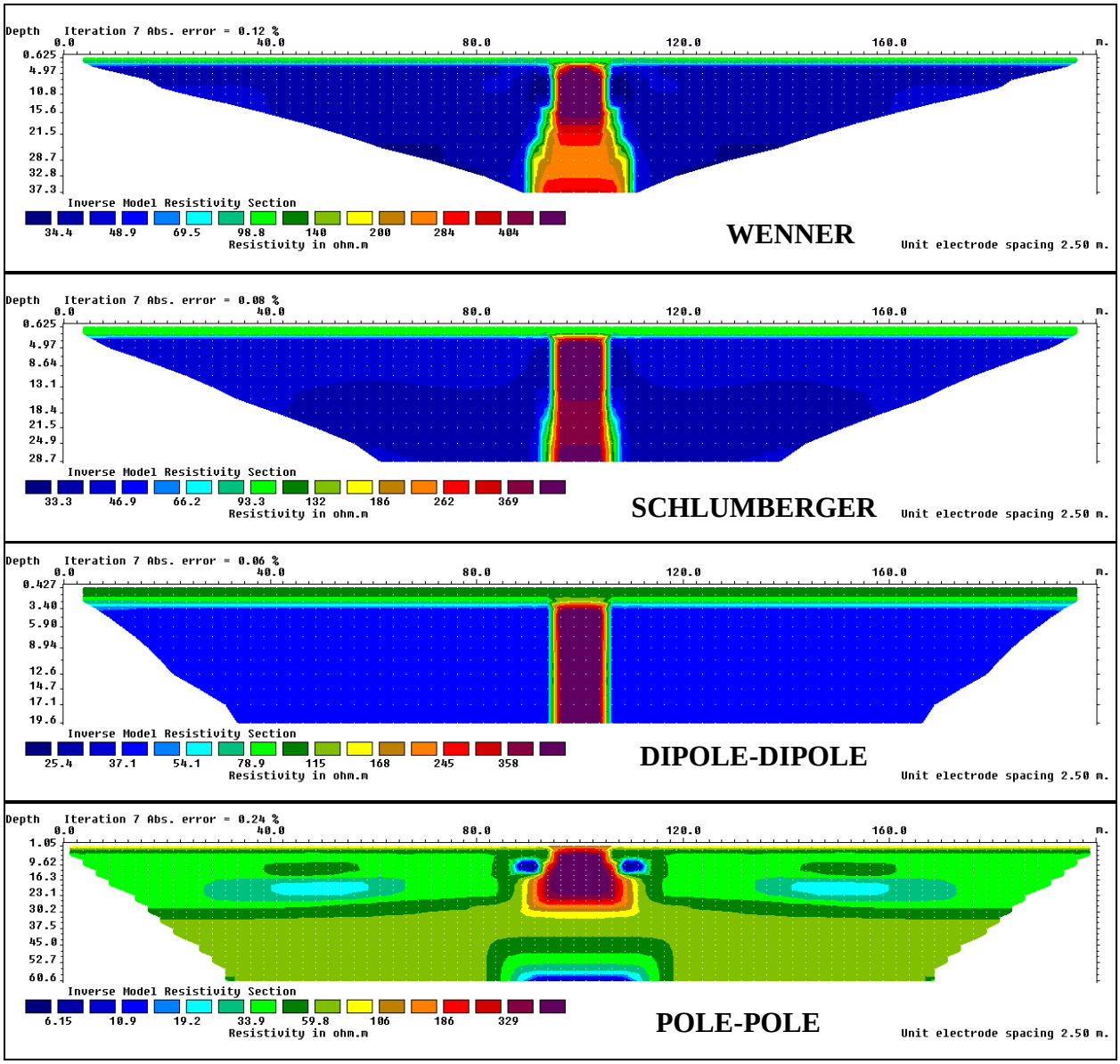

Figure 6-8: Modelled resistivity sections for a vertical thin dyke

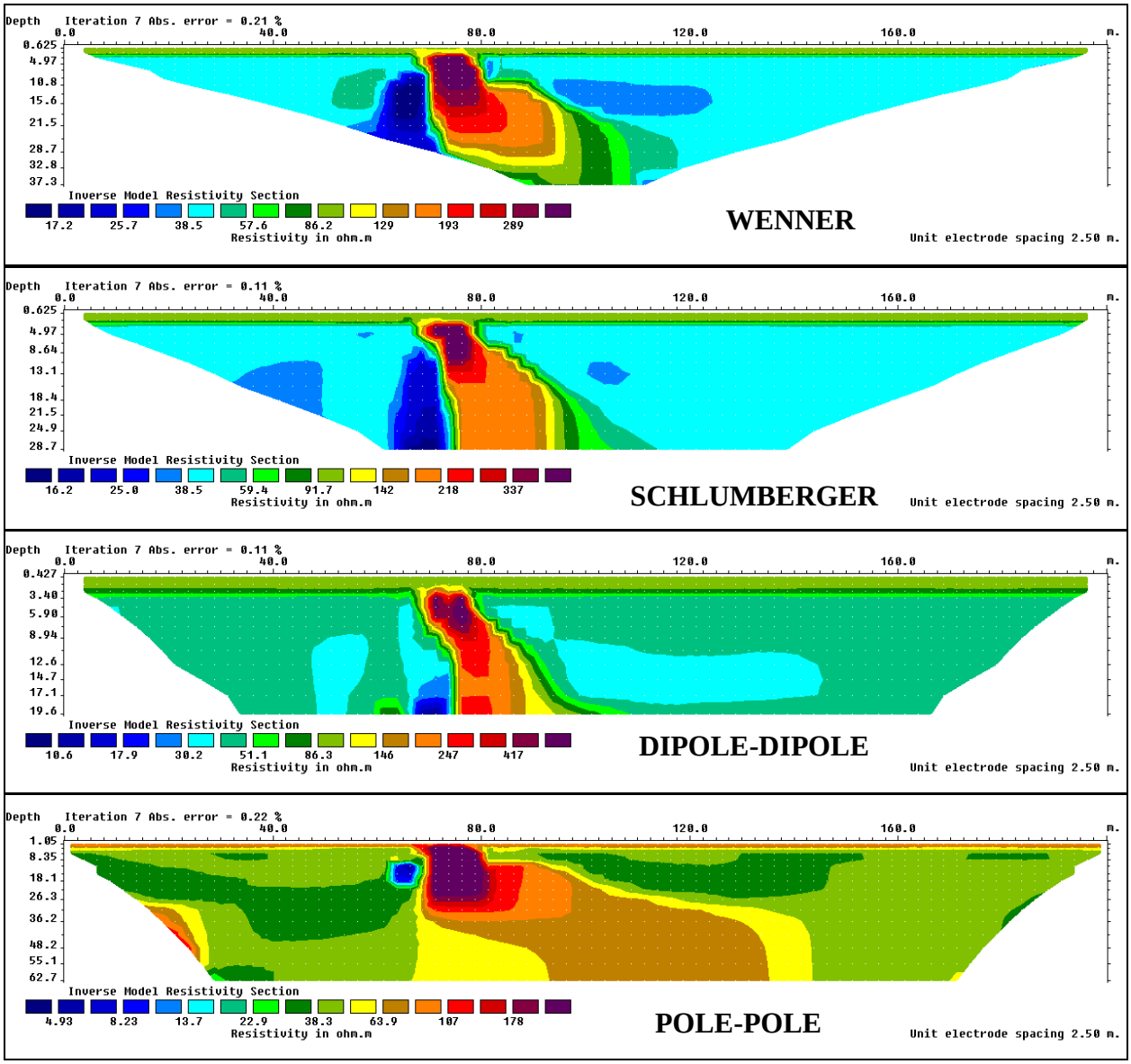

Figure 6-9: Modelled resistivity sections for a dipping thin dyke

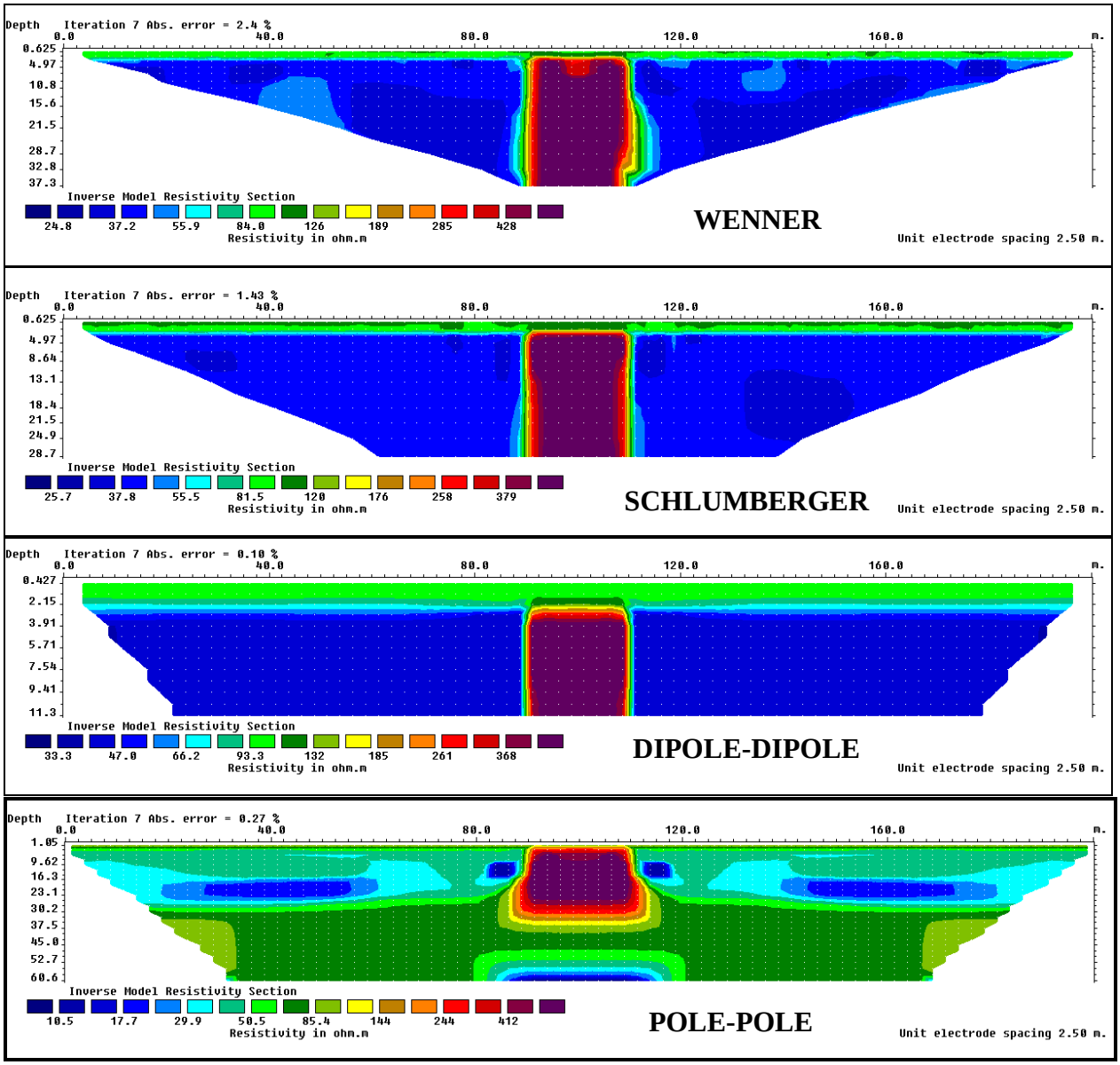

Figure 6-10: Modelled resistivity sections for a vertical thick dyke

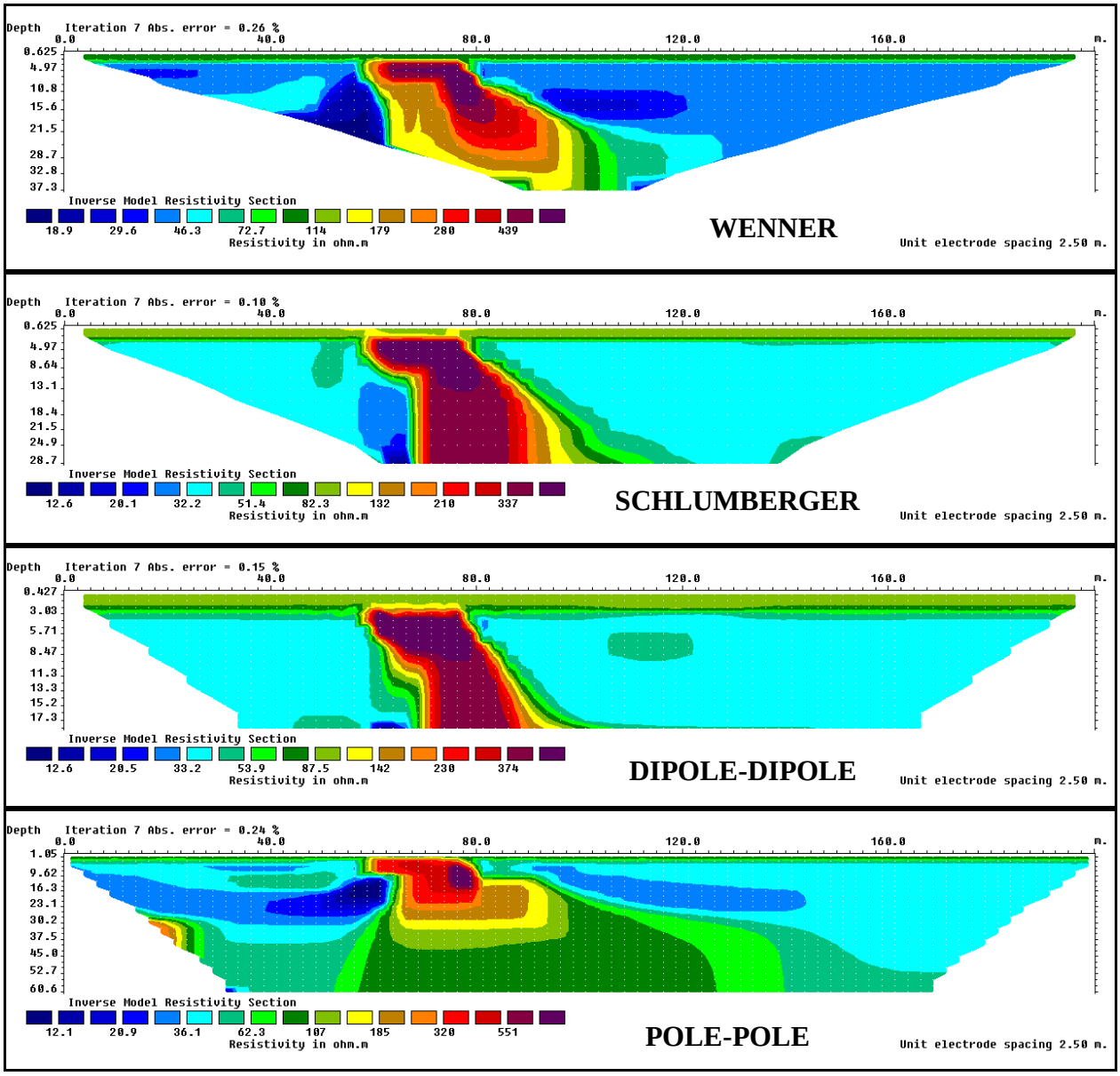

Figure 6-11: Modelled resistivity sections for a dipping thick dyke

Table 6-1 displays the RMS errors for the Wenner, the Schlumberger, the Dipole-Dipole and the Pole-Pole arrays for the four models.

Table 6-1: RMS errors of the vertical and dipping dyke models after seven iterations

MODELS	Root Mean Square errors (in %)			
	Wenner	Schlumberger	Dipole-Dipole	Pole-Pole
Vertical thin dyke	0.12	0.08	0.06	0.24
Dipping thin dyke	0.21	0.11	0.11	0.22
Vertical thick dyke	2.40	1.43	0.10	0.27
Dipping thick dyke	0.26	0.10	0.15	0.24

For every model, comparison between the input resistivity model and the modelled responses (inverse model resistivity sections), was made. It clearly revealed that:

- For the vertical thin dyke and the vertical thick dyke, the modelled resistivity section of the Dipole-Dipole corresponds best with the input resistivity model, followed by the Schlumberger array and the Wenner array. The modelled resistivity section for the Pole-Pole array gives the poorest agreement. The Schlumberger resistivity section shows the presence of a resistive vertical body, the dyke, but the vertical contact between that intrusion and the host rock is not very well defined, as it is for the Dipole-Dipole array. The modelled resistivity section for the Wenner array also reveals the presence of a resistive body, yet the thickness of the body is seen to increase with depth, resulting in a weaker agreement with the input model at depth.

- Concerning the dipping thin dyke and the dipping thick dyke, none of the four electrode arrays performed very well when the modelled resistivity sections are compared to the input resistivity models. The Dipole-Dipole, Schlumberger and Wenner resistivity sections illustrate dipping resistive bodies near the surface, but at greater depths the resistivity models of all of the arrays indicate near-vertical contacts between the resistive dyke and the host rock. The inverse models therefore fail to resolve the dip of the dyke at large depths. The modelled resistivity section for the Pole-Pole array performed the worst in mapping the dipping dykes. The Dipole-Dipole array performs the best in mapping dipping dykes, followed by the Schlumberger array, then the Wenner array.

Results from this analysis suggest that, for field surveys carried out across vertical and dipping structures such as vertical and dipping dolerite dykes (thin or thick), the Dipole-Dipole, Schlumberger and Wenner arrays may be considered, while the Pole-Pole array should be avoided. The Dipole-Dipole array is seen to define vertical and dipping contacts the best, followed by the Schlumberger and Wenner arrays.

Horizontal resistivity changes from the host rock (40 Ω.m) to the vertical or dipping dolerite intrusion (500 Ω.m), and then back to the host rock again, are very well identified by the Dipole-Dipole array compare to the other arrays. However, sharp vertical changes in the resistivity from the overburden material to the dolerite dyke are displayed as gradual changes in the modelled resistivity section of the Dipole-Dipole array. The Dipole-Dipole array is

therefore more sensitive to horizontal changes in the subsurface resistivity. This array may therefore be successful in mapping vertical and dipping structures, but less successful in imaging horizontal contacts.

6.3 MODELLING SILLS ALONE

Dolerite sills are one of the most important geological structures encountered in the Karoo (Botha *et al*., 1998). Groundwater is often encountered at the contact zones between the sill and the surrounding host rock. Since the sill may form a barrier to vertical groundwater flow, groundwater may collect at the top boundary between the sill and the host rock. Sills may also act as barriers to the vertical migration of groundwater contaminants.

In order to investigate the ERT response of dolerite sills in Karoo sedimentary rocks, modelling of these sills as horizontal structures is done in this section. Modelling the responses obtained with various arrays may assist in choosing the most appropriate electrode array for any geological surveys across such structures. In this section, only two synthetic geological models, simulating a thin sill and a thick sill, were used to examine the sensitivities of the Wenner, the Schlumberger, the Dipole-Dipole and the Pole-Pole arrays. The apparent resistivity pseudo-sections for both these models (thin and thick sills) and for the four mentioned electrode arrays are displayed in APPENDIX 2.

6.3.1 Construction of the input resistivity models

As was done during the investigations into the responses from dolerite dyke intrusions (Section 6.2), the input models of a thin sill (Figure 6-12) as well as a thick sill (Figure 6-13) were constructed in a text file which was then saved with the extension .MOD in order to be read by RES2DMOD. The thin sill was 7.5 m-wide, while the thick sill had a thickness of 10.5 m. Both intrusions had a resistivity of 500 Ω.m, and were overlain by an overburden material with a resistivity of 100 Ω.m and underlain by rock material of a low resistivity (40 Ω.m). Both dolerite sills were approximately 150 m-long. For the modelling, an electrode spacing of 2.5 m was used and a total number of 81 electrodes were included. The software RES2DMOD was thereafter used to calculate the apparent resistivity values corresponding to the two models.

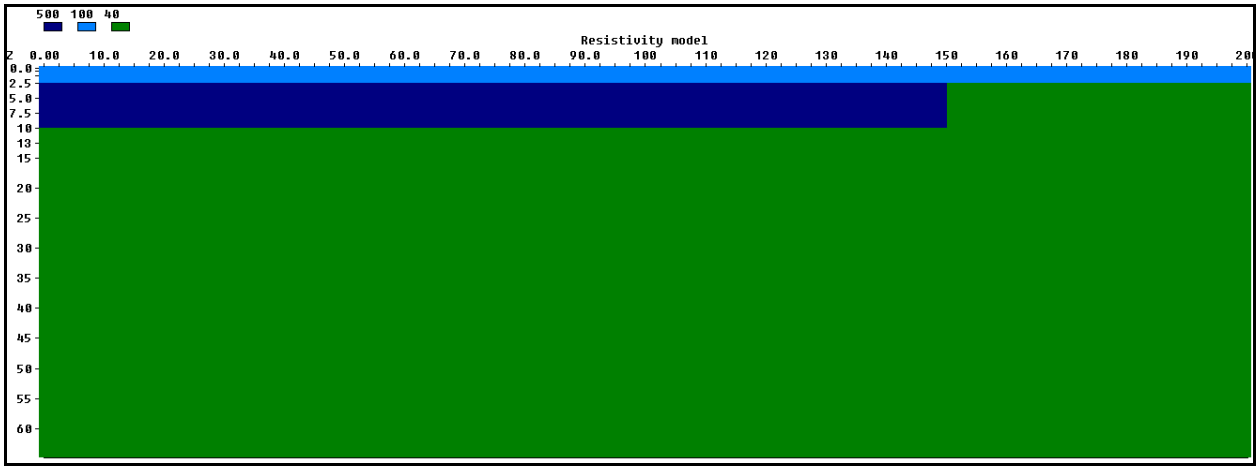

Figure 6-12: Input resistivity model for a thin sill

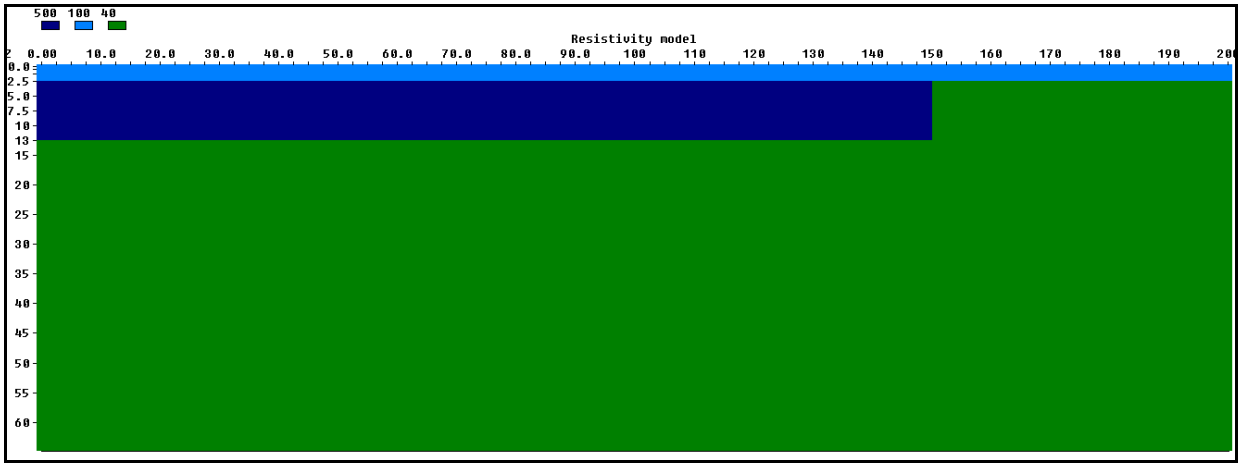

Figure 6-13: Input resistivity model for a thick sill

6.3.2 Inverse model resistivity sections

The least-square inversions were carried out using the L1-norm (robust constraint). The inverse model resistivity sections of the different electrode arrays used are presented in Figure 6-14 and Figure 6-15. Table 6-2 displays the RMS errors obtained after seven iterations for both models.

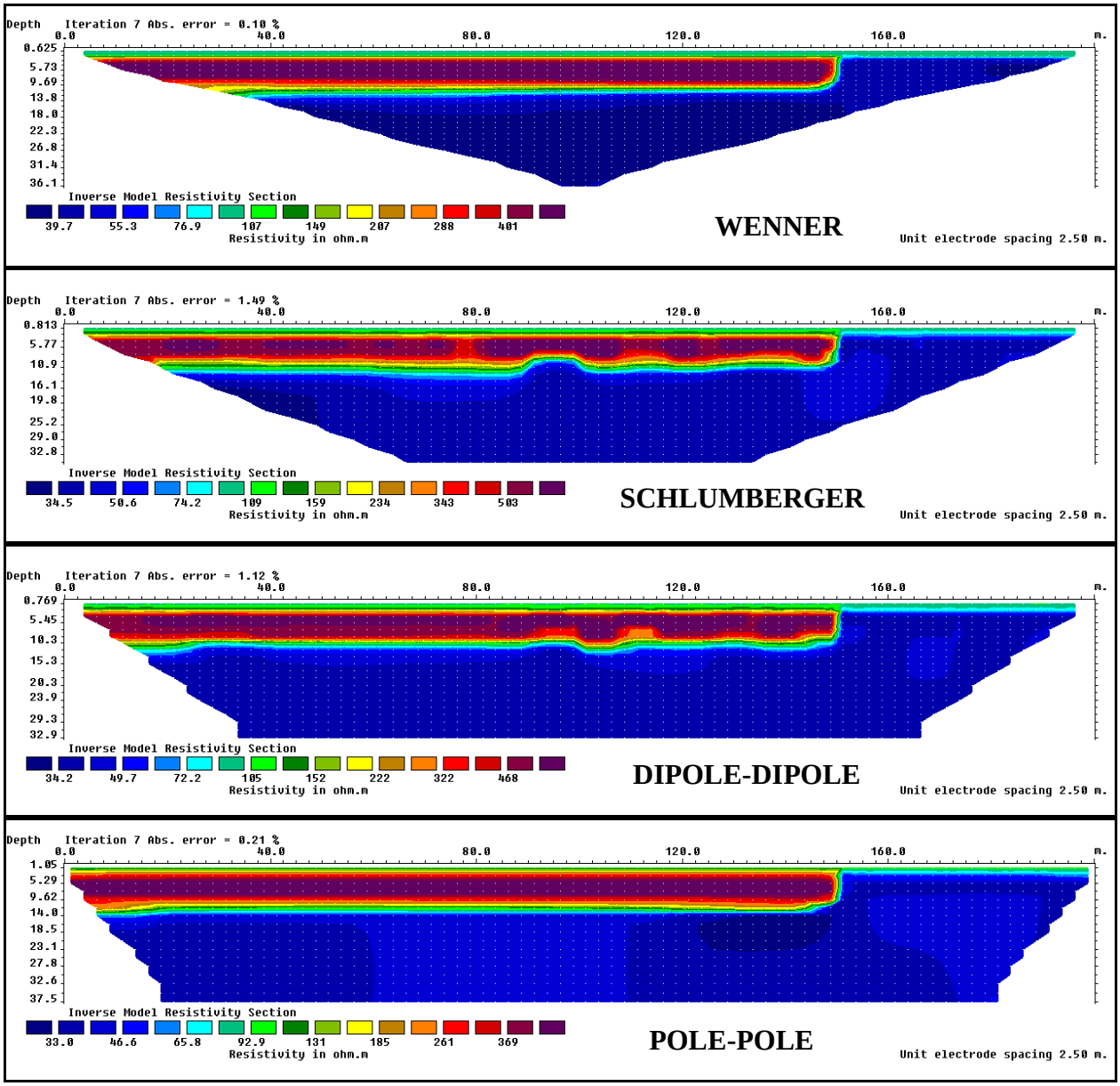

Figure 6-14: Modelled resistivity sections for a thin sill

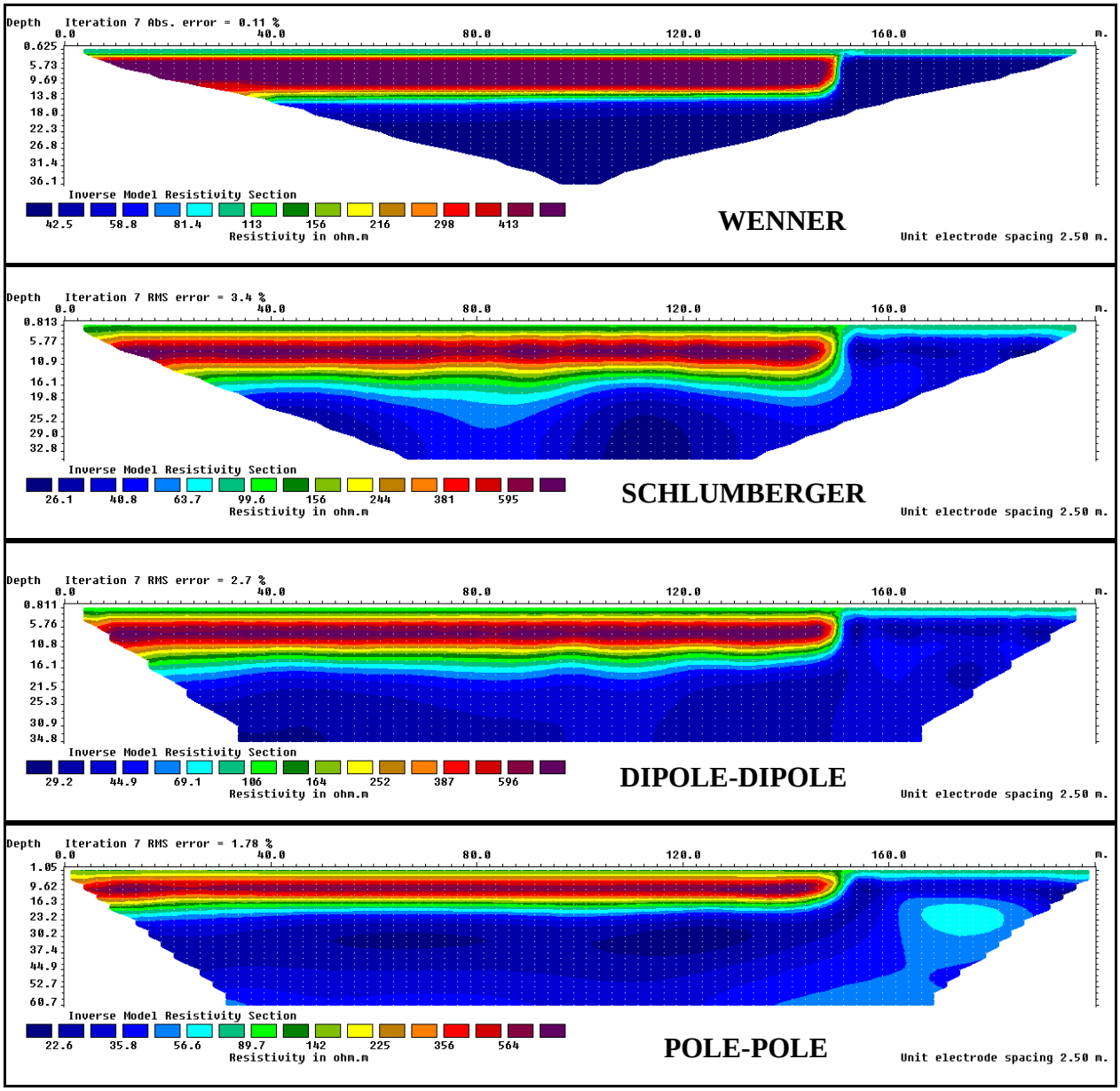

Figure 6-15: Modelled resistivity sections for a thick sill

Table 6-2: RMS errors of the sill models after seven iterations

MODELS	Root Mean Square errors (in %)			
	Wenner	Schlumberger	Dipole-Dipole	Pole-Pole
Thin sill	0.10	1.49	1.12	0.21
Thick sill	0.11	3.40	2.70	1.78

Comparison of the input resistivity models and the modelled responses, for both the thin and the thick sill, shows that the modelled resistivity section of the Wenner array corresponds the best to the input resistivity models, followed by the Pole-Pole array, then the Schlumberger and finally the Dipole-Dipole array. The Schlumberger and Dipole-Dipole modelled

resistivity sections, although showing the presence of the sill, tend to over-estimate the thickness of the sill. The contact between the intrusions and the host rocks is therefore not very well defined by the two arrays. The Wenner array is seen to be the most successful in defining the contact between the sill and the soil materials. Although the modelled resistivity section of the Pole-Pole array also defines the horizontal contacts well, this array is known to be very sensitive to noise (in particular, telluric currents). Due to this limitation, the Pole-Pole array may be less suitable for the mapping of horizontal structures.

The Wenner array successfully identified the sharp vertical changes in resistivity from the overburden material (100 Ω.m), to the dolerite sill intrusion (500 Ω.m), and from the dolerite sill to the soil material (40 Ω.m). On the other hand, the Schlumberger and the Dipole-Dipole arrays produced gradual changes in the modelled subsurface resistivity. The Wenner array is therefore seen to be more sensitive to vertical changes in the subsurface resistivity and may be successfully applied to image horizontal structures such as sills.

From the above modelling results it is concluded that, for ERT surveys across horizontal structures such as thin or thick dolerite sills, the Wenner, Schlumberger and Dipole-Dipole arrays may be considered. For such structures, the Wenner array is the most suitable due to its high sensitivity to vertical changes in the subsurface resistivity.

6.4 MODELLING DYKES WITH SILLS

Dolerite dyke and sill intrusions present in the Karoo are not only encountered as single structures. Very often, many years after the genesis of the first intrusion, another plutonic event can occur, generating a second intrusion which may intersect the first one. The contacts between the two intrusions are usually sought in geohydrological studies, for such contacts may be associated with fresh groundwater or may act as preferential pathways for contaminants.

In this section, the following eight synthetic geological models were simulated and used to examine the sensitivities of four electrode arrays:

- A thin sill intruded by a vertical thin dyke;
- A thin sill intruded by a dipping thin dyke;
- A thin sill intruded by a vertical thick dyke;

- A thin sill intruded by a dipping thick dyke;
- A thick sill intruded by a vertical thin dyke;
- A thick sill intruded by a dipping thin dyke;
- A thick sill intruded by a vertical thick dyke; and
- A thick sill intruded by a dipping thick dyke.

6.4.1 Construction of the input resistivity models

The input resistivity models (Figure 6-16 to Figure 6-23) were again constructed as text files used as inputs to RES2DMOD. Thicknesses of 10 and 20 m were assigned to the thin and thick dykes, respectively, while the thin and thick sills were respectively assigned thicknesses of 5 and 12.5 m. Dips of approximately 60^{o} to 70^{o} were assigned to the dipping dykes. The resistivity values of the overburden, the intrusions and the host rock used were set at 100 Ω.m, 500 Ω.m and 40 Ω.m, respectively. The apparent resistivity pseudo-sections are all displayed in APPENDIX 3.

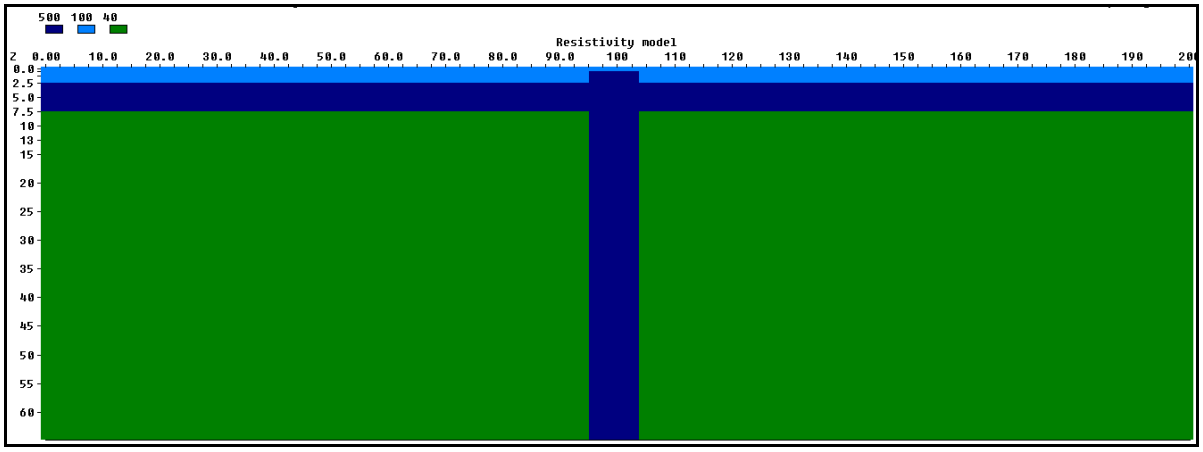

Figure 6-16: Input resistivity model for a thin sill intruded by a vertical thin dyke

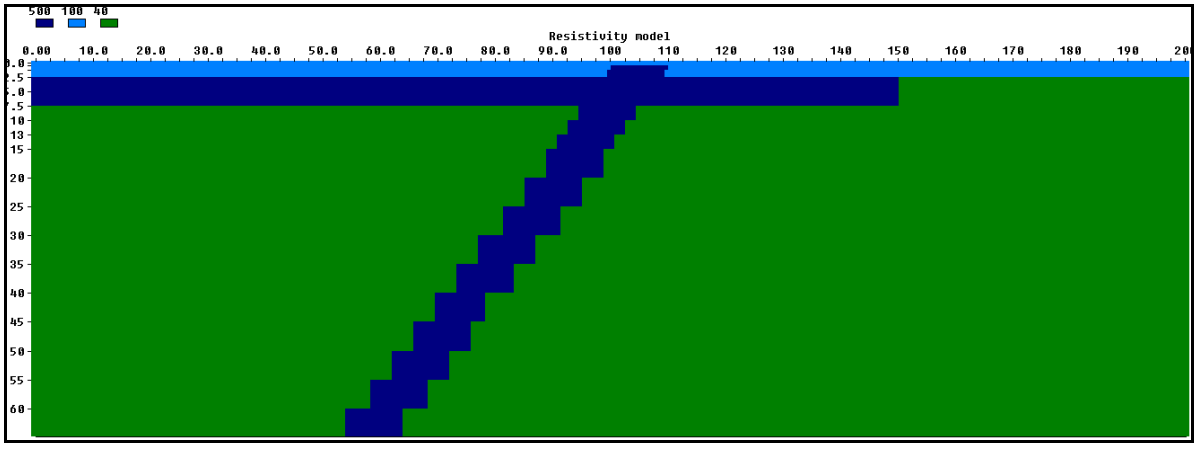

Figure 6-17: Input resistivity model for a thin sill intruded by a dipping thin dyke

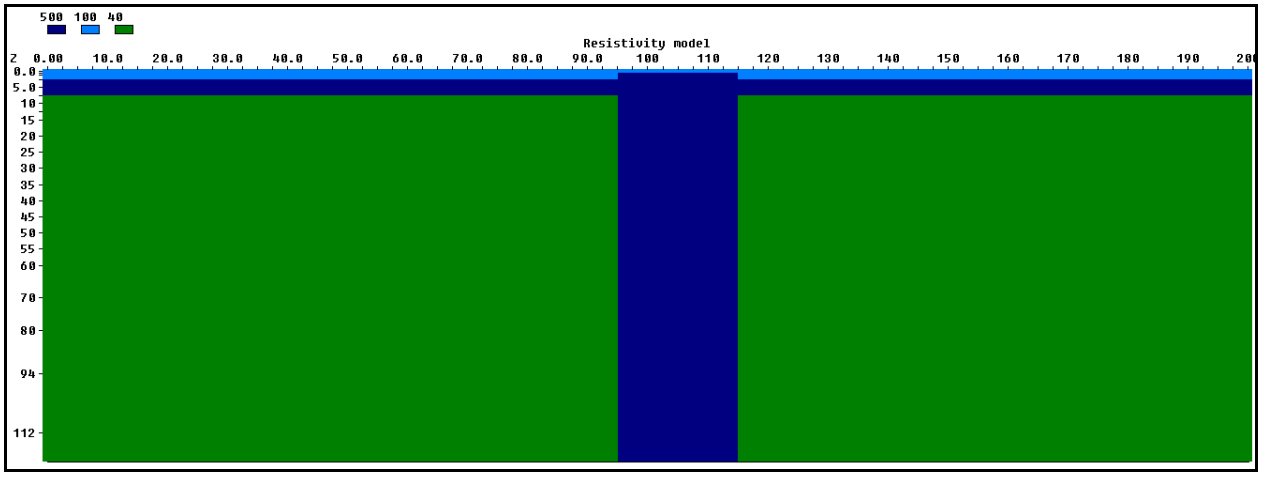

Figure 6-18: Input resistivity model for a thin sill intruded by a vertical thick dyke

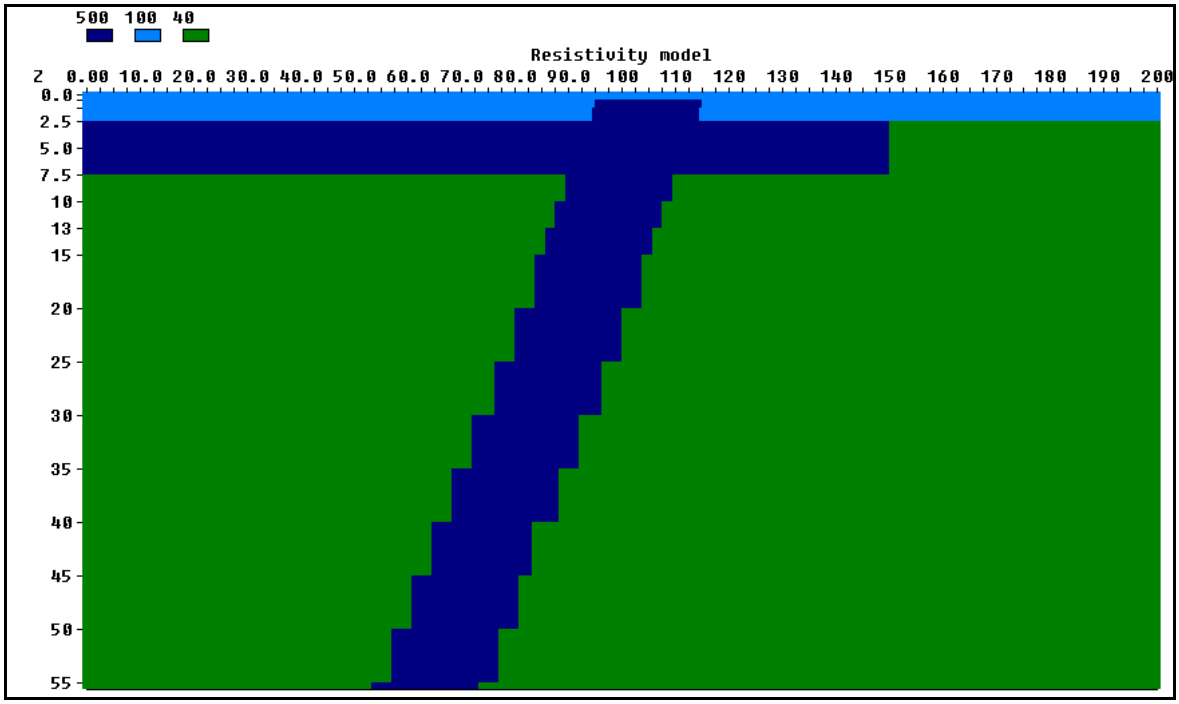

Figure 6-19: Input resistivity model for a thin sill intruded by a dipping thick dyke

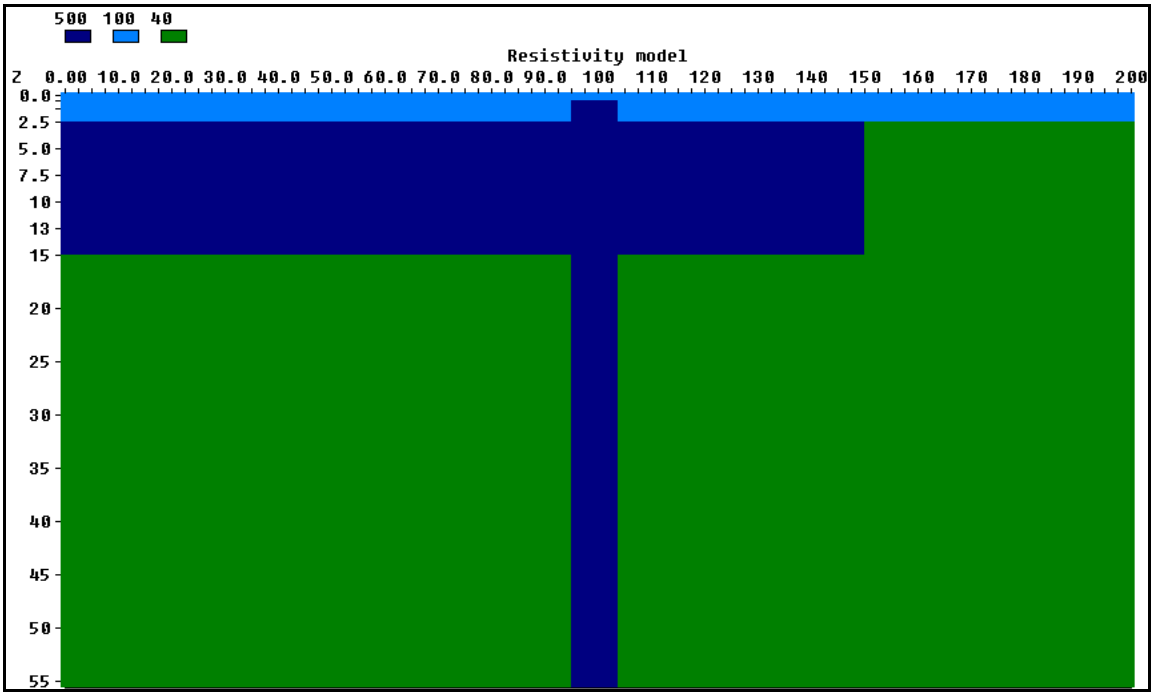

Figure 6-20: Input resistivity model for a thick sill intruded by a vertical thin dyke

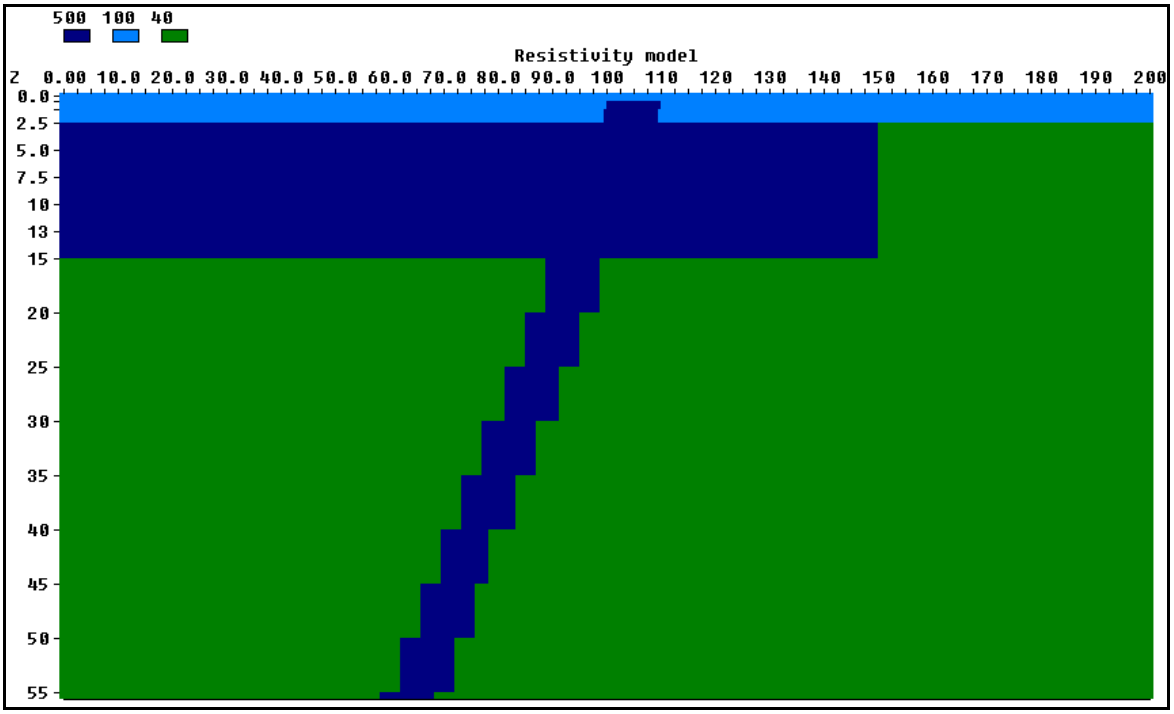

Figure 6-21: Input resistivity model for a thick sill intruded by a dipping thin dyke

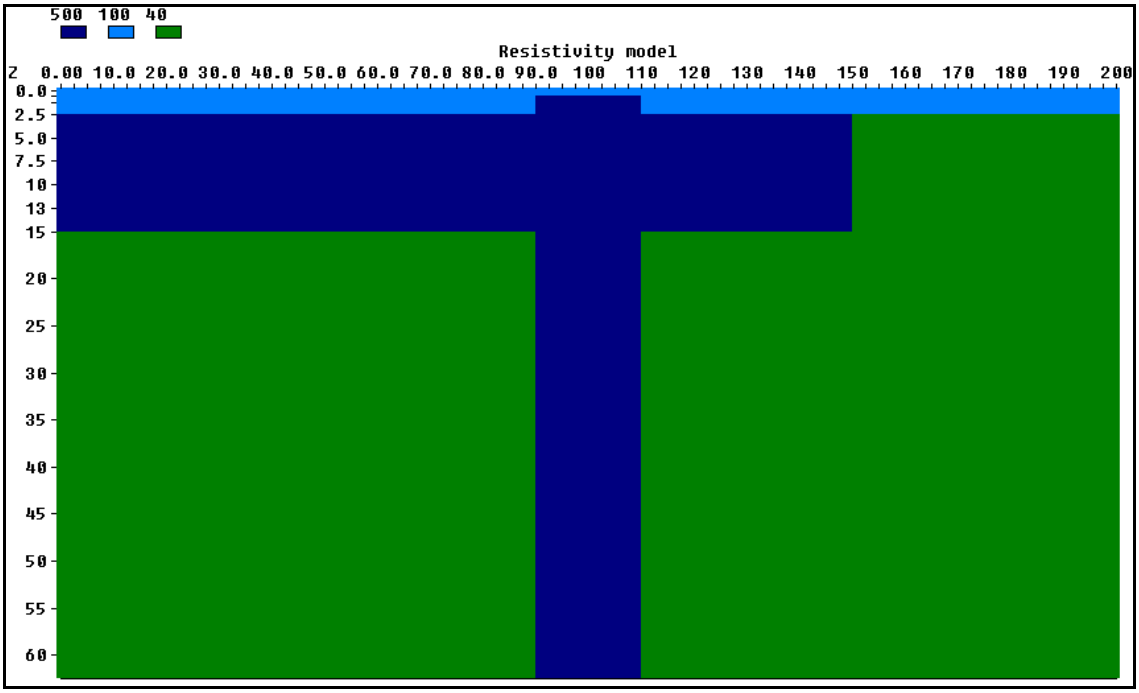

Figure 6-22: Input resistivity model for a thick sill intruded by a vertical thick dyke

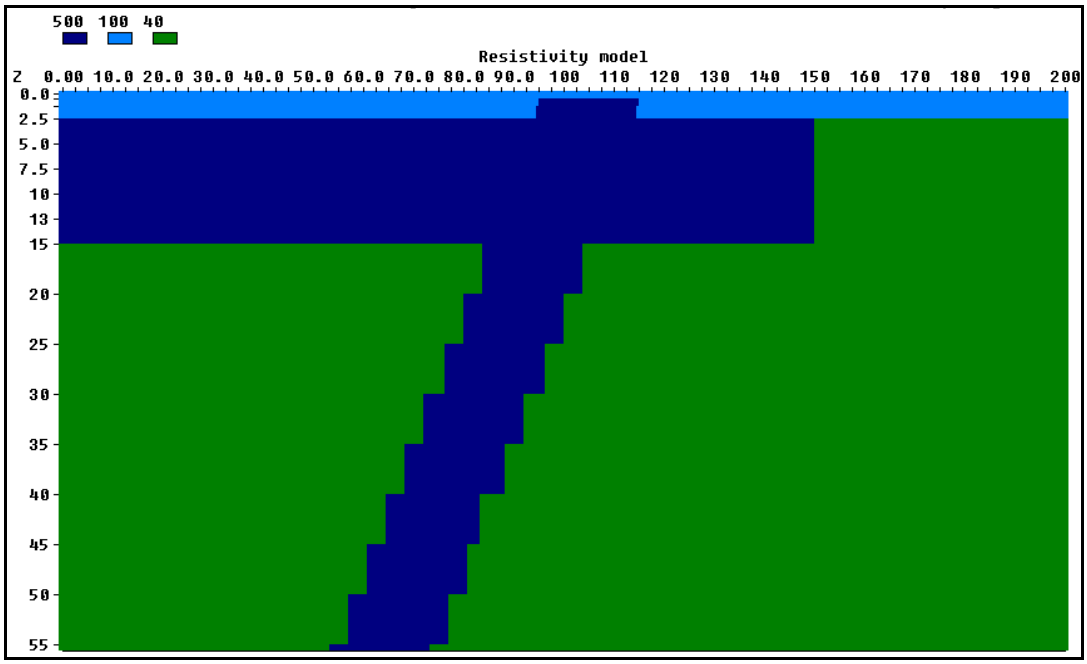

Figure 6-23: Input resistivity model for a thick sill intruded by a dipping thick dyke

6.4.2 Inverse model resistivity sections

The least-square inversions were carried out using the L1-norm (robust constraint). The modelled resistivity sections of the different electrode arrays are presented from Figure 6-24 to Figure 6-31.

It is evident that different electrode arrays produced significantly different modelled resistivity sections, when comparing the input resistivity models to the modelled responses.

For a thin sill intruded by a vertical thin dyke model, the inverse model resistivity section of the Wenner array imaged the sill very well but the dyke is only shown as a resistive body not deeper than 20 m. The modelled resistivity section of the Schlumberger array defined both the dyke and the sill very well, although the transition from the host rock to the dyke appeared to be gradual rather than sharp. The thicknesses of both structures were accurately modelled. This array is thus very sensitive to both the sill and the dyke. The Dipole-Dipole resistivity section displayed both structures well but with some imperfections: Firstly, the thickness of the dyke appeared to be slightly less than 10 m; Secondly, the transition from the overburden material to the intrusion and then to the host rock appeared gradual rather than sharp, and finally, from 105 m to 120 m the upper part of the sill showed some undulations. The Pole-Pole array was the least successful in imaging both the dyke and the sill. It can be seen on the inverse model resistivity section that the vertical thin dyke is only displayed as a resistive high resistivity body not deeper that 26 m. Under the horizontal sill intrusion, appears a zone with resistivity values ranging between 43 Ω.m and 72 Ω.m. Table 6-3 lists the RMS errors obtained after seven iterations for each of the eight models.

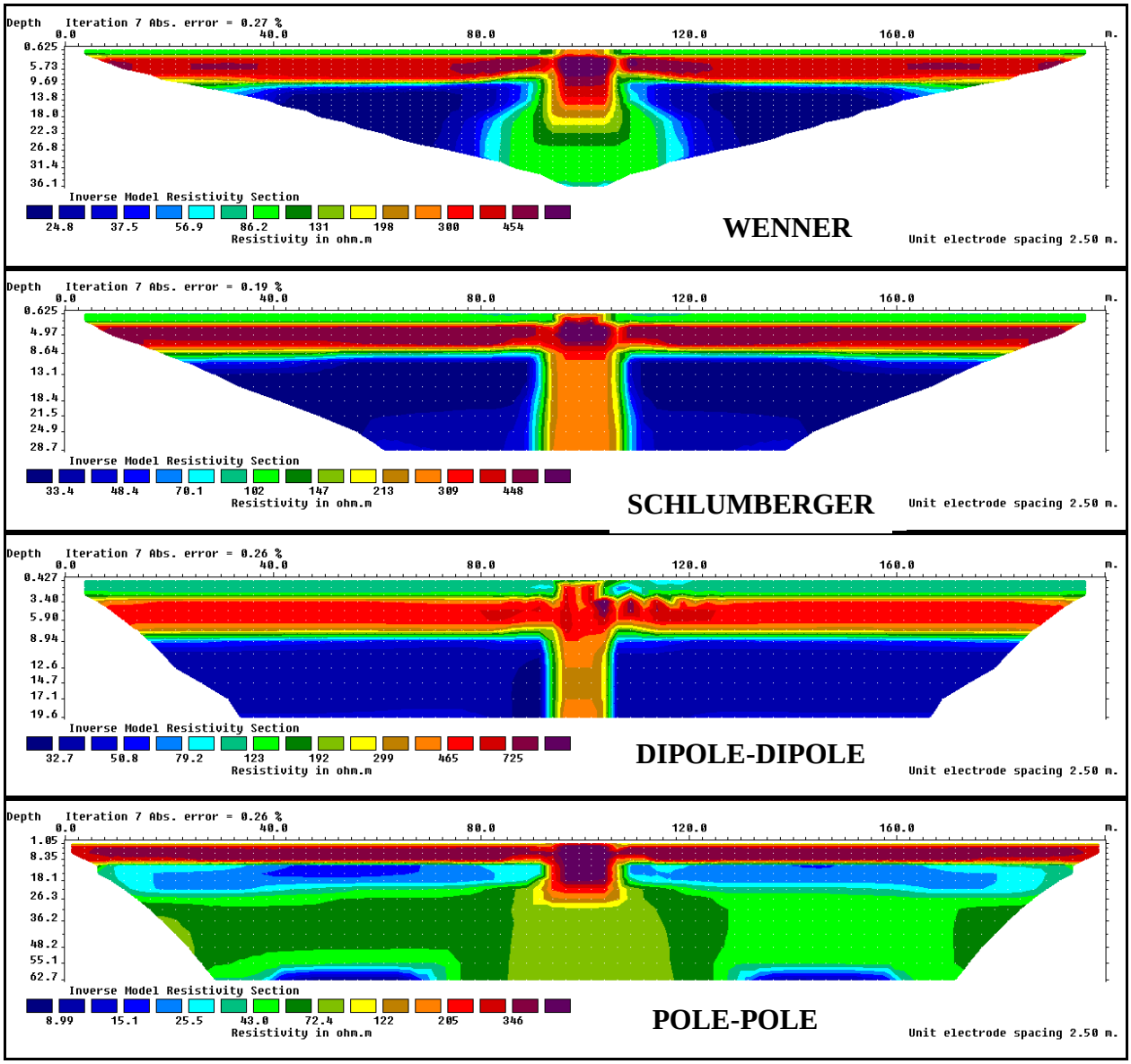

Figure 6-24: Modelled resistivity sections for a thin sill intruded by a vertical thin dyke

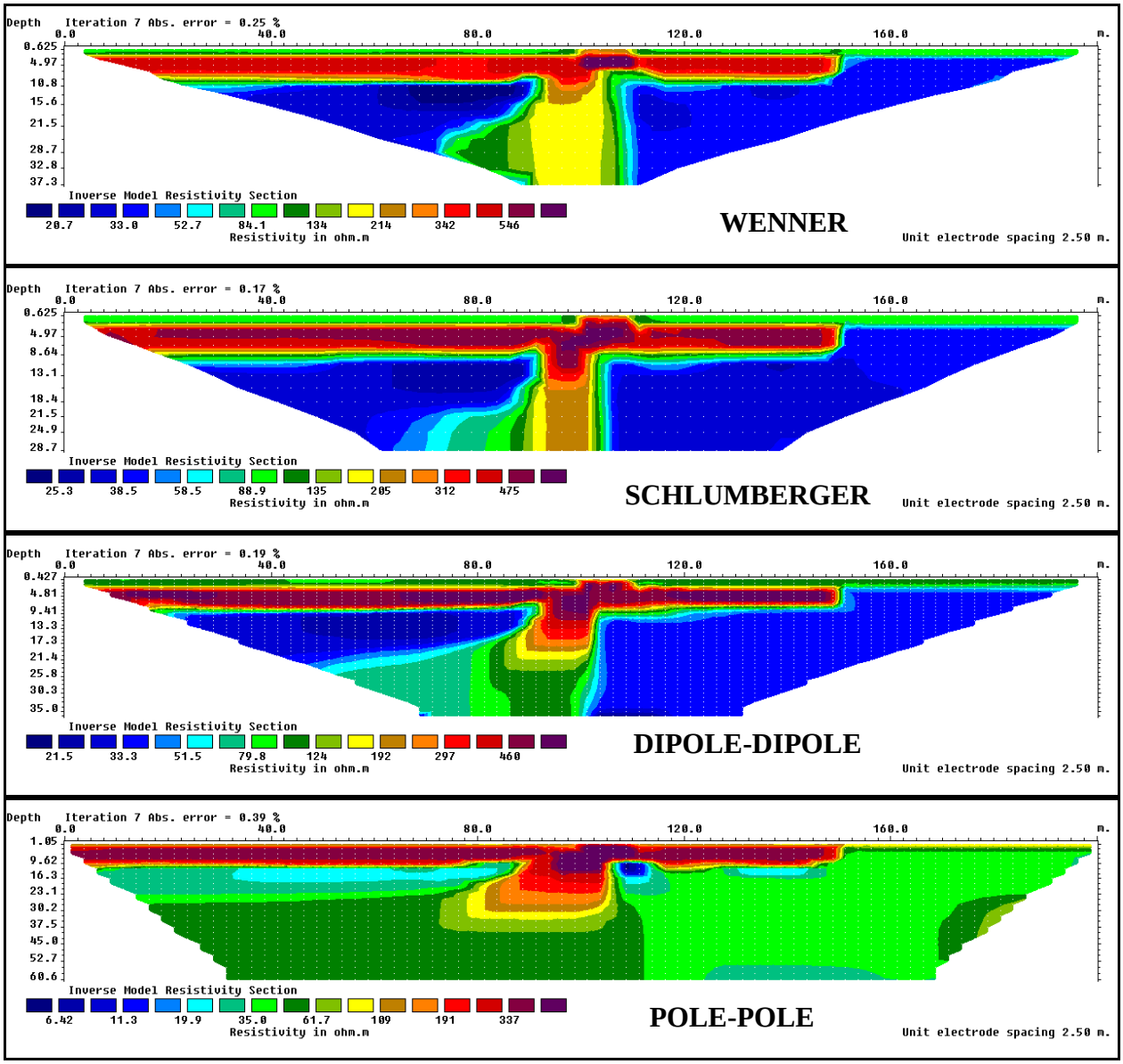

Figure 6-25: Modelled resistivity sections for a thin sill intruded by a dipping thin dyke

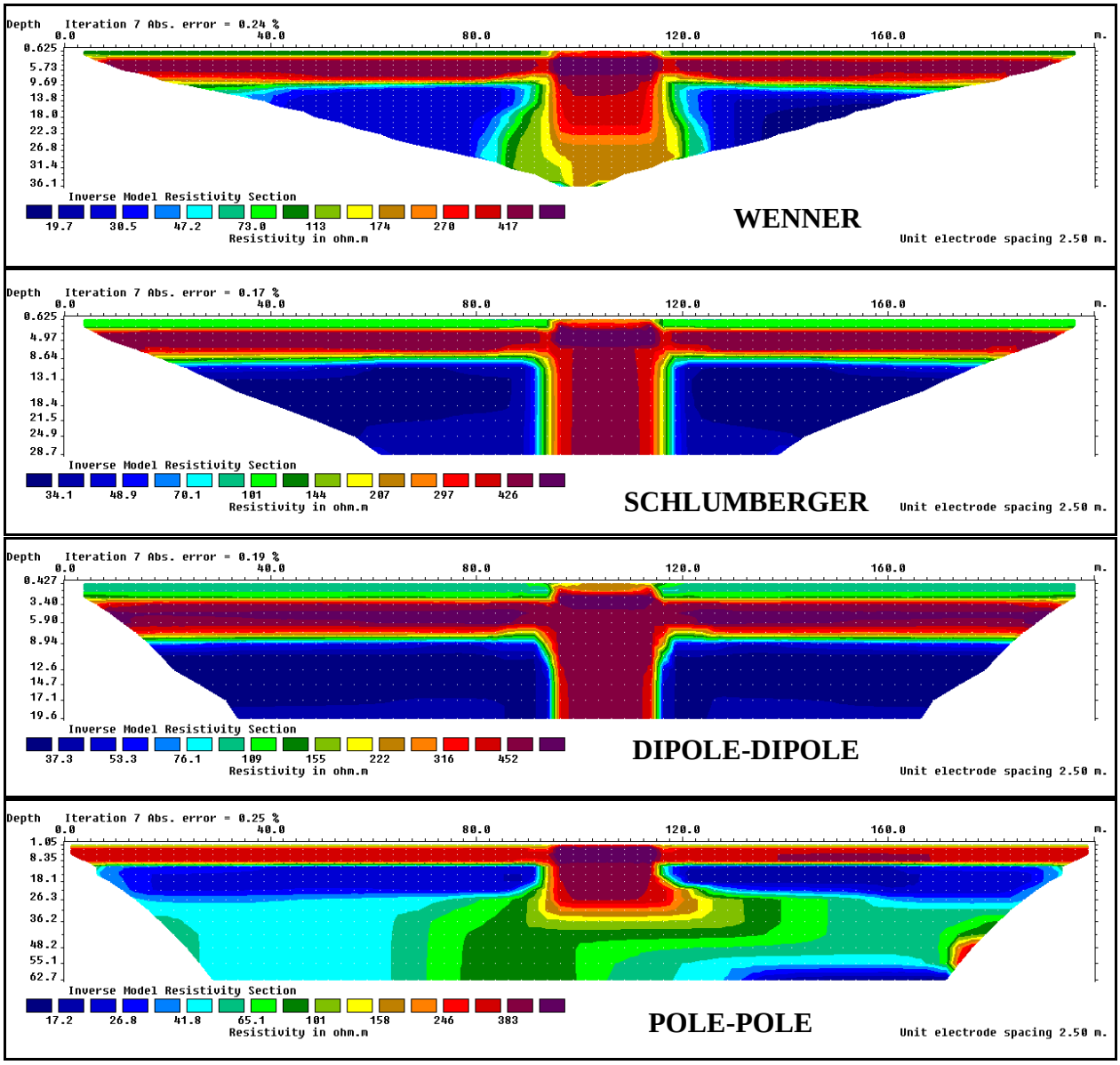

Figure 6-26: Modelled resistivity sections for a thin sill intruded by a vertical thick dyke

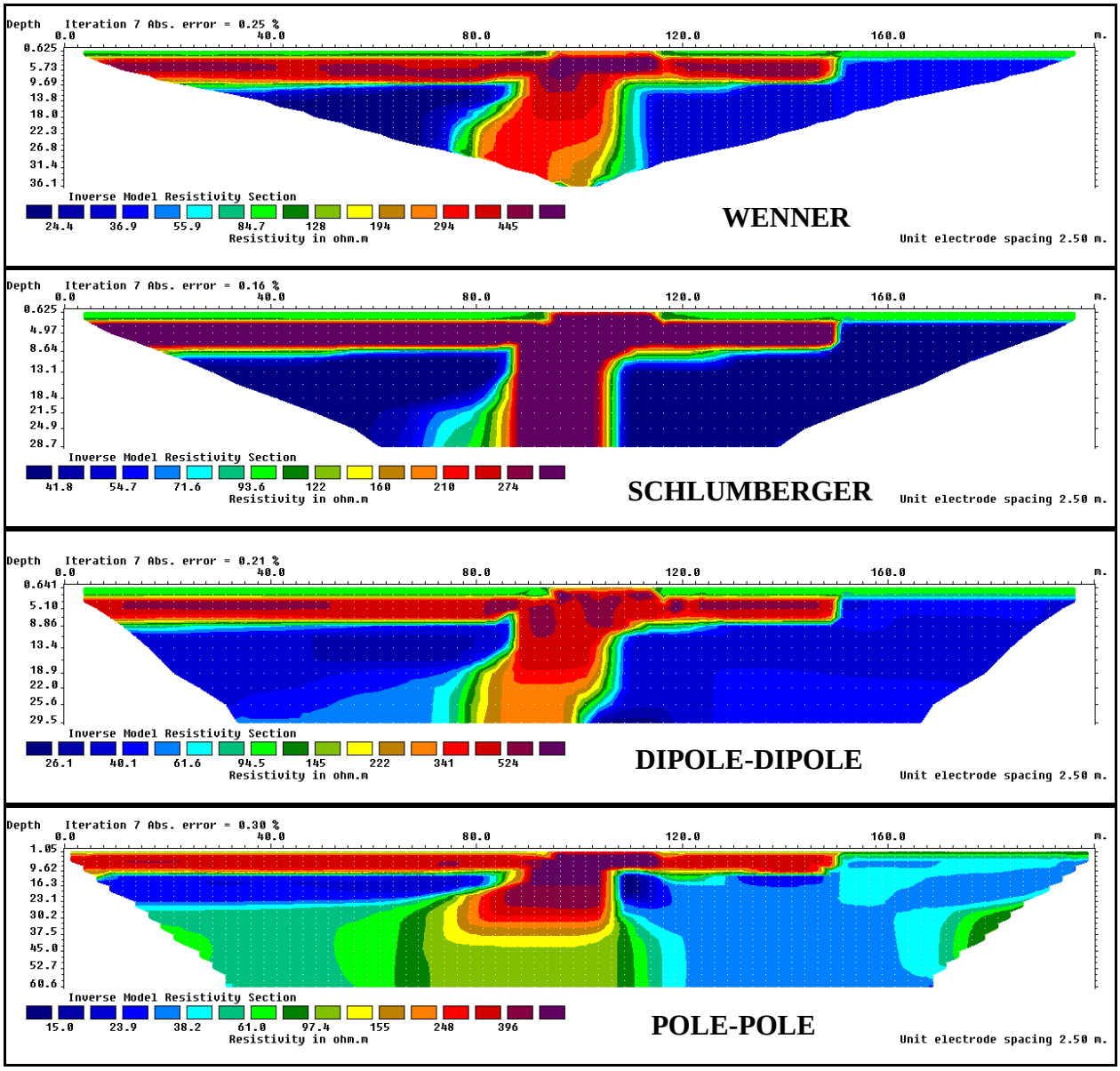

Figure 6-27: Modelled resistivity sections for a thin sill intruded by a dipping thick dyke

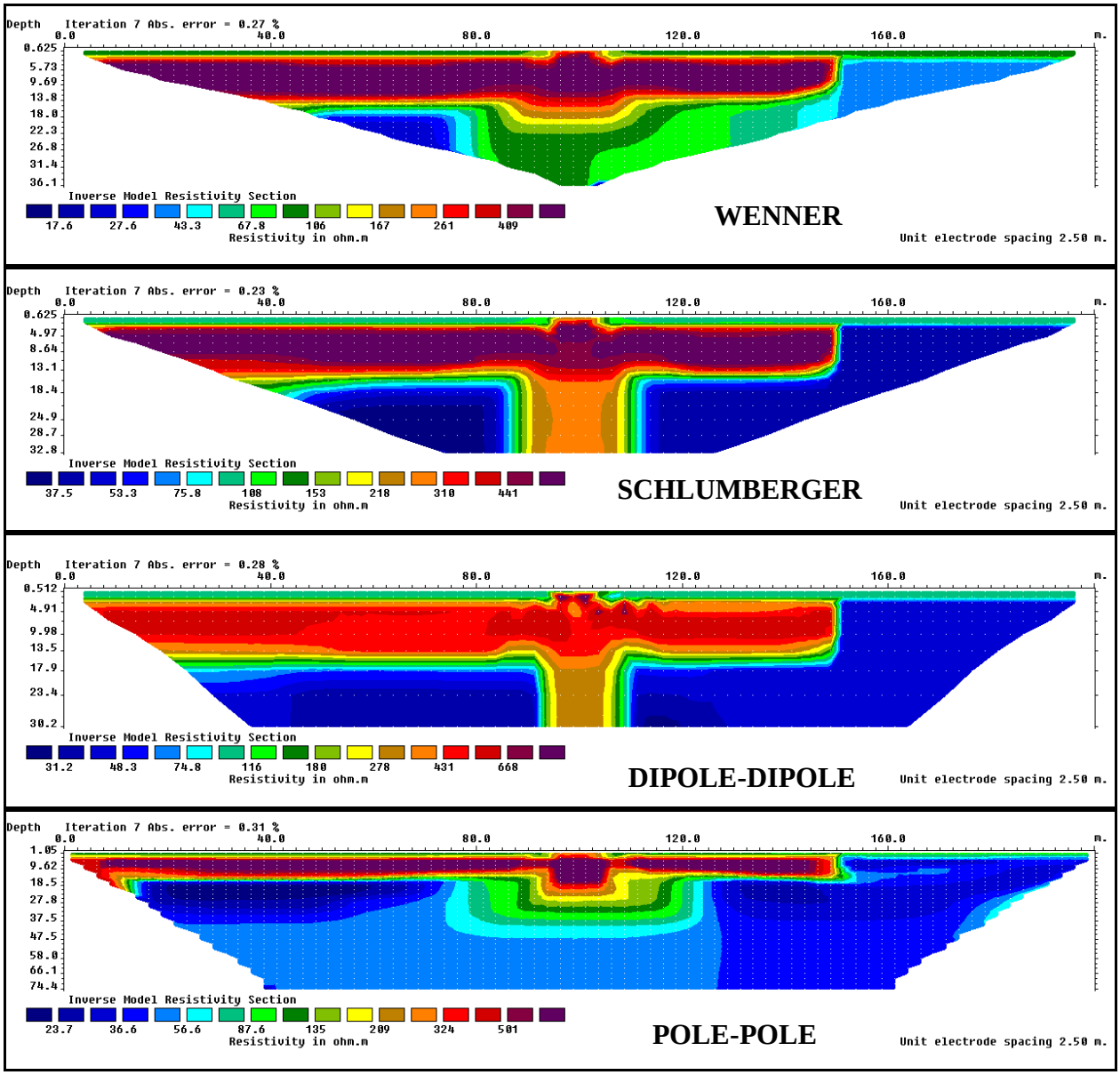

Figure 6-28: Modelled resistivity sections for a thick sill intruded by a vertical thin dyke

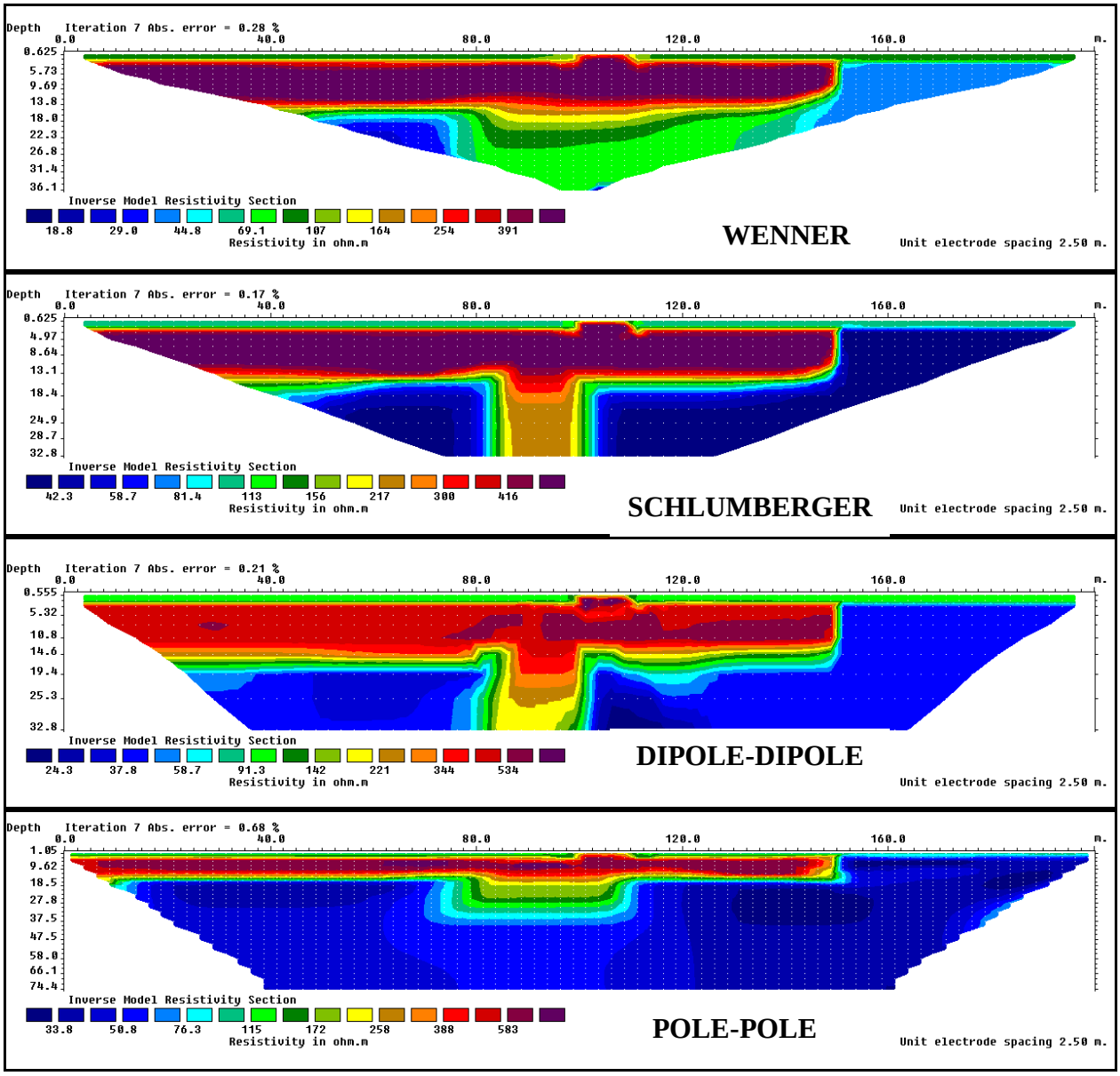

Figure 6-29: Modelled resistivity sections for a thick sill intruded by a dipping thin dyke

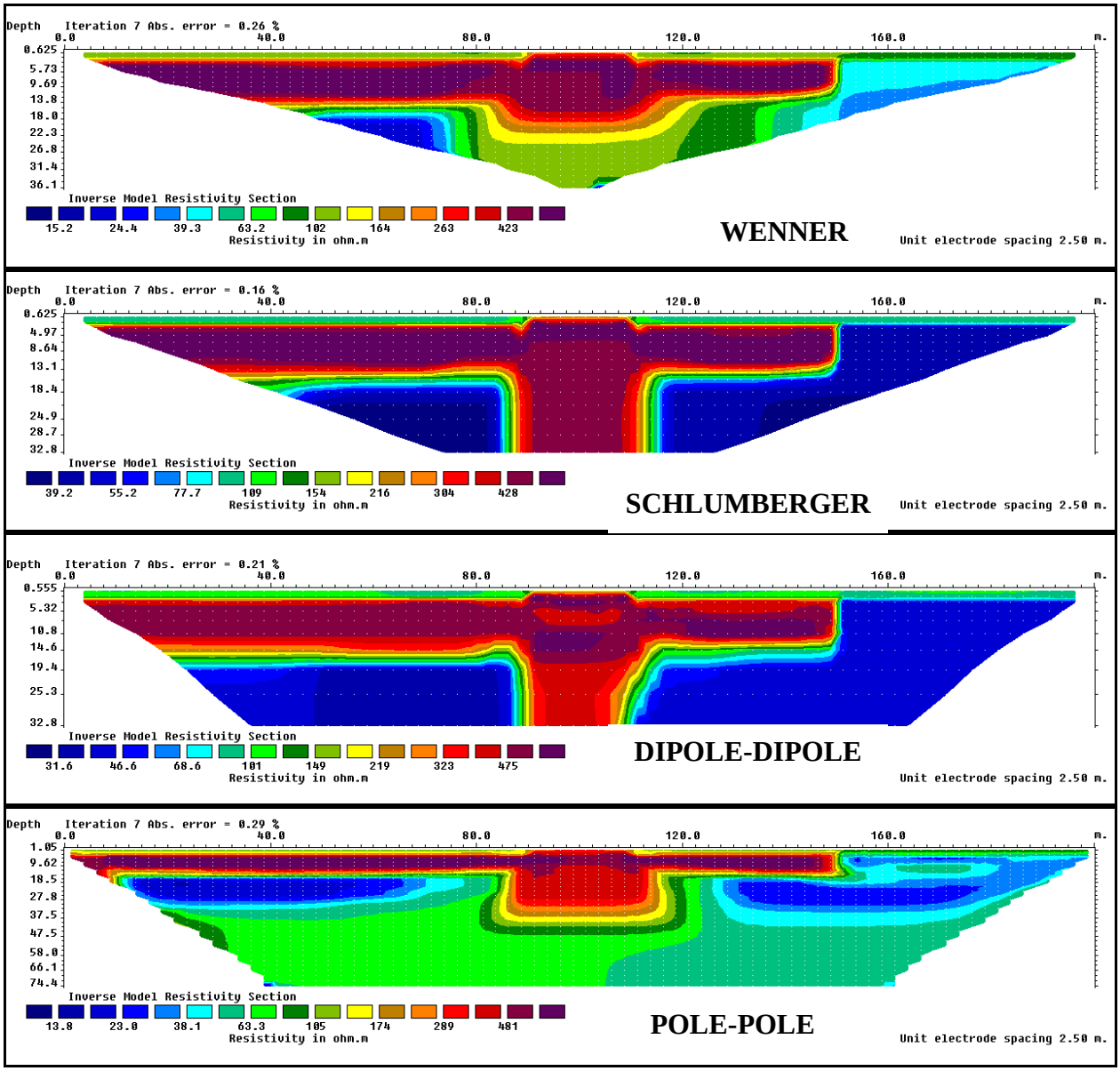

Figure 6-30: Modelled resistivity sections for a thick sill intruded by a vertical thick dyke

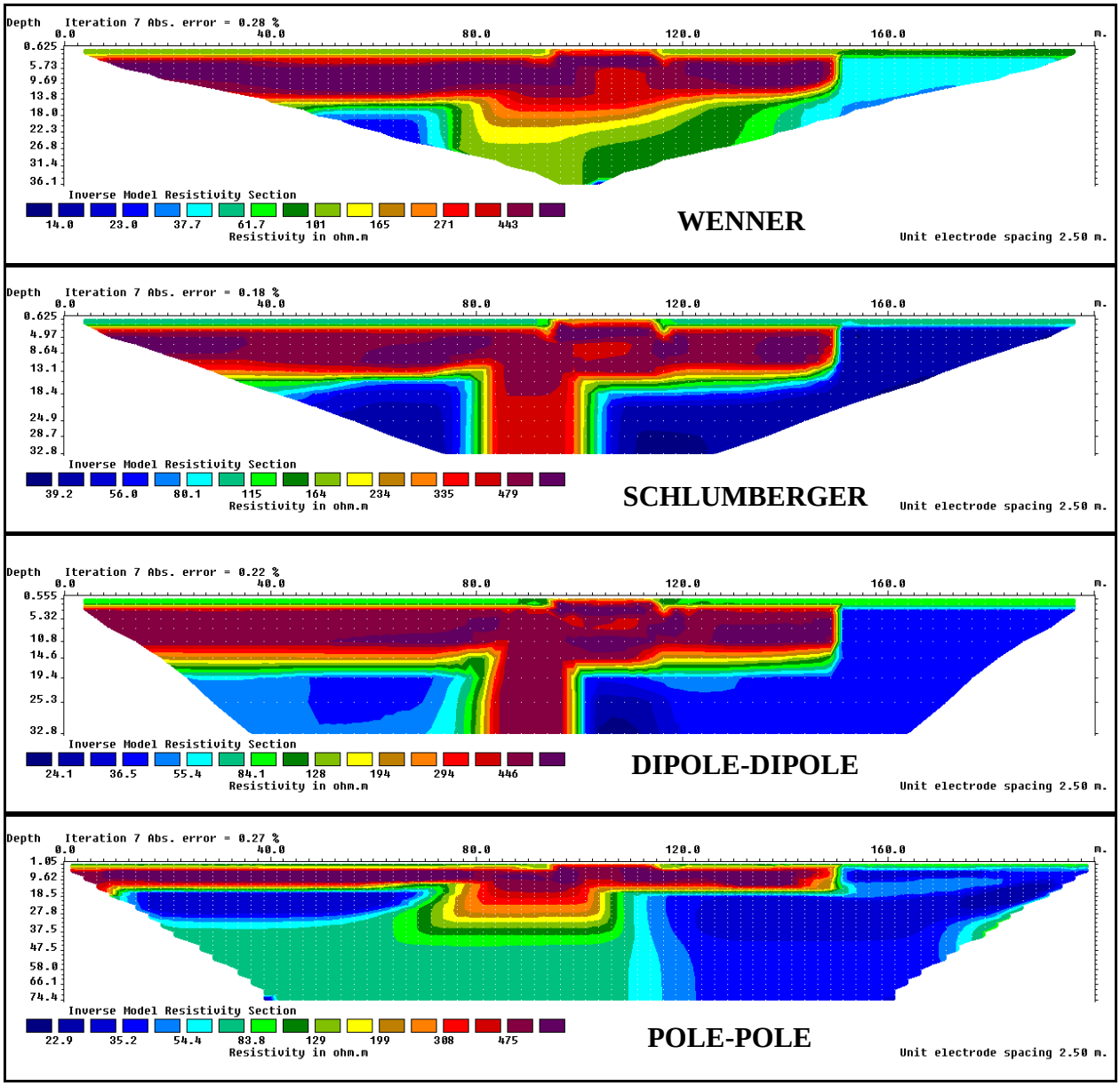

Figure 6-31: Modelled resistivity sections for a thick sill intruded by a dipping thick dyke

Among the four electrode geometries used to evaluate the resistivity responses from vertical thin dykes intruding thin sills, the Schlumberger array was the most successful in defining both the vertical and horizontal contacts. The performances of the different arrays for this model may be ranked in terms of their success in imaging the boundaries as follows: the Schlumberger array, the Dipole-Dipole array, the Wenner array and lastly the Pole-Pole array. Consequently, for resistivity field surveys in areas where both sills and dykes are expected, the Schlumberger array is recommended. The Wenner and Dipole-Dipole arrays may also be used, but the Pole-Pole array should be avoided.

Table 6-3: RMS errors of the sill intruded by vertical and dipping dyke models after seven iterations

MODELS	Root Mean Square errors (in %)			
	Wenner	Schlumberger	Dipole-Dipole	Pole-Pole
Vertical thin dyke - thin sill	0.27	0.19	0.26	0.26
Dipping thin dyke - thin sill	0.25	0.17	0.19	0.39
Vertical thick dyke - thin sill	0.24	0.17	0.19	0.25
Dipping thick dyke - thin sill	0.25	0.16	0.21	0.30
Vertical thin dyke – thick sill	0.27	0.23	0.28	0.31
Dipping thin dyke – thick sill	0.28	0.17	0.21	0.68
Vertical thick dyke – thick sill	0.26	0.16	0.21	0.29
Dipping thick dyke – thick sill	0.28	0.18	0.22	0.27

As was done for a thin sill intruded by a thin dyke (Figure 6-24), modelling investigations were also conducted for a thin sill intruded by a vertical thick dyke (Figure 6-26), a thick sill intruded by a vertical thin dyke (Figure 6-28), and a thick sill intruded by a vertical thick dyke (Figure 6-30). The results from these models were similar with regard to the successes of the arrays in defining the horizontal and vertical contacts: The modelled resistivity sections of the Schlumberger array give the best agreement with the input resistivity models, since both vertical and horizontal contacts are well defined. The performances of the different arrays in imaging both horizontal and vertical structures are ranked as follows: the Schlumberger array, the Dipole-Dipole array, the Wenner array and finally the Pole-Pole array. Once again, the Schlumberger array appeared to be a good compromise between the Wenner and the Dipole-Dipole array in simultaneously mapping both horizontal and vertical geological structures (sills and dykes).

For resistivity surveys in areas where both horizontal and vertical structures are expected, the following arrays may be considered (in order of preference): the Schlumberger, the Wenner and the Dipole-Dipole arrays.

For thin and thick sills intruded by dipping thin and thick dykes models, none of the four electrode arrays performed very well. The Wenner array identified faultlessly the sills, but its model resistivity sections showed weaknesses in picking up the dipping dykes. Results from the Schlumberger profiles demonstrated that this array has a poor capability in resolving dipping structures; it tends to model them as vertical structures. Nonetheless, its image

resolution towards horizontal structures is very good. The Dipole-Dipole model resistivity sections displayed both structures (sills and dipping dykes) but less effective than the Schlumberger array. The vertical changes were gradually made, which consequently increased the thicknesses of the sills; the dykes are displayed as vertical structures rather than dipping structures as made initially in the conceptual models. The modelled resistivity sections from the Pole-Pole array illustrated the most uncertainties in the modelling process.

Although the Schlumberger array itself presented some pits in its inverse model resistivity sections, this array is the most suitable configuration that offers less anomalies in detecting or mapping thin and thick sills intruded by dipping thin and thick dykes. The array performance for these models is ranked as follow: the Schlumberger array, the Dipole-Dipole array, the Wenner array and the Pole-Pole array. Once more, the Schlumberger array showed to be the most sensitive to dipping and horizontal structures. Indeed, resistivity field surveys across such structures should be conducted by the Schlumberger, the Dipole-Dipole and the Wenner arrays.

This modelling exercise indicates that the suitable arrays for field investigations carry out over two or many structures displayed horizontally and vertically/obliquely are the Schlumberger, the Wenner and the Dipole-Dipole arrays. Among these arrays, the Schlumberger is the most appropriate for it defines the best the horizontal and vertical/dipping contacts between the Earth subsurface materials.

6.5 MODELLING WEATHERED ZONE

6.5.1 A conceptual model of a weathered zone

A numerical model simulating a weathered zone was designed in this section for the purpose of evaluating the suitability of the Wenner, the Schlumberger, the Dipole-Dipole and the Pole-Pole arrays for resistivity field surveys across such features. The resistivity model (Figure 6-32) consisted of an overburden with a 1 m thickness, with a resistivity value of 500 Ω.m; a weathered zone with a width of 10 m and a thickness of 3.4 m, with very low resistivity (10 Ω.m), overlain by the overburden and underlain by rocks with resistivity value of 200 Ω.m. A number of 81 electrodes were used in the program, with a spacing of 1 m. The apparent resistivity pseudo-sections are displayed in APPENDIX 4.

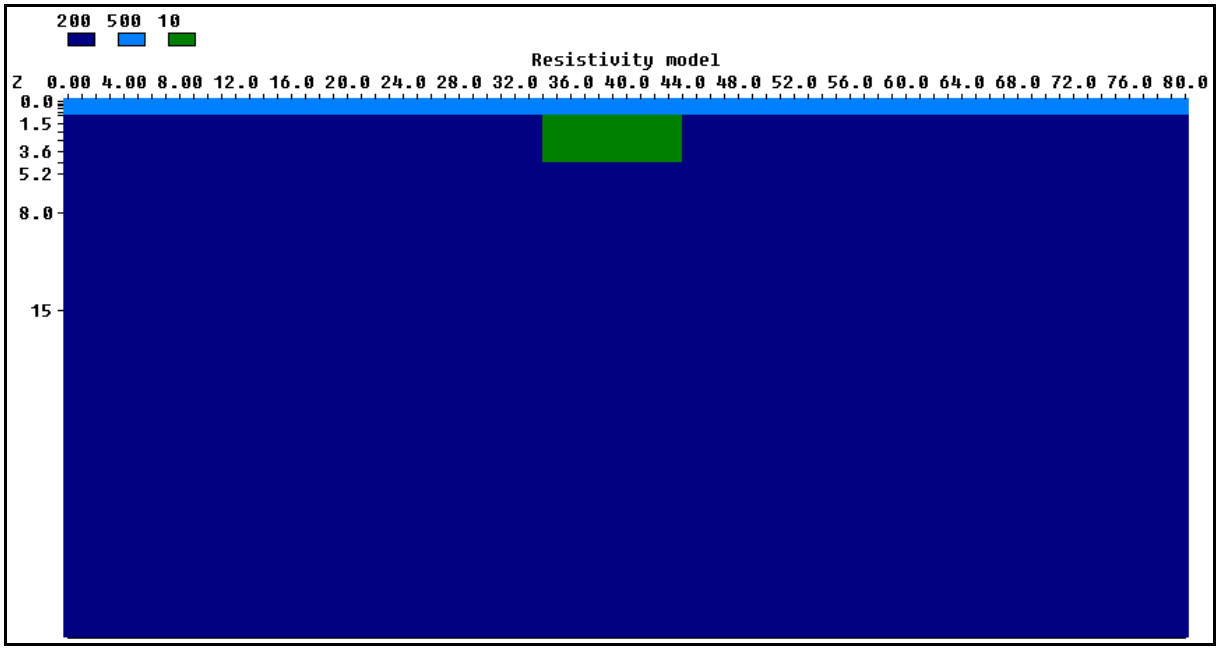

Figure 6-32: Input resistivity model for a weathered zone

6.5.2 Inverse model resistivity sections

For the least-square inversion, the L1-norm (robust constraint inversion) was selected. The model resistivity sections of the different electrode arrays are presented in Figure 6-33.

The RMS errors, obtained after seven iterations, for the Wenner, the Schlumberger, the Dipole-Dipole and the Pole-Pole arrays are respectively 0.12%, 0.12%, 0.26% and 0.17%.

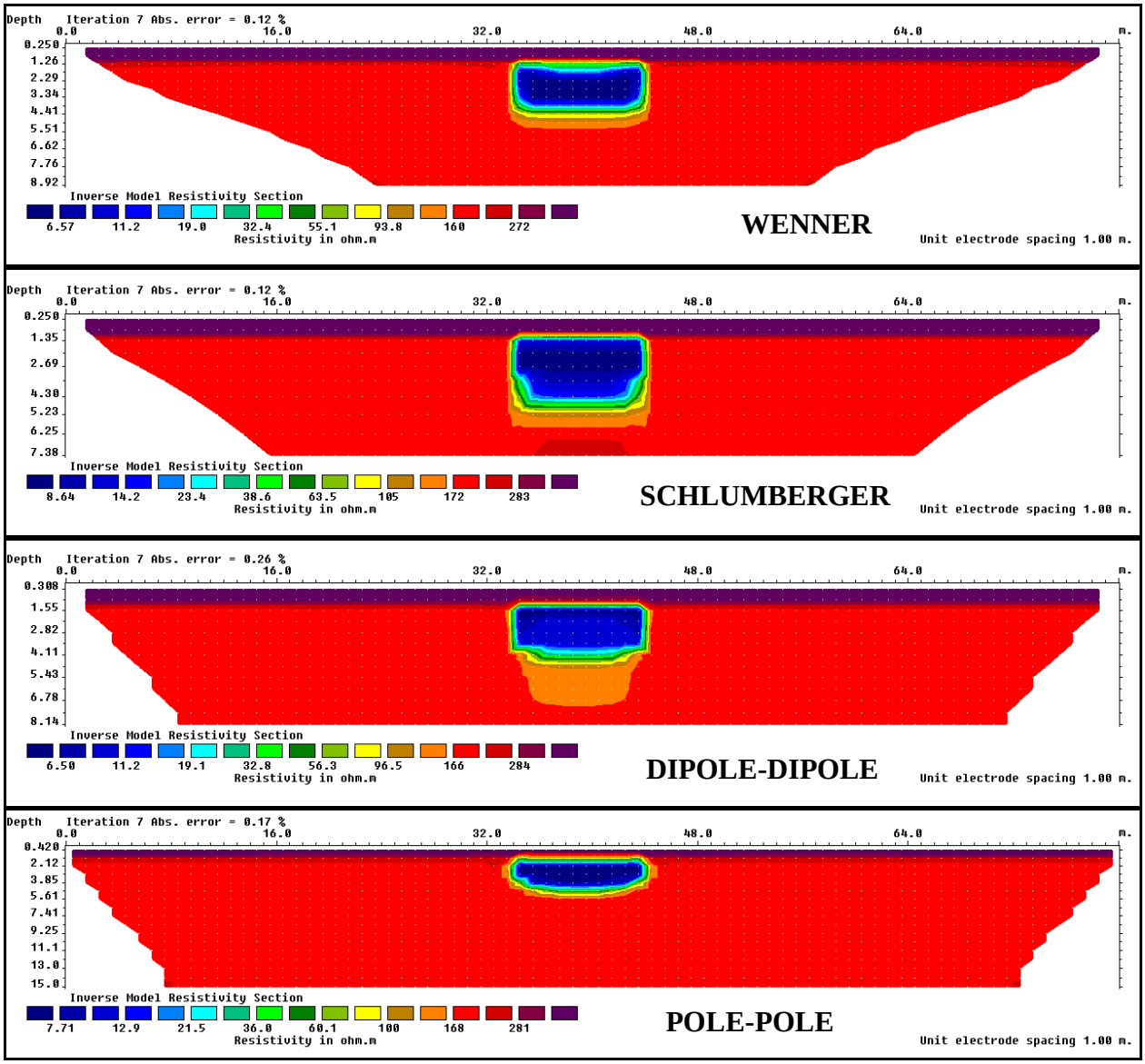

Figure 6-33: Modelled resistivity sections for a weathered zone

The Wenner, Schlumberger and Dipole-Dipole arrays identified the low resistivity zone well compared to the Pole-Pole array whose inverse model resistivity section tended to represent an oval low resistivity zone rather than a rectangular body as in the input resistivity model. The Schlumberger and the Dipole-Dipole modelled resistivity sections imaged the horizontal changes in resistivity very well, but were less successful in imaging the vertical changes in resistivity. Compared to the Schlumberger and Dipole-Dipole arrays, the Wenner array imaged the vertical changes in resistivity better. This result confirmed once more the sensitivity of the Dipole-Dipole array to horizontal changes in subsurface resistivity as well as the sensitivity of the Wenner array to vertical changes in the subsurface resistivity. Thus, for resistivity field surveys carried out across weathered zones, it is recommended that the

following three electrode arrays be used in order of preference: the Wenner, the Dipole-Dipole and the Schlumberger arrays.

6.6 MODELLING BOUNDARIES

Vertical, dipping and horizontal boundaries models are the three synthetic geological models used in this section to examine the sensitivities of four electrode arrays. The input models consist of two materials of different resistivities (500 Ω.m and 100 Ω.m) making a vertical contact with one another (Figure 6-34), having a dipping boundary of 45^{o} (Figure 6-35), and finally having a horizontal boundary (Figure 6-36). The apparent resistivity pseudo-sections are displayed in APPENDIX 5. The inverse model resistivity sections are displayed from Figure 6-37 to Figure 6-39. In Table 6-4, the RMS errors obtained after seven iterations for each model are presented for the different arrays.

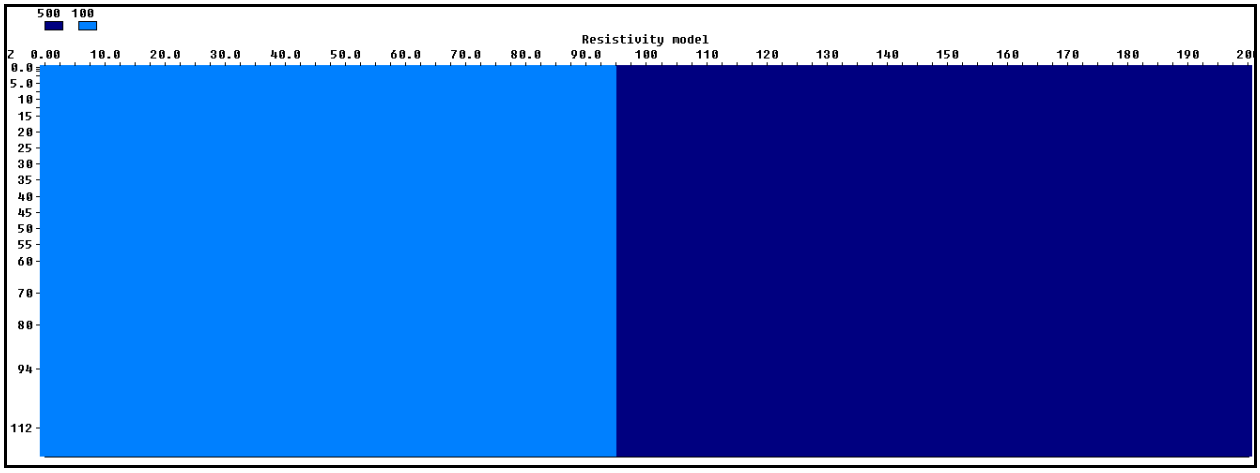

Figure 6-34: Input resistivity model for a vertical boundary

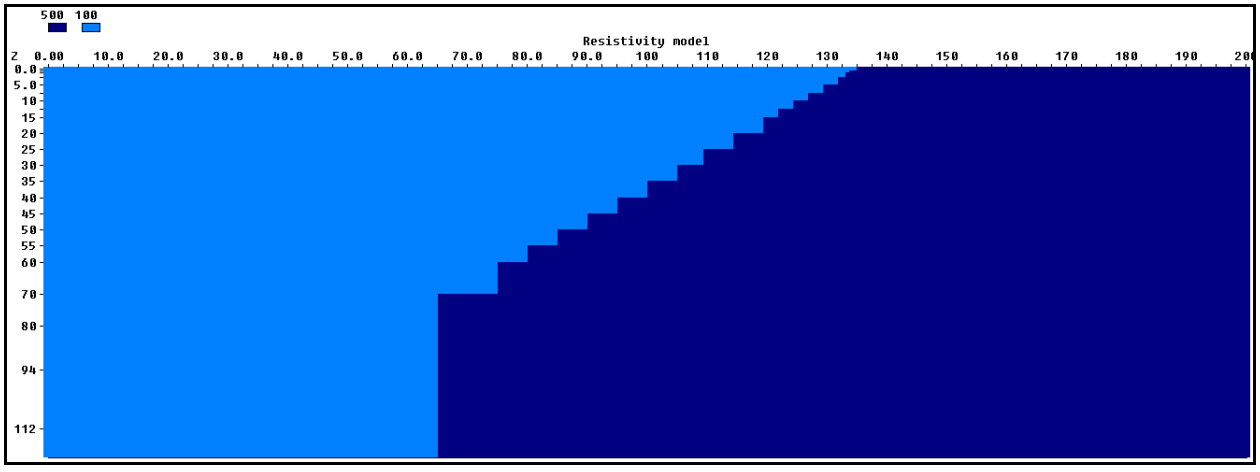

Figure 6-35: Input resistivity model for a dipping boundary

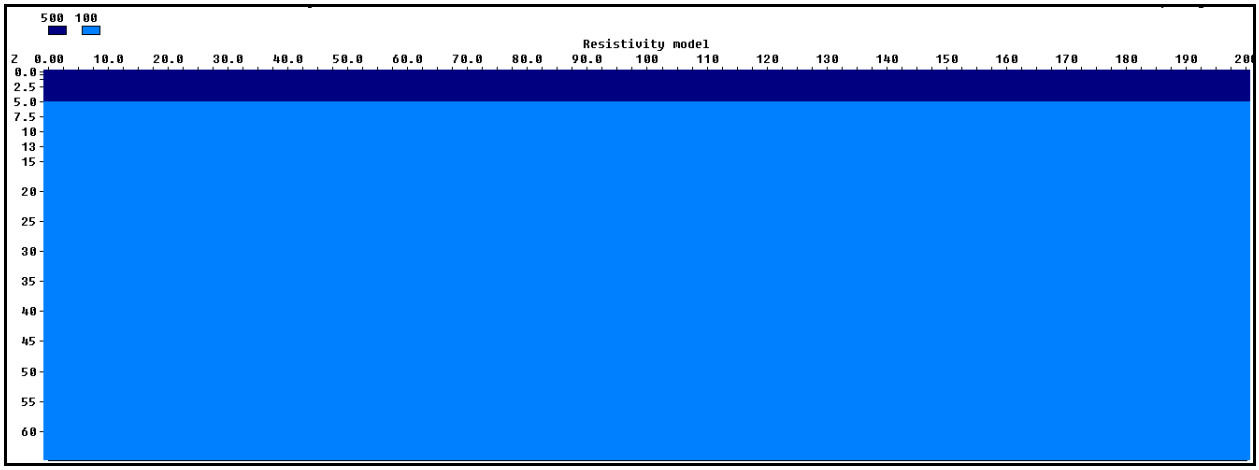

Figure 6-36: Input resistivity model for a horizontal boundary

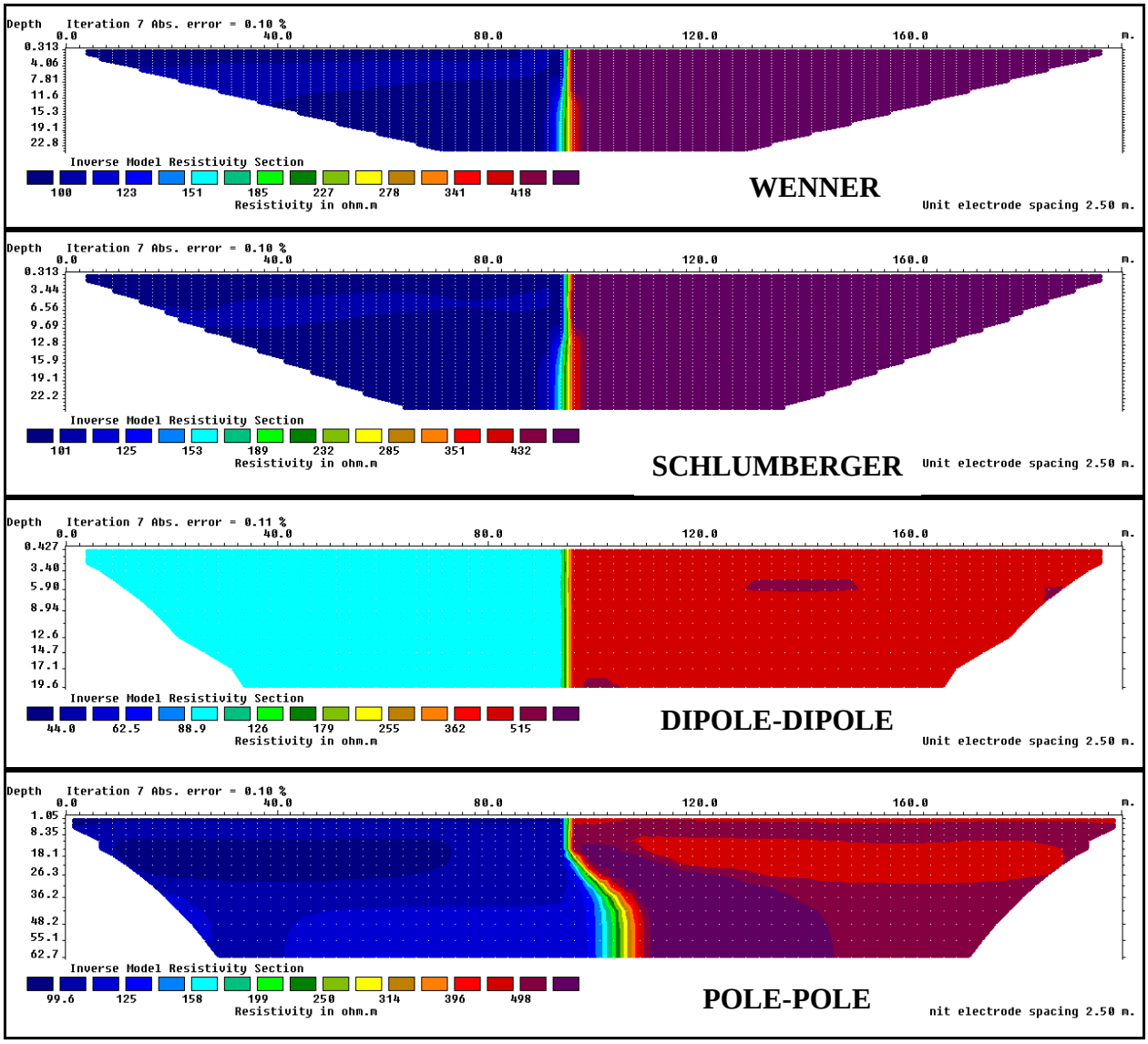

Figure 6-37: Modelled resistivity sections for a vertical contact zone

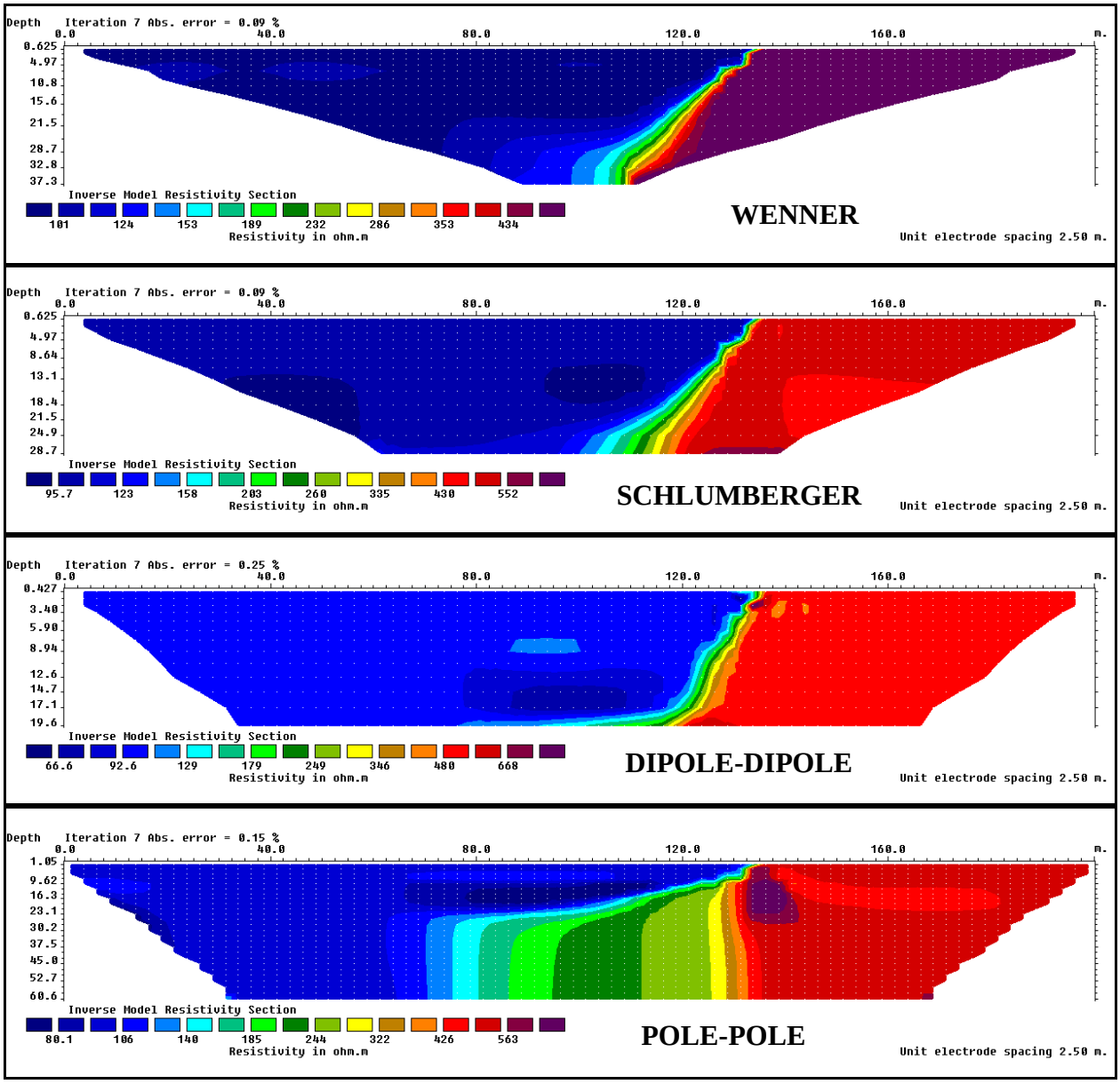

Figure 6-38: Modelled resistivity sections for a dipping contact zone

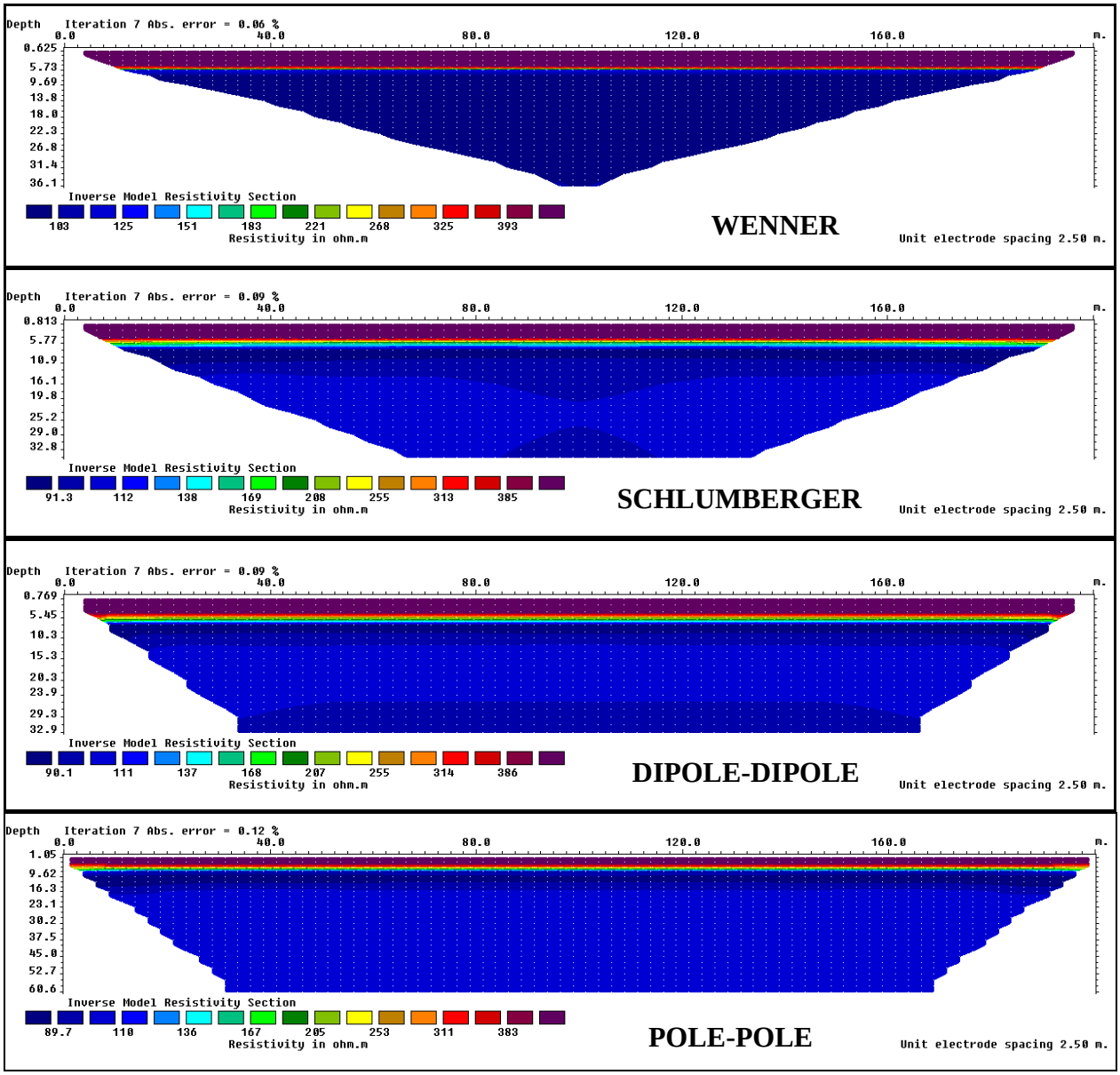

Figure 6-39: Modelled resistivity sections for a horizontal contact zone

Table 6-4: RMS errors of the boundary models after seven iterations

MODELS	Root Mean Square errors (in %)			
	Wenner	Schlumberger	Dipole-Dipole	Pole-Pole
Vertical contact zone	0.10	0.10	0.11	0.11
Dipping contact zone	0.09	0.09	0.25	0.15
Horizontal contact zone	0.06	0.09	0.09	0.05

Figure 6-37 shows that all the electrode arrays located the vertical boundary within the model but the position and the width of the boundary differ from one array to another. At the shallower portion of the model, the Wenner, Schlumberger and Pole-Pole arrays performed

well in mapping the vertical boundary. The resistivity mismatches begin at the intermediate depth portion of the model and get progressively worse with depth, particularly for the Pole-Pole array. The Dipole-Dipole array performed the best in matching the input model resistivity. The vertical boundary is shown as a straight vertical thin line from the top to the bottom of the inverse model section. For the vertical boundary model, the Dipole-Dipole array defined the vertical contact the best, followed by the Schlumberger array, then the Wenner array. The three above-mentioned arrays are recommended for resistivity field surveys across such features.

Except for the Pole-Pole array, all the arrays performed well in matching the input model resistivities of the dipping boundary model (Figure 6-38). The width of the oblique boundary differs from one array to another and from the surface to the depth. Although none of the arrays reproduced the dipping transitional zone perfectly sharp as it is in the input resistivity model, the Dipole-Dipole array resolved the horizontal changes in resistivity thoroughly, followed by the Schlumberger array and then the Wenner array. The transition zone between the high resistive block at the left side of the modelled section to the low resistive block at the right side is broader in the Wenner and Schlumberger inverse model sections; the corresponding transitional zone is thinner in the Dipole-Dipole inverse model section. The Dipole-Dipole array thus defined the dipping contact the best. For surveys across such features, it is recommended that the Dipole-Dipole, Wenner and Schlumberger arrays be considered in order of preference while surveys with the Pole-Pole array should be avoided.

For the horizontal boundary model, all the arrays performed well in matching the input model resistivity (Figure 6-39). The Wenner array identified the vertical changes in resistivities the best. It performed slightly better than the Schlumberger array. The Schlumberger, Dipole-Dipole and Pole-Pole inverse model resistivity sections showed broader transitions zones across the horizontal boundary than the Wenner array.

This modelling exercise revealed that the Dipole-Dipole array is more sensitive to horizontal changes in subsurface resistivities, yet less sensitive to vertical changes, while conversely the Wenner array is more sensitive to vertical changes in subsurface resistivities, but less sensitive to horizontal changes. The Schlumberger array showed to be sensitive to both vertical and horizontal resistivity changes in the subsurface. The Pole-Pole array presented some limitations in mapping the vertical and dipping boundaries.

6.7 MODELLING FAULT ZONES

Plutonic, metamorphic, volcanic and tectonic events always generate multiples fractures in the Earth's subsurface. Bedding plane, vertical and dipping fractures are often sought during groundwater exploration in the Karoo rocks. Two synthetic geological models simulating vertical (Figure 6-40) and dipping (Figure 6-41) faults, similar to subsurface conditions encountered in Karoo formations, were used in this section to evaluate the suitability of four electrode arrays. The input models consist of an overburden, the host rocks and 10 m-wide vertical and dipping fault zones associated with extensive fracturing and a higher water content. The resistivity values of the overburden, the host rocks and the fault are 500 Ω.m, 200 Ω.m and 40 Ω.m, respectively. The apparent resistivity pseudo-sections are displayed in APPENDIX 6. As before, the arrays selected during forward and inverse modelling operations were: the Wenner, Schlumberger, Dipole-Dipole and Pole-Pole arrays.

Figure 6-42 and Figure 6-43 illustrate the inverse model resistivity sections of both models for each electrode array, obtained from the RES2DINV program after least-square inversions by the means of the L1-norm (Robust constraint inversion). Table 6-5 displays the RMS errors the modelled resistivity sections obtained after seven iterations.

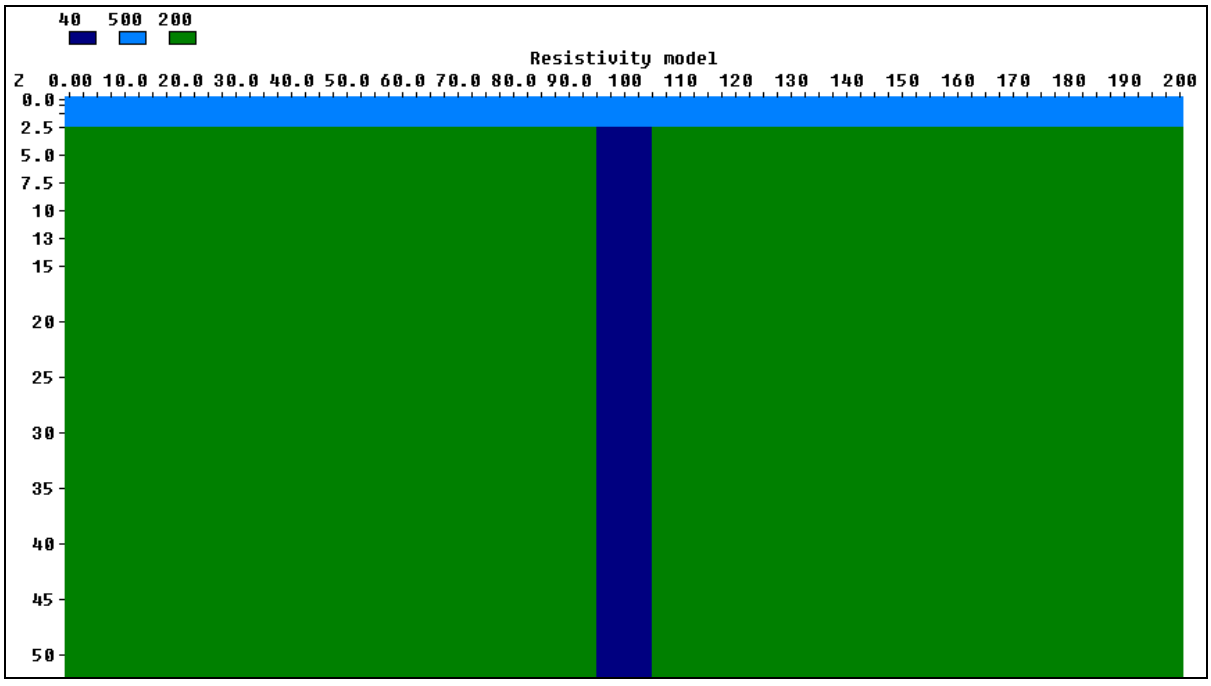

Figure 6-40: Input resistivity model for a vertical fault

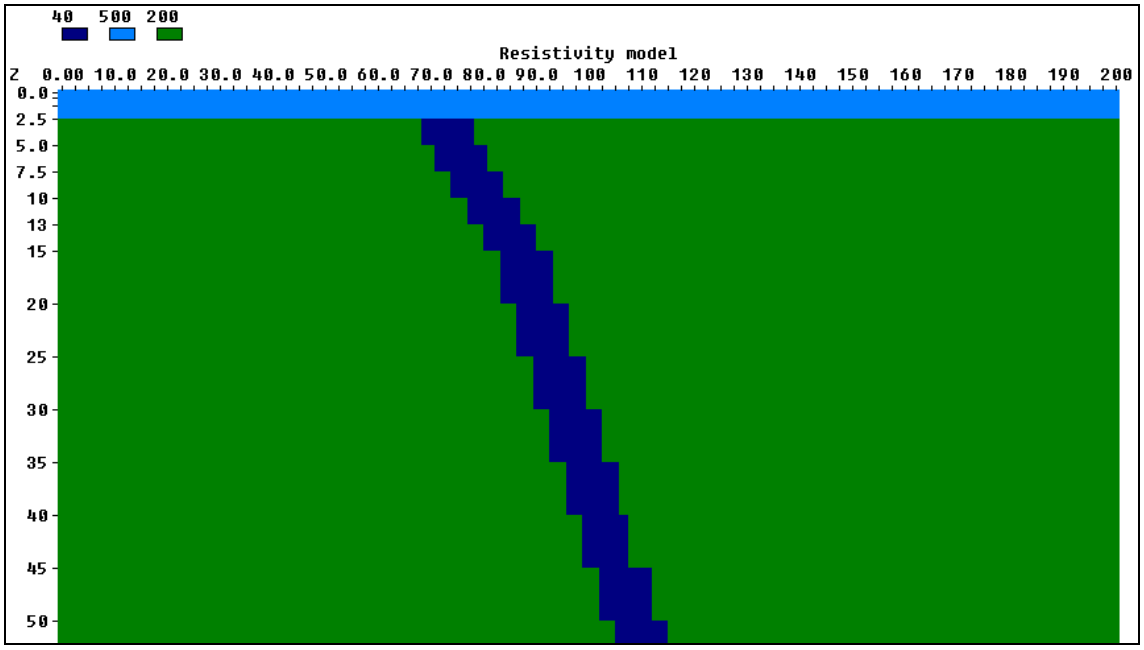

Figure 6-41: Input resistivity model for a dipping fault

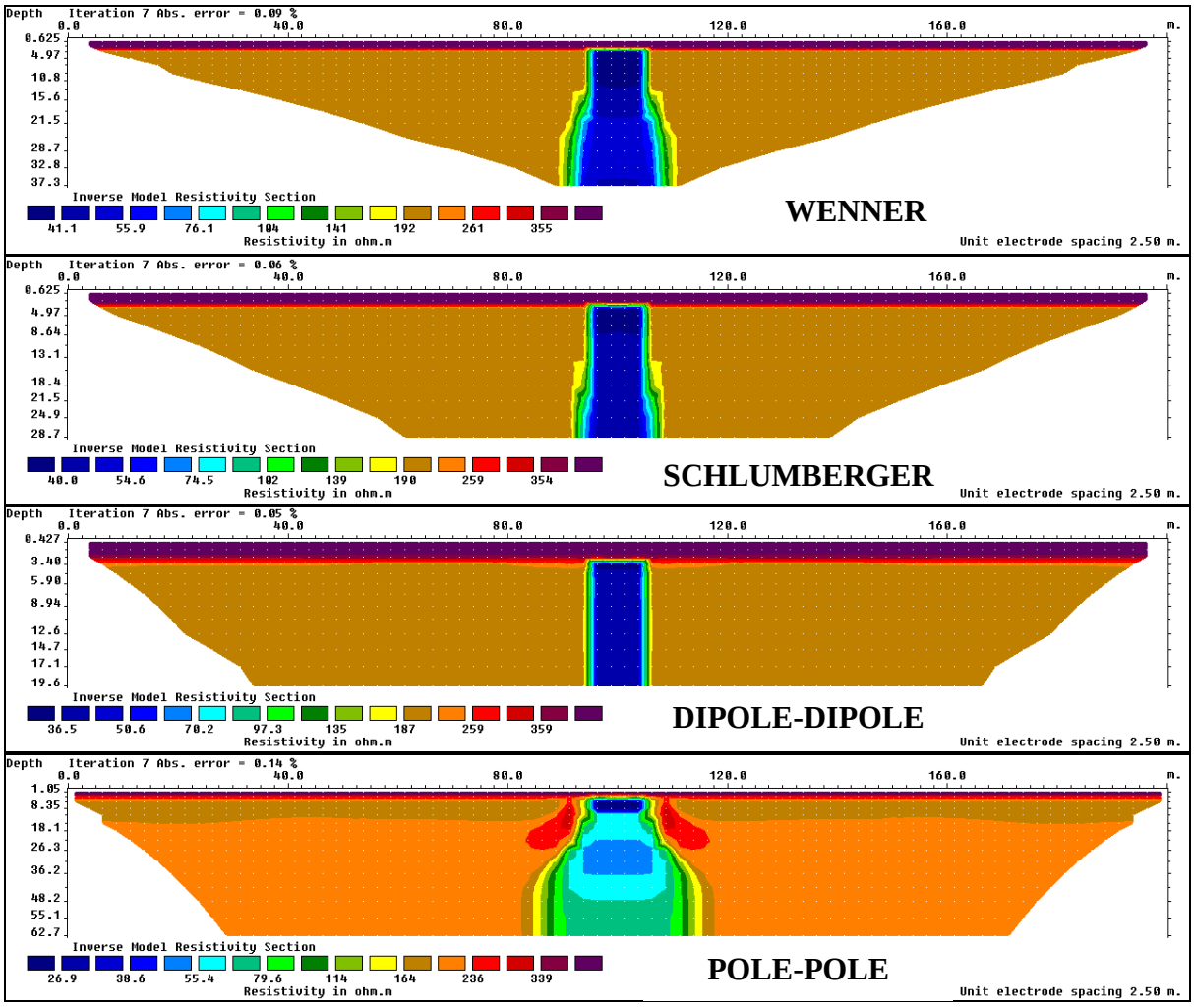

Figure 6-42: Modelled resistivity sections for a vertical fault

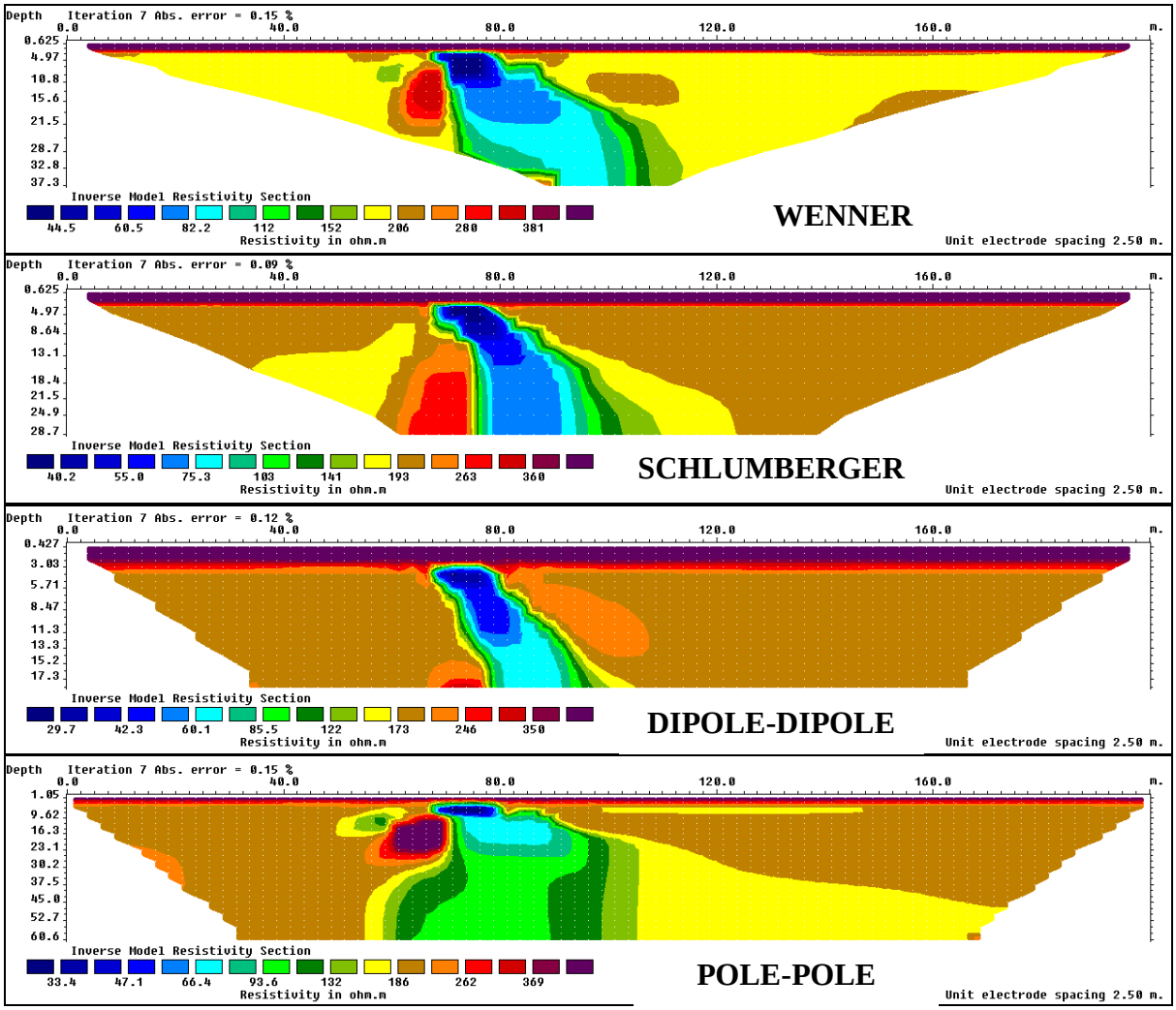

Figure 6-43: Modelled resistivity sections for a dipping fault

Table 6-5: RMS errors of the fault models after seven iterations

MODELS	Root Mean Square errors (in %)			
	Wenner	Schlumberger	Dipole-Dipole	Pole-Pole
Vertical fault	0.09	0.06	0.05	0.14
Dipping fault	0.15	0.09	0.12	0.15

Comparisons between the input resistivity model and the modelled responses (Figure 6-42) for the vertical fault model show that the Dipole-Dipole array was the most successful in imaging the side contacts of the vertical fault zone, followed by the Schlumberger array. The Wenner array also detected the vertical fault at shallow depth, but failed to image its thickness at greater depth. However, both the Wenner and Schlumberger arrays performed very well in imaging the vertical changes in resistivity compared to the Dipole-Dipole array. It is seen in the Wenner and Schlumberger inverse model resistivity sections (Figure 6-42)

that the vertical transition from the overburden to the host rock is well defined, while a gradual transition is seen in the Dipole-Dipole inverse model resistivity section. The Dipole-Dipole and Schlumberger arrays, conversely to the Wenner array, imaged the horizontal changes in resistivity well. The Pole-Pole array was the less successful in mapping the vertical fault zone. Its inverse model resistivity section shows a very broad feature of more than 20 m at the centre of the profile. The horizontal changes in resistivity are gradual rather than sharp as in the input resistivity model.

Results from this analysis again exhibit the sensitivity of the Wenner array to vertical resistivity changes, the performance of the Schlumberger array in identifying both vertical and horizontal changes in the ground surface, and the capability of the Dipole-Dipole array in resolving horizontal changes in the subsurface. These three arrays may therefore be considered for resistivity field surveys across vertical fault zones.

Figure 6-43 shows that the Dipole-Dipole, Schlumberger and Wenner arrays were much more successful in locating the dipping fault zone than the Pole-Pole array. The Dipole-Dipole array was the most successful in imaging the dipping fault zone. The contact between the host rock and the dipping fault is significantly narrower than in the modelled resistivity sections of the Wenner and Schlumberger arrays. However, the contact between the host rock and the overburden is less sharply defined in the Dipole-Dipole modelled section than in the Wenner and Schlumberger inverse models. The Pole-Pole array failed in mapping the dipping fault. The dipping low resistivity zone is not imaged clearly, but a near-vertical zone of low resistivity is seen in the inverse model. It is thus recommended that the Dipole-Dipole, Schlumberger and Wenner arrays be considered for ERT field surveys across dipping fault zones.

The above modelling exercises indicate that different electrode arrays perform differently in the detection of vertical, horizontal and dipping structures, as well as when dealing with a combination of vertical and horizontal structures. Knowledge of the geological structures being targeted during an ERT survey may therefore assist in the selection of an appropriate array for the survey.

7 FIELD SURVEYS

Because numerical modelling experiments (as studied in the previous chapter) only produce an idealised representation of the characteristics of the real system present in the field, it is always very important to supplement numerical modelling results with data gathered from field surveys in order to prove or to invalidate the theory (numerical modelling agreement) on the one hand, and to have a better understanding of the real system on the other hand. The ERT method has become one of the most important geophysical techniques for investigating near-surface underground structures. It is used in this study to investigate into the sensitivities of different electrode arrays. The present chapter describes the field method of investigations undertaken to collect resistivity data in the framework of this research.

7.1 SITE DESCRIPTIONS

The 2-D ERT field surveys were conducted during the current project on three different sites where the geology is well known, namely: near the Krugersdrift Dam, at the Paradise Agricultural Test Site and the Meadows area south-east of Bloemfontein (Figure 7-1). All three sites are located on Karoo sedimentary formations intruded by dolerites.

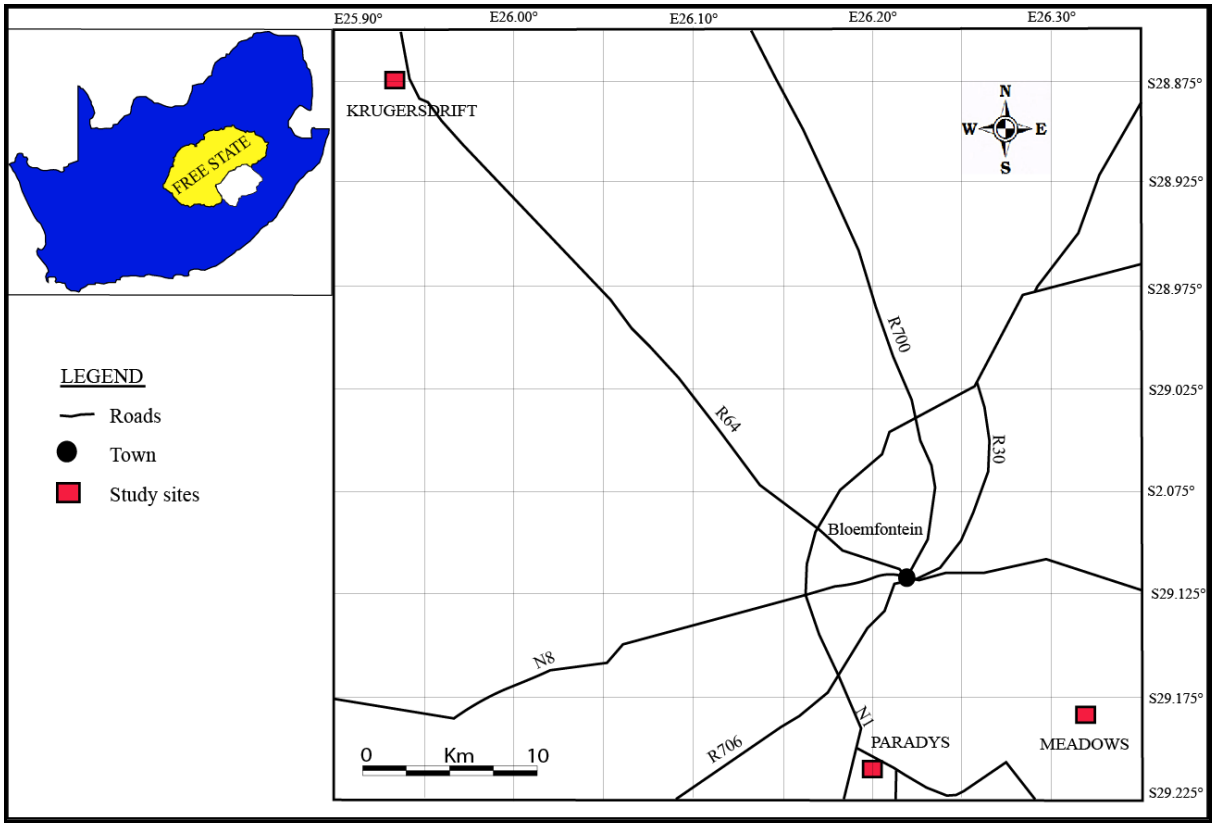

Figure 7-1: Geographical location of the three study sites

❖ KRUGERSDRIFT SITE

This site is located in the Free State Province, approximately 40 km from the town of Bloemfontein. The survey in this area was undertaken on a farm where a thick dolerite dyke (approximately 20 m wide) is known to occur. This dyke has a north-west/south-east strike (Figure 7-2). The 2-D ERT data were recorded on a single profile perpendicular to the strike of the dyke.

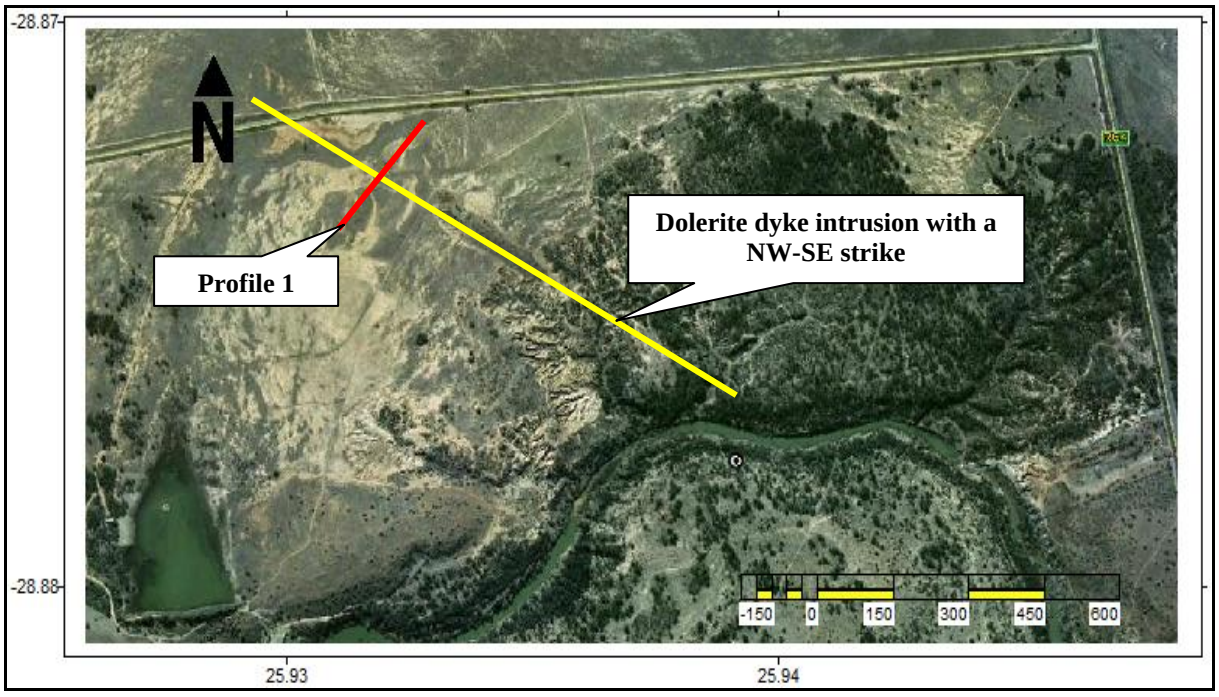

Figure 7-2: Geographical location of the Krugersdrift site (Google Earth)

❖ PARADISE SITE

This site is situated approximately 10 km south of Bloemfontein (Figure 7-1), within the Sydenham neighbourhood (Figure 7-3). Resistivity measurements were collected on a farm under where a dolerite sill is known to occur. The contact between the sill and the Karoo sedimentary rocks has an approximate north/south strike. The site has been used by the University of the Free State as an experimental site for geohydrological studies.

❖ MEADOWS SITE

The Meadows site (Figure 7-4) is located approximately 12 km south-east of the city of Bloemfontein (Figure 7-1). A weathered dolerite sill body, intruded by a fresh dolerite dyke, are the main geological features present at the site. The strike of the dyke (south-south-west/north-north-east) was determined from a magnetometer field survey using the automatic GEM Walkmag, as shown in Figure 7-5.

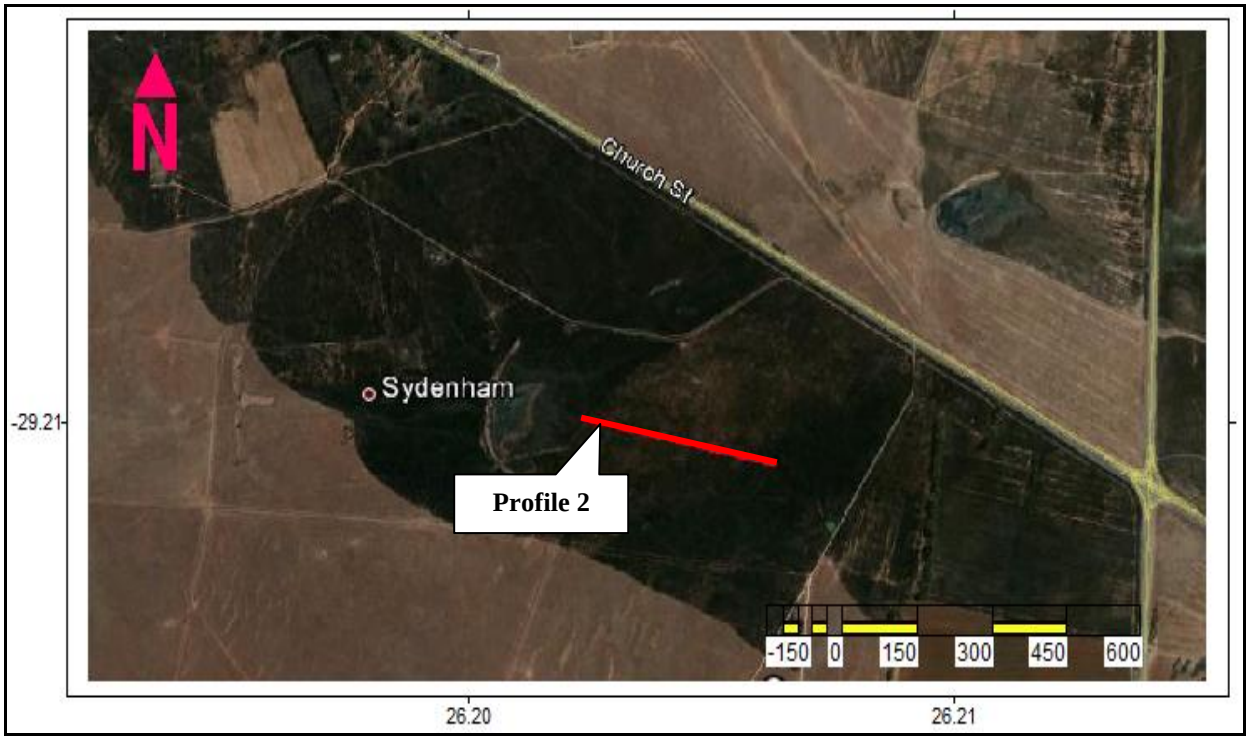

Figure 7-3: Geographical location of the Paradise site (Google Earth)

Figure 7-4: Geographical location of Meadows site (Google Earth)

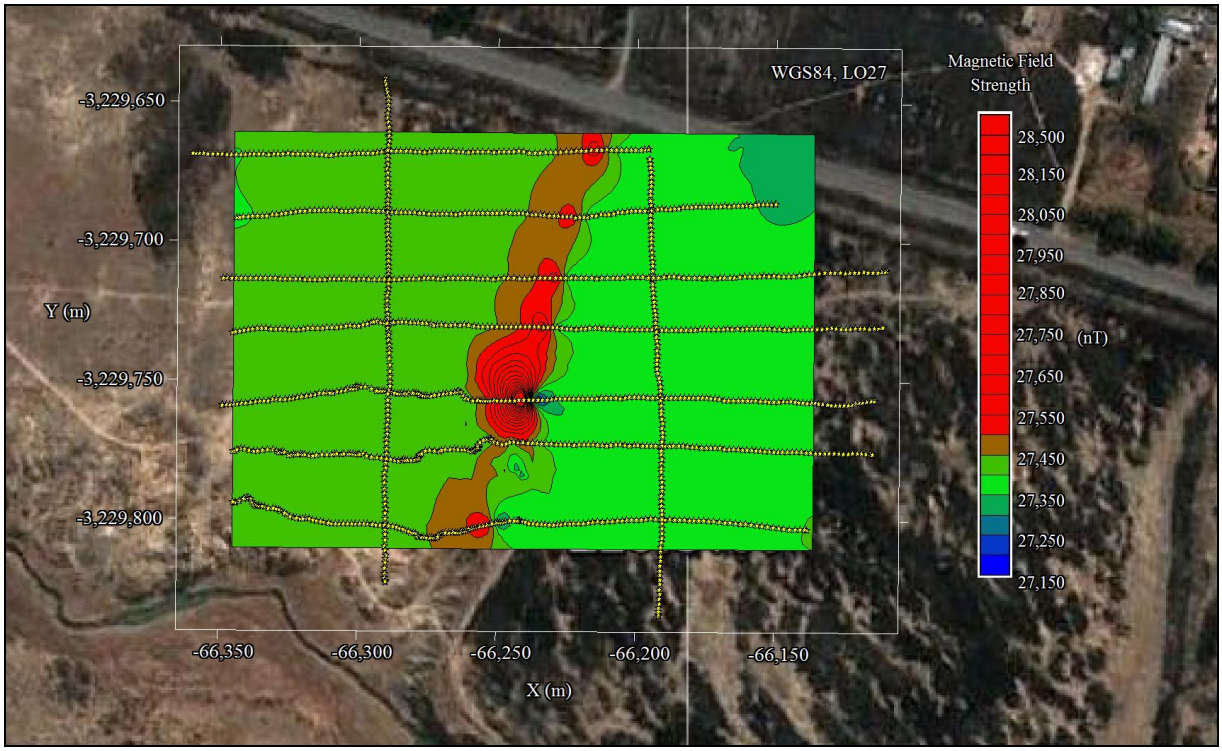

Figure 7-5: Dolerite dyke direction at Meadows site (Google Earth)

7.2 METHOD OF INVESTIGATIONS

❖ THE ARRAYS CHOSEN FOR THE SURVEY

Based on the type of structures present in the different study areas (as described in Section 7.1), the sensitivities of the arrays (discussed in detail in Chapter 4), the background noise levels and the numerical modelling results (discussed in Chapter 6), only three electrode arrays were selected to carry out the 2-D ERT field surveys.

Because of its high signal strength and its sensitivity to vertical changes in the subsurface resistivities, the Wenner array was selected to be used for the surveys at each site. The Schlumberger array was chosen because of its greater depth of investigation and higher data coverage when compared with the Wenner array. It also has a symmetric electrode configuration for normal and reciprocal measurements: this facilitates the data quality control needed to obtain reliable, well-resolved images (Dahlin and Zhou, 2004). The Dipole-Dipole array was chosen because of its depth of investigation and sensitivity to vertical structures. The Pole-Pole array was not selected because the field conditions did not allow the position of remote electrodes at a sufficient distance from the profile lines. In addition, this array is very sensitive to noise.

❖ THE EQUIPMENT

The Lund Imaging System developed by ABEM was used during the field surveys. This system consists of a Terrameter SAS1000 (Figure 7-6), an Electrode Selector, a 12 Volt battery, four multi-core cables, each with 21 take-outs on a 5 m-spacing, two cable joints, 81 electrodes and other accessory tools.

Figure 7-6: Resistivity equipment

The configuration of the Lund Imaging System used for the resistivity field surveys is shown in Figure 7-7. In this configuration, the four multi-core cables are laid out on a straight line (the profile) across the geological features investigated. Cables 1 and 2, as well as 3 and 4 are connected by means of cable connectors, shown in Figure 7-8. The Terrameter and Electrode Selector are positioned at the midpoint of the four-cable setup. Cables 2 and 3 are connected to the Electrode Selector, which is in turn connected to the Terrameter through a communication cable. A 12 Volt battery serves as power source to the system.

Each of the four cables has 21 take-outs at which electrical connection may be achieved. Electrodes are installed into the ground at each of the take-outs and connected to the multi-core cables. Where the cables meet, they are connected to a shared electrode, so that a total number of 81 electrodes are connected in this configuration.

Prior to the fieldwork, measurement protocols are designed and installed on the Terrameter. These protocols inform the Terrameter which of the 81 electrodes should be used as current electrodes and potential electrodes during a particular measurement. The Electrode Selector connected to the Terrameter performs the switching between the different electrodes.

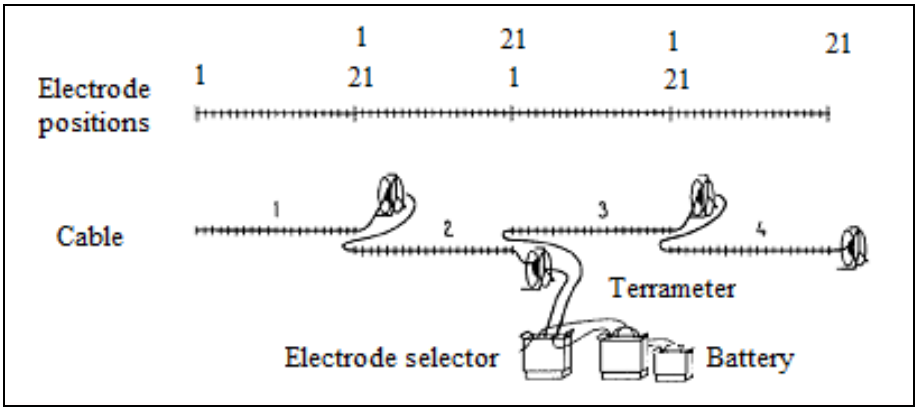

Figure 7-7: Arrangement of the equipment for a 2-D survey (Modified from Loke, 2012)

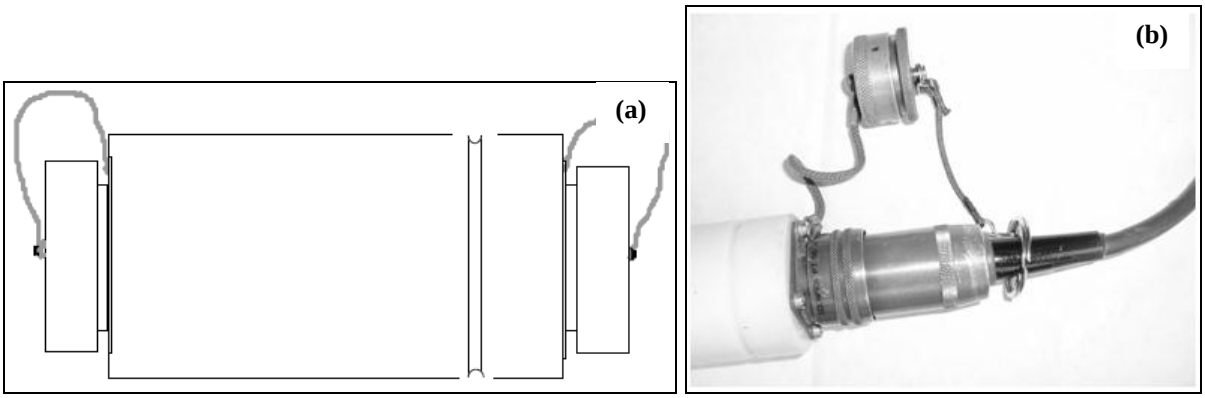

Figure 7-8: Cable joint (a) and cable joint connected to a cable (b) (ABEM, 2010)

❖ MEASUREMENT PROTOCOLS

Measurement protocol files written using the SAS4000/SAS1000 Utilities software were loaded onto the Terrameter of the Lund Imaging System. Measurements were taken using two protocol types for each array, namely protocols using large distances between the electrodes to record deeper data at lower resolution and protocols using smaller electrode spacings to record high-resolution data at shallow depths. For example, the field surveys conducted with the Wenner geometry employed protocols Wenner_L and Wenner_S to record the deeper and shallower data, respectively. The Wenner_L protocol uses electrodes on all four cables, but only every second electrode is active. The Wenner_S protocol uses only electrodes on the central two cables, but every electrode on these cables is active during the survey.

The measurement protocols used during the field surveys were designed to include all possible measurement positions and depths. Although many of the data points may be considered redundant, the maximum data coverage was desired in order to investigate the

resolution and limitations of each array. Redundant data points could be removed at a later stage to investigate the responses that would be obtained from a more typical data coverage as normally employed during a field survey limited by time constraints.

The vertical and horizontal data coverage obtained with the Wenner_L and Wenner_S protocols is shown schematically in Figure 7-9. The green dots in this figure represent the subsurface positions at which measurements are taken. A total number of 260 measurements are possible with this particular Wenner_L protocol, while the Wenner_S protocol includes 197 measurements.

Similar protocols were designed for the Schlumberger and Dipole-Dipole arrays. Again, both long (L) and short (S) protocols were used. The data coverage obtained with the protocols of the three electrode geometries are listed in Table 7-1. It is seen that the data coverage with the Schlumberger and Dipole-Dipole arrays are significantly greater than with the Wenner array. This may be considered a limitation of the Wenner array.

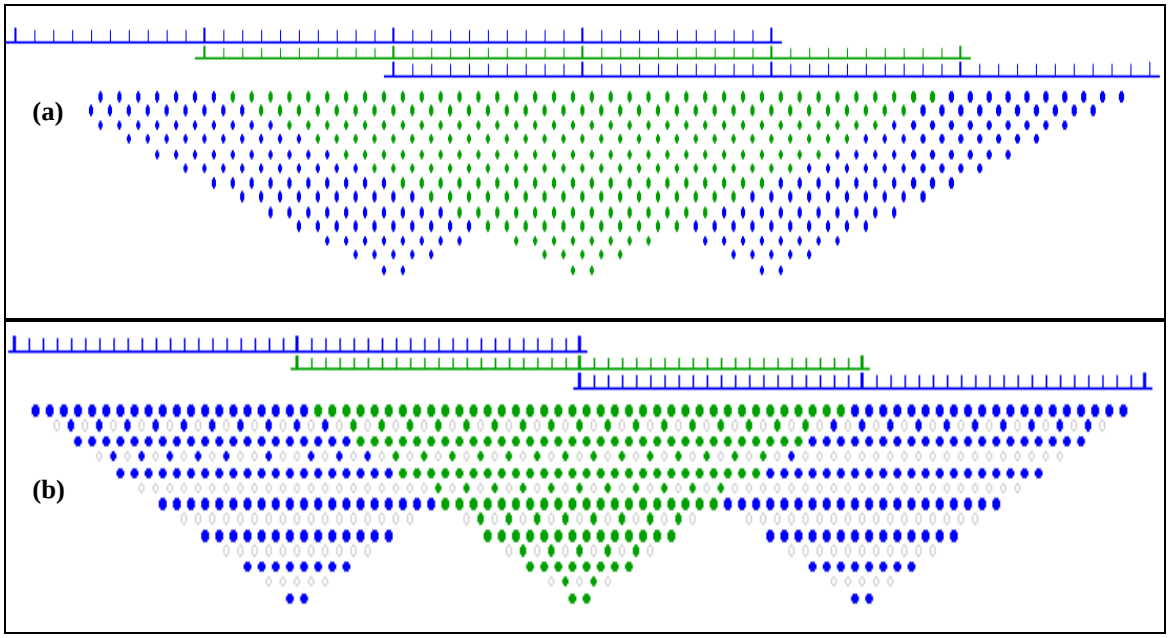

Figure 7-9: Data points distribution for all possible measurements taken with Wenner_L (a) and Wenner_S (b)

Table 7-1: All possible measurements taken for each electrode array

Arrays	**Number of measurements**		**Total number of measurements**
	L	S	
Wenner	260	197	457
Schlumberger	637	501	1138
Dipole-Dipole	1057	924	1981

For this research, the maximum electrical current was set at 200 mA. The Terrameter allows subtraction of external power line noise from the recorded data. The power line frequency was set at 50 Hz, corresponding to the frequency of the power grid in South Africa. The AUTO setting was used for the voltage, which implied that the instrument set the optimum value for each measurement. After reading the control file, the Terrameter automatically selected the appropriate electrodes for each measurement. Each measurement was automatically stored in the Terrameter. The background noise levels were checked before measurements began.

❖ THE PROFILE LINES

The resistivity measurements were collected along Profiles 1, 2 and 3 at the Krugersdrift (Figure 7-2), Paradise (Figure 7-3) and Meadows (Figure 7-4) sites, respectively. The ERT profiles were laid out perpendicular to the strikes of the dykes and sills that occur at these sites. Unit electrode spacings of 2.5 m were used at the Krugersdrift and Meadows sites along profiles with total lengths of 200 m, while 5 m-unit electrode spacings were used at Paradise site, resulting in a total profile length of 400 m. The coordinates of each profile are presented in Table 7-2.

Table 7-2: Resistivity profile lines coordinates

	Station N^o	**-100**	**-50**	**0**	**50**	**100**
PROFILE 1 (Krugersdrift)	**Latitude**	-28.87331^o	-28.87296^o	-28.87261^o	-28.87225^o	-28.87191^o
	Longitude	25.93142^o	25.93175^o	25.93207^o	25.93239^o	25.93270^o
	Station N^o	**-200**	**-100**	**0**	**100**	**200**
PROFILE 2 (Paradise)	**Latitude**	-29.20994°	-29.21015°	-29.21035°	-29.21055°	-29.21073°
	Longitude	26.20237°	26.20334°	26.20433°	26.20534°	26.20636°
	Station N^o	**-100**	**-50**	**0**	**50**	**100**
PROFILE 3 (Meadows)	**Latitude**	-29.18243^o	-29.18254^o	-29.18266^o	-29.18279^o	-29.18291^o
	Longitude	26.31820^o	26.31869^o	26.31919^o	26.31968^o	26.32016^o

7.3 RESULTS OF THE FIELD INVESTIGATIONS

After studying the performance of different electrode configuration from a theoretical perspective (Chapter 4) and through numerical modelling (Chapter 6), the suitability of the Wenner, the Schlumberger and the Dipole-Dipole arrays were evaluated by carrying out field surveys over some geological structures encountered in Karoo formations. The primary aim of the field surveys was to investigate which electrode arrays are the most successful in imaging vertical/horizontal/dipping contacts associated with different geological structures, and then to compare the field results with the theoretical considerations, in order to draw appropriate conclusions regarding the applications of the selected arrays.

A total number of 457 measurements were collected at each study site using the Wenner array. The measurement for one data point takes place in several measurement cycles which are called stacks. For this study, a maximum of four stacks for each data point was chosen. The apparent resistivity value obtained was therefore the average of the measurements taken at a particular electrode selection. The standard deviation for each stack was monitored during the measurements as an indicator of the quality of the measurements. At least two resistivity measurements were taken at each study site (along the same profile line) and then compared with each other. Apparent resistivity values with an error (standard deviation) of less than 2% were accepted as valid measurements. Measurements with standard deviation greater than 2% were considered as data resulting from poor measurements. These measurements were therefore either removed or processed prior to the creation of the final inverse models.

Two sets of field measurements were collected with the Schlumberger array at each site, along the same profile line. Because all possible measurements were included in the protocols used for data collection, some measurements corresponding to large “n” factors (n > 6) were negative or abnormally high due to poor data quality. These values had to be processed by means of averaging prior to inverse modelling. Apparent resistivity values with standard deviation greater than 4% were processed. A total of 1138 measurements were taken with the Schlumberger array at each study site. Measurements were taken up to an “n” factor of 36.

Although 1981 measurements are possible with the Dipole-Dipole array (Table 7-1), only 1177, 1135 and 1408 numbers of measurements were collected at Paradise, Krugersdrift and Meadows sites, respectively. All the possible measurements could not be collected due to the large number of negative values recorded for large “n” factors. With increasing “n”, the

signal strength decreases and the data quality deteriorates. Measurements were taken with "n" up to 76. Two sets of measurements were also taken with this array at each site, along the same profile line. While processing the data, only apparent resistivity values with standard deviation less than 10% were accepted as valid data measurements.

Resistivity field data collected using the different arrays are presented on the disc attached to this document.

7.3.1 Field survey across a dolerite sill

The suitability of the Wenner, Schlumberger and Dipole-Dipole arrays to image horizontal structures present in the Earth's subsurface was evaluated by conducting an ERT survey across a dolerite sill intrusion. The survey was carried out at the Paradise site near the city of Bloemfontein. The description of the current study area and the methods of investigation undertaken were discussed in Sections 7.1 and 7.2 respectively. Least-square inversions of the field data sets were performed using the software RES2DINV. Because the investigation site consists of discrete subsurface structures with sharp boundaries between the dolerite sill body and the surrounding rocks, the robust constraint inversion technique (L1-norm) was selected. The modelled responses are displayed in Figure 7-10, which presents the inverse model resistivity sections of the Wenner, the Schlumberger and the Dipole-Dipole arrays.

The different electrode arrays produced significantly different modelled resistivity sections for the same structure being mapped along the same profile line. The location, the thickness, the vertical depth and the horizontal extent of the dolerite sill are all different from one modelled resistivity section to another.

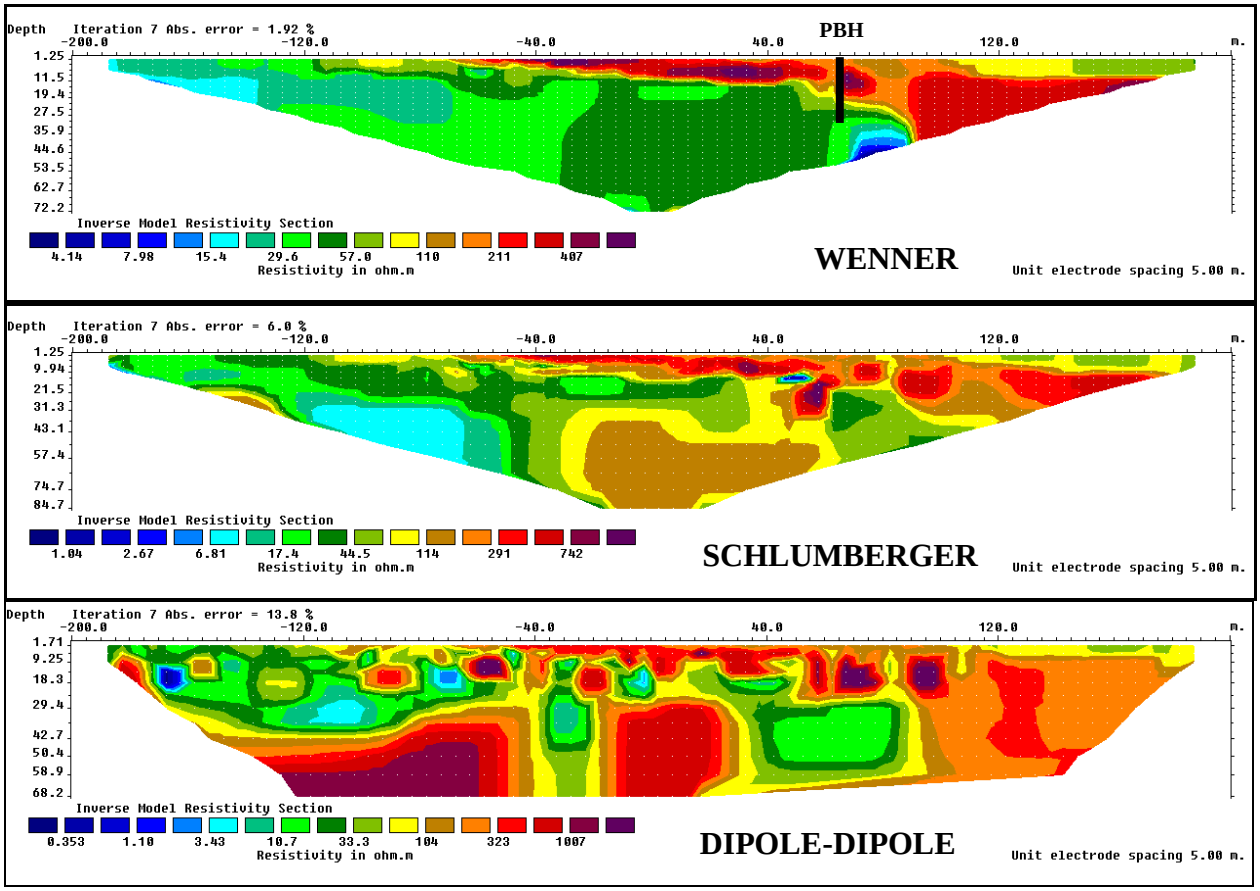

Figure 7-10: Modelled resistivity sections across a dolerite sill at the Paradise site

The Wenner array: The modelled resistivity section at the top of Figure 7-10 is the inverse model section of the Wenner array. Seven iterations were used during the inversion and an RMS error of 1.92% was obtained. The dolerite sill intrusion was clearly detected (high resistivity body running from -10 m to the right were it becomes thicker). The modelled resistivity section shows that the sill is very shallow in place, almost outcropping. The vertical transition in resistivity is sharp, which implies the sensitivity of this array to vertical changes in resistivity or its capability of accurately mapping horizontal structures. The image is less noisy and has good resolution. Compared to the other two inverse modelled sections, this array has the lowest horizontal data coverage. With a total array length of 400 m, the investigation with this array gives a depth of 72.2 m in the modelled resistivity section.

The vertical black line observed in the Wenner resistivity section (Figure 7-10) is a 30 m-deep borehole drilled 65 m from the centre of the profile. The corresponding borehole log (Figure 7-11) shows that the dolerite was encountered between depths of 1 m and 16 m during the drilling process. The vertical changes in resistivity displayed by the Wenner array at 65 m (horizontal depth) on the profile are thus in fairly good agreement with the drilling results.

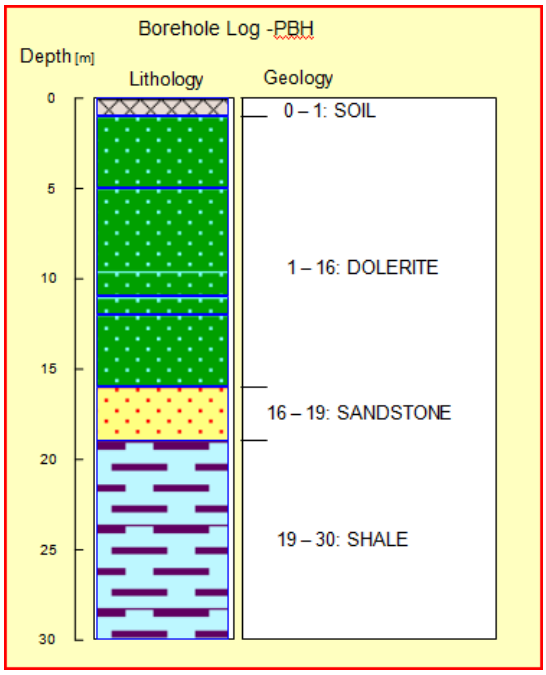

Figure 7-11: Borehole log

The Schlumberger array: The 2-D resistivity tomography data obtained using the Schlumberger array was also inverted using the robust inversion technique. The results are shown in the middle image of Figure 7-10. After seven iterations, the inversion process converged with an RMS of 6.0%, which is greater than the RMS error for the inversion obtained for the Wenner array (1.92%). This difference is partly due to the greater signal strength of the Wenner array, especially when a high resistivity contrast exists.

The Schlumberger resistivity model revealed the presence of the sill, but was less successful in accurately defining the continuous intrusive body. Although the Schlumberger array produced a greater depth of investigation along the profile line than the Wenner array, the inversion of the resistivity data obtained for both arrays showed clearly that the Wenner array has better depth resolution that the Schlumberger array. The vertical transition in resistivity is not as well defined for the Schlumberger array. The results clearly demonstrate the superiority of the Wenner array over the Schlumberger configuration for the determination of the vertical distribution of subsurface resistivities.

The Dipole-Dipole array: The inverse model resistivity section displayed at the bottom of Figure 7-10 is the modelled response obtained for the Dipole-Dipole array. After seven iterations, the inversion process converged with an RMS of 13.8%, which is greater than errors obtained with both the Wenner (1.92%) and Schlumberger (6.0%) arrays. The larger error is again partly due to the sensitivity of the Dipole-Dipole array to noise. Among the three arrays, the Dipole-Dipole array has the lowest signal strength.

The horizontal dolerite sill intrusion is not very well defined in the modelled resistivity section. The quality and coherence of the modelled resistivity section are worse when compared to the results of the Wenner and Schlumberger arrays. This can be explained by the considerable number of bad data points recorded with the Dipole-Dipole array, which consequently affected the inverse modelling process. During inversion the quality of the modelled resistivity sections appears to deteriorate with an increasing number of iterations as the program starts to model the bad data points. These observations indicate that the Dipole-Dipole array is less suitable for mapping horizontal structures, such as sill intrusions.

Before processing the resistivity data collected in the field with the Dipole-Dipole array, the inverse model was run and a median depth of investigation of 103.6 m was displayed in the modelled resistivity section. Among the three arrays, the Dipole-Dipole array thus has the greatest potential depth of investigation but the modelled resistivity section on Figure 7-10 shows that, in practice, this array has greater difficulty in imaging deep features than the Wenner and Schlumberger arrays. Figure 7-10 also shows that, compared to the Wenner and Schlumberger arrays, the Dipole-Dipole array has the largest horizontal data coverage at depth, yet the quality of many of the data points may be adversely affected by the inherent low signal strength of the array.

From the above results it can be concluded that the electrode arrays selected to map a horizontal dolerite sill intrusion greatly differed from one to another in terms of their successes in imaging the horizontal contacts between the sill and the host rock. The results showed that the Wenner array was the most successful in defining the horizontal contacts, despite its smaller depth of investigation and lower horizontal data coverage.

❖ Dipole-Dipole model sections for truncated data sets

Resistivity field data collected with the Dipole-Dipole array, using protocols containing all the possible measurements, often include bad data points: some measurements contain either negative or abnormally high apparent resistivity values. The standard deviations of these apparent resistivity measurements are usually high (greater than 10% but sometimes as high as 100%). The standard deviation is a valid indicator of the quality of the measurements: the smaller this value, the better the quality of the data point. Conversely, high standard deviations imply bad data quality.

The presence of poor data in an apparent resistivity data set negatively affects the inverse modelling process. It is therefore recommended that data cleaning and processing be done prior to inversion. Processing the data may consist of removing or correcting bad data points by means of averaging adjacent measurements. For example, Figure 7-12 displays the Dipole-Dipole inverse model resistivity sections (for a survey carried out across a dolerite sill) for apparent resistivity data after removal of all data points with standard deviations in excess of 50% (top image), 20% (middle image) and 10% (bottom image).

After seven iterations using the three truncated data sets, different RMS errors were obtained, namely 25.8%, 23.9% and 23.2 % for the data sets with standard deviations below 50%, 20% and 10%, respectively. Comparison between Figure 7-12 and the Dipole-Dipole resistivity section at Figure 7-10 revealed that inverse model resistivity sections produced by data sets containing many data points of poor quality generate poor quality images. It is also seen in Figure 7-12 that the dolerite sill intrusion has not been clearly defined. In addition, two other resistive bodies appear in the resistivity models.

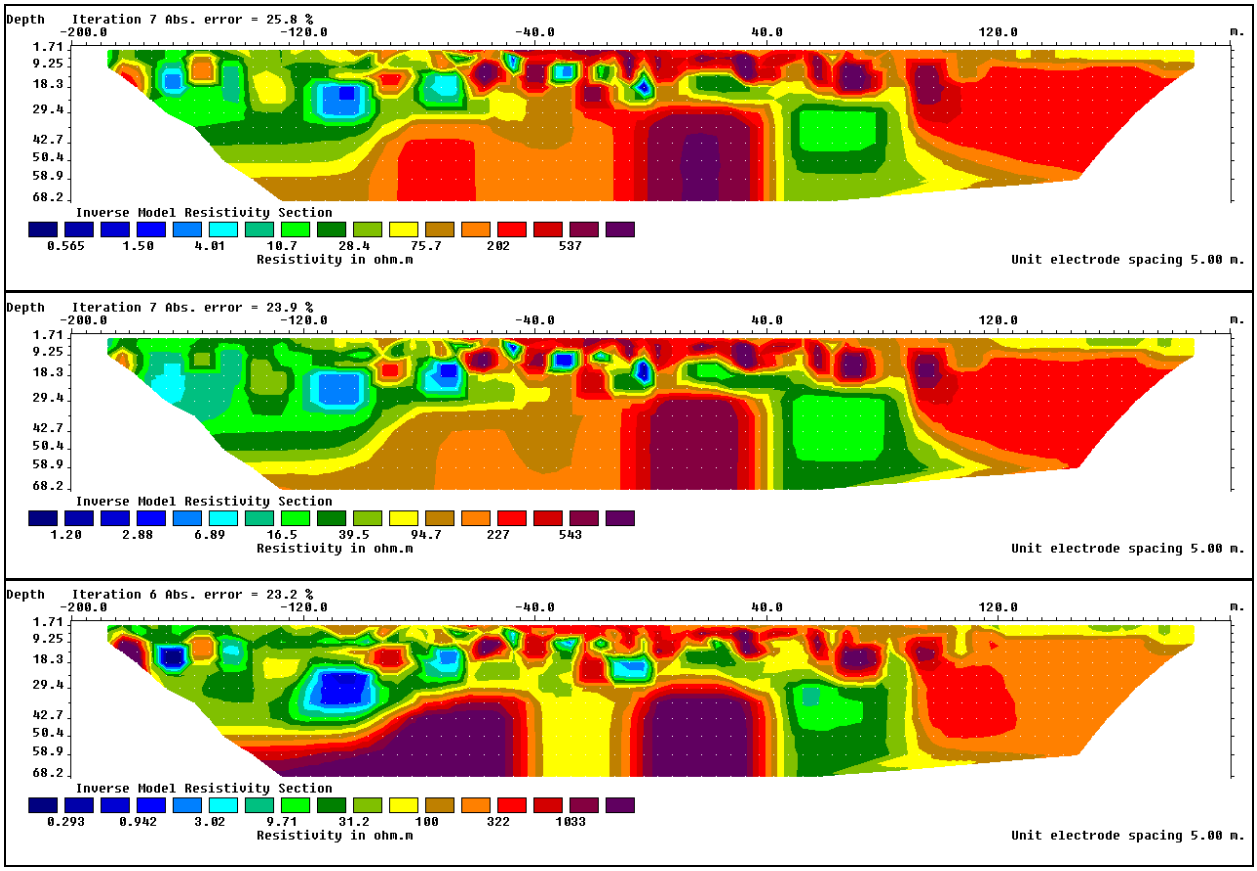

Figure 7-12: Inverse resistivity models for data recorded across a sill using the Dipole-Dipole array. Data sets have been truncated to include data points with standard deviations less than 50% (top), 20% (middle) and 10% (bottom)

❖ 2-D ERT using typical survey protocols

Measurement protocol files used during the current research and explained in detail in Section 7.2 were designed to include all possible measurement positions and depths. This implies a significant increase in the amount of time required to collect the field data. In practice, protocols including fewer measurements are employed to collect field data that give a good representation of the subsurface without redundancy. For example, for a typical field survey the Wenner_L and Wenner_S protocols may be as shown in Figure 7-13. The green dots represent the subsurface positions at which measurements are taken. The data coverage obtained with this particular protocol for the three electrode arrays are listed in Table 7-3. The numbers in red are the numbers of measurements of the protocols that employ all possible measurements, as described in Section 7.2. In this example, measurements with the Wenner_S are only taken at three shallow depths of investigation. It is seen that even for the typical protocols employed in practice, the Dipole-Dipole array has the largest number of measurements.

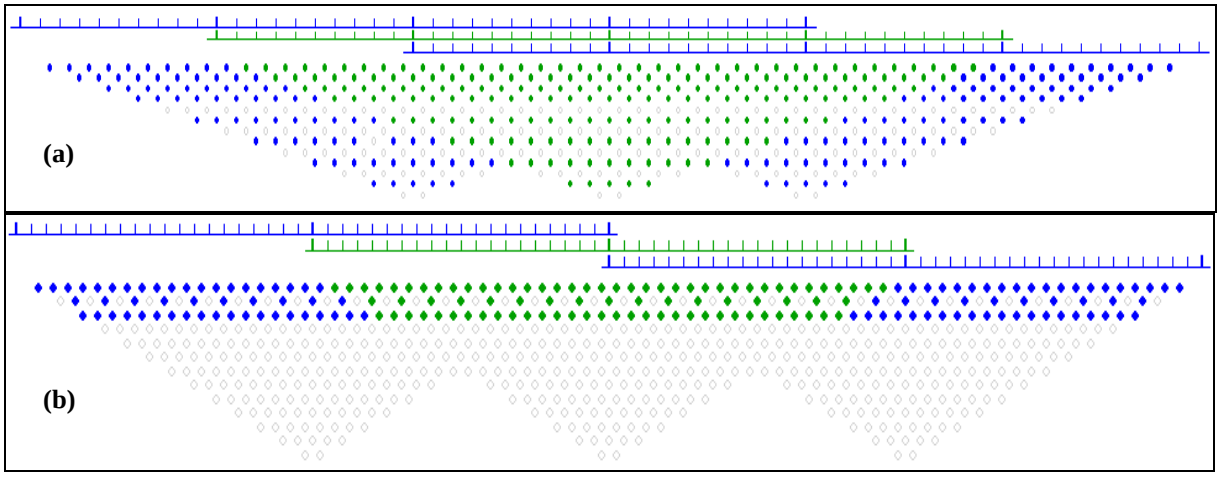

Figure 7-13: Data points distribution for rapid surveys with (a) Wenner_L and (b) Wenner_S

Table 7-3: Possible measurements for a typical field surveys

Arrays	**Number of measurements**		**Total number of measurements**
	L	S	
Wenner	190 (260)	87 (197)	277 (457)
Schlumberger	418 (637)	330 (501)	748 (1138)
Dipole-Dipole	414 (1057)	356 (924)	770 (1981)

The 2-D resistivity field data, collected across the dolerite sill intrusion at the Paradise site using the more typical protocols were inverted and Figure 7-14 displays the corresponding inverse model resistivity sections for the Wenner, Schlumberger and Dipole-Dipole arrays. The Wenner and Schlumberger arrays imaged the sill body better than the Dipole-Dipole array, but for all three arrays the continuous dolerite body is not very well defined. Comparison of Figure 7-14 with Figure 7-10 (the modelled resistivity sections using the protocols that include all possible measurements) shows that complete protocols generate inverse resistivity models which define the subsurface structures more successfully. The contacts between the dolerite body and the surrounding sedimentary rocks are more clearly resolved. The typical protocols employed in practice generate model sections with artefacts. It is seen particularly on the Wenner model section that the dolerite sill seems to have an extension towards the bottom of the profile.

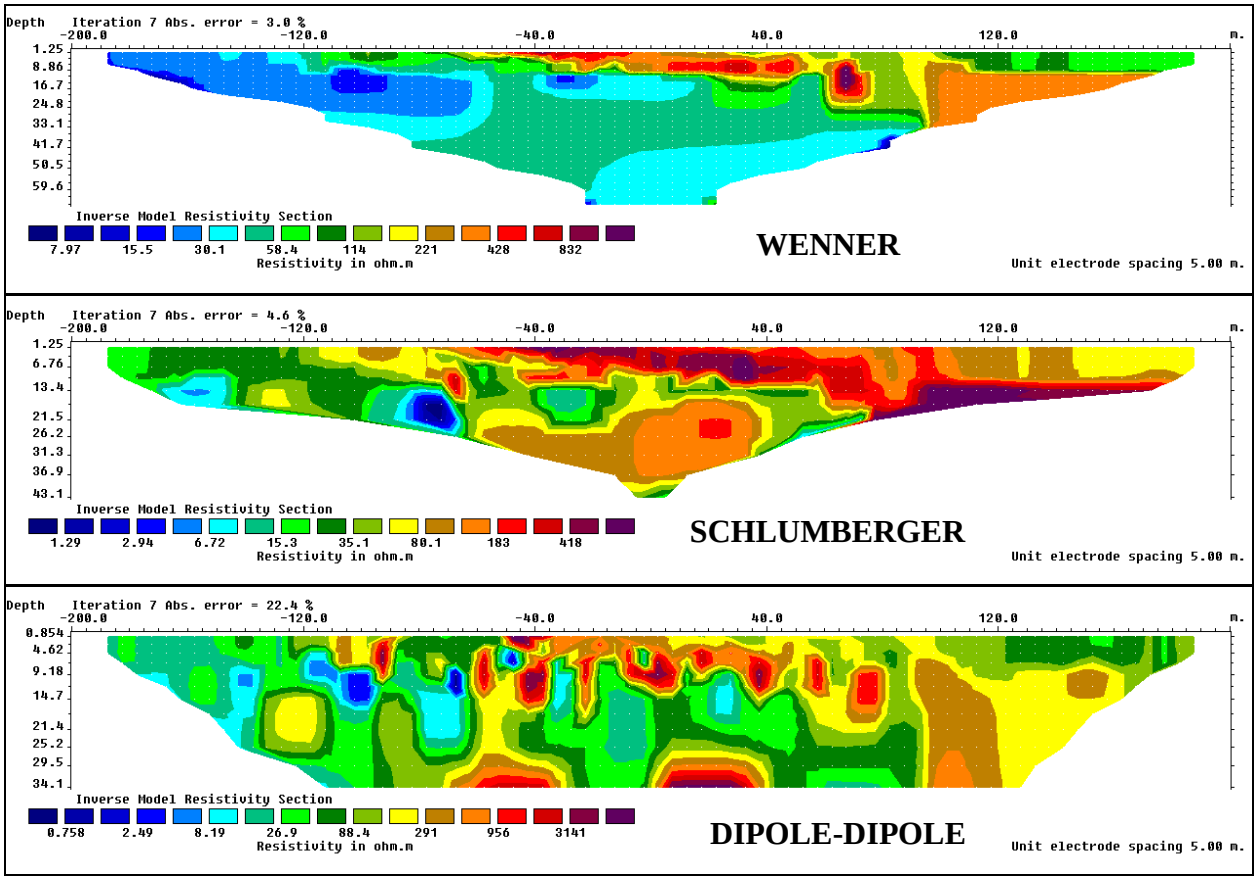

Figure 7-14: Modelled sections using the typical survey protocols across a dolerite sill at the Paradise site

7.3.2 Field survey across a dolerite dyke

The suitability of the Wenner, Schlumberger and Dipole-Dipole arrays in imaging vertical structures in the subsurface was evaluated by undertaking resistivity fieldwork across a dolerite dyke intrusion. The survey was conducted at the Krugersdrift site, near Bloemfontein. The current study area and the methods of investigation undertaken were both discussed in Chapter 7. In the field, the dolerite intrusion is outcropping (Figure 7-15) and has a width at surface of 35 to 45 m. This indicates that the intrusion present here is a thick dyke. The resistivity investigations were carried out in an area where the dyke is not visible at surface but has a depth of approximately 5 m. Interpretation of magnetic data recorded on a traverse perpendicular to the dyke (shown in Figure 7-16) suggested that the dyke is vertical or near-vertical.

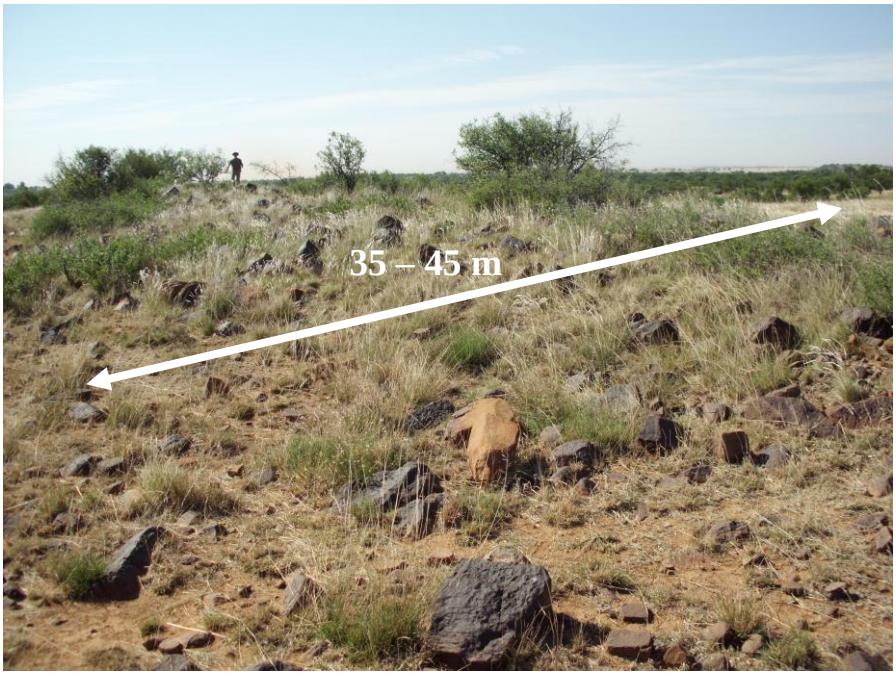

Figure 7-15: Thick dolerite dyke outcropping at the Krugersdrift site

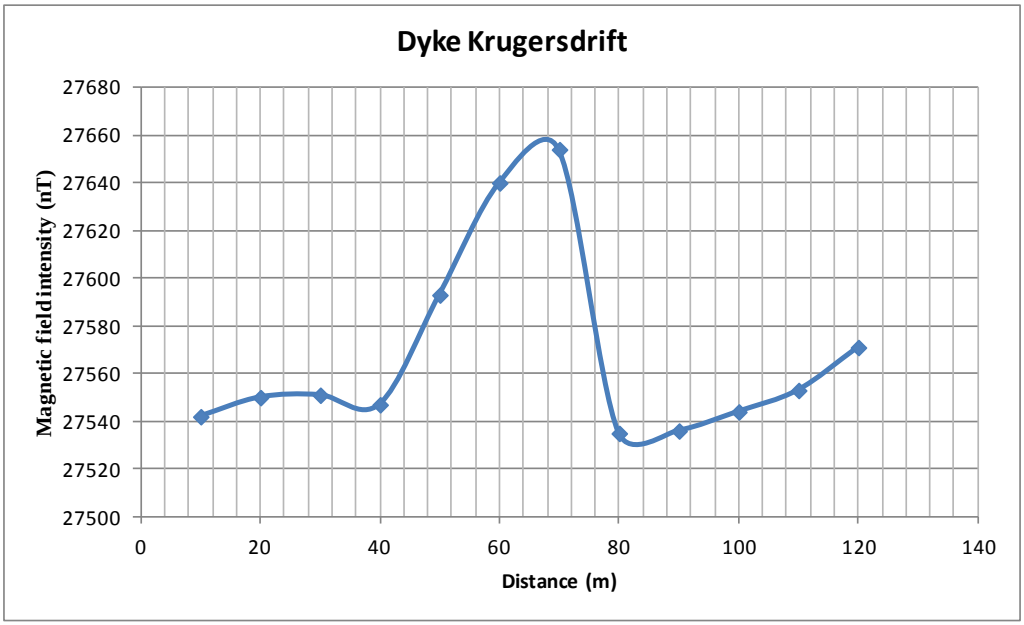

Figure 7-16: Magnetic profile across a dolerite dyke at the Krugersdrift site

During field investigations, the survey was planned in such a way that the dyke would be at the centre of the survey profile line. The RES2DINV program was used to invert the resistivity field data. During the least-square inversion, the robust constraint inversion (L1-norm) was selected, since the investigation site consists of discrete subsurface structures with sharp boundaries between the dolerite dyke and the surrounding rocks. Figure 7-17 presents the inverse model resistivity sections of the Wenner (top), the Schlumberger (middle) and the Dipole-Dipole (bottom) arrays.

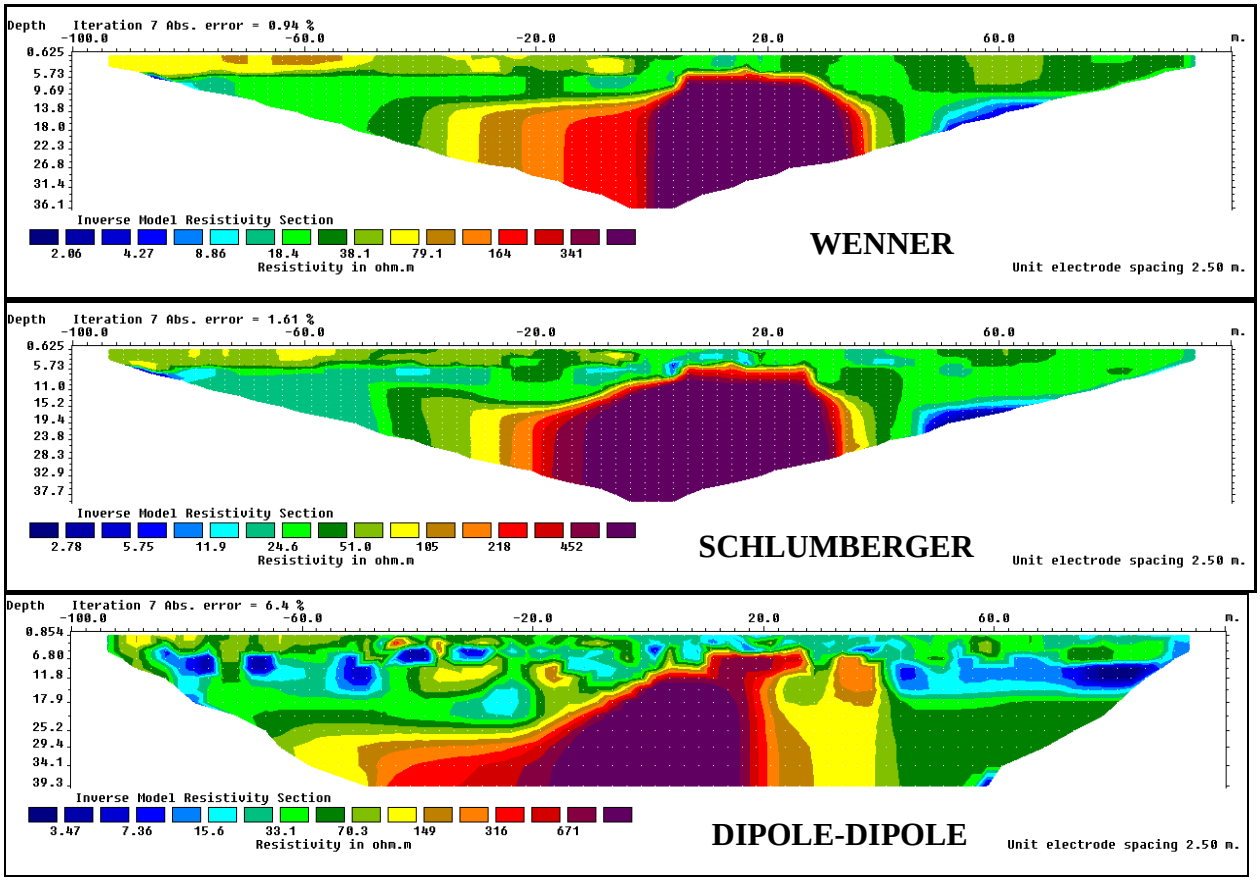

Figure 7-17: Modelled resistivity sections across a dolerite dyke at the Krugersdrift site

All three electrode arrays detected the dyke intrusion, but the shape of the dyke, its location, thickness, depth and horizontal extent are all different from one resistivity model to the next.

The Wenner array: Seven iterations were used during the inversion and an RMS error of 0.94% was obtained. In the modelled resistivity section (Figure 7-17), the vertical resistive body (resistivity > 341 Ω.m) present between positions 0 m and 30 m is the thick vertical dolerite dyke intrusion. The resistivity model of the Wenner array clearly imaged the dyke as a thick, vertical structure of high resistivity. The vertical change in resistivity, from the overburden to the dyke is very well defined, but the horizontal changes in resistivity, from the host rock to the dyke and from the dyke to the host rock, are gradual, especially on the left side of the dyke. This indicates the sensitivity of the Wenner array to vertical changes in the subsurface resistivity and its limits in accurately resolving horizontal changes in resistivity. For this survey carried out over a 200 m-total array length, the median depth of investigation for this array is approximately 36.1 m. The image is clear, not too noisy, which is due to the good signal strength obtained with the Wenner array.

The Schlumberger array: As with the Wenner array, seven iterations were done during inversion and an RMS error of 1.61% was obtained, which is greater than the RMS error (0.94%) of the Wenner array. The dolerite dyke intrusion is also identified as a vertical and thick structure. The dyke is located in the centre of the modelled resistivity section, (from -10 m to nearly 35 m), while it is displayed a little to the right in the Wenner modelled section. The Schlumberger array therefore more successfully identified the position of the dyke compared to the results using the Wenner array.

The vertical change in resistivity, observed on the Schlumberger modelled section, is almost similar to that observed in the Wenner modelled section. Significant differences are however noticed regarding the horizontal changes in resistivity between the host rock and the dyke. The horizontal changes in resistivity, although also gradual in the Schlumberger inverse model, are sharper than observed in the Wenner modelled section, especially on the left side of the dyke. The dyke thickness presented by the Schlumberger inverse model resistivity section (approximately 40 to 45 m) agrees better with the observed thickness of the outcrop.

The Schlumberger array is moderately sensitive to both vertical and horizontal changes in resistivity and produces a greater depth of investigation (almost 40 m) compared to the Wenner array (36.1 m). Results demonstrate the larger horizontal data coverage of the Schlumberger array compared to the Wenner configuration. The above observations and comments lead to the conclusion that the Schlumberger array is more suitable than the Wenner array in mapping vertical dyke intrusions.

The Dipole-Dipole array: The Dipole-Dipole inverse model resistivity section is displayed at the bottom of Figure 7-17. All data points with standard deviations greater than 7% were removed prior to inversion. Seven iterations were used during the inversion and an RMS of 6.4% was obtained. This RMS error is greater than the Wenner RMS error (0.94%) and the Schlumberger RMS error (1.61%). The vertical thick dolerite dyke intrusion is observed in the centre of the profile. The dyke intrusion here is not well represented by the resistivity model of the Dipole-Dipole array: large resistivity variations are seen adjacent to the structure. The dyke shape and thickness are different from the ones seen in the Wenner and Schlumberger modelled sections. These differences are partly due to the large number of bad data points collected with the Dipole-Dipole array during the resistivity field survey. During the inverse modelling process, although measurements with errors greater than 8% were removed, the remaining bad data points were still modelled as the number of iteration was

increased, consequently affecting the final inverse model section. These observations again illustrate the problems associated with the low signal strength of this array and its susceptibility to noise.

Before processing the field data, the inverse model was run and a median depth of investigation of 56.1 m was observed in the resistivity section, while the Wenner and Schlumberger depth were respectively 36.1 and 37.7 m. The Dipole-Dipole array thus has the greatest potential depth of investigation but the modelled resistivity section shows that, in practice, this array has greater difficulty in imaging deep features than the Wenner and Schlumberger arrays. Due to the fact that small distances between the potential electrodes are employed for many of the deeper measurements, small electrical potentials and small signal-to-noise ratios result. This is one of the limitations of this array. It is the reason for the poor data points obtained when measuring the resistivity of deeper structures. Figure 7-17 also shows that the Dipole-Dipole array has the widest horizontal data coverage, compared to the Wenner and Schlumberger arrays, yet the quality of many of the data points may be adversely affected by the inherent low signal strength of the array.

- **Dipole-Dipole model sections for truncated data sets**

Figure 7-18 displays the Dipole-Dipole inverse model resistivity sections (for a survey carried out across a dolerite dyke) for apparent resistivity data after removal of all data points with standard deviations in excess of 50% (top image), 20% (middle image) and 10% (bottom image). After seven iterations using the three truncated data sets, different RMS errors were obtained, namely 9.2%, 7.2% and 6.4% for the data sets with standard deviations below 50%, 20% and 10%, respectively. Figure 7-18 shows that the inverse model resistivity sections produced by data sets containing many data points of poor quality generate poor quality models compared to the Dipole-Dipole resistivity section in Figure 7-17.

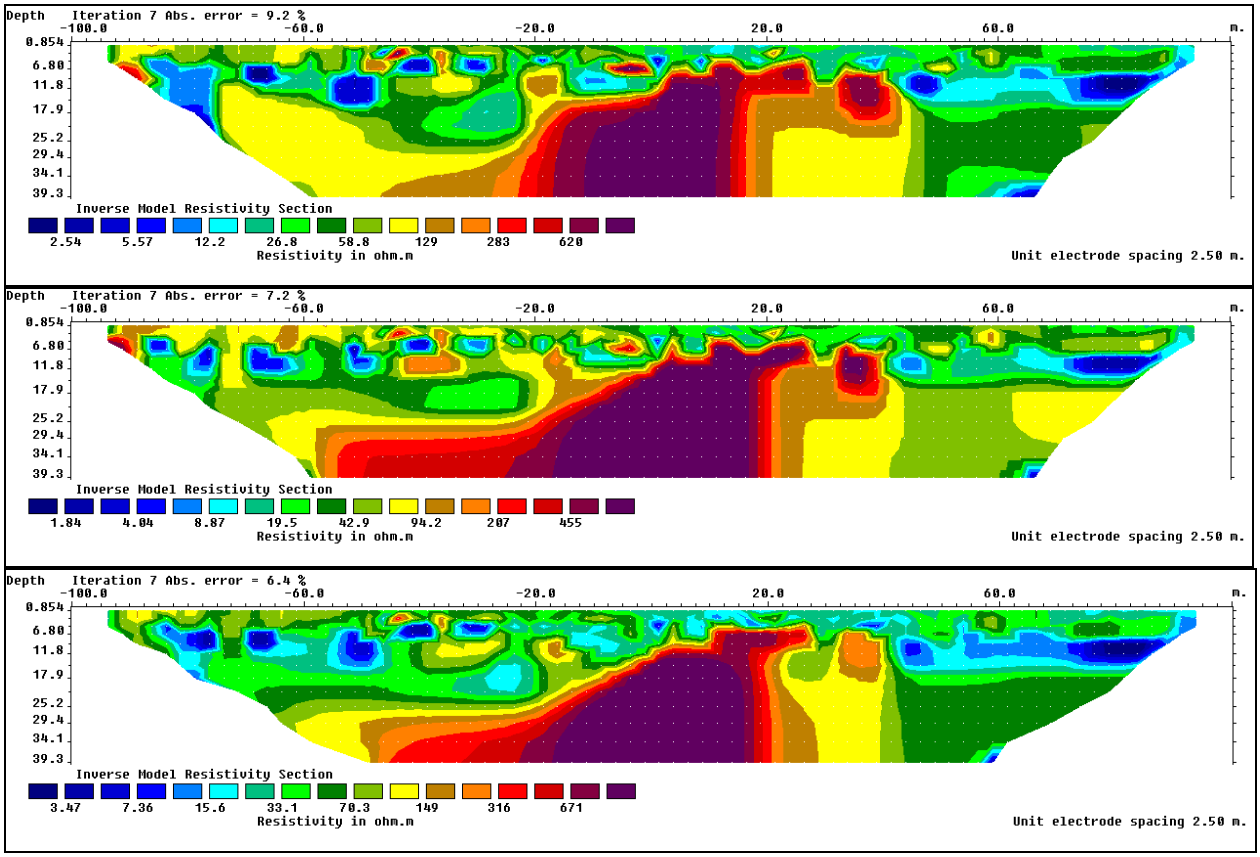

Figure 7-18: Inverse resistivity models for data recorded across a dyke using the Dipole-Dipole array. Data sets have been truncated to include data points with standard deviations less than 50% (top), 20% (middle) and 10% (bottom)

The suitability of the Wenner, the Schlumberger and the Dipole-Dipole arrays for producing inverse models imaging the vertical thick dolerite dyke intrusion differed from one array to another. Results showed that the Wenner and the Schlumberger arrays have almost similar sensitivities when mapping vertical dykes, but the Dipole-Dipole array, due to its poor signal strength and high susceptibility to noise might be less appropriate to map such structures. Both the Wenner and the Schlumberger arrays defined the horizontal and vertical contacts better than the Dipole-Dipole array. They have similar imaging resolution but different depths of investigation and different signal strengths. For field surveys across such vertical dyke intrusions, both arrays may be used, but the Schlumberger array showed to be the most successful array in mapping such structures.

❖ 2-D ERT using typical survey protocols

Resistivity field data collected across the dolerite dyke using the typical protocols that do not take into consideration all the possible measurements were inverted and Figure 7-19 displays the corresponding model sections for the Wenner, Schlumberger and Dipole-Dipole arrays.

Comparing Figure 7-19 to Figure 7-17 shows that the continuous dolerite body is not very well defined when using the truncated protocol. The protocols that include all possible measurements generate inverse model resistivity sections which define the subsurface structures more successfully. The contacts between the dyke and the surrounding sedimentary rocks are more clearly resolved. The typical protocols employed in practice generate model sections with depths shallower than the depths observed in model sections produced by the protocols that include all possible measurements. It also underestimated the width of the dyke, its position, as well as its shape.

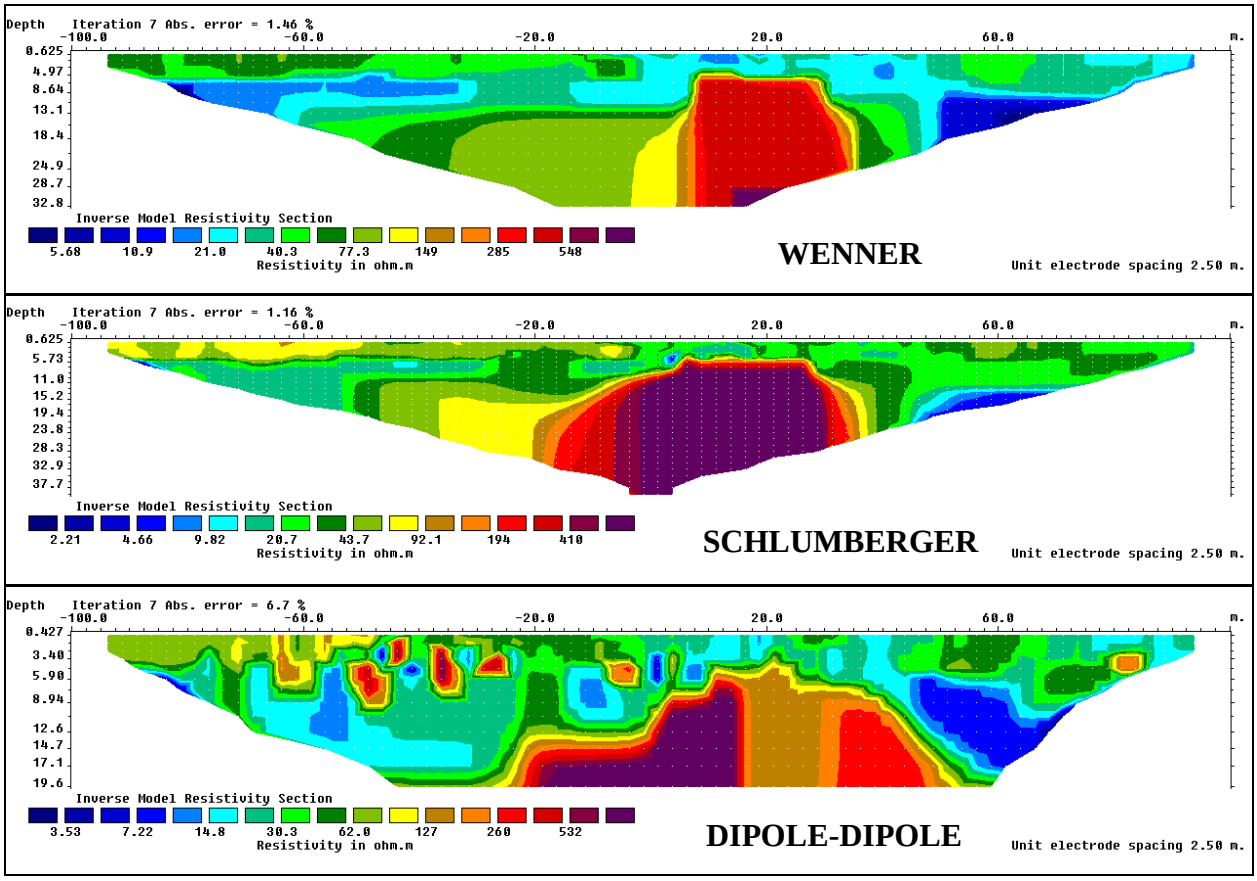

Figure 7-19: Modelled sections using the typical survey protocols across a dolerite dyke at the Krugersdrift site

7.3.3 Field survey across a dolerite sill intruded by a dyke

An example of a horizontal dolerite sill intruded by a dolerite dyke with thickness greater than 5 m (Figure 7-20) was observed on a farm located near the city of Bloemfontein. The current study site and the methods of investigation undertaken were both discussed in Sections 7.1 and 7.2.

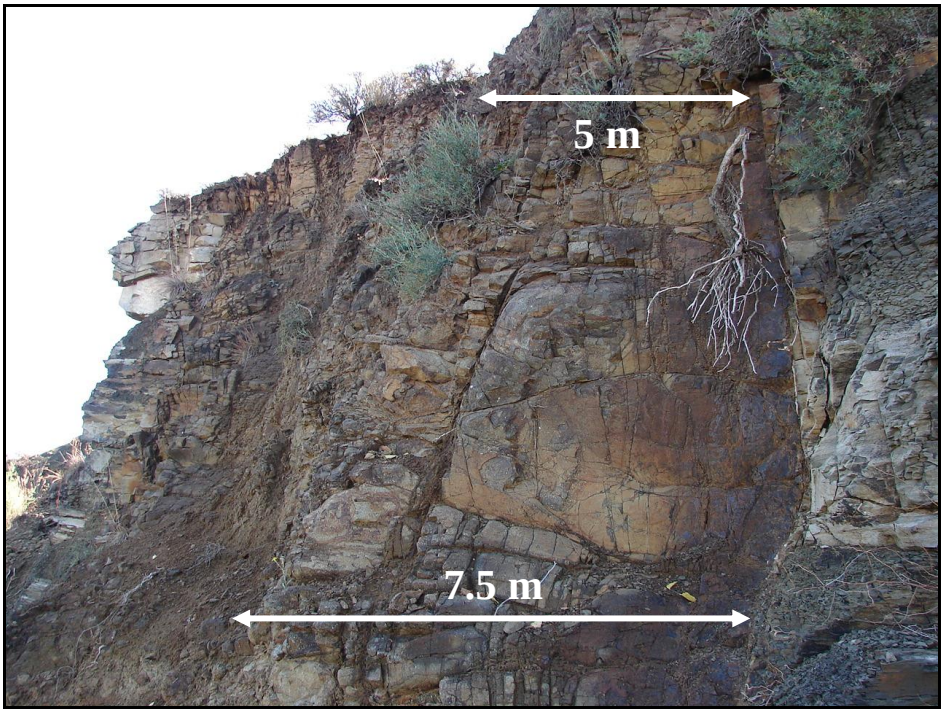

Figure 7-20: Trench showing the dyke thickness at the Meadows site

The performance of the Wenner, Schlumberger and Dipole-Dipole arrays in imaging both these structures was evaluated by conducting 2-D resistivity field surveys perpendicular to the strike of the dyke. Least-square inversions of the field data sets were performed using the software RES2DINV. Figure 7-21 presents the inverse model resistivity sections of the Wenner, Schlumberger and Dipole-Dipole arrays.

It is obvious that different electrode arrays produced significantly different modelled resistivity sections: the sensitivities to resistivity changes, the depths of investigation and the horizontal data coverage are all different from one model section to another. The shapes, the locations and the thicknesses of both structures are imaged differently in the three resistivity sections.

The Wenner array: The sill and the dyke are defined by this array (topmost model section of Figure 7-21). In the modelled resistivity section the sill is shown as a horizontal high resistive body (47.1 to 83.4 Ω.m), intersected by a vertical high resistive body, which is the dyke. The dyke appears here as a vertical to near-vertical structure. The horizontal changes in resistivity from the host rock to the dyke are gradual. In the field, a value of 7.5 m corresponding to the dyke thickness was measured at 3 to 4 m below the surface (Figure 7-20). In the Wenner model, at 3 m below the surface the thickness of the dyke is almost 10 m. This array overestimated the thickness of the dyke. The horizontal sill on the left side of the dyke

appears just as a rectangular resistive body. The vertical changes in resistivity, from the sill to the host rock, are gradual, rather than sharp as expected. This array might have difficulties in simultaneously mapping both horizontal and vertical structures. The image quality demonstrates the strong signal strength of this array, although the investigation only considers depths up to 74.7 m.

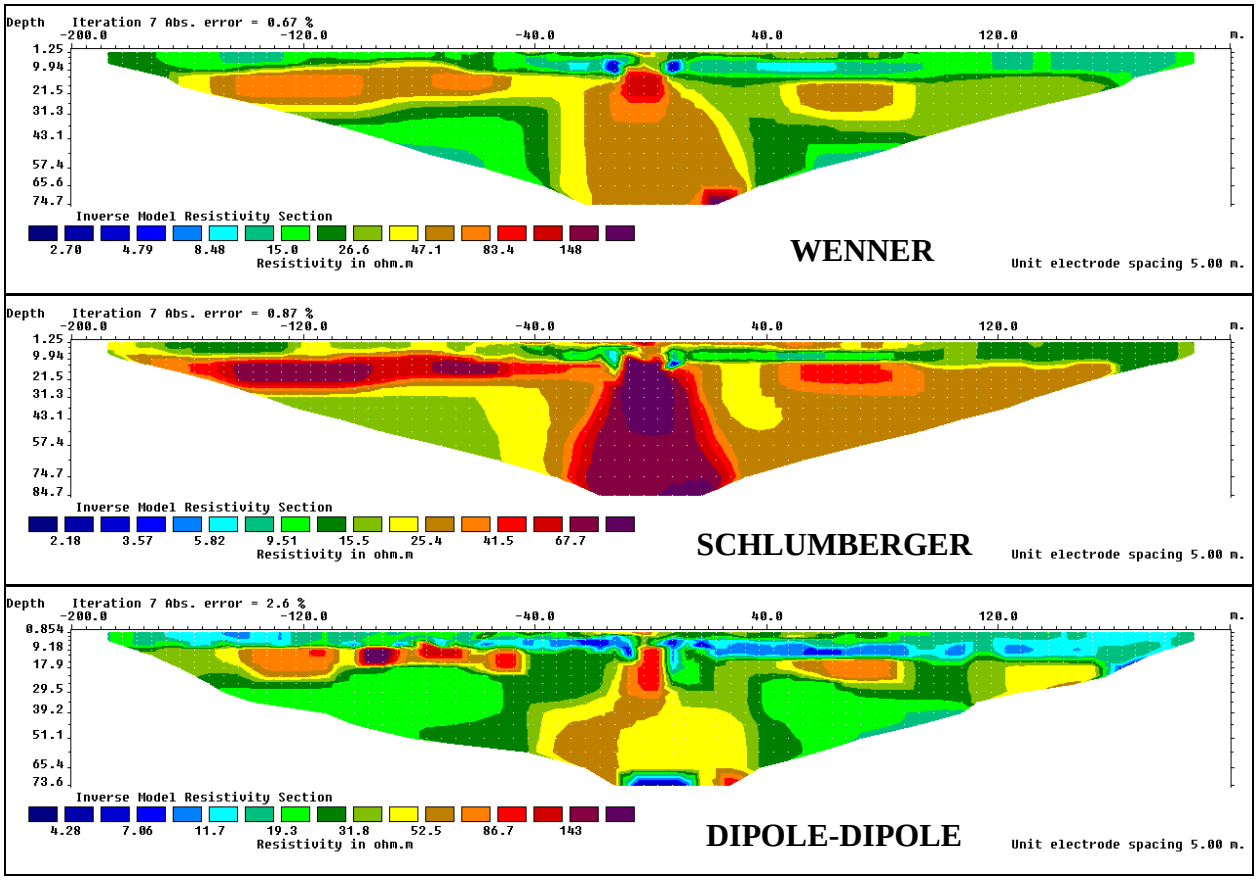

Figure 7-21: Modelled resistivity sections across a sill intruded by a dyke at the Meadows site

The Schlumberger array: The modelled resistivity section of the Schlumberger array displayed as the centre image of Figure 7-21 revealed that this array was very successful in detecting and defining both the dyke and the sill known to occur in the study area. The vertical resistive body, with a resistivity of approximately 70 Ω.m, is the dyke intrusion. The Schlumberger array imaged the sill as a resistive horizontal structure on the left side of the dyke. It was fairly successful in defining the horizontal structure as well as the vertical contacts between the two intrusions and the host rocks. At 3 m below the surface the thickness of the dyke is almost 7.5 m, which correspond to the dyke thickness measured at 3 m below the surface in the field (Figure 7-20). For a total array length of 400 m, the depth of investigation obtained was 42.3 m, which is 6.2 metres greater than the maximum depth of

the Wenner array. Compared to the Wenner array, the Schlumberger array is the most suitable configuration recommended for simultaneously mapping both vertical and horizontal structures in the earth's subsurface.

The Dipole-Dipole array: With an RMS error of 2.6% obtained after seven iterations, the inversion process converged and displayed the Dipole-Dipole inverse model presented at the bottom of Figure 7-21. The sill and the dyke were detected but could not be well defined in the profile. The dyke is shapeless; the sill is less thick than in the Wenner and Schlumberger models. The model produced some artefacts: for example, a low resistive zone (4.28 Ω.m) appears at large depths in the centre of the model section. The horizontal and vertical extents of the sill and dyke, as well as their thicknesses are totally different from the Wenner and Schlumberger inverse models. This array may have the widest data coverage and the deepest depth (the inverse model obtained prior to data processing gave a 103.6 m-depth of investigation), yet it is less successful in imaging both the vertical and horizontal structures known to occur at the site of investigation.

- **Dipole-Dipole model sections for truncated data sets**

The Dipole-Dipole inverse model sections for a survey carried out across a dolerite sill intruded by a dyke are displayed in Figure 7-22 for truncated data sets after removal of all data points with standard deviations in excess of 50%, 20%, 10%, 5% and 2%. Different RMS errors were obtained after seven iterations using the three truncated data sets: 15.6%, 11.6%, 8.8%, 6.1% and 4.0% for the data sets with standard deviations below 50%, 20% 10%, 5% and 2%, respectively. Compared to the Dipole-Dipole inverse model at Figure 7-21, these model sections (Figure 7-22) show that data sets containing many data points of poor quality generate models in which the representation of subsurface structures are inaccurate and less detailed. It is also noticed that as more data of poor quality are removed, the horizontal sill intrusion becomes better imaged in the model sections.

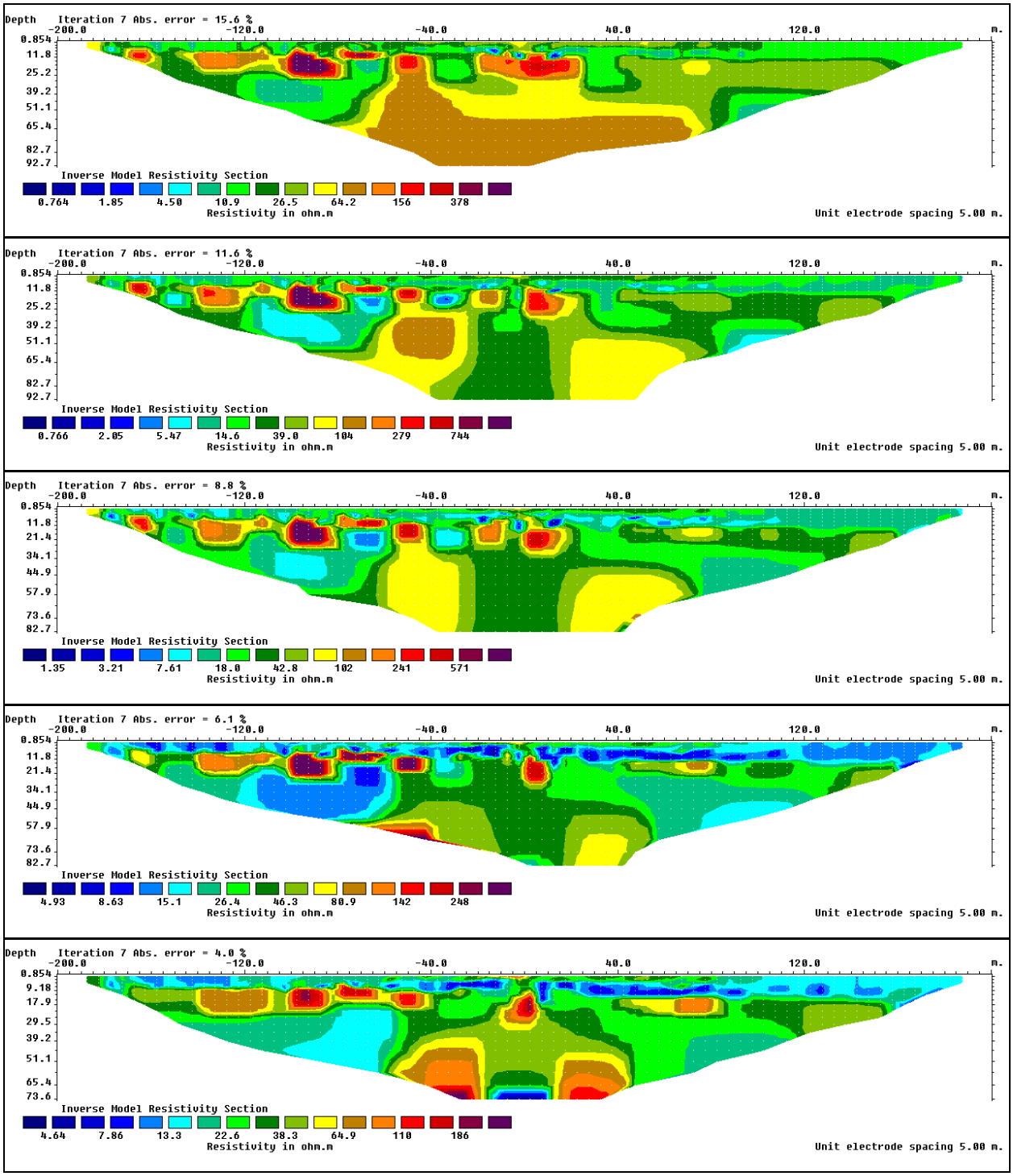

Figure 7-22: Inverse resistivity models for data recorded across a sill intruded by a dyke using the Dipole-Dipole array. Data sets have been truncated to include data points with standard deviations less than 50%, 20% 10%, 5% and 2%

❖ 2-D ERT using typical survey protocols

Figure 7-23 presents the inverse model resistivity sections obtained from the 2-D resistivity field data, collected across a dolerite sill intruded by a dyke, employing the typical protocols used in practice. Only the Dipole-Dipole array failed in imaging both the vertical and

horizontal structures very well. Yet here also, it is seen that the horizontal sill intrusion is imaged, although less clearly than with the Wenner and Schlumberger arrays. The model resistivity sections obtained from the protocols that include all possible measurements (refer to Figure 7-21), compared to the inverse model sections of the typical protocols used in practice, show that complete protocols generate models which define the subsurface structures more successfully. The contacts between the dolerite bodies and the surrounding rocks are clearly resolved. The typical protocols employed in practice may generate model sections with artefacts, particularly with the Dipole-Dipole array.

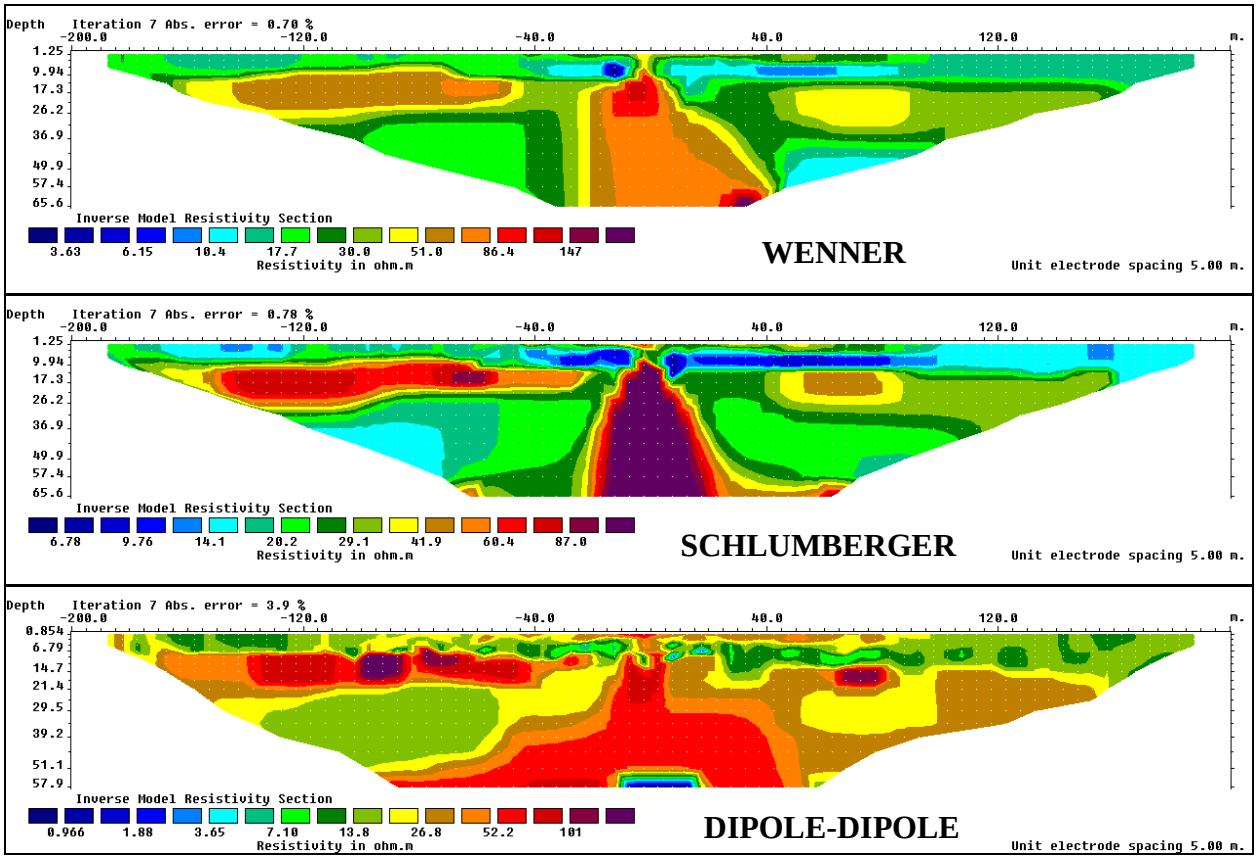

Figure 7-23: Modelled sections using the typical survey protocols across a sill intruded by a dyke at the Meadows site

As Figure 7-10, Figure 7-17 and Figure 7-21 showed, different arrays used to map the same region can give rise to very different resistivity models. These figures also give an idea of the data coverage that can be obtained with different arrays. Note that the Dipole-Dipole array gives the widest horizontal coverage, while the coverage obtained with the Wenner and the Schlumberger arrays decrease much more rapidly with increasing electrode spacing.

The sensitivities of the three selected electrode arrays used to map a horizontal dolerite sill intrusion differed from one array to another. Results showed that the Wenner array defined

the horizontal contacts the most successfully, followed by the Schlumberger array. This array (Wenner) was the most successful in defining the vertical changes in resistivity compared to the other two arrays. Its signal strength is the greatest, even though it has a smaller depth of investigation and less horizontal data coverage. From these observations the following conclusions may be drawn: for 2-D ERT field surveys across horizontal structures such as dolerite sill intrusion, the most appropriate electrode array appears to be the Wenner array. Conversely, because of its susceptibility to noise, it is advised to avoid the use of the Dipole-Dipole array to map such structure in the Karoo rocks.

The suitability of the Wenner, the Schlumberger and the Dipole-Dipole electrode geometries evaluated in mapping a vertical dolerite dyke intrusion revealed: the Schlumberger array defined and imaged the vertical contacts the most successfully, followed by the Wenner array. Its depth of investigation was greater than the depth of investigation of the Wenner array. These results imply the following: for 2-D ERT field surveys across vertical structures, such as vertical dolerite dyke intrusion in Karoo rocks, the most appropriate electrode arrays are the Schlumberger and Wenner arrays. The Dipole-Dipole array is not recommended due to its susceptibility to noise.

Regarding the evaluation of the suitability of the three arrays selected to map a horizontal sill intruded but a vertical dolerite dyke, once again the results differed from one electrode array to another. The Schlumberger array was revealed to be the most appropriate in defining both the vertical and horizontal contacts, followed by the Wenner array. Its depth of investigation was greater than that of the Wenner array. These results suggest the following: for 2-D ERT field surveys across a combination of vertical and horizontal structures, such as a dolerite sill intruded by a dolerite dyke, the most suitable configurations are the Schlumberger and the Wenner arrays, but preferably the Schlumberger array. The Dipole-Dipole array, because of its numerous limitations, is not recommended for mapping such structures in Karoo rocks.

7.4 COMPARISONS OF FIELD RESULTS TO THEORETICAL CONSIDERATIONS

Theoretical considerations in this section refer to the results obtained from the numerical modelling investigations (Chapter 6) as well as the findings of several authors.

7.4.1 Results obtained from surveys across dolerite sills

Results from the 2-D ERT field surveys conducted across horizontal structures such as dolerite sill intrusions in the Karoo revealed that the Wenner array is the most suitable electrode array to map such structures. It detected, identified and defined the horizontal contacts the most successfully and represented the vertical changes in resistivity more accurately than the Schlumberger and Dipole-Dipole arrays. These results are completely in agreement with the results predicted by the numerical modelling investigations of Chapter 6. These results also confirm the theoretical results of Dahlin and Zhou (2004), Loke (1999) and Loke (2012). These authors indicated that the Wenner array is relatively sensitive to vertical changes in the subsurface resistivity.

Seaton and Burbey (2002), as well as Zhou *et al.* (2002) conducted two different studies in the USA, respectively titled: "Evaluation of 2-D resistivity methods in a fractured crystalline-rock terrain" and "Effective electrode array in mapping karst hazards in electrical resistivity tomography". Both studies revealed the great suitability of the Wenner array for detecting vertical changes in resistivity, results in accordance with the current findings in Karoo rocks. Recently, Ahmad *et al.* (2010) conducted 3-D resistivity field surveys over an underground cavity in Malaysia using both the Wenner and Dipole-Dipole arrays, and concluded that the Wenner array is very suitable for determining the vertical distribution of the subsurface resistivity. Once again, these results are in accordance with the current findings in the Karoo rocks.

7.4.2 Results obtained from surveys across dolerite dykes

For the 2-D ERT field surveys conducted in the Karoo across vertical structures such as dolerite dyke intrusions, the current study revealed the superiority of the Schlumberger array over the Wenner and Dipole-Dipole arrays. This electrode array (Schlumberger) was shown to be the most sensitive to vertical structures: it successfully detected and defined the vertical contacts and represented the horizontal changes in resistivity quite accurately. For such structures, the numerical modelling results (Chapter 6) recommended both the Dipole-Dipole and Schlumberger arrays: the Dipole-Dipole array if low noise levels occur, but the Schlumberger array if the survey is conducted in an area with high background noise levels. The field results are therefore in accordance with the numerical modelling results. Perren (2005) investigated the performance of the common electrical resistivity arrays used in

resistivity method and concluded that the Schlumberger array performs well in mapping the boundaries of vertical structures – a conclusion in accordance with the current findings regarding the suitability of the Schlumberger array for mapping dolerite dykes in Karoo rocks. Zhou *et al.* (2002) also state that the Schlumberger array is very successful in mapping vertical structures.

Some other authors however, found that the most successful electrode array in mapping vertical structures is the Dipole-Dipole array, but also concluded that the Schlumberger array could be used to map such structures (Loke, 1999; Loke, 2012; Seaton and Burbey, 2002). Note that conclusions of Loke were based on only numerical modelling results; no resistivity field surveys were undertaken to confirm or contradict that theory. However, the research of Seaton and Burbey (2002) emanated from field investigations where both the Dipole-Dipole and Schlumberger arrays were used. During the 2-D ERT surveys undertaken, the "a" spacings and the "n" factor were limited up to 3 and 6 respectively, for both arrays. This considerably limits the depth of investigation and the level of accuracy of the results in defining the borders of the continuous body being investigated. By using measurement protocols that include fewer measurements, many details about the subsurface resistivity distribution may be missed (see Section 7.3). For this reason it is recommended that more complete survey protocols be employed when time- and financial constraints allow.

Some authors employ measurement protocols that contain fewer measurements to avoid recording very noisy and unusable data (such as data recorded with the Schlumberger and Dipole-Dipole arrays when the "n" factor becomes large). Inverse model resistivity sections obtained from these types of surveys might be less accurate and give less detail about the distribution of the structures present within the subsurface. While conducting 2-D ERT field investigations across dolerite dykes in the Karoo, the protocol that contains all the possible measurements, in which the "a" spacings and the "n" factor are considered more than 3 and 6, respectively, was used. This explains why the current field results are different from the results obtained by Seaton and Burbey (2002).

7.4.3 Results obtained from surveys across dolerite sill intruded by dyke

Comparisons of the field results obtained after surveys conducted across dolerite sills intruded by dolerite dykes in the Karoo to the theoretical considerations revealed many similarities. Field results demonstrated that the Schlumberger array is the most suitable

electrode array when both vertical and horizontal structures are present in the subsurface. It defined both the vertical and horizontal contacts the best and represented the vertical and horizontal changes in resistivity more accurately than the Wenner and Dipole-Dipole arrays. These field results are entirely in agreement with the results obtained from the numerical modelling investigations studied in Chapter 6. Loke (1999), Loke (2012), as well as Dahlin and Zhou (2004), after several numerical modelling investigations predicted that the Schlumberger array is moderately sensitive to both horizontal and vertical structures. Loke (1999) furthermore stated that in areas where both types of geological structures are expected, this array might be a good compromise between the Dipole-Dipole and the Wenner arrays: considerations now confirmed by the results of the resistivity field surveys conducted over the sill intruded by the dyke in the Karoo rocks.

Regarding the signal strength, the median depth of investigation, the horizontal data coverage as well as the image resolution, results obtained from the 2-D ERT surveys conducted over various structures present in the Karoo Formations, are in accordance with the numerical modelling findings of Chapter 6 of the current thesis. These results also confirm the theoretical considerations of several authors (Loke, 1999; Loke, 2012; Dahlin and Zhou, 2002) and are in agreement with the findings of other authors (Seaton and Burbey, 2002; Zhou *et al.*, 2002; Ahmad *et al.*, 2010).

- The Wenner array has the strongest signal strength, followed by the Schlumberger array. Among the three electrode arrays, the Dipole-Dipole array has the lowest signal-to-noise ratio.

- The Dipole-Dipole has the greatest theoretical depth of investigation (although the smallest depth resolution), followed by the Schlumberger array and finally the Wenner array.

- In terms of horizontal data coverage, from the widest to the narrowest, the electrode arrays rank as follows: the Dipole-Dipole, the Schlumberger, and the Wenner array.

- However, Dahlin and Zhou (2004) found that the Dipole-Dipole array can under certain circumstances yield better results than the Schlumberger and Wenner arrays, although it is more susceptible to noise contamination.

Table 7-4: Summary regarding the advantages/disadvantages of the arrays

MAPPING DYKES					
		Wenner	Schlumberger	Dipole-Dipole	Pole-Pole
Sensitivity	Rank	2nd	1st	3rd	4th
	Quality	Good	Good	Fair	Very bad
Depth of investigation	Rank	4th	3rd	2nd	1st
	Quality	Shallowest	Deep	Deep	Deepest
Signal strength	Rank	1st	2nd	3rd	4th
	Quality	Best	Good	Very bad	Poorest
Horizontal data coverage	Rank	4th	3rd	2nd	1st
	Quality	Narrow	Large	Large	Largest
Suitability (rank)		**2nd**	**1st**	**3rd**	**4th**
MAPPING SILLS					
		Wenner	Schlumberger	Dipole-Dipole	Pole-Pole
Sensitivity	Rank	1st	2nd	3rd	4th
	Quality	Best	Good	Poor	Very bad
Depth of investigation	Rank	4th	3rd	2nd	1st
	Quality	Shallowest	Deep	Deep	Deepest
Signal strength	Rank	1st	2nd	3rd	4th
	Quality	Best	Good	Very bad	Poorest
Horizontal data coverage	Rank	4th	3rd	2nd	1st
	Quality	Narrow	Large	Large	Largest
Suitability (rank)		**1st**	**2nd**	**3rd**	**4th**
MAPPING SILLS INTRUDED BY DYKES					
		Wenner	Schlumberger	Dipole-Dipole	Pole-Pole
Sensitivity	Rank	2nd	1st	3rd	4th
	Quality	Good	Good	Poor	Poorest
Depth of investigation	Rank	4th	3rd	2nd	1st
	Quality	Shallowest	Deep	Deep	Deepest
Signal strength	Rank	1st	2nd	3rd	4th
	Quality	Best	Good	Bad	Poorest
Horizontal data coverage	Rank	4th	3rd	2nd	1st
	Quality	Narrow	Large	Large	Largest
Suitability (rank)		**2nd**	**1st**	**3rd**	**4th**

8 CONCLUSIONS AND RECOMMENDATIONS

The present thesis evaluates the suitability of different electrodes arrays used during 2-D ERT surveys for geohydrological studies in Karoo rocks. Experience has shown that, in Karoo rocks, groundwater often occurs within joints and fractures in the contact zones between intrusive plutonic bodies and the host rock. Boreholes intersecting such features more often have high yields. It follows that the methods which accurately map the contact zones between the Karoo rocks and the intrusive bodies could increase the success rate of groundwater exploration programmes in Karoo rocks.

Mapping the contacts between dolerite intrusions and their host rocks also has application in other geohydrological investigations, such as the study of contaminant migration in the subsurface. Since fresh dolerite intrusions may act as barriers to groundwater flow and contaminant migration in directions perpendicular to the strikes of the bodies, being able to accurately map the boundaries between the sedimentary and igneous rocks could assist in predicting pollution plume migration.

The goals of the current research were to study, examine and evaluate different electrode arrays (the Wenner, Schlumberger, Dipole-Dipole and Pole-Pole arrays) in terms of their suitabilities for mapping vertical/horizontal/dipping contacts associated with different geological structures present in the Karoo rocks. Such structures could include not only intrusive dolerite dykes and sills, but also fault zones and weathered zones.

To achieve these goals the following actions were taken:

- ✓ Theoretical studies on the sensitivity functions, depths of investigation, signal strengths and horizontal data coverage of various electrode arrays;
- ✓ Several numerical modelling investigations were performed in order to study the expected responses of different arrays for 2-D ERT measurements over sills, dykes, sills intruded by dykes, weathered zones and faults;
- ✓ 2-D ERT field surveys were conducted on Karoo rocks at three different sites where dolerite dyke and sill intrusions are known to occur.

Theoretical studies

As part of the theoretical studies, the sensitivity functions of different electrode arrays were investigated. Each electrode array could potentially define the horizontal and vertical contact zones between the abovementioned dyke and sill intrusions and their hosts. However, these arrays do not yield the same response to such target bodies. The choice of the appropriate electrode arrays which responds the most successfully to a specific target body is based on a characteristic of the array called the **sensitivity function**. The sensitivity function describes the degree to which a change in the resistivity of a section of the subsurface influences the electrical potential measured by the array. The sensitivity functions of the Wenner, Schlumberger, Dipole-Dipole and Pole-Pole arrays were calculated and the results showed different sensitivity functions for the different electrode arrays, due to their different geometrical arrangements. Note that the term "Schlumberger array" was used in this thesis to describe the Wenner-Schlumberger array.

Results from the theoretical studies showed that the Wenner array is good in resolving vertical changes (horizontal structures), but relatively poor in detecting horizontal changes. The Dipole-Dipole array is rather very sensitive to horizontal changes in resistivity, but relatively insensitive to vertical changes in the resistivity, while the Schlumberger array is moderately sensitive to both horizontal and vertical changes in the Earth's subsurface.

Modelling investigations

Several characteristics of the different electrode arrays, such as the sensitivity of the array to vertical and horizontal resistivity changes in the Earth's subsurface, the median depth of investigation, the signal strength, as well as the horizontal data coverage were evaluated while studying the suitability of the different arrays. These characteristics were studied by performing several numerical modelling investigations. In this research, the differences in the sensitivity functions were examined in order to explain the response of the different arrays to different types of structures and to compare to the suitability of these arrays for a particular survey. The suitability of four electrode arrays was examined by means of 20 synthetic geological models, simulating dykes and sill intrusions, weathered zones, faults as well as contact zones.

The modelled responses, obtained by performing robust inversion (using the L1-norm) revealed that the Dipole-Dipole array is more sensitive to horizontal changes in the earth subsurface resistivity variations; it has a very good depth penetration, a wide horizontal data

coverage, but a low signal-to-noise ratio. The Wenner array is very sensitive to vertical changes, has the strongest signal strength, yet the smallest depth of investigation and the narrowest horizontal data coverage. The Schlumberger array might not be the most suitable array in resolving dipping structures, but its performance when mapping sills intruded by dykes is good; it has a moderate depth of investigation and is less contaminated by noise compared to the Dipole-Dipole array. The Pole-Pole array has the largest depth of investigation, the widest horizontal data coverage, yet the lowest signal strength and is therefore inherently sensitive to noise.

Based on the results of the modelling investigations, it was decided to employ only the Wenner, Schlumberger and Dipole-Dipole arrays for the field surveys.

Field measurements

The 2-D ERT field surveys were conducted at three different sites (all underlain by rocks of the Karoo Supergroup) where the geology is well known, namely a site near the Krugersdrift Dam, the Paradise agricultural test site and a site in the Meadows area, south-east of Bloemfontein. ERT surveys were conducted across an intrusive dyke at the Krugersdrift site, across a dolerite sill intrusion at the Paradise site, and across a dolerite sill intruded by a dolerite dyke at the Meadows site.

The three different electrode arrays used for field surveys produced significantly different inverse resistivity models for each geological structure being mapped.

For the ERT surveys conducted across a dolerite sill intrusion, the Wenner array performed the best in defining the contacts. The field data was of a good quality due to the strong signal strength of this array. The Wenner array detected and identified the horizontal boundaries of the sill very well. The inverse resistivity model obtained for the Wenner array displayed sharp vertical changes in resistivity, corresponding to the geological conditions known to exist in the study area. The results were also compared to the findings of several authors and were found to be in good agreement. The Wenner array is thus shown to be very sensitive to vertical changes in resistivity within the Earth's subsurface, and is therefore suitable for mapping horizontal structures such as dolerite sill intrusion in Karoo rocks.

Regarding the 2-D ERT surveys carried out across a dolerite dyke intrusion, the Schlumberger array was the most successful in imaging the vertical contacts. Although the field data had some noise, this array imaged the vertical structure better than the other arrays.

It successfully imaged the vertical boundaries of the dyke. Moreover, it gave a better depth penetration compared to the Wenner array. The results obtained from the Schlumberger array in mapping vertical dyke intrusions were compared to the predictions of several authors regarding the applicability of this array when mapping vertical structures. Some authors predicted that the Dipole-Dipole array would be the best configuration to map such structures, while others suggested that the Schlumberger array would be the most suitable. The limitations of the Dipole-Dipole array in mapping such structure were illustrated during the current research. For large depths of investigation, electrode configurations with "n" factors larger than 6 were employed. However, large values of the "n" factor led to small differences in the recorded electrical potentials at the potential electrodes and hence poor data quality. The poor data quality in turn produced resistivity models containing many artefacts. For "n" factors less or equal to 6, only shallow depths of investigation could be attained. Taking these limitations into account, the Schlumberger array is revealed to be the most suitable array to map vertical structures such as dolerite dyke intrusion in the Karoo rocks.

The field results obtained from surveys conducted over a horizontal dolerite sill intruded by a vertical dolerite dyke showed that the Schlumberger array is the most suitable electrode array to simultaneously image both vertical and horizontal changes in resistivity in the subsurface. The inverse resistivity model obtained from the Schlumberger array imaged the vertical and horizontal changes in resistivity more sharply than the Wenner and Dipole-Dipole arrays. The field results were in perfect agreement with the considerations of the numerical modelling investigations performed during this study, as well as the conclusions from previous modelling investigations by several authors. The Schlumberger array is thus shown to be very sensitive to both vertical and horizontal changes in resistivity within the earth subsurface, and is therefore suitable for surveys where both vertical and horizontal structures are present.

Recommendations for ERT surveys in Karoo rocks

Based on the findings of the current study, the following recommendations are made:

⇒ For 2-D ERT surveys across horizontal structures such as dolerite sill intrusions, horizontal sedimentary layers, and horizontal boundaries between two geological bodies with different resistivities, the Wenner array is recommended, although the Schlumberger array may also yield acceptable results. However, the Dipole-Dipole array is not recommended for such structures due to its lower sensitivity to vertical changes in resistivity.

⇒ For 2-D ERT surveys over vertical or near-vertical geological structures such as dolerite dyke intrusions, fault zones, and vertical boundaries between two geological bodies with different resistivities, the Schlumberger array is recommended. The Wenner array, although less sensitive to horizontal changes in resistivity, may also be considered, especially if the surveys are conducted in areas with high background noise, since this array has the largest signal strength. Due to its susceptibility to noise, the Dipole-Dipole array is not recommended.

⇒ For resistivity field measurements conducted in areas where both vertical and horizontal structures are expected, the Schlumberger array appears to be the most suitable array. This array may successfully image both vertical and horizontal contacts.

⇒ For 2-D ERT surveys carried out across weathered zones, the Schlumberger and the Wenner arrays are both recommended.

⇒ For resistivity field surveys undertaken across dipping structures, both the Wenner and the Schlumberger arrays may be considered.

⇒ During groundwater exploration in Karoo rocks, the contact zones between dolerite intrusions and the surrounding host rock are often targeted. There is therefore a need to accurately map such contacts. Since the robust constraint inversion (L1-norm) produces models with sharp boundaries between different geological bodies, it is recommended that this inversion algorithm be employed when performing inversion of the resistivity data recorded from the field.

⇒ For 2-D ERT surveys aimed at mapping groundwater pollution or targeting the extent of a contaminant plume, it is recommended that either the Wenner or the Schlumberger array be employed. The Wenner array may be considered if the pollution has occurred within horizontal sedimentary layers, or if horizontal structures such as dolerite sills occur in the study area. The Schlumberger array would be suitable in the case where a dyke (which might also act as a barrier to the contaminant migration) or other vertical structures occur within the site under investigation.

⇒ Resistivity field data collected by either the Wenner or the Schlumberger array when investigating groundwater pollution should be inverted using the L2-norm (smoothness-constrained least-squares inversion) because the diffusion boundary of a contaminant plume in the subsurface geology exhibits a smooth variation. The L2-norm inversion method will give optimal results under such conditions where gradual changes in the subsurface resistivities are expected.

REFERENCES

ABEM (2010). *Instruction manual: Terrameter SAS 4000 / SAS 1000, ABEM Instrument AB.* ABEM printed matter 93109. Sweden: ABEM Instrument AB.

Acworth, R.I. (1987). The development of crystalline basement aquifers in a tropical environment. *Quarterly Journal Engineering Geology*, **20**, 265-272.

Advanced Geosciences Inc. (AGI). (1997). *Sting R1 instruction manual*, release 2.5.5. Austin, Texas: Advanced Geosciences.

Agramakova, Y. (2005). *Time-Lapse Electrical Resistivity Tomography Applied to Cave Sustainability (Barbados) and Groundwater Exploration (Saint Lucia).* MSc. Thesis (unpublished), Moscow State University. 69pp.

Ahmad, N., Wan Abdullah, W.A.T., Samsudin, T. and Behrang, N. (2010). Comparison of Wenner and Dipole–Dipole arrays in the study of an underground three-dimensional cavity. *Journal of Geophysics and Engineering*, **7** (2010), 30–40.

Archie, G. (1942). Electrical Resistivity Log as an aid in determining some reservoir characteristics. *Transactions of AIME*, **146** (1), 54-62.

Barker, R.D. (1991). Depth of investigation of collinear symmetrical four-electrode arrays. *Geophysics*, **54**, 1031-1037.

Barker, R.D. (1996). The application of electrical tomography in groundwater contamination studies. *EAGE 58th Conference and Technical Exhibition Extended Abstracts*, P082.

Binley, A., Cassiani, G., Middleton, R. and Winship, P. (2002). Vadose zone flow model parameterisation using cross-borehole radar and resistivity imaging. *Journal of Hydrology*, **267**:147-159.

Botha, J.F., Verwey, J.P., Van der Voort, I., Vivier, J.J.P., Buys, J., Colliston, W.P. and Loock, J.C. (1998). *Karoo aquifers – Their geology, geometry and physical properties.* Report to the Water Research Commission by the Institute for Groundwater Studies, University of the Free State. (WRC Report No. 487/1/98). Pretoria.

Carpenter, E.W. and Habberjam, G.M. (1956). A tri-potential method of resistivity prospecting. *Geophysical Prospecting*, **29**:128-143.

Cassiani, G., Bruno, V., Villa, A., Fusi, N. and Binley, A.M. (2006). A saline trace test monitored via time-lapse surface Electrical Resistivity Tomography. *Journal of Applied Geophysics*, **59**(3):244-259.

Chevallier, L. and Woodford, A.C. (1999). Morpho-tectonics and mechanism of emplacement of the dolerite rings and sills of the Western Karoo, South Africa. *South African Journal of Geology*, **102** (1), 43-54.

Chevallier, L., Goedhart, M. and Woodford, A.C (2001). The influences of dolerite sill and ring complexes on the occurrence of groundwater in Karoo fractured aquifers: a morpho-tectonic approach. WRC report No 937/1/01.

Chevallier, L., Cole, J., Ngcofe, L., Nhleko, L., and Viljoen, J. (2005). Geospatial and structural analysis of the Kalkveld catchment area for the groundwater management plan. Council for Geoscience, Report number 2005_0078.

Dahlin T. (1996). 2-D resistivity surveying for environmental and engineering applications. *First Break*, **14**, 275-284.

Dahlin, T. and Bernstone, C. (1997). *A roll-along technique for 3-D resistivity data acquisition with multi-electrode arrays*. Symposium on the Application of Geophysics to Engineering and Environmental Problems, Reno, Nevada, March 23-26, vol. 2, 927-935.

Dahlin, T. and Loke, M.H. (1997). *Quasi-3-D resistivity imaging-mapping of three dimensional structures using two dimensional DC resistivity techniques*. Proceedings of the 3rd Meeting of the Environmental and Engineering Geophysical Society, Aarhus, Denmark, pp. 143-146.

Dahlin, T. and Owen, R. (1998). Geophysical investigations of alluvial aquifers in Zimbabwe. Proceedings of the IV Meeting of the Environmental and Engineering Geophysical Society (European Section), Sept. 1998, Barcelona, Spain, 151-154.

Dahlin, T. and Zhou, B. (2004). A numerical comparison of 2-D resistivity imaging with 10 electrode arrays. *Geophysical Prospecting*, **52**, 379-398.

Dahlin, T., Bernstone, C. and Loke, M.H. (2002). A 3-D resistivity investigation of a contaminated site at Lernacken, Sweden. *Geophysics*, **67,** 1692-700.

Daily, W. and Ramirez, A.L. (2000). Electrical imaging of engineered hydraulic barriers. *Geophysics*, **65**, 83-94.

Daily, W., Ramirez, A. and Johnson, R. (1998). Electrical impedance tomography of a perchloroethelyne release. *Journal of Environmental and Engineering Geophysics*, **2**, 189-201.

Daily, W., Ramirez, A., LaBrecque, D. and Nitao, J. (1992). Electrical Resistivity Tomography of Vadose water movement. *Water resources research*, **28**(5), 1429-1442.

Daniels, F. and Alberty, R.A. (1966). *Physical Chemistry*. 3rd edition. John Wiley and Sons, Inc., New York.- 365pp.

Darcy Groundwater Scientists and Consultants (2004). *Establishment of a groundwater management plan for the Kalkveld water user association*. Final Report prepared for DWAF, Free State Region, Bloemfontein.

Dey, A. and Morrison, H.F. (1979). Resistivity modelling for arbitrary shaped two-dimensional structures. *Geophysical Prospecting***, 27**, 1020-1036.

Duncan, A.R. and Marsh, J.S. (2006). The Karoo Igneous Province. In Johnson, M.R., Anhaeusser, C.R. and Thomas, R.J. (Eds). *The Geology of South Africa*. Geological Society of South Africa, Johannesburg,/Council for Geoscience, Pretoria. pp 501-519.

Duncan, R.A., Hooper, P.R., Ehacek, J. and Marsh, J.S. (1997). The timing and duration of the Karoo igneous event, Southern Gondwana. *Journal of Geophysical Res.* **102**, 18127-18138.

Du Toit, A.L. (1905). *Geological survey of Glen Grey and parts of Queenstown and Woodhouse, including the Indwe area*. Geological Commission of the Cape of Good Hope, Tenth Annual Report, 95-140.

Du Toit, A.L. (1920). The Karoo dolerites of South Africa: a study in hypabyssal injection. *Transactions of the Geological Society of South Africa*, **23**(1920), 1-42.

Edwards, L.S. (1977). A modified pseudo-section for resistivity and induced-polarization. *Geophysics*, **42**, 1020-1036.

Ekinic, Y.L. and Kaya, M.A. (2007). 3-D resistivity imaging of buried tombs at the Parion necropolis (NW Turkey). *Journal of Balkan Geophysics Society*, **2**, 30-45.

Ellis, R. and Oldenburg, D.W. (1994). Applied geophysical inversion. *Geophysics Journal Int.*, **116,** 5-11.

El-Quady, G., Monteiro, Santos, F.A., Hassaneen, A.G. and Trindade, L. (2005). 3-D inversion of VES data from Saqqara archaeological area. *Egypt Near Surface Geophysics*, **3**, 227-233.

Fitch, F.J. and Miller, J.A. (1984). Dating Karoo igneous rocks by the conventional K-Ar and $^{40}Ar/^{39}Ar$ age spectrum methods. In Erlank, A.J. (Ed), Pretrogenesis of the volcanic rocks of the Karoo Province. *Geological Society of South Africa.* Special Publication No **13**, 247-256.

Geotomo Software (2012). *RES2DINV version 3.71. Rapid 2-D Resistivity and IP inversion using the least-squares method.* Penang, Malaysia.

Goes, B.J.M. and Meekes, J.A.C. (2004). An effective electrode configuration for the detection of DNAPLs with electrical resistivity tomography. *Journal of Environmental and Engineering Geophysics*, **9**, 127-141.

Griffiths, D.H. and Turnbull, J. (1985). A multi-electrode array for resistivity surveying. *First Break*, **3**(7), 16-20.

Griffiths, D.H., Turnbull, J. and Olayinka, A.I. (1990). Two-dimensional resistivity mapping with a computer- controlled array. *First Break*, **8**, 121-129.

Hallenburg, J.K. (1984). *Geophysical logging for mineral and engineering applications*. Tulsa: Pennwell Corp.

Johansson, S. and Dahlin, T. (1996). Seepage monitoring in an earth embankment dam by repeated resistivity measurements. *European Journal of Engineering and Geophysics*, **1**, 229-247.

Johnson, M.R., C.J. van Vuuren, Visser, J.N.J., Cole, D.I., Wickens, H. de V., Christtie, A.M.D., Roberts, D.L. and Brandi, G. (2006). Sedimentary Rocks of the Karoo Supergroup. In Johnson, M.R., Anhaeusser, C.R. and Thomas, R.J. (Eds). *The Geology of South Africa*. Geological Society of South Africa, Johannesburg/Council for Geoscience, Pretoria. pp 461-499.

Kaufmann, O. and Quinif, Y. (2001). An application of cone penetration tests and combined array 2-D electrical resistivity to delineate cover-collapse sinkhole prone areas. In: Beck, B.F. and Herring, J.G. (Eds). *Geotechnical and environmental applications of Karst geology and hydrology*, pp. 359–364. Rotterdam: Balkema.

Keller, G.V. and Frischknecht, F.C. (1966). *Electrical methods in geophysical prospecting*. Oxford: Pergamon Press.

Koefoed, O. (1979). *Geosounding principles 1: Resistivity sounding measurements*. Amsterdam: Elsevier Science.

Loke, M.H. (1999). *Electrical imaging surveys for environmental and engineering studies: a practical guide to 2-D and 3-D surveys*. Penang, Malaysia.

Loke, M.H. (2002). *RES2DMOD version 3.01. Rapid 2-D resistivity forward modelling using the finite-difference and finite-element methods.* Penang, Malaysia.

Loke, M.H. (2007). *Res3Dinv software. Version 2.14, Geoelectrical Imaging 2D and 3D,* Pinang, Malaysia

Loke, M.H. (2012). *Tutorial: 2-D and 3-D electrical imaging surveys*.

Loke, M.H. and Barker, R.D. (1995). Least-square deconvolution of apparent resistivity pseudo-sections. *Geophysics,* **60**(6), 499-523.

Loke, M.H. and Barker, R.D. (1996). Practical techniques for 3D resistivity surveys and data inversion. *Geophysical Prospecting*, **44**, 499-523.

Loke, M.H. and Dahlin, T. (2002). A comparison of the Gauss-Newton and quasi-Newton methods in resistivity imaging inversion. *Journal of Applied Geophysics,* **49**, 149-462.

Maske, S. (1966). *The petrography of the Ingeli Mountain Range*. Annals from the University of Stellenbosch, vol. 41.

McGillivray, P.R. and Oldenburg, D.W. (1990). Methods for calculating Frechet derivatives and sensitivities for the non-linear inverse problem: A comparative study. *Geophysical Prospecting,* **38**, 499-524.

Meads, L.N., Bentley, L.R. and Mendoza, C.A. (2003). Application of electrical resistivity imaging to the development of a geologic model for a proposed Edmonton landfill site. *Canadian Geotechnical Journal,* **40**, 551-558.

Merrick, N.P. (1997). A new resolution index for resistivity electrode arrays. *Exploration Geophysics,* **28**, 106-109.

Miller, C.R., Routh, P.S., Brosten, T.R. and McNamara, J.P. (2008). Application of time-lapse ERT imaging to watershed characterization. *Geophysics*, **73(**3), G7-G17.

Mochales, T., Casas, A.M., Pueyo, E.L., Pueyo, O., Roman, M.T., Pocovi, A., Soriano, M.A. and Anson, D. (2008). Detection of underground cavities by combining gravity, magnetic and ground penetrating radar surveys: a case study from the Zaragoza area, NE Spain. *Environmental Geology*, **53**(2007), 1067-1077.

Parasnis, D.S. (1997). *Principles of Applied Geophysics*. 5th ed. Chapman & Hall, London, New York.

Park, J., You, Y.J. and Kim, H.J. (2009). Electrical resistivity surveys for gold-bearing veins in the Yongjang mine, Korea. *Journal of Geophysics and Engineering*, **6**, 73-81.

Pazdirek, O. and Blaha, V. (1996). *Examples of resistivity imaging using ME-100 resistivity field acquisition system*. EAGE 58th Conference and Technical Exhibition Extended Abstracts. Houten, The Netherlands: EAGE.

Perren, L.J. (2005). *Investigating the Performance of Electrical Resistivity Arrays*. M.Sc.Thesis, Virginia Polytechnic Institute and State University.

Richardson, S.H. (1984). Sr, Nd and O isotope variation in an extensive Karoo dolerite sheet, Southern Namibia. In Erlank, A.J. (Ed), Pretrogenesis of the volcanic rocks of the Karoo Province. *Geological Society of South Africa.* Special Publication No **13**, 289-293.

Rogers, A.W. and Du Toit, A.L. (1903). *Geological survey of parts of the divisions of Ceres, Sutherland and Calvinia*. Annual Report of Cape Geol. Comm., 36-43.

Roy, A. and Apparao, A. (1971). Depth of investigation in direct current methods. *Geophysics*, **36**, 943-959.

Sami, K.I., Neumann, Gqiba, D., de Kock, G. and Grantham, G. (2002). *Groundwater exploration in geologically complex and problematic Terrain – Guidelines*, vol. 1. WRC Report No.966/1/02, Pretoria: Water Research Commission.

Sandberg, S.K., Slater, L.D. and Versteeg, R. (2002). An integrated geophysical investigation of the hydrogeology of an anisotropic unconfined aquifer. *Journal of Hydrology*, **267**, 227-243.

Seaton, W.J. and Burbey, T.J. (2002). Evaluation of two-dimensional resistivity methods in a fractured crystalline-rock terrain. *Journal of Applied Geophysics*, **51** (2002) 21- 41

Soupios, P.M., Georgakopoulos, P., Papadopoulos, N., Saltas, V., Andeadakis, A., Vallianatos, F., Sarris, A. and Makris, J.P. (2007). Use of engineering geophysics to investigate a site for a building foundation. *Journal of Geophysics and Engineering*, **4**, 94-103.

Spitzer, K. (1998). The three-dimensional DC sensitivity for surface and subsurface sources. *Geophysical Journal International*, **134**(3), 736-746.

Sultan, S.A., Monteiro, Santos, F.A. and Helal, A. (2006). A study of the groundwater seepage at Hibis Temple using geoelectrical data, Kharga Oasis, Egypt. *Near Surface Geophysics*, **4**(6), 347-354.

Telford, W.M., Geldart, L.P. and Sheriff, R.E. (1990). *Applied Geophysics*. 2nd edition. Cambridge University Press.

Tohon, D.S., Vannesta, K., Sintubin, M., Muchez, P. and Waelkens, M. (2004). *Two-dimensional resistivity imaging: a tool in archaeoseismology: an example from Ancient Sagalassos (Southwest Turkey)*. Archaeol. Prospect. 11 1–18.

Tsourlos, P. and Ogilvy, R. (1999). An algorithm for the 3-D inversion of topographic resistivity and induced polarization data: preliminary results. *Journal of Balkan Geophysics Society*, **2**, 30-45.

Walker, F. and Poldervaart, A. (1949). Karoo dolerite of the Union of South Africa. *Bulletin of the Geological society of America*, **60**, 591-706.

Van Wyk, W.L. (1963). *Groundwater studies in northern Natal, Zululand and surrounding areas*. Memoir 52, Geological Survey of South Africa, p. 135.

Woodford, A.C., Chevallier, L., Botha, J.F., Cole, D., Johnson, M.R., Meyer, R., Simonic, M., Van Tonder, G.J. and Verhagen, B.T. (2002). *Hydrogeology of the main Karoo Basin: Current knowledge and future research needs*. Water Research Commission**. (**WRC Report No. TT 179/02).

Zhao, S. and Yedlin, M.J. (1996). Some refinements on the finite-difference method for 3-D DC resistivity modelling. *Geophysics*, **61,** 1301-1307.

Zhou, B. and Dahlin, T. (2003). Properties and effects of measurement errors on 2-D resistivity imaging. *Near Surface Geophysics*, **1**(3), 105-117.

Zhou, W., Barry, F.B. and Angela, L.A. (2002). Effective electrode array in mapping karst hazards in electrical resistivity tomography. *Environmental Geology*, **42** (2002), 922-928.

Zhou, W.F., Beck, B.F. and Stephenson, B.J. (1999). *Defining the bedrock/overburden boundary in covered karst terrains using Dipole-Dipole electrical resistivity tomography*. In: Powers, M.H., Ibrahim, A.B. and Cramer, L. (Eds), *Proc Symp: Application of geophysics to engineering and environmental problems*, Oakland, California, 14–18 March, pp. 331–339. Environmental and Engineering Geophysical Society, Colorado.

http://www.sanparks.org/parks/golden_gate/images/geology/dykes_sills. Accessed on the 14th of February 2012.

http://www.encyclopedia.com/doc/1O13-electrodeconfiguration.html. Accessed on the 6th of March 2012.

APPENDICES

APPENDIX 1: Vertical and dipping dyke's apparent resistivity pseudo-sections

A. VERTICAL THIN DYKE

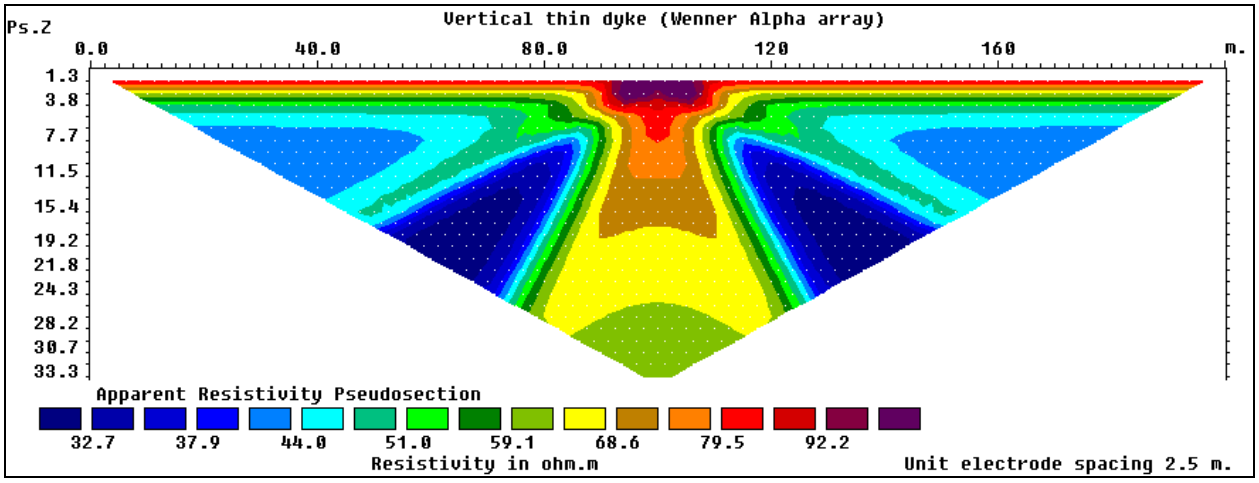

Wenner array

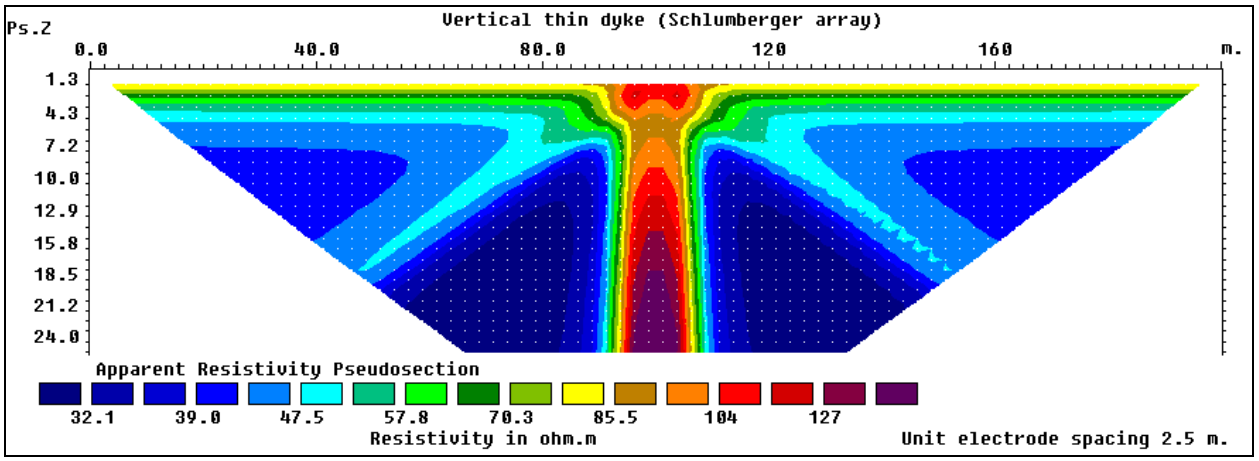

Schlumberger array

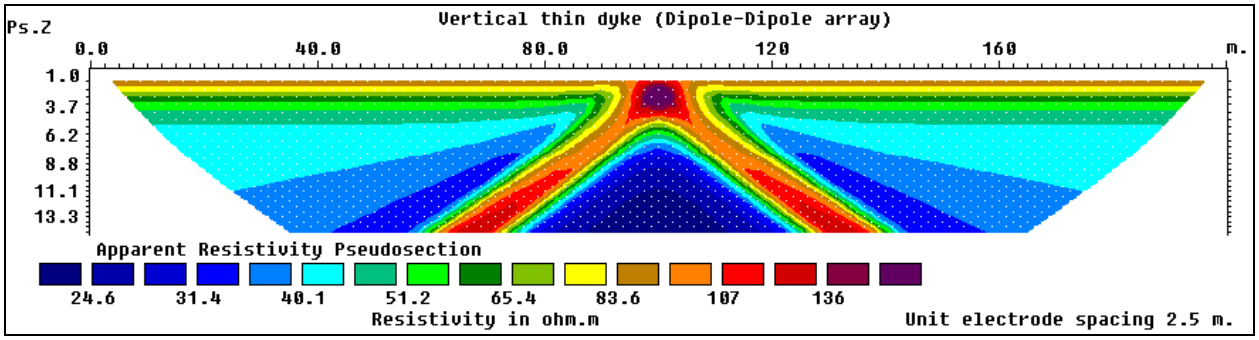

Dipole-Dipole array

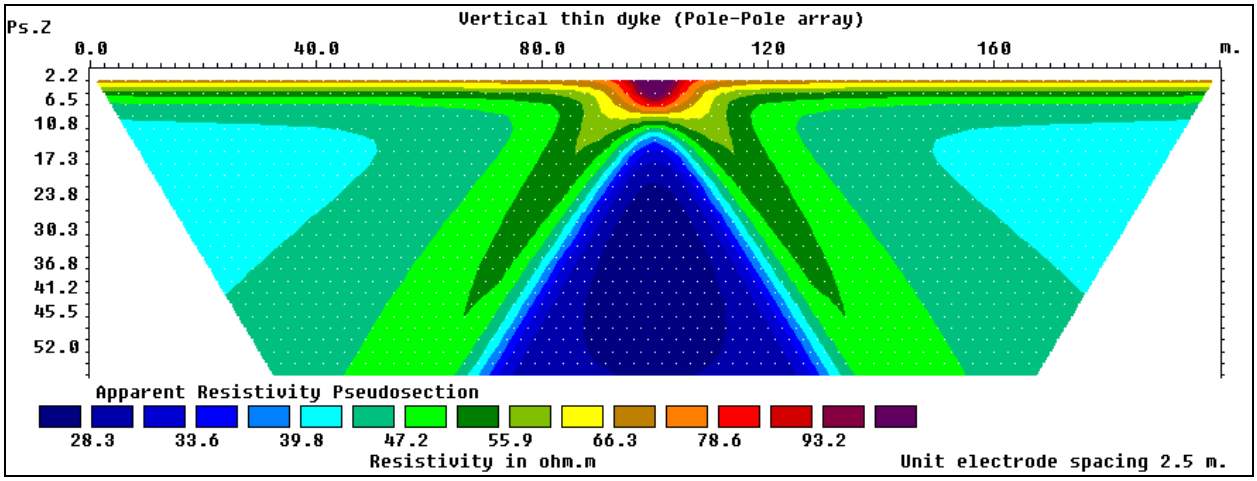

Pole-Pole array

B. DIPPING THIN DYKE

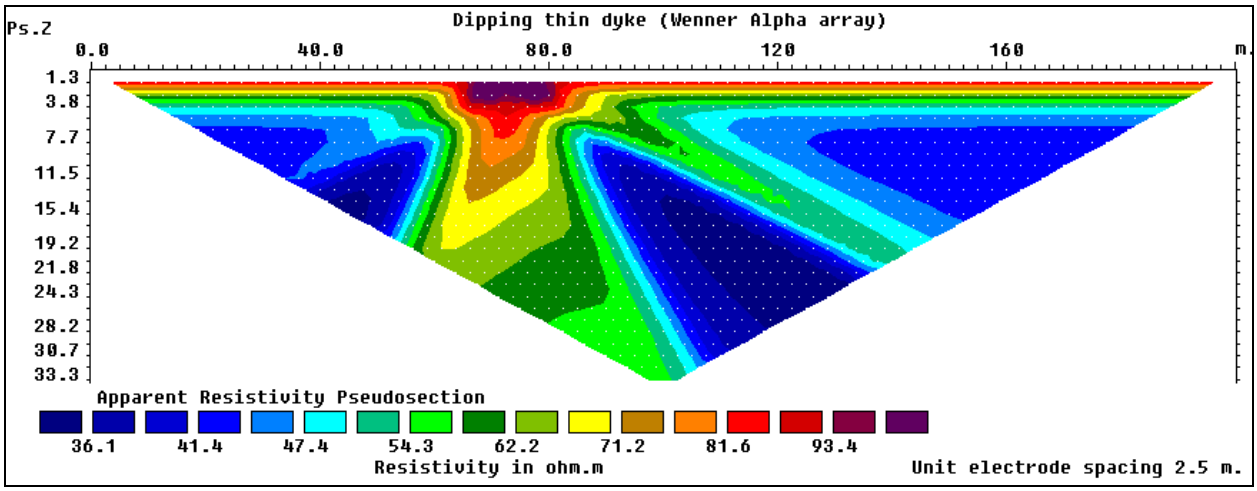

Wenner array

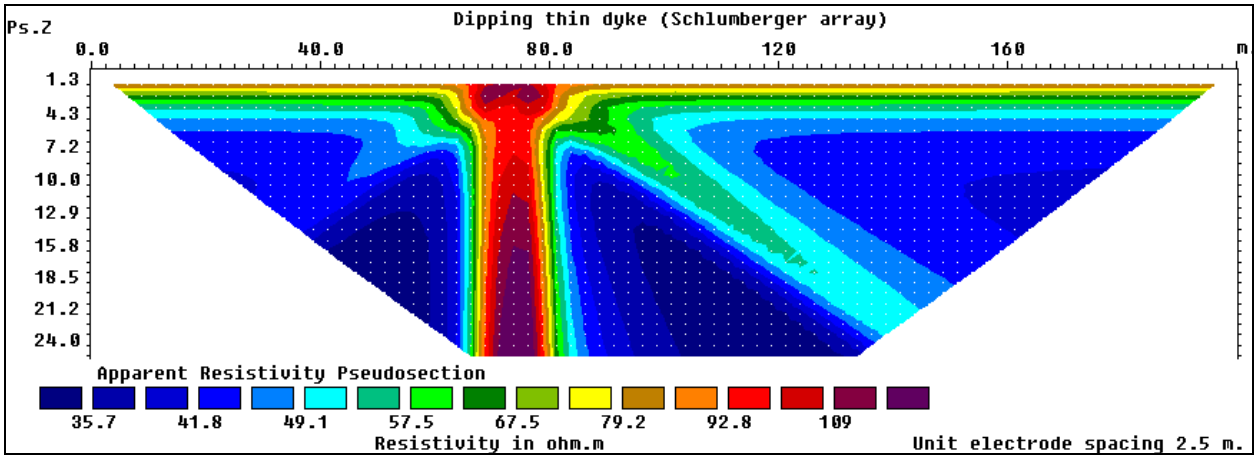

Schlumberger array

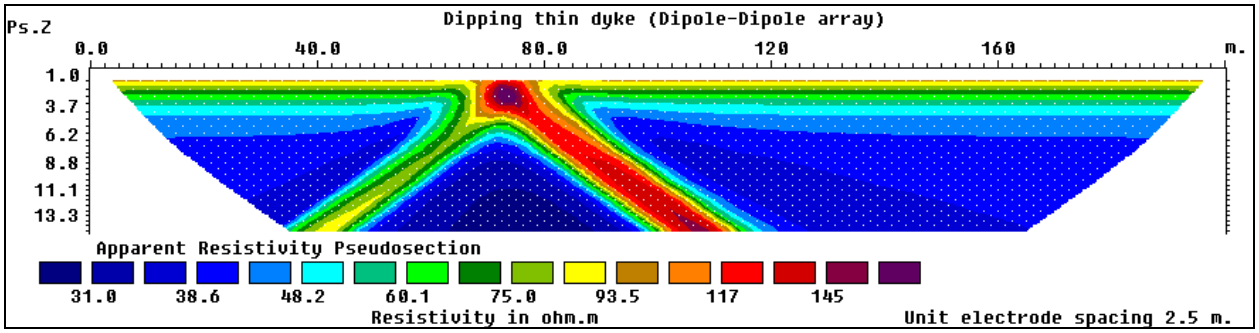

Dipole-Dipole array

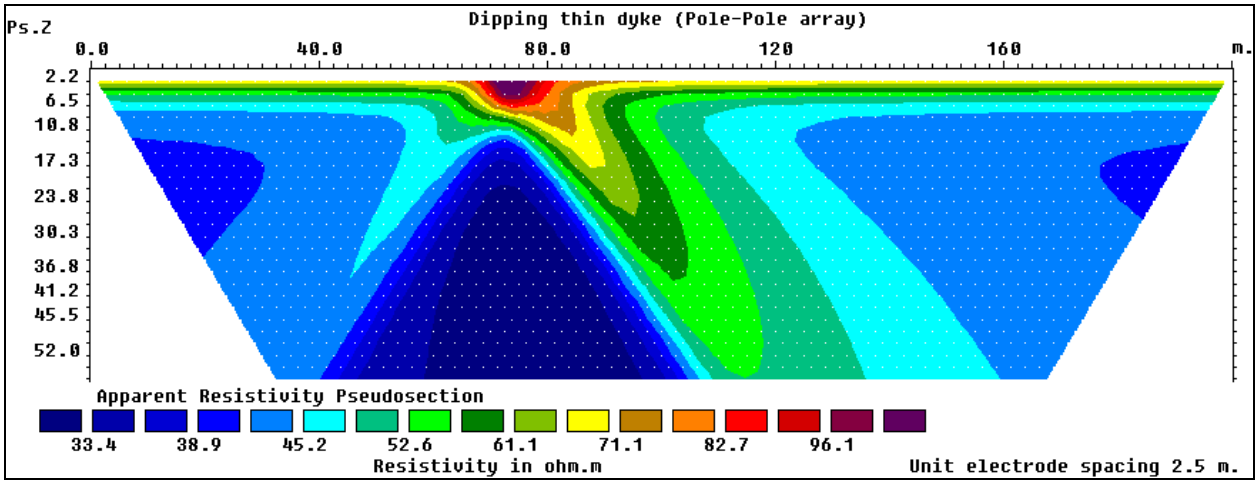

Pole-Pole array

C. VERTICAL THICK DYKE

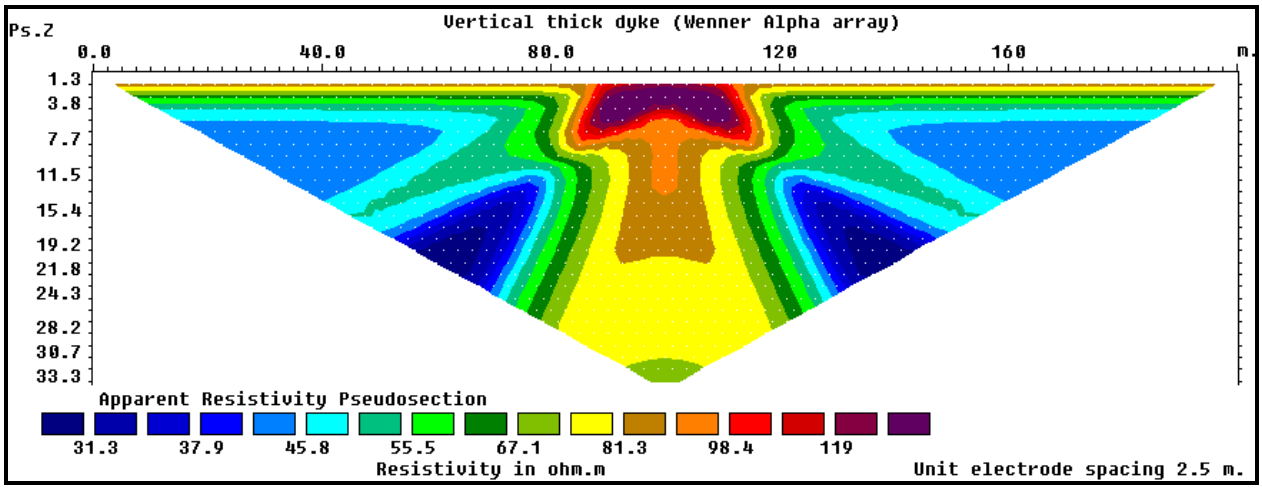

Wenner array

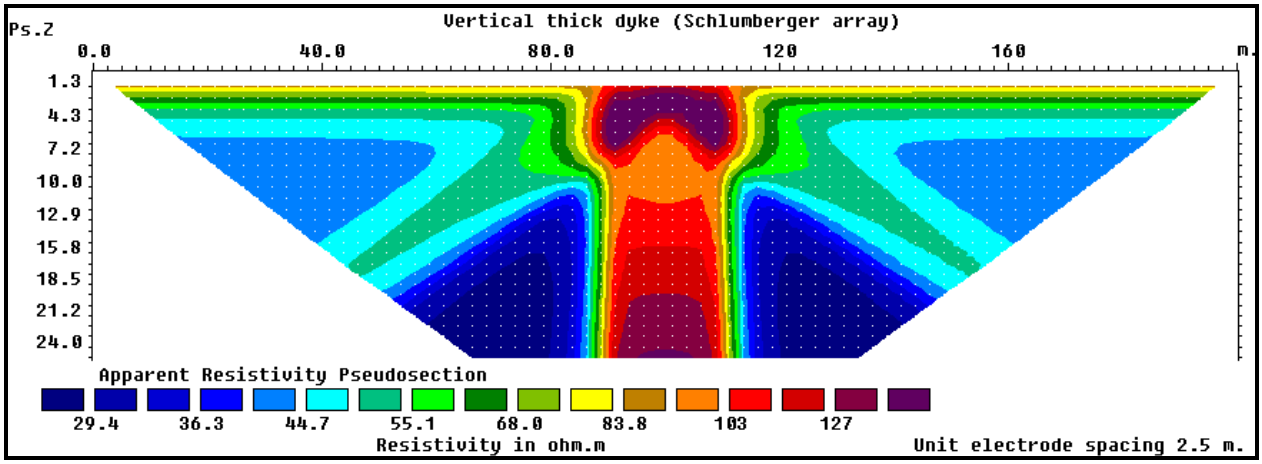

Schlumberger array

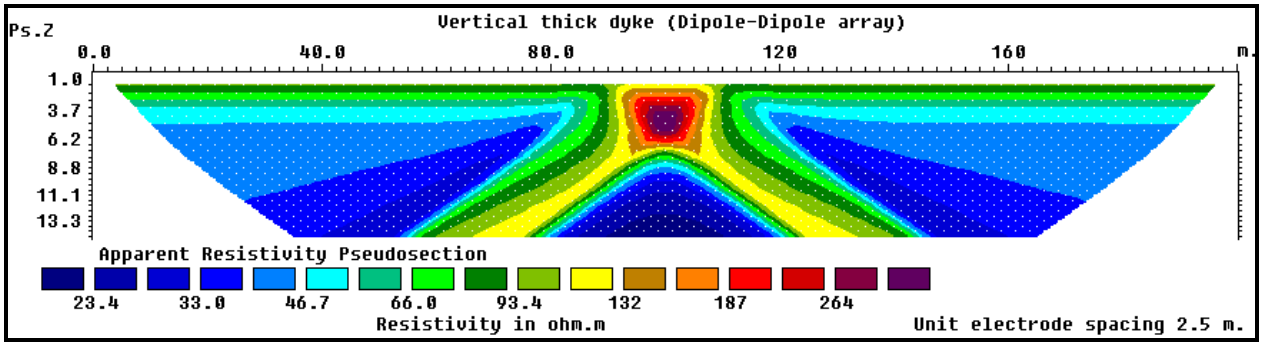

Dipole-Dipole array

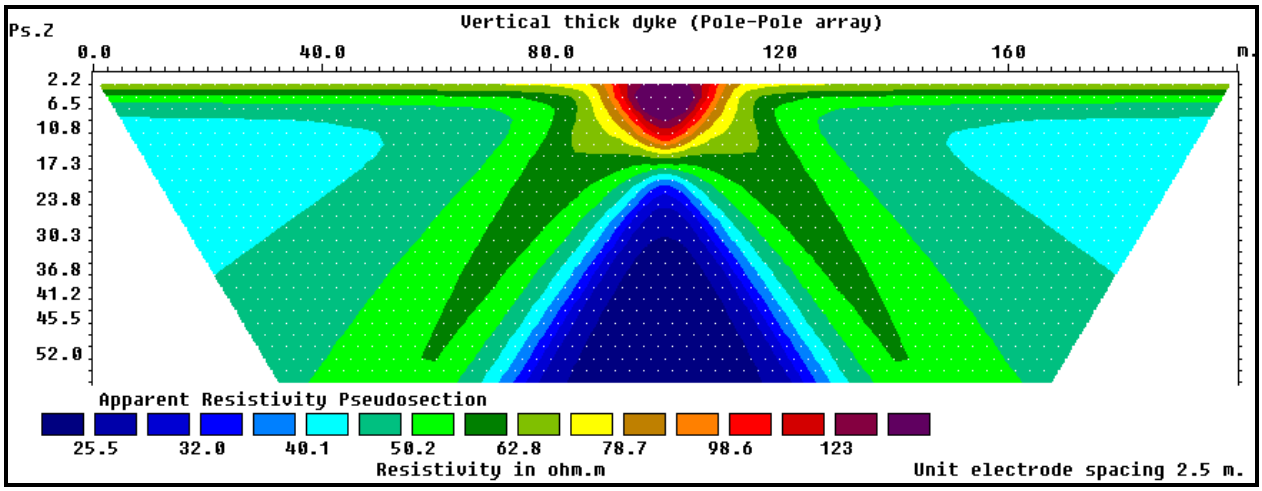

Pole-Pole array

D. DIPPING THICK DYKE

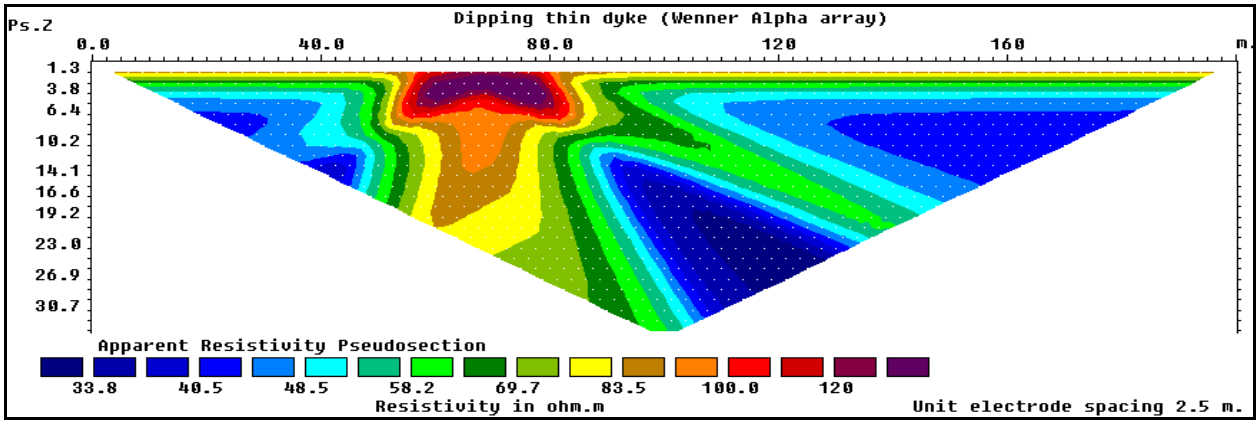

Wenner array

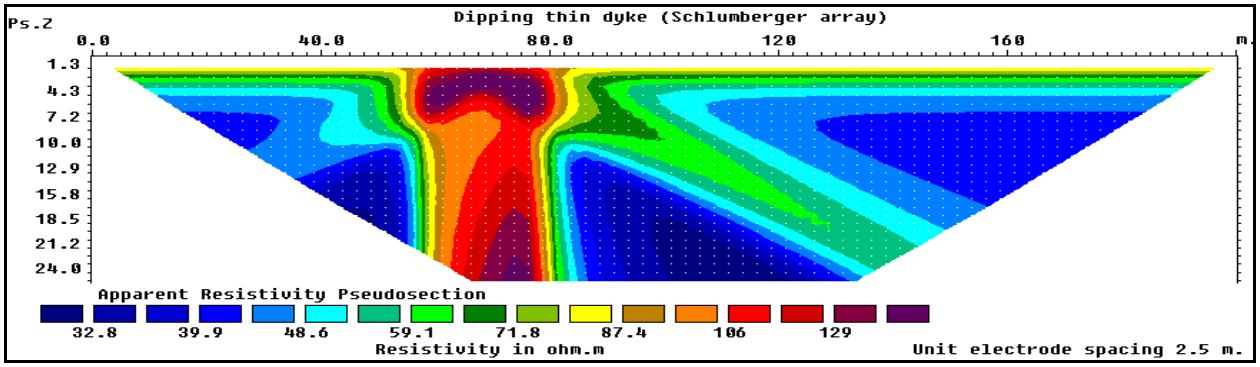

Schlumberger array

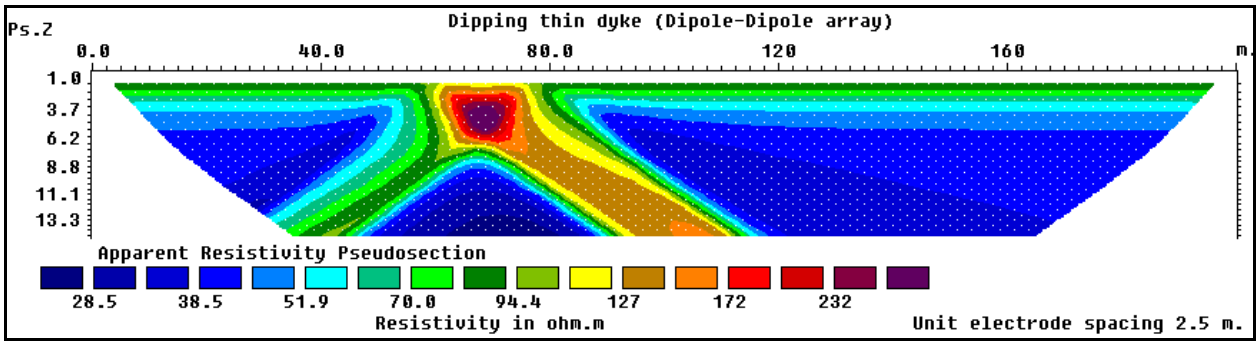

Dipole-Dipole array

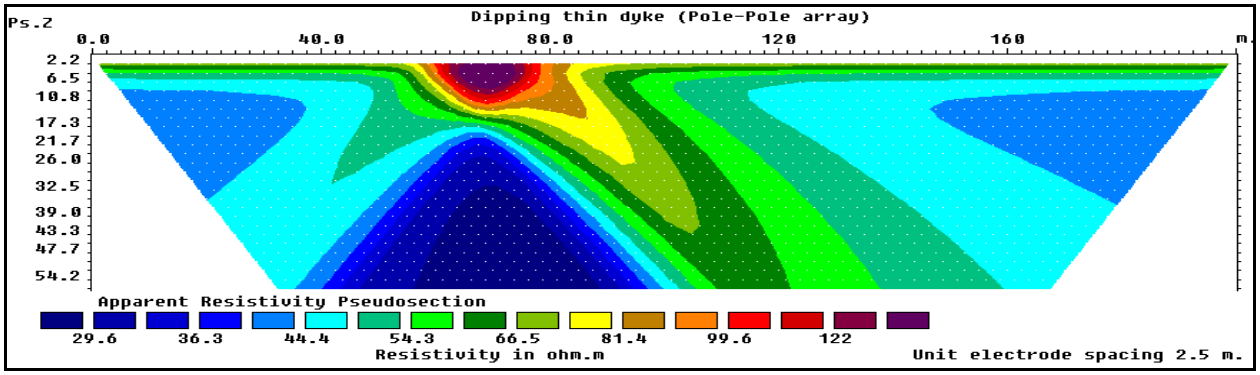

Pole-Pole array

APPENDIX 2: Sill's apparent resistivity pseudo-sections

A. THIN SILL

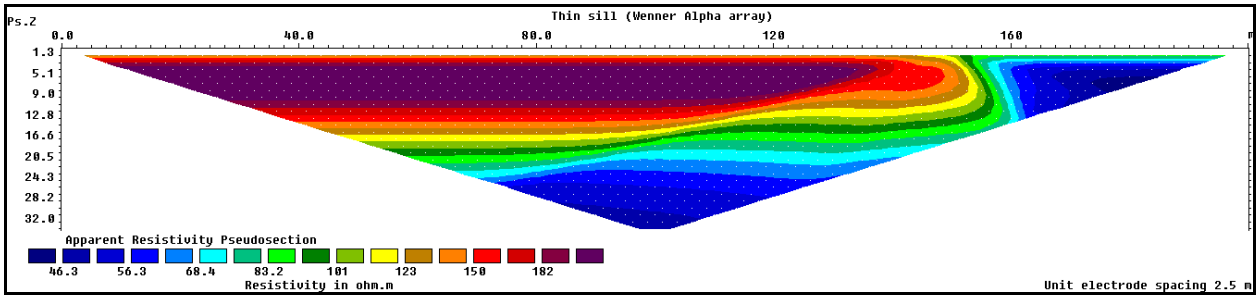

Wenner array

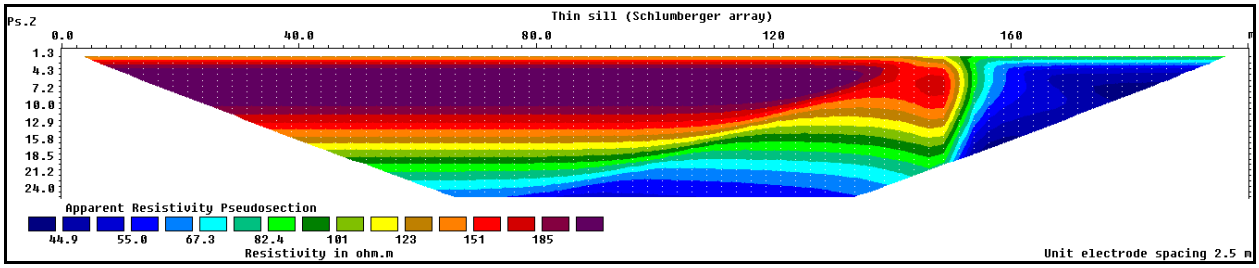

Schlumberger array

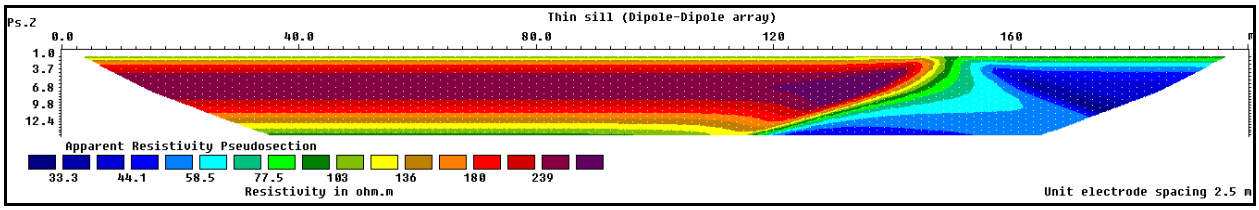

Dipole-Dipole array

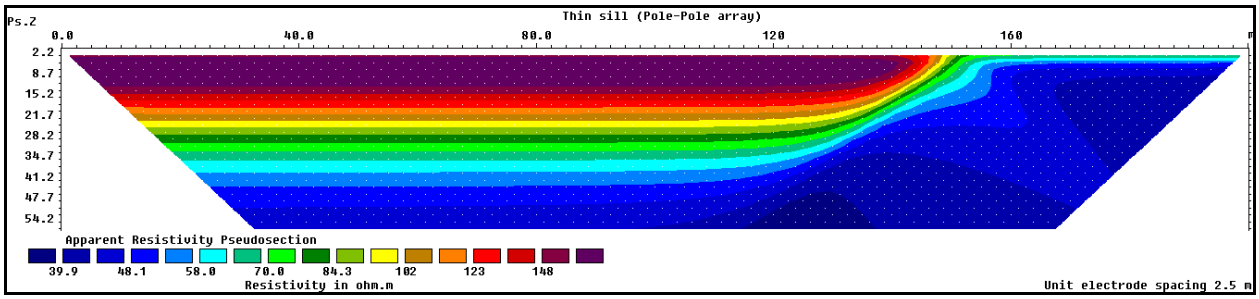

Pole-Pole array

B. THICK SILL

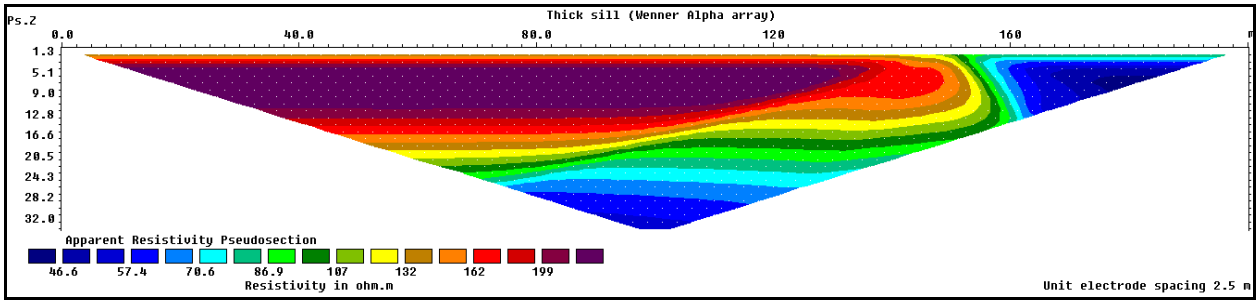

Wenner array

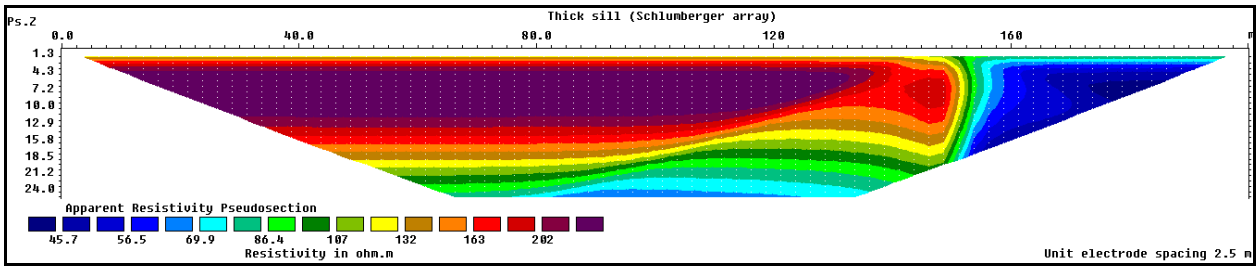

Schlumberger array

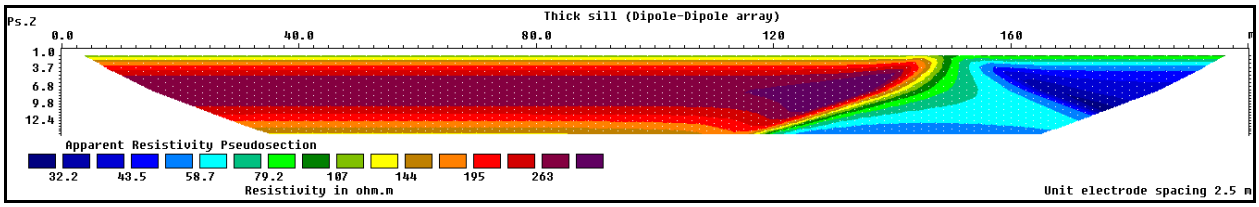

Dipole-Dipole array

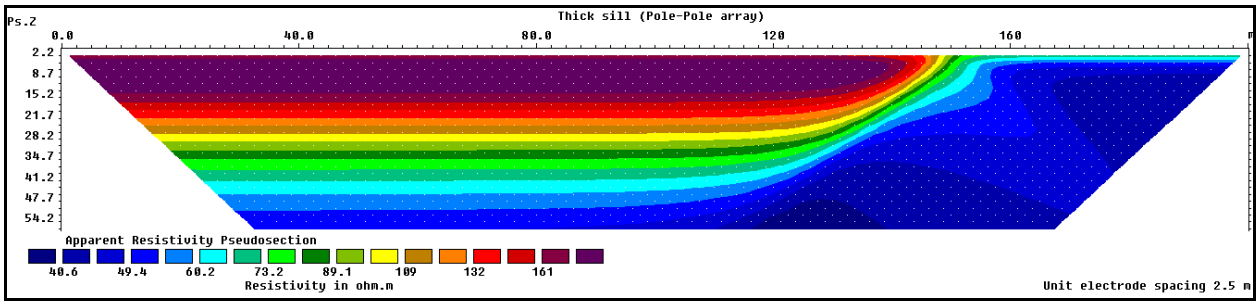

Pole-Pole array

APPENDIX 3: Sill intruded by vertical and dipping dyke's pseudo-sections

A. VERTICAL THIN DYKE WITH THIN SILL

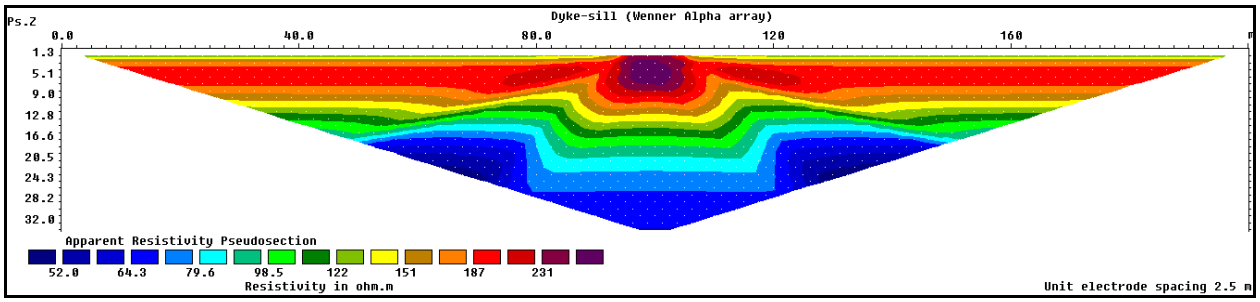

Wenner array

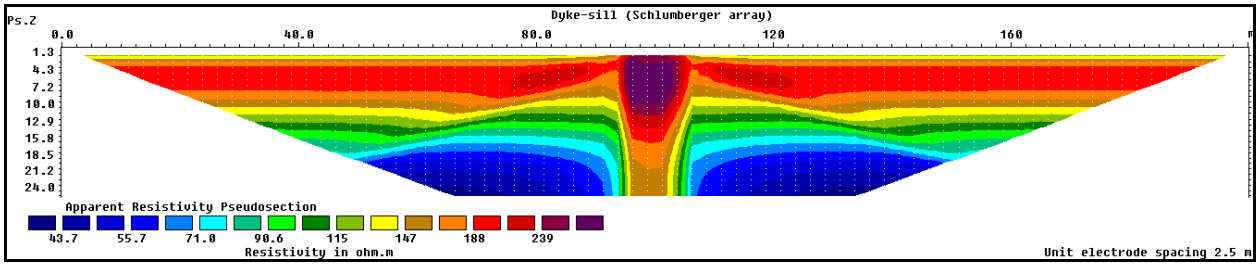

Schlumberger array

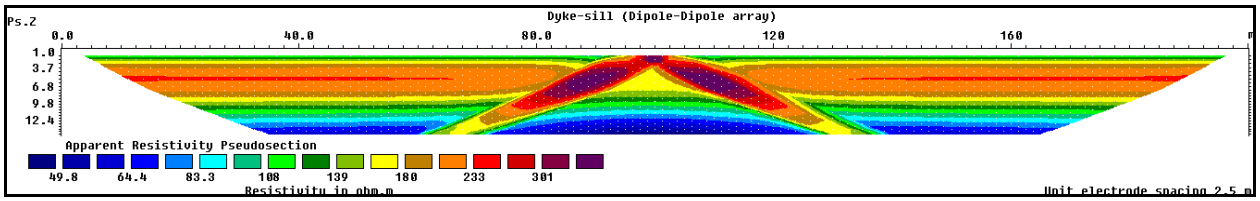

Dipole-Dipole array

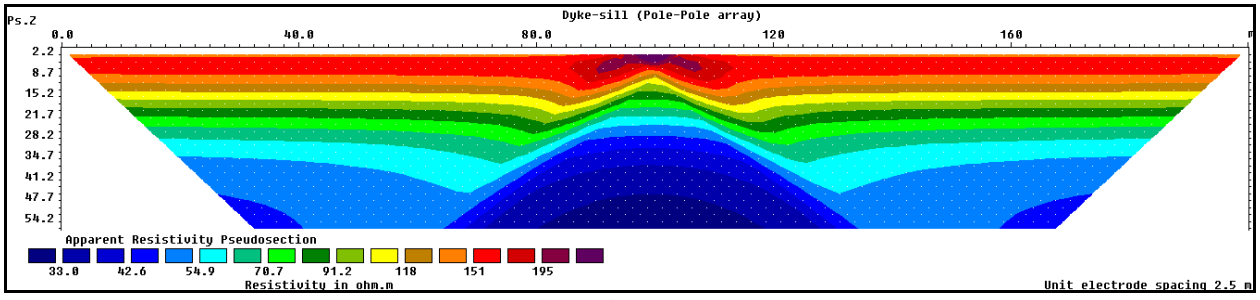

Pole-Pole array

B. DIPPING THIN DYKE WITH THIN SILL

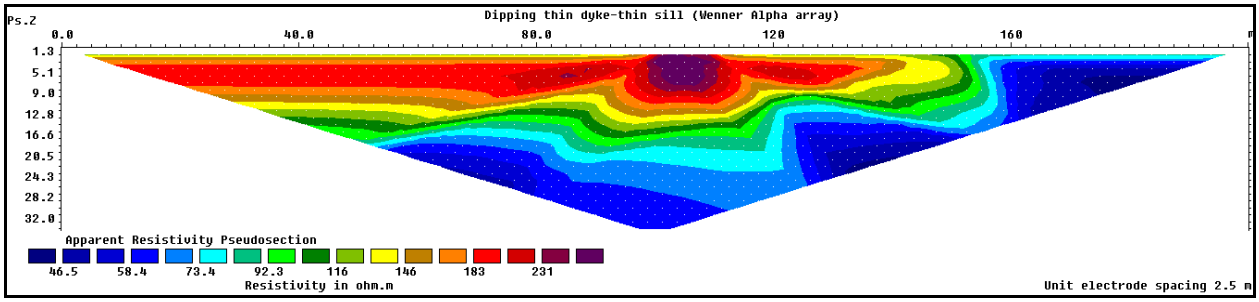

Wenner array

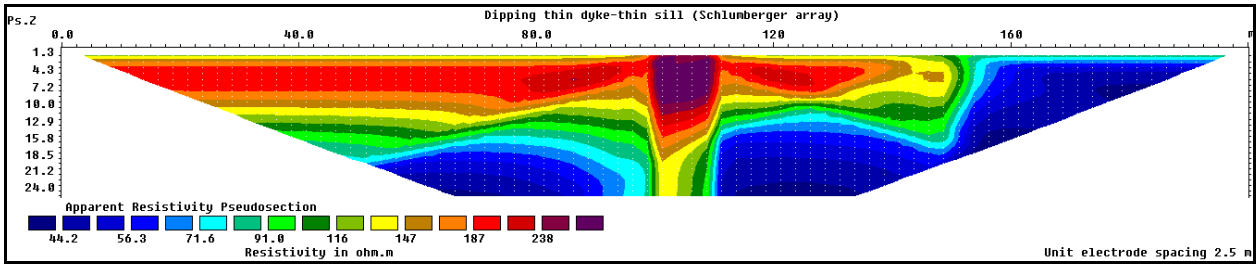

Schlumberger array

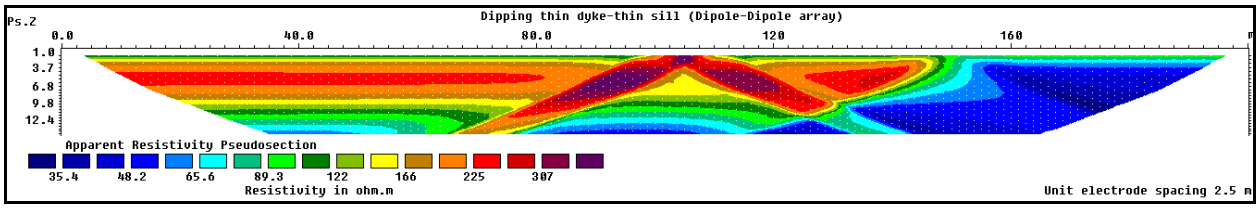

Dipole-Dipole array

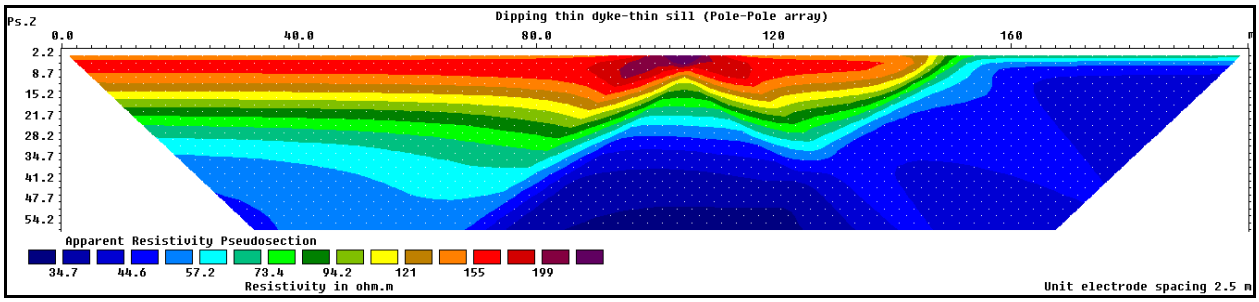

Pole-Pole array

C. VERTICAL THICK DYKE WITH THIN SILL

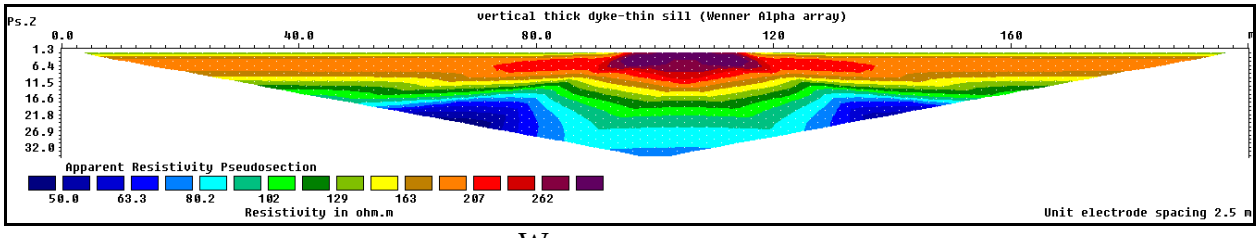

Wenner array

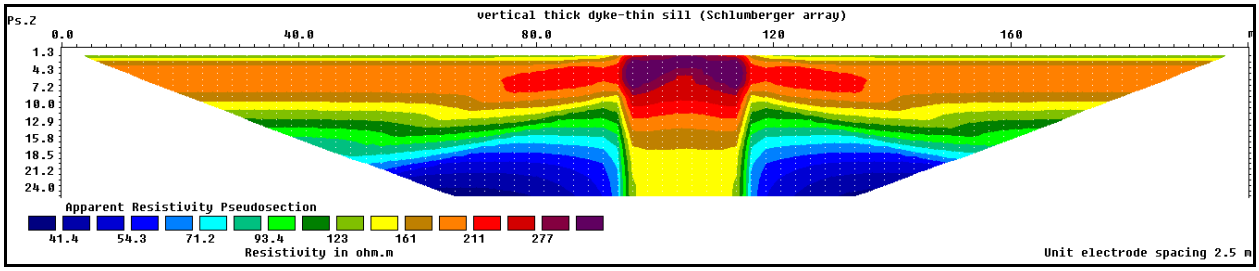

Schlumberger array

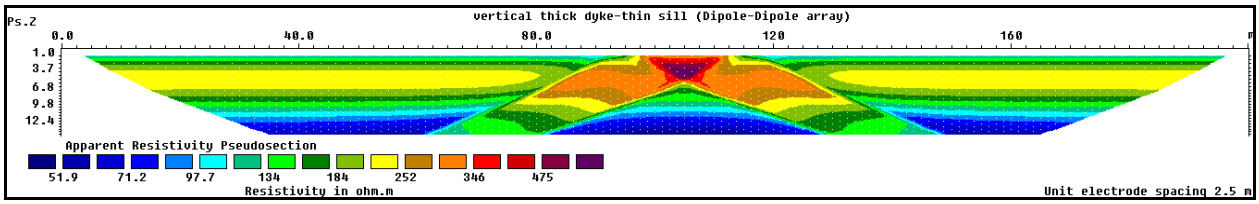

Dipole-Dipole array

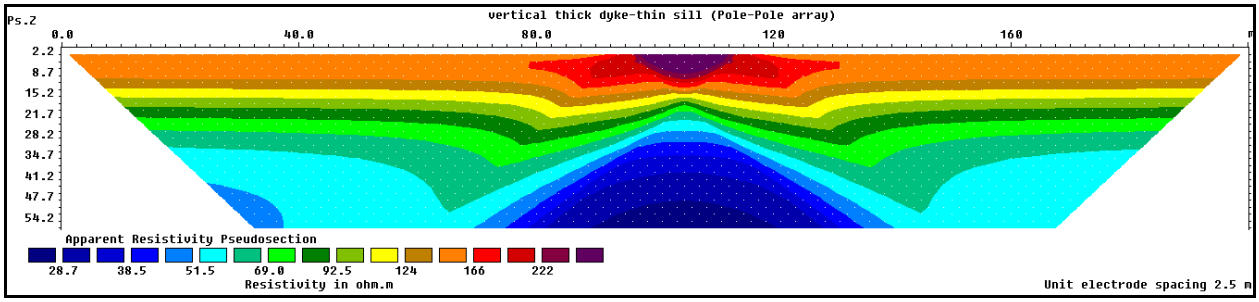

Pole-Pole array

D. DIPPING THICK DYKE WITH THIN SILL

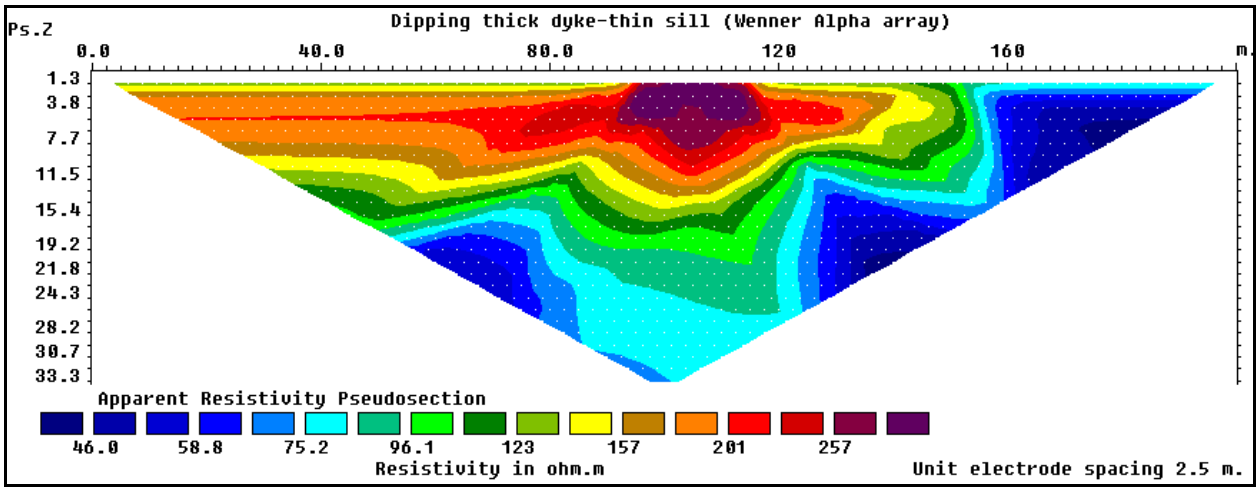

Wenner array

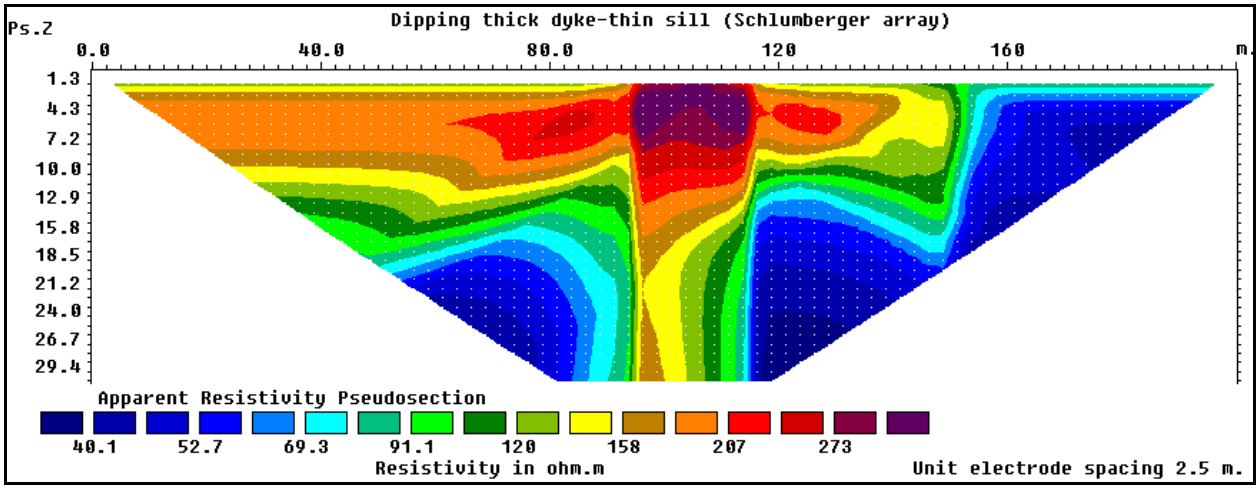

Schlumberger array

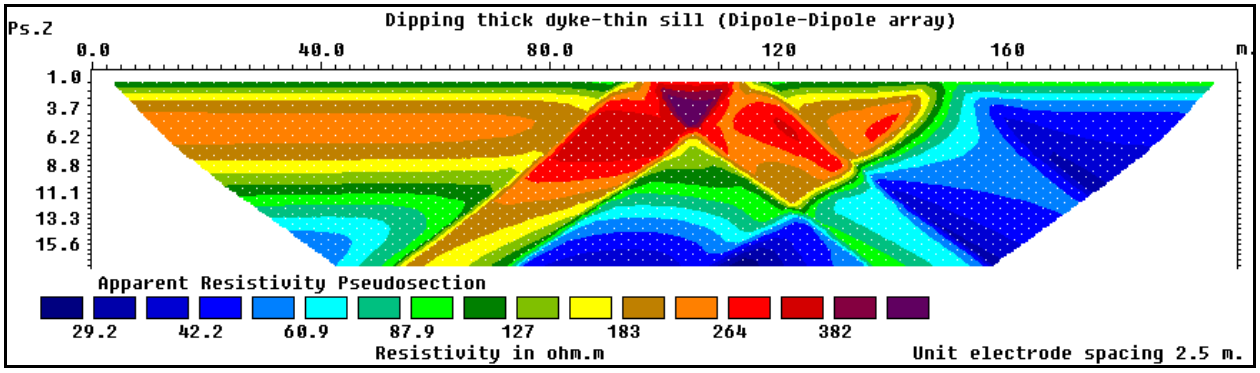

Dipole-Dipole array

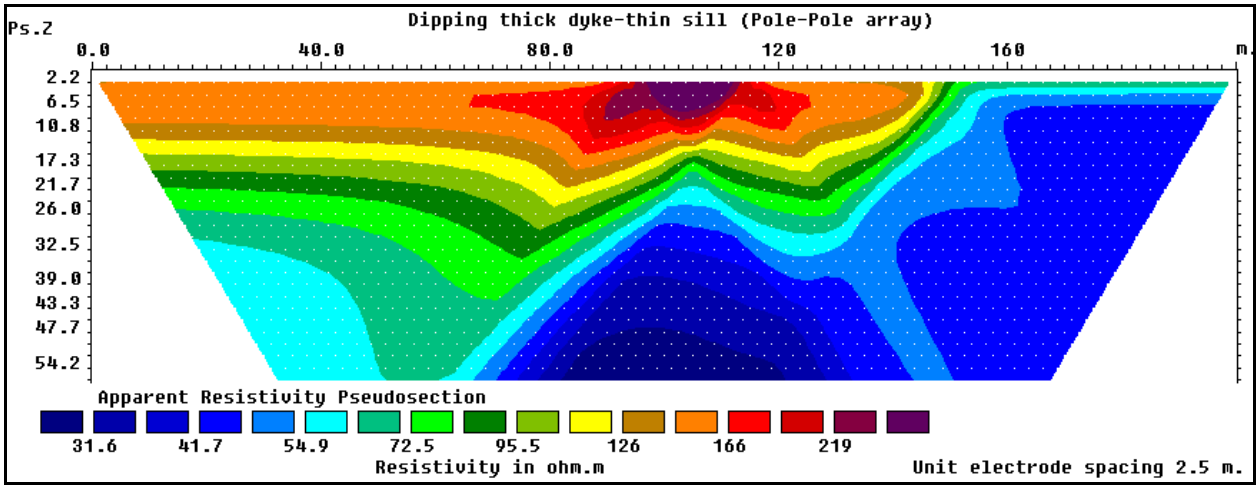

Pole-Pole array

E. VERTICAL THIN DYKE WITH THICK SILL

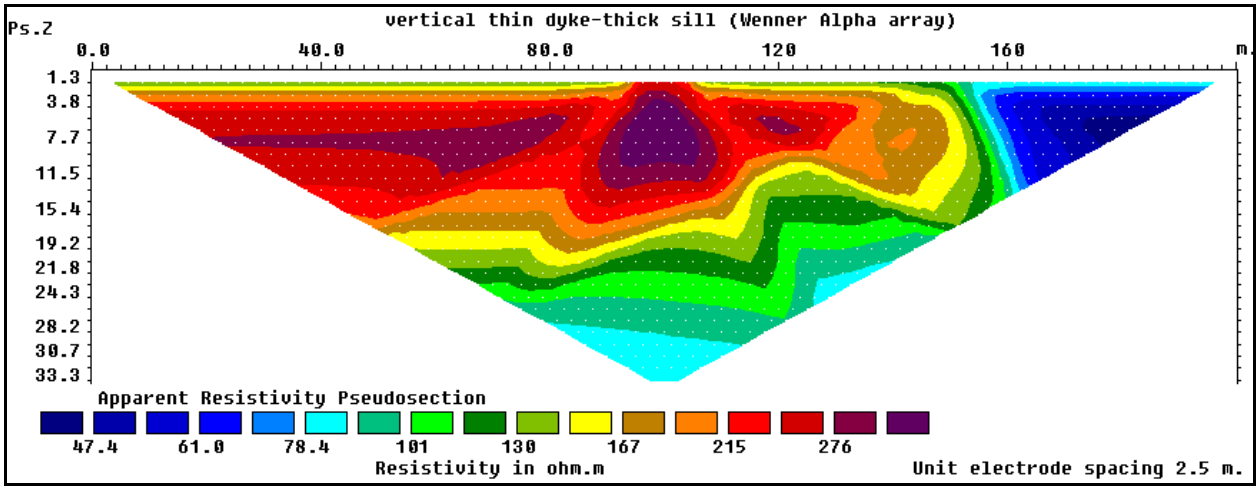

Wenner array

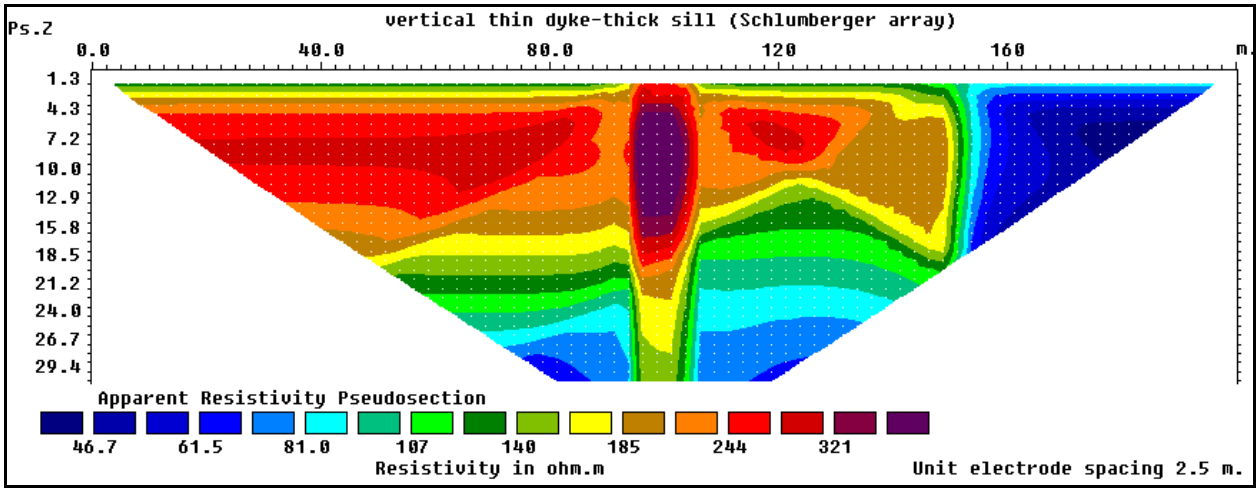

Schlumberger array

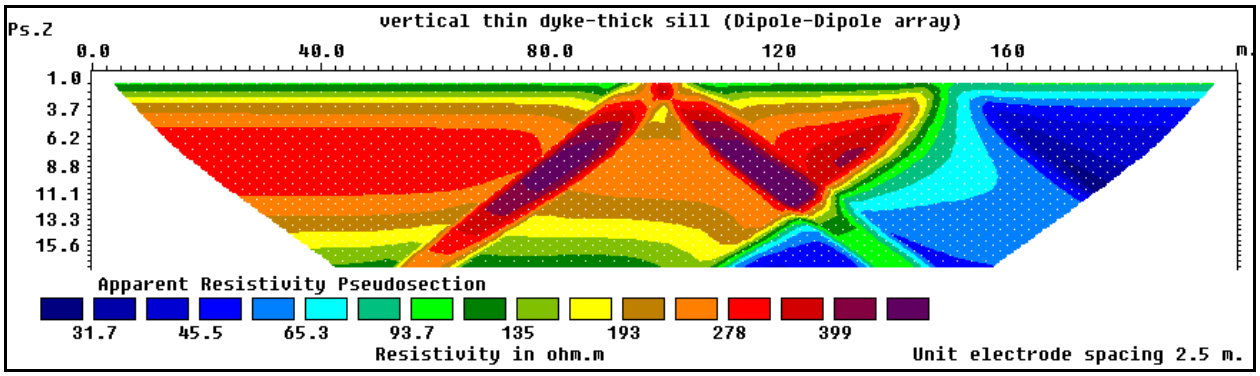

Dipole-Dipole array

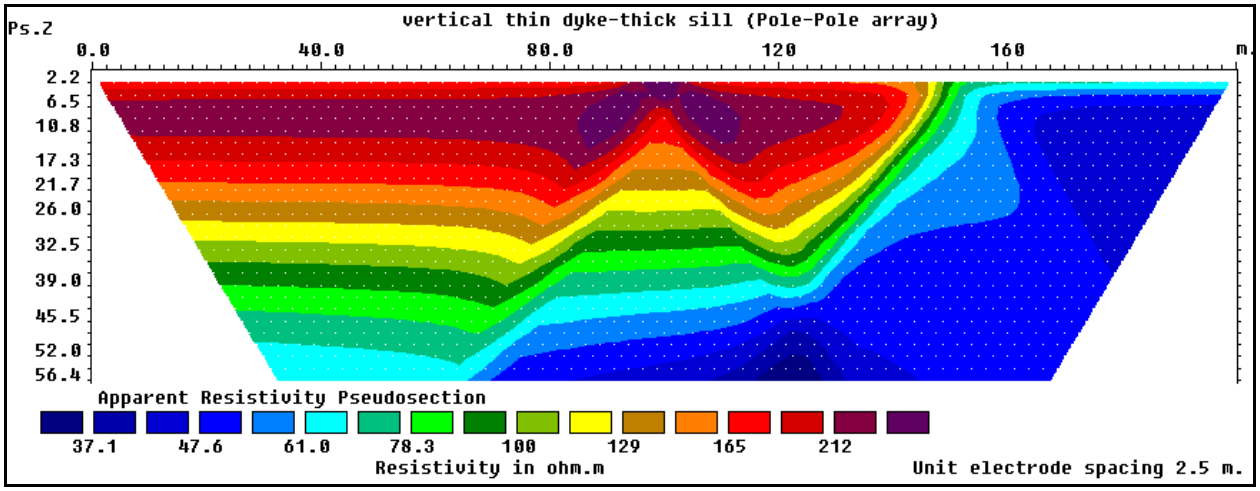

Pole-Pole array

F. DIPPING THIN DYKE WITH THICK SILL

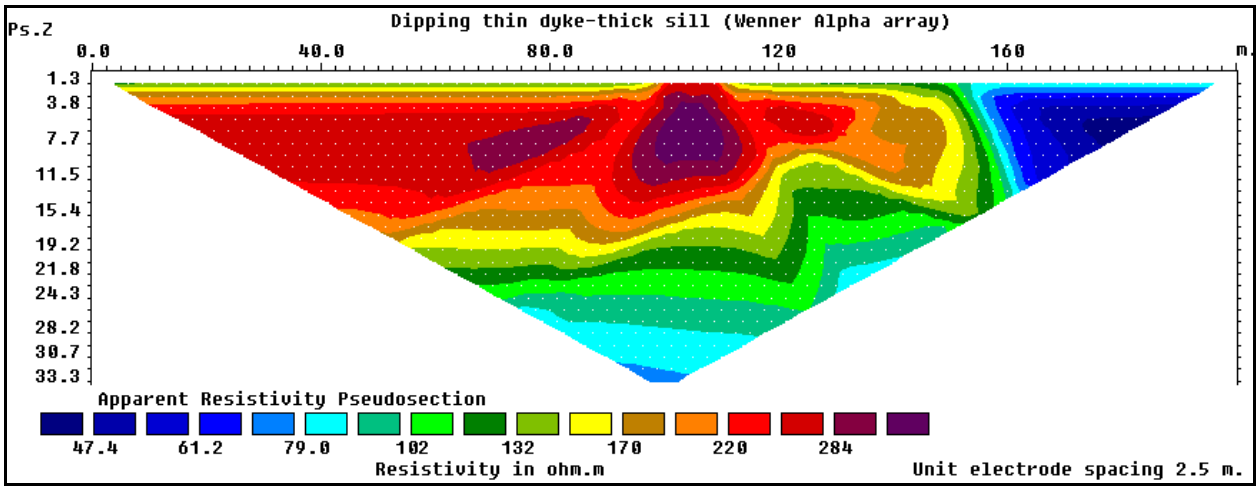

Wenner array

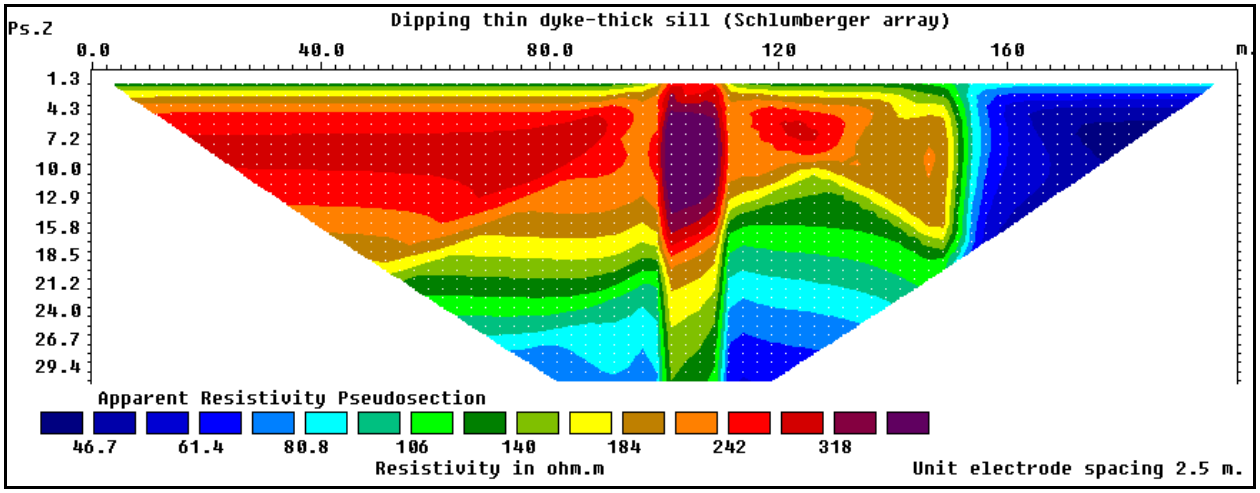

Schlumberger array

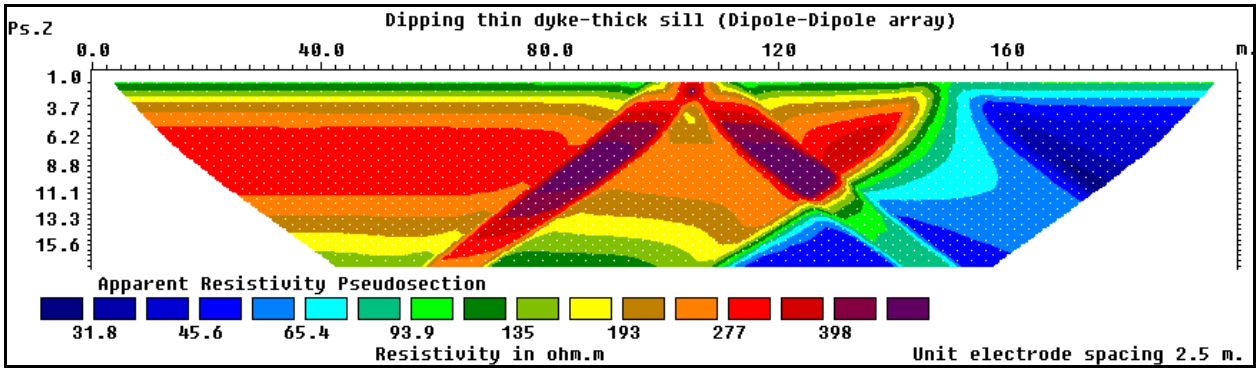

Dipole-Dipole array

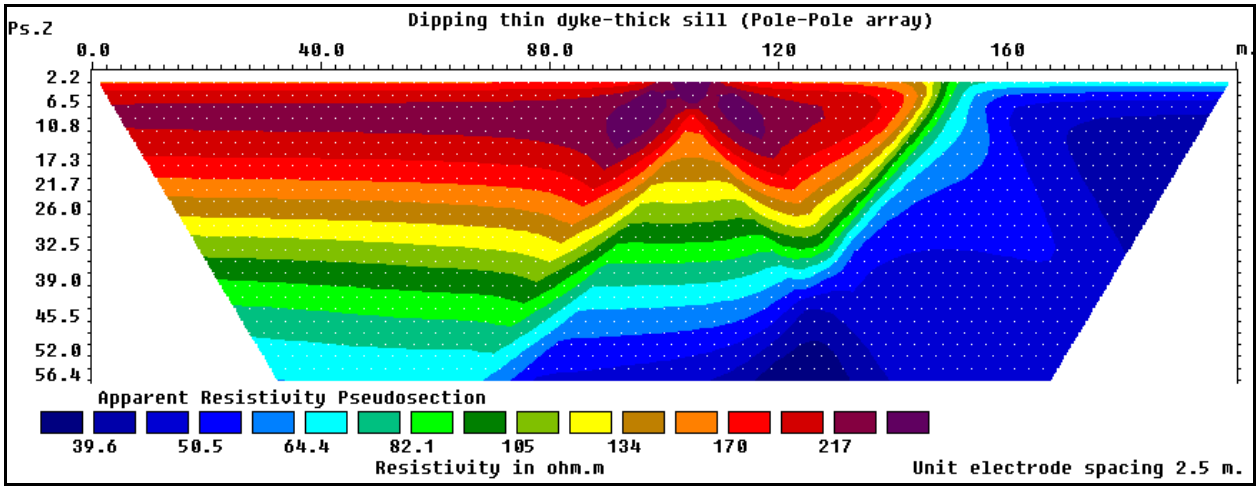

Pole-Pole array

G. VERTICAL THICK DYKE WITH THICK SILL

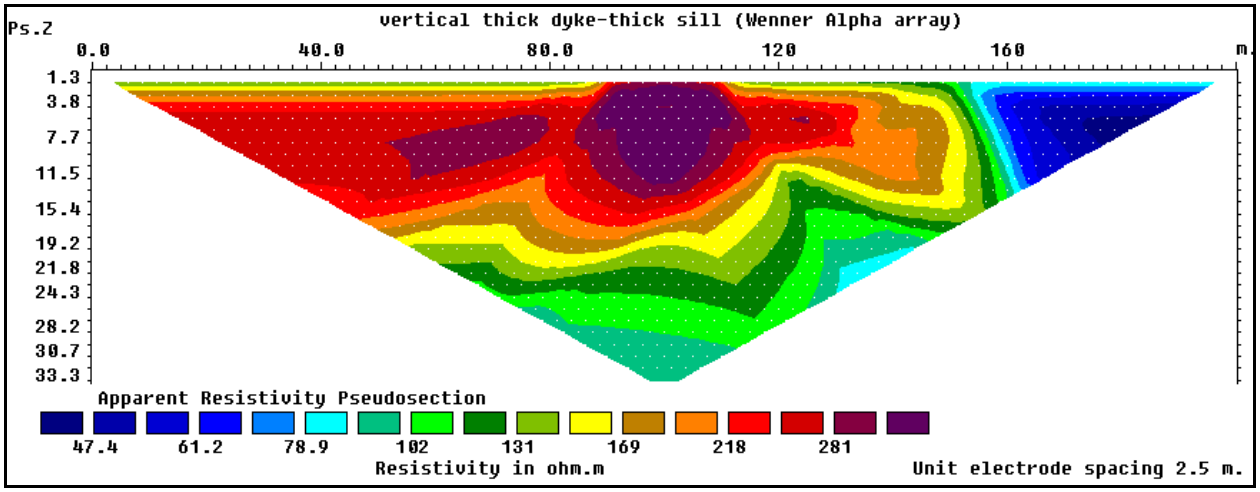

Wenner array

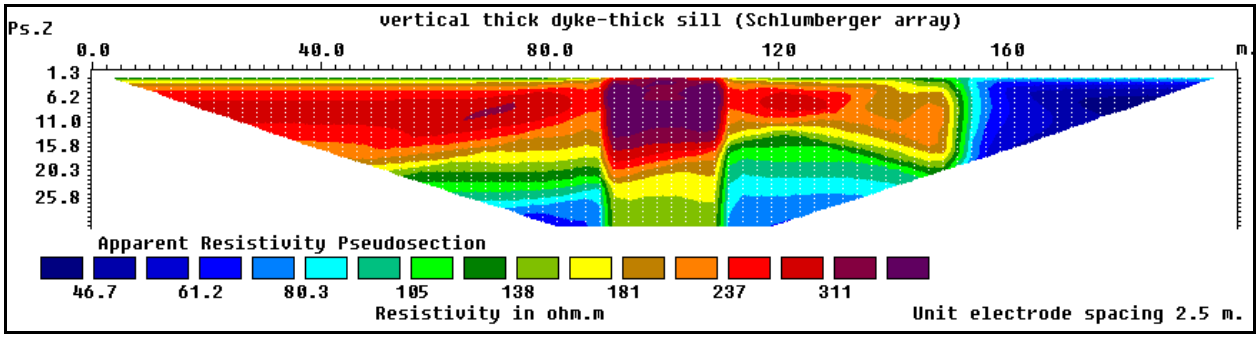

Schlumberger array

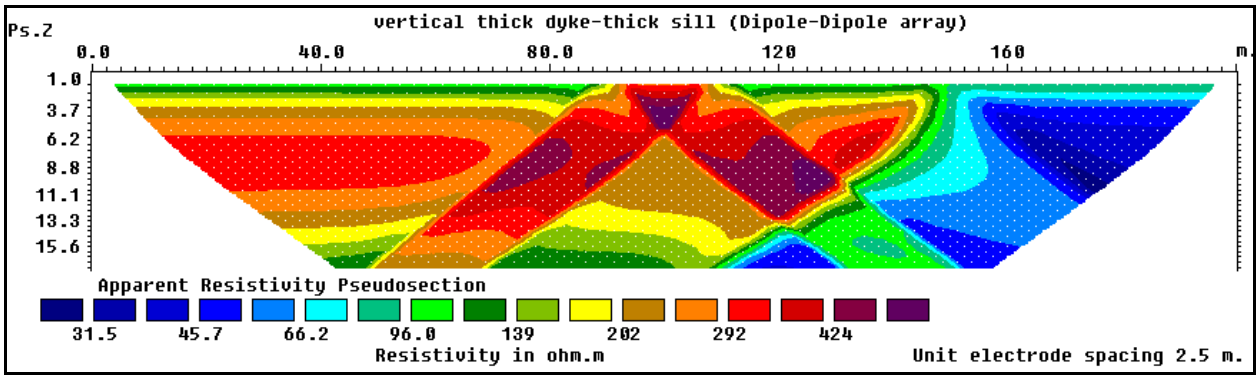

Dipole-Dipole array

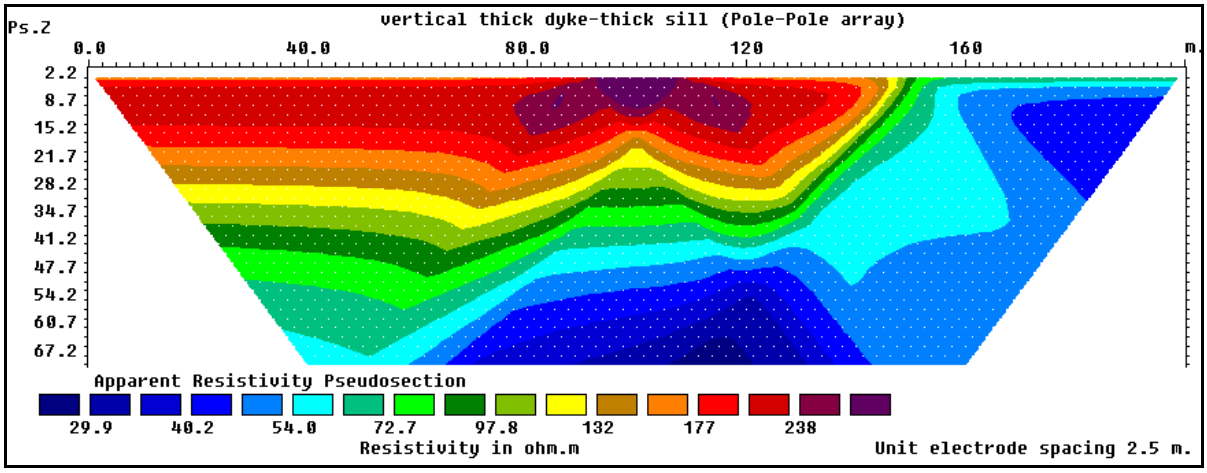

Pole-Pole array

H. DIPPING THICK DYKE WITH THICK SILL

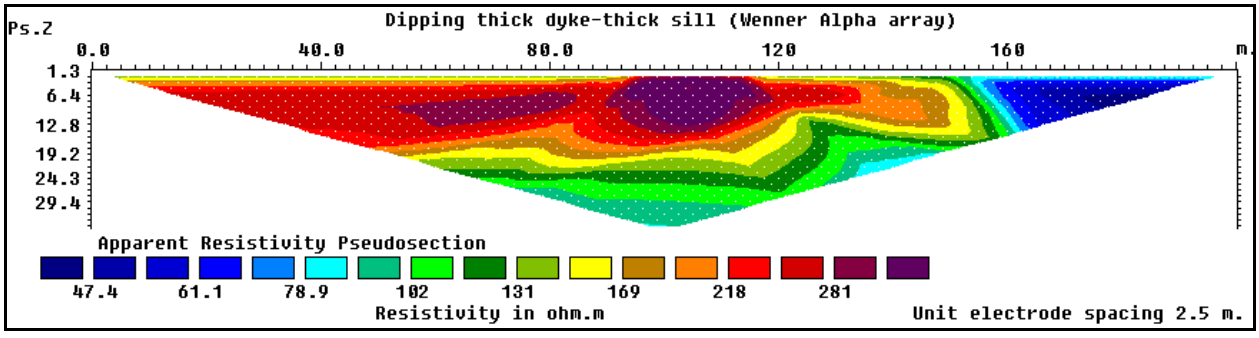

Wenner array

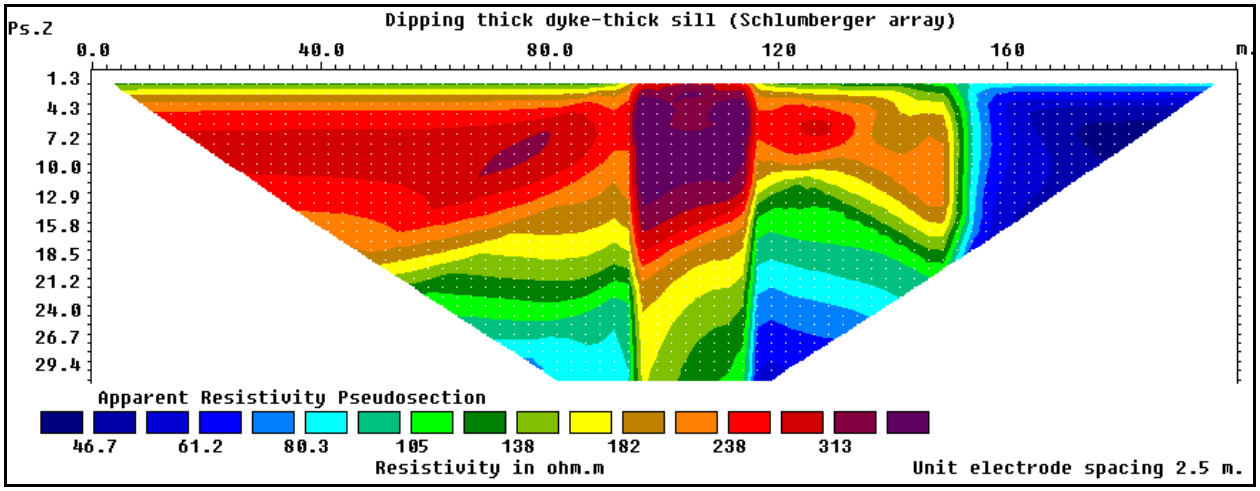

Schlumberger array

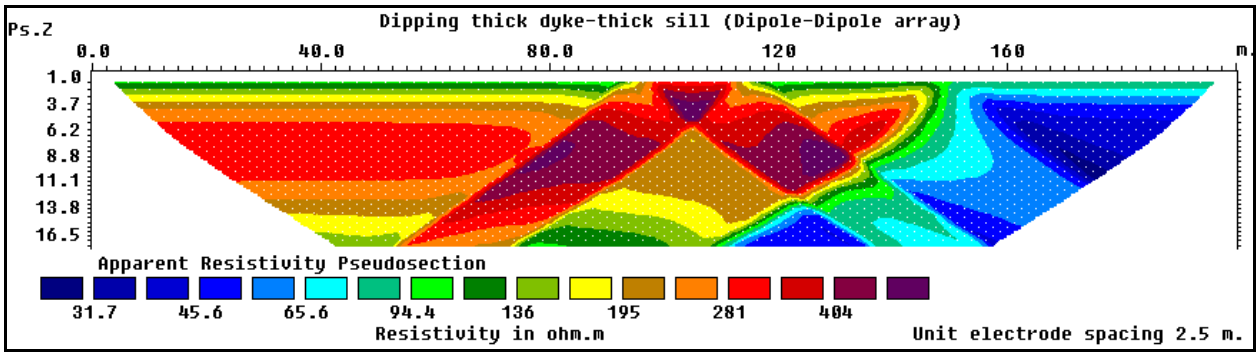

Dipole-Dipole array

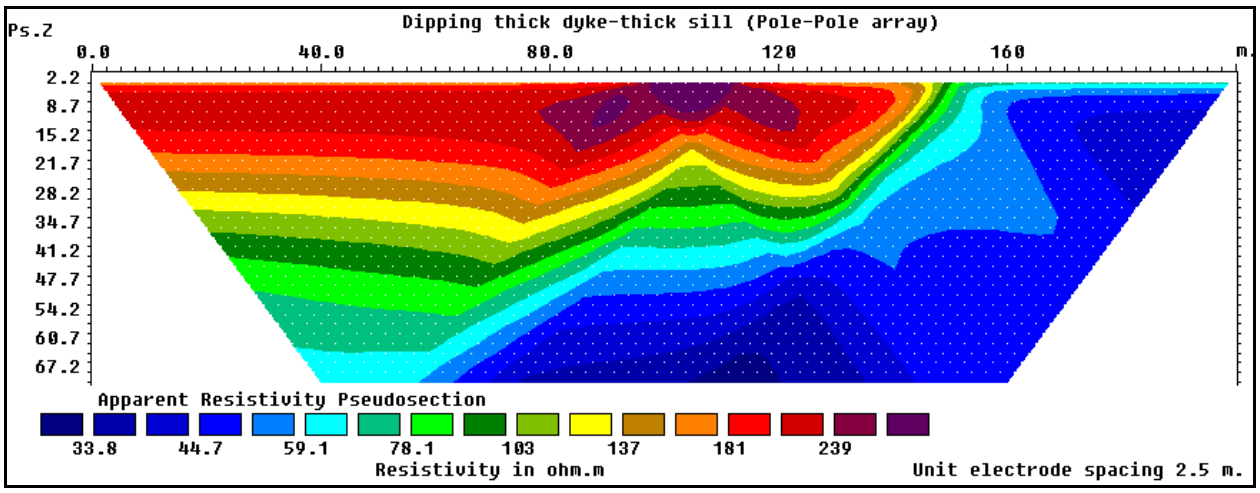

Pole-Pole array

APPENDIX 4: Weathered zone's apparent resistivity pseudo-sections

A. WEATHERED ZONE

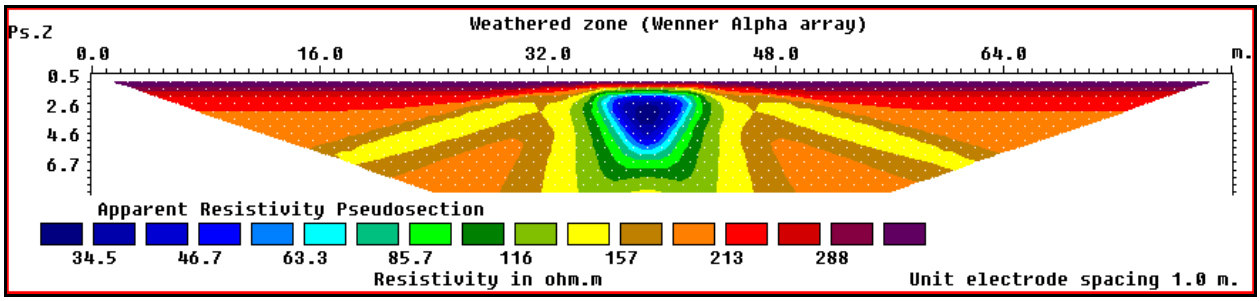

Wenner array

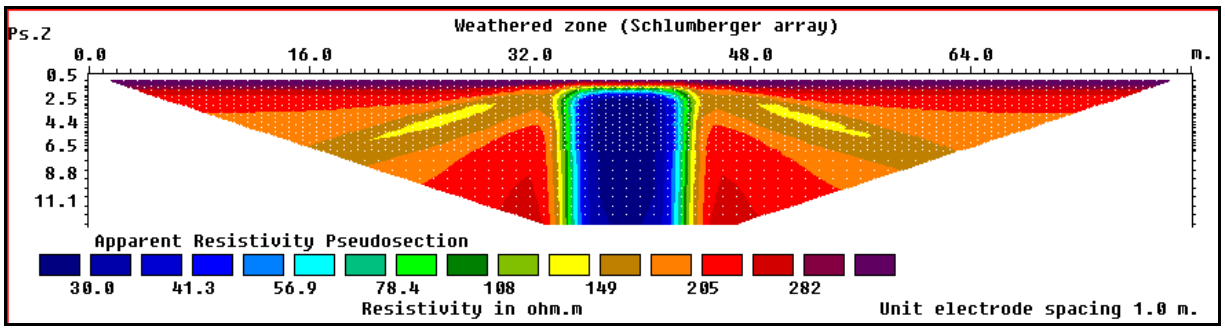

Schlumberger array

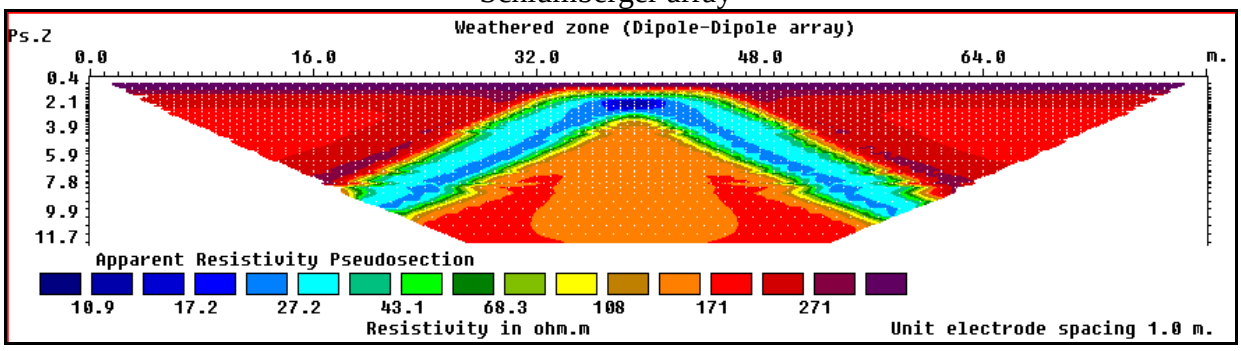

Dipole-Dipole array

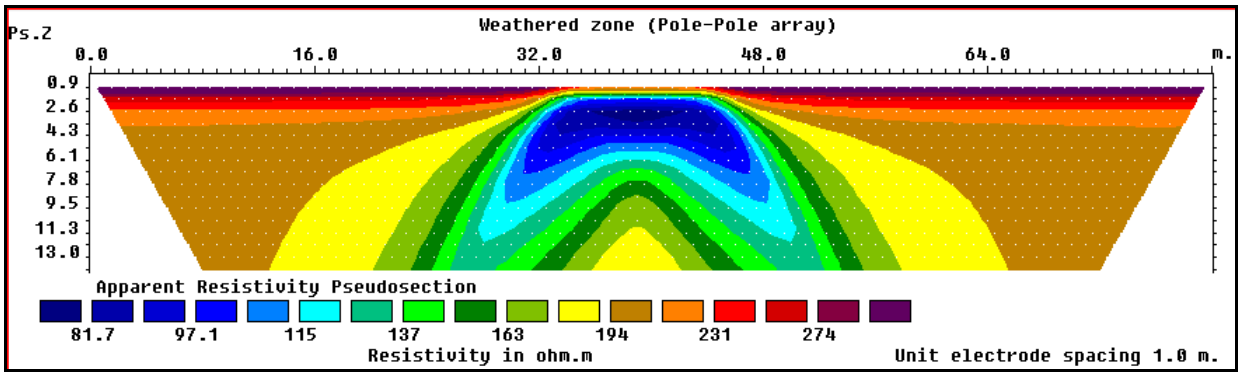

Pole-Pole array

APPENDIX 5: Contacts and boundary's apparent resistivity pseudo-sections

A. VERTICAL CONTACT

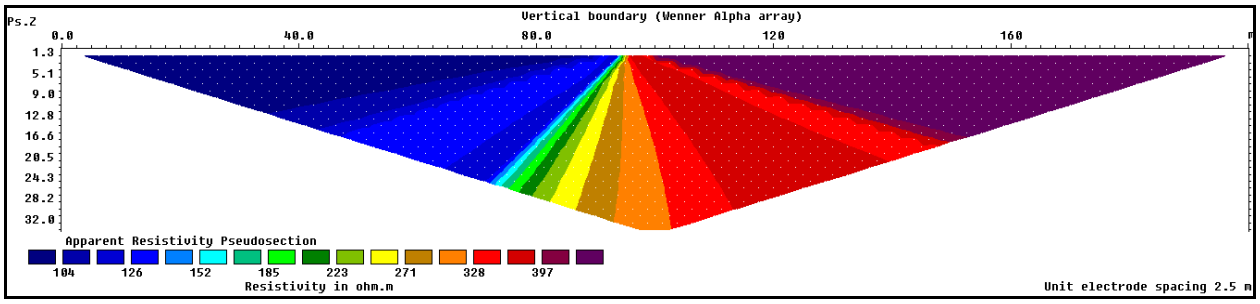

Wenner array

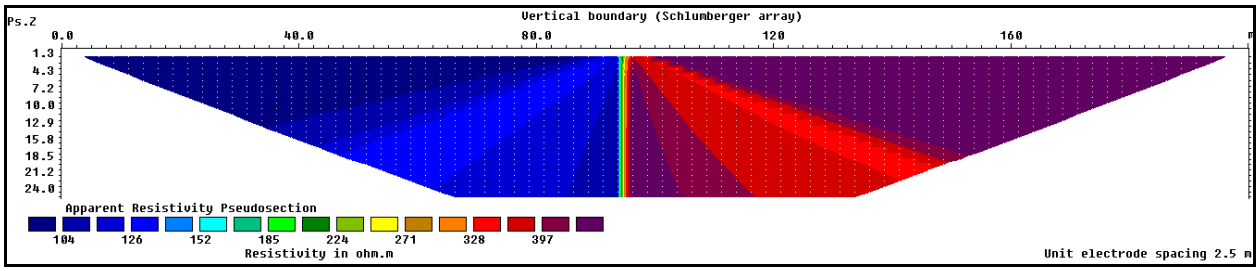

Schlumberger array

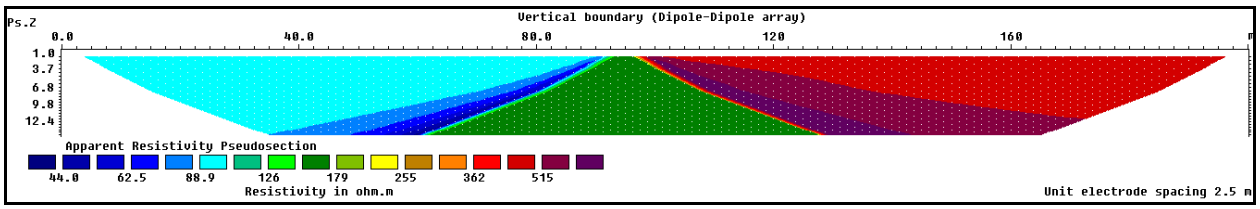

Dipole-Dipole array

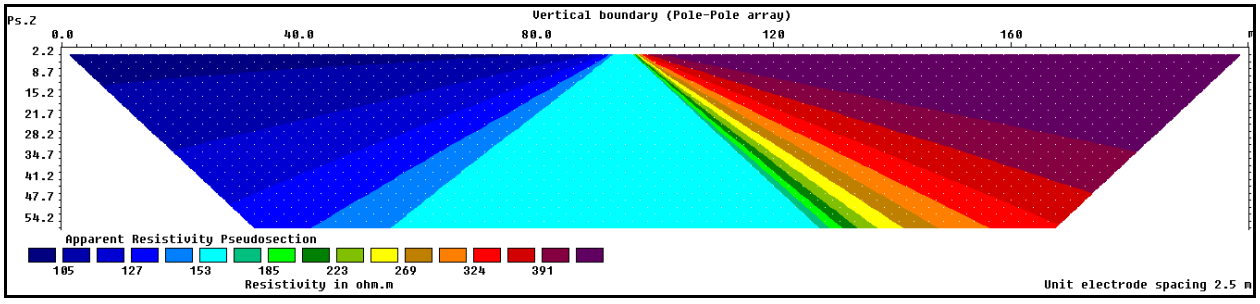

Pole-Pole array

B. DIPPING CONTACT

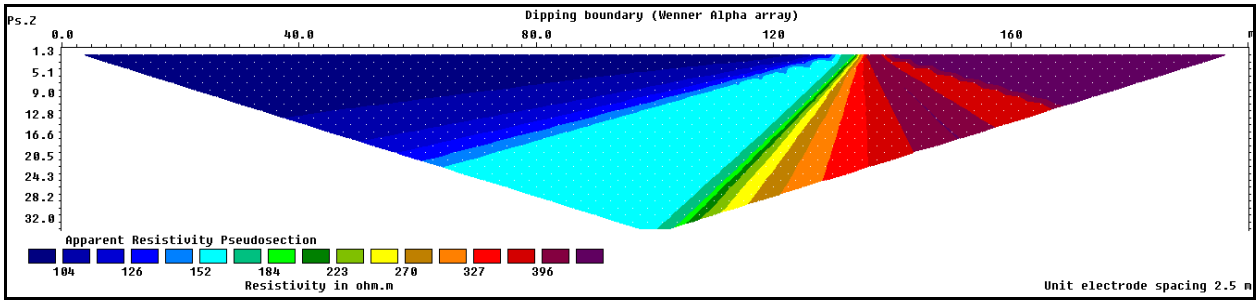

Wenner array

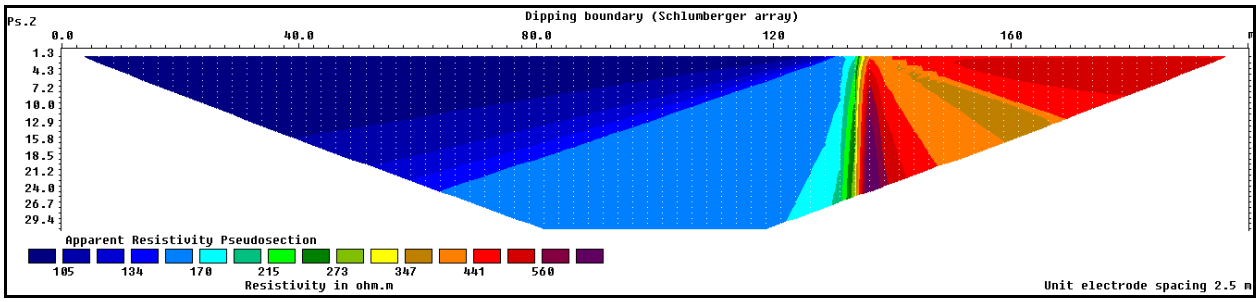

Schlumberger array

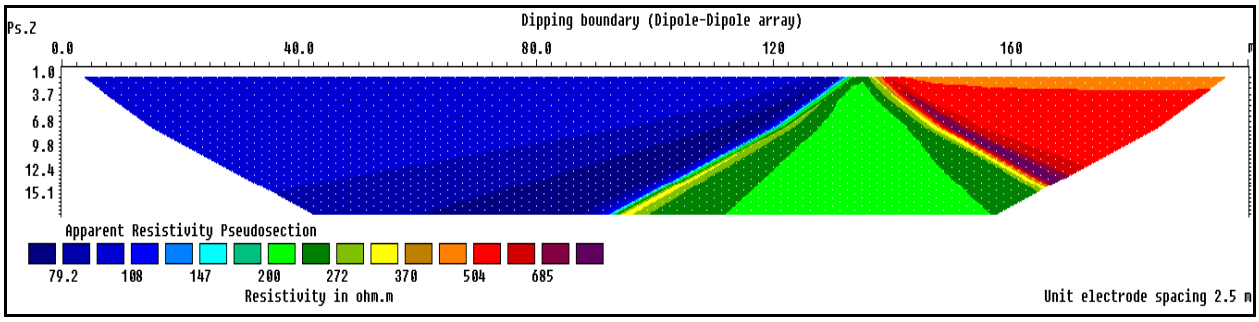

Dipole-Dipole array

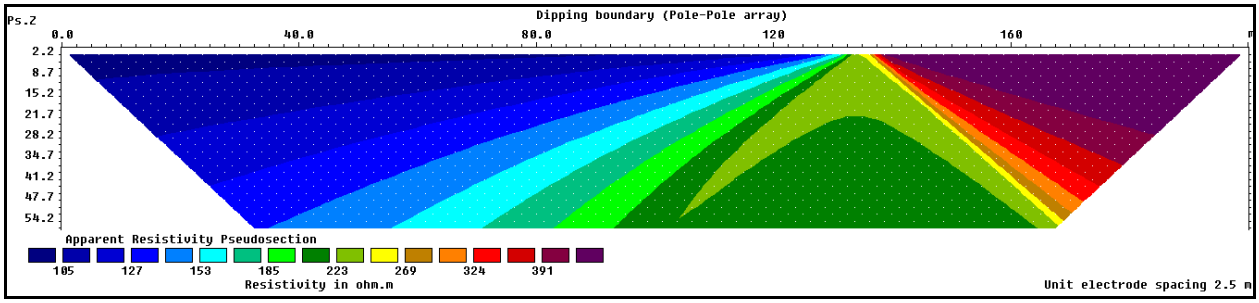

Pole-Pole array

C. HORIZONTAL CONTACT

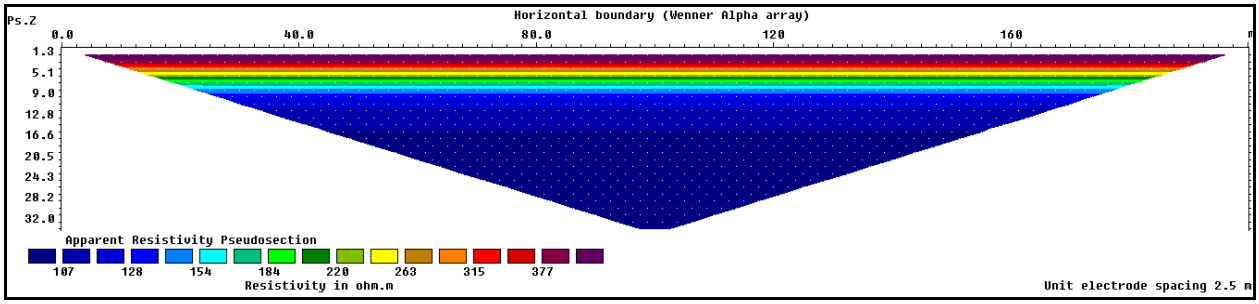

Wenner array

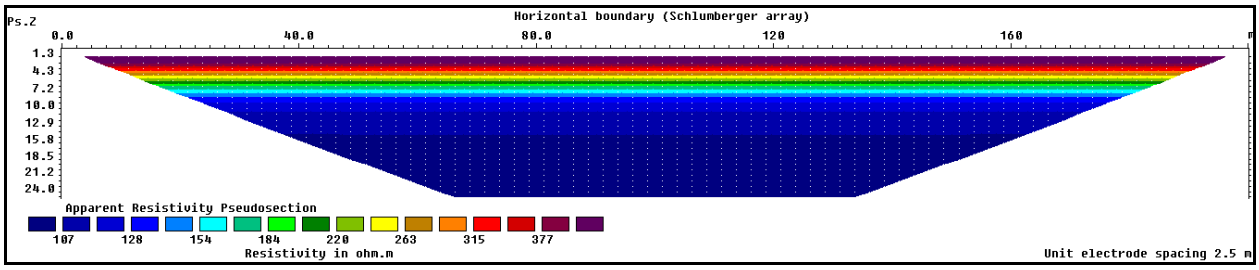

Schlumberger array

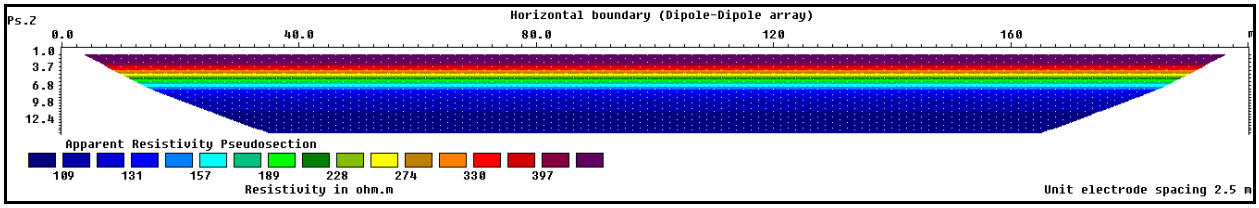

Dipole-Dipole array

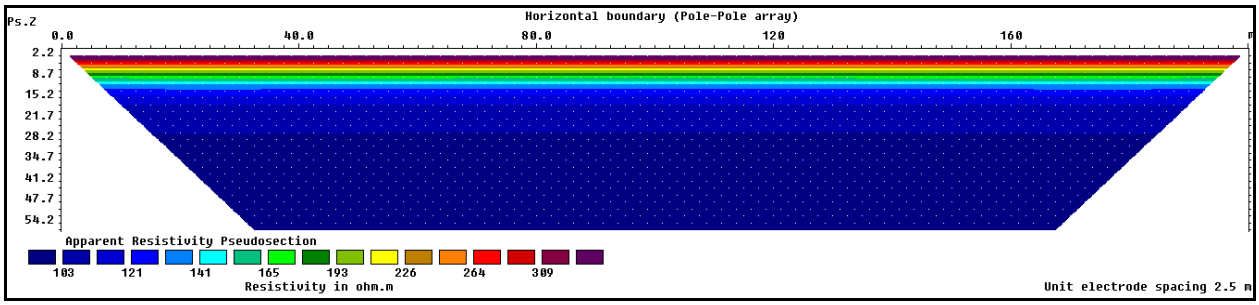

Pole-Pole array

APPENDIX 6: Fault's apparent resistivity pseudo-sections

A. VERTICAL FAULT

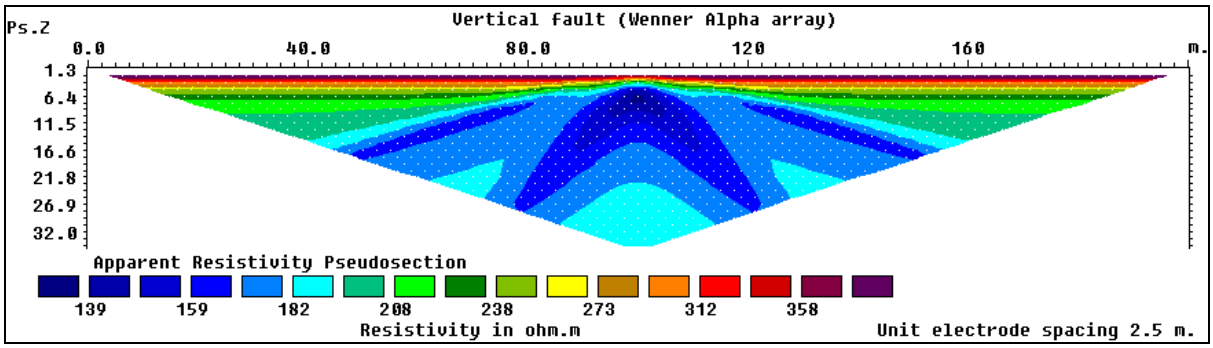

Wenner array

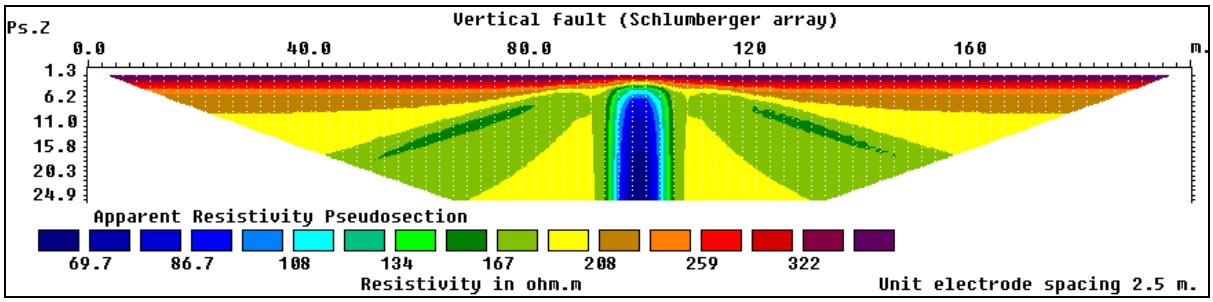

Schlumberger array

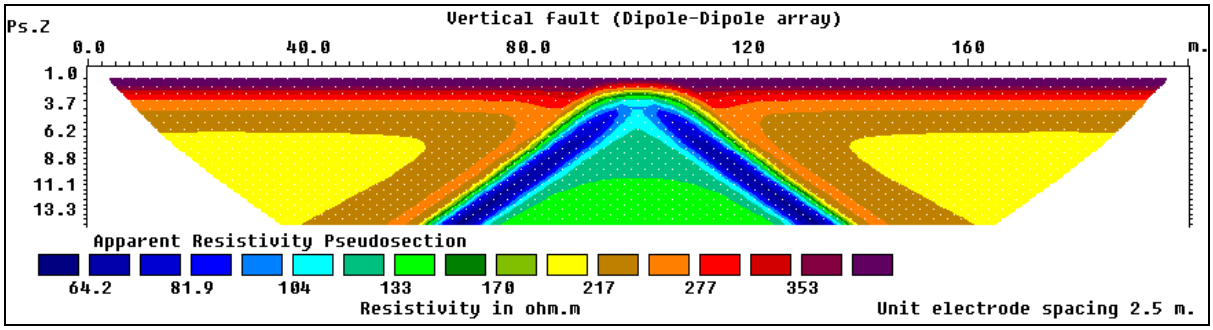

Dipole-Dipole array

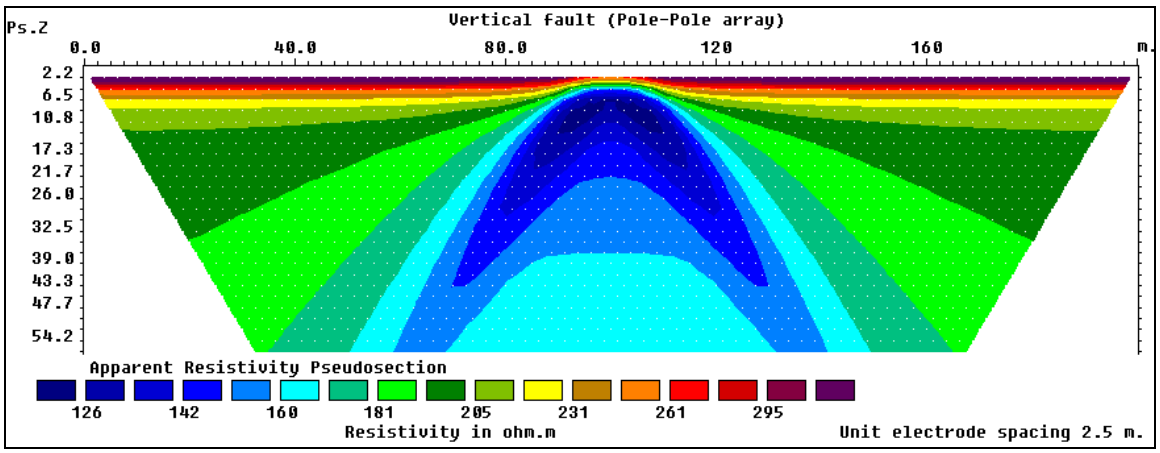

Pole-Pole array

B. DIPPING FAULT

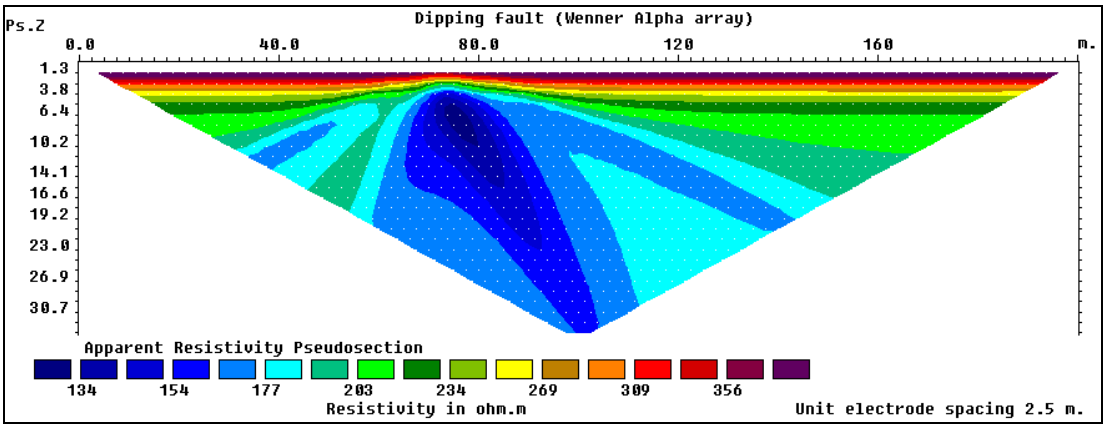

Wenner array

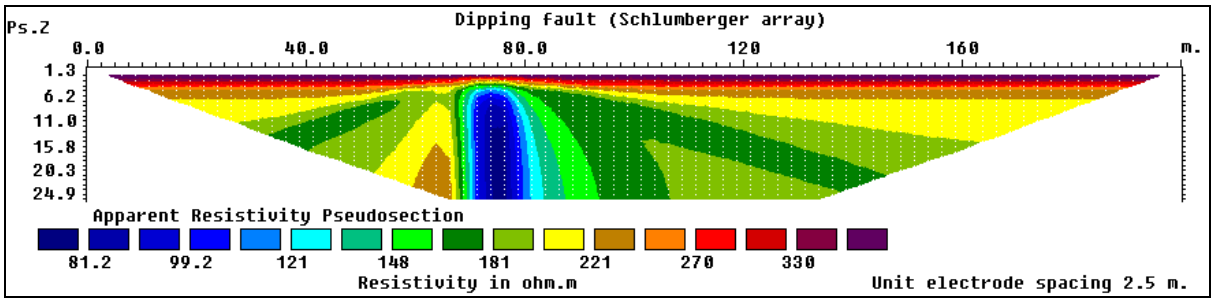

Schlumberger array

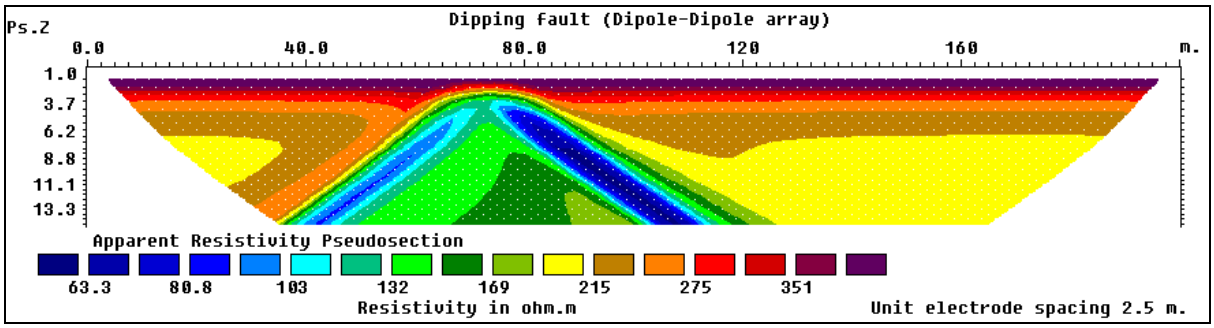

Dipole-Dipole array

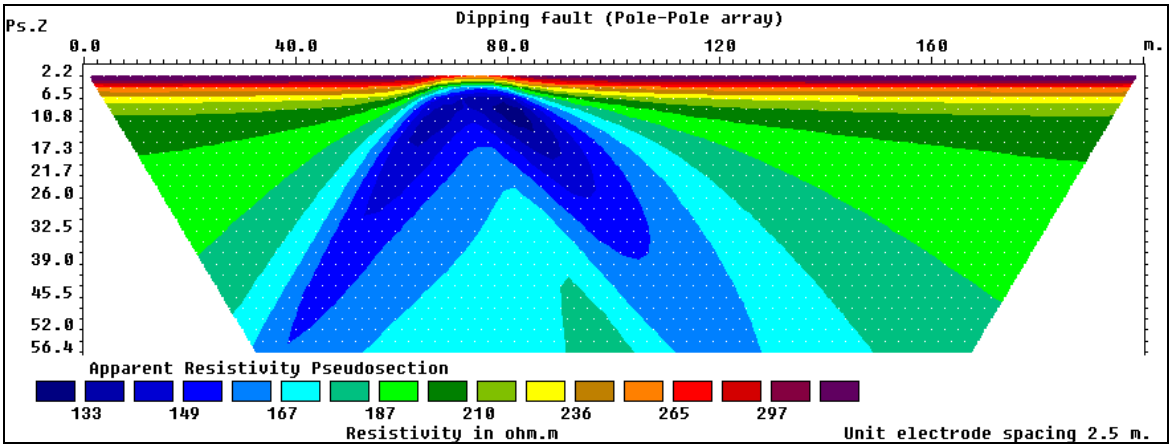

Pole-Pole array

ABSTRACT

The suitability of different electrodes arrays used during electrical resistivity tomography surveys for geohydrological studies in the Karoo rocks is evaluated through theoretical considerations, numerical modelling and field surveys.

The theoretical considerations predict that the Wenner array is sensitive to vertical changes in resistivity in the subsurface, while the Dipole-Dipole array is sensitive to horizontal changes in resistivity and the Schlumberger array is sensitive to both vertical and horizontal changes in resistivity. The theoretical considerations also show that the arrays with the strongest signal strength, the greatest depth of investigation and the broadest horizontal data coverage are the Wenner, the Dipole-Dipole and the Pole-Pole arrays, respectively.

Twenty synthetic geological models, simulating dolerite dyke and sill intrusions, weathered zones, faults zones or bedding plane fractures and different types of geological boundaries, are used to evaluate the sensitivity, depth of investigation, signal strength, as well as horizontal data coverage of the Wenner, Schlumberger, Dipole-Dipole and Pole-Pole arrays. Responses of these numerical models to the L1-norm, L2-norm and to random noise are also investigated.

Numerical modelling results indicate that the Wenner array is sensitive to vertical changes in the Earth's subsurface resistivity, has the strongest signal strength, yet the shallowest depth of investigation and the narrowest horizontal data coverage. The Schlumberger array, sensitive to both vertical and horizontal resistivity changes in the subsurface, has high signal-to-noise ratio and better depth coverage compared to the Wenner array. The Dipole-Dipole array is seen to be sensitive to horizontal resistivity changes in the subsurface, has great depth penetration, but a low signal-to-noise ratio. Although the Pole-Pole array has the broadest horizontal data coverage and the greatest depth of investigation this array is the most vulnerable to noise contamination.

The robust constraint inversion (L1-norm) should be selected for inverse modelling if the goal of the surveys concerns groundwater exploration since this algorithm produces models with sharp boundaries between different geological bodies. Conversely, the smoothness-constrained least-squares inversion (L2-norm) is appropriate when studying groundwater migration and contaminant transport because the diffusion boundary of a contaminant plume

in the subsurface geology is likely to be associated with a smoother variation in the resistivities. The L2-norm inversion method gives optimal results under such conditions where gradual changes in the subsurface resistivities are expected.

Two-dimensional electrical resistivity tomography surveys were carried out at three different sites near the city of Bloemfontein where dolerite dyke and sill intrusions occur. Results showed that the Wenner array is the most suitable electrode array to use for field surveys conducted across sill intrusions, while the Schlumberger array is the most appropriate for field surveys over dyke intrusions or sills intruded by dykes. The Dipole-Dipole array presented significant limitations for the field investigations due to its low signal-to-noise ratio. Results from the field studies conducted around Bloemfontein are in agreement with theoretical considerations as well as numerical modelling except the minor limitation of the Dipole-Dipole array (array recommended in theory by some authors).

Results demonstrate that the two-dimensional electrical resistivity tomography surveys employing either the Wenner or Schlumberger arrays, in conjunction with the appropriate inversion technique, would be of great benefit to geohydrological studies in Karoo rocks, particularly for boreholes siting and during contaminant transport studies.

Keywords: Suitability, Electrode arrays, Electrical resistivity tomography, Karoo rocks, Geohydrological studies, Dykes, Sills.

OPSOMMING

Die geskiktheid van verskillende elektrode-opstellings wat gebruik word tydens elektriese weerstandstomografie opnames vir geohidrologiese studies on Karoo-gesteentes word bestudeer deur teoretiese oorwegings, numeriese modellering en veldopnames.

Die teorie voorspel dat die Wenner-opstelling sensitief is vir vertikale veranderinge in die soortlike weerstand van die ondergrondse formasies, terwyl die Dipool-Dipool-opstelling sensitief is vir horisontale verandering in die soortlike weerstand en die Schlumberger-opstelling sensitief is vir beide vertikale en horisontale veranderinge in soortlike weerstand. Dit is getoon dat die elektrode-opstelling met die grootste seinsterkte, die grootste diepte van ondersoek en die breedste horisontale data-dekking onderskeidelik die Wenner-, die Dipool-Dipool- en die Schlumberger-opstelling is.

Twintig sintetiese geologiese modelle wat: dolerietgangintrusies, dolerietplaatintrusies, verweerde sones, verskuiwings of laagvlak frakture en verskillende tipe geologiese grense voorstel was gebruik vir die ondersoek. Die modelle was gebruik om die sensitiwiteit, ondersoekdiepte, seinsterkte, asook horisontale data-dekking van die Wenner-, Schlumberger-, Dipool-Dipool- en Pool-Pool-opstellings te ondersoek. Die response van hierdie numeriese modelle op die L1-norm, L2-norm en op ewekansige geraas is ook ondersoek.

Die resultate van die numeriese modellering dui daarop dat die Wenner-opstelling sensitief is vir vertikale verandering in die ondergrondse soortlike weerstand, die grootste seinsterkte het, maar dat dit die vlakste diepte van die ondersoek en die smalste horisontale data-dekking het. Die Schlumberger-opstelling, sensitief is vir beide vertikale en horisontale soortlike weerstandveranderinge ondergronds, het 'n hoë sein-tot-geraas verhouding en 'n groter ondersoekdiepte in vergelyking met die Wenner-opstelling. Die Dipool-Dipool-opstelling is sensitief is vir horisontale soortlike weerstandsveranderinge in die ondergrond, het ‘n groot penetrasiediepte, maar het egter ‘n lae sein-tot-geraas verhouding. Alhoewel die Pole-Pole rangskikking die wydste horisontale data-dekking het en die grootste diepte van ondersoek, , is hierdie elektrode-opstelling die mees kwesbaarste vir geraas-kontaminasie.

Die robuuste-beperking-inversie-norm (L1-norm) moet gekies word vir inverse modellering indien die weerstandopname fokus op grondwatereksploraie, aangesien hierdie algoritme modelle produseer met skerp grense tussen die verskillende geologiese liggame. Daarenteen

behoort die gladheid-beperkte kleinste-kwadraat-inversie (L2-norm) gebruik te word gedurende die studie van grondwatermigrasie en besoedelingsvervoer aangesien die diffusie-grens van ‘n kontaminantpluim waarskynlik geassosieer is met ‘n meer geledelike verandering in soortlike weerstande.

Twee-dimensionele elektriese weerstandstomografie opnames is uitgevoer by drie verskillende areas naby Bloemfontein waar dolerite-gangintusies en dolerite-plaatintrusies voorkom. Resultate toon dat die Wenner-opstelling die beste electrode-opstelling is om van gebruik te maak vir veldopnames oor doleriet-plaatintrusies. Die Schlumberger-opstelling is die mees geskikte opstelling is vir veldopnames oor dolerite-gangintrusies of waar ‘n doleriet-gang ‘n plaat ingedring het. Die Dipool-Dipool-opstelling het baie beperkings getoon vir veldopnames as gevolg van die lae sein-tot-geraas verhouding. Die resultate van die veld-opnames in die omgewing van Bloemfontein stem in die algemeen goed ooreen met die teoretiese voorspellings en numeriese modellering behalwe vir die beperkings van die Dipool-Dipool-opstelling (opstelling teroeties aanbeveel deur sekere outeurs).

Resultate toon dat die twee-dimensionele elektriese-weerstandstomografie-opnames met beide die Wenner- en die Schlumberger-opstellings, in kombinasie met die toepaslike inversie tegnieke, van groot belang kan wees vir geohidrologiese studies in Karoo-gesteentes, veral vir die aanwysing van boorgate en gedurende ondersoeke van kontaminantverspreiding.